Report No. FHWA-RD-76-165

HIGHWAY-VEHICLE-OBJECT SIMULATION MODEL--1976

Vol. 4 Engineering Manual--Validation

February 1976
Final Report

Document is available to the public through
the National Technical Information Service,
Springfield, Virginia 22161

Prepared for
FEDERAL HIGHWAY ADMINISTRATION
Offices of Research & Development
Washington, D. C. 20590

NOTICE

This document is disseminated under the sponsorship of the Department of Transportation in the interest of information exchange. The United States Government assumes no liability for its contents or use thereof.

The contents of this report reflect the views of Calspan Corporation, which is responsible for the facts and the accuracy of the data presented herein. The contents do not necessarily reflect the official views or policy of the Department of Transportation. This report does not constitute a standard, specification, or regulation.

FHWA DISTRIBUTION NOTICE

Limited copies of this report are being distributed by memorandum to individual researchers involved in computer simulations of highway vehicles and impacts with roadside obstacles.

A limited number of additional copies of this report is available from the Protective Systems Group of the Structures and Applied Mechanics Division, Office of Research.

Copies may also be obtained from the National Technical Information Service (NTIS), Department of Commerce, 5285 Port Royal Road, Springfield, Virginia 22161. A small charge is imposed for copies provided by NTIS.

Technical Report Documentation Page

1. Report No.	2. Government Accession No.	3. Recipient's Catalog No.
FHWA-RD-76-165		

4. Title and Subtitle	5. Report Date
Highway-Vehicle-Object Simulation Model - 1976 Engineering Manual - Validation	February 1976
	6. Performing Organization Code
7. Author(s) David J. Segal	8. Performing Organization Report No. ZR-5461-V-4-R
9. Performing Organization Name and Address Calspan Corporation P. O. Box 235 Buffalo, New York 14221	10. Work Unit No. (TRAIS) FCP 31H2232
	11. Contract or Grant No. DOT-FH-11-8265
12. Sponsoring Agency Name and Address U.S. Department of Transportation Federal Highway Administration Contracts and Procurement Division Washington, D.C. 20590	13. Type of Report and Period Covered Final Report February 1974 - February 1976
	14. Sponsoring Agency Code S0610

15. Supplementary Notes

FHWA Contract Manager: Morton S. Oskard

16. Abstract

A series of reports have been written to document revised and updated versions of the simulation of highway-vehicle-object interactions in a single vehicle highway environment. The programs documented were developed under FHWA sponsorship to provide the highway safety community with an analytical means of evaluating the effects of highway/roadside environment on safety.

This manual is addressed to the engineer and contains evidence of the validity of the HVOSM mathematical model and computer simulation. Both rigorous tests of validity by comparisons with extensively documented full-scale tests and general comparisons are included.

This manual is one of four volumes.

Contractors Report No. ZR-5461-V	Short Title
-6	HVOSM - 1976 Users Manual
-7	HVOSM - 1976 Programmers Manual
-8	HVOSM - 1976 Engineering Manual - Analysis
-4-R	HVOSM - 1976 Engineering Manual - Validation

17. Key Words	18. Distribution Statement
HVOSM, Vehicle Dynamics Computer Simulation	No restrictions. This report is available to the public through the National Technical Information Service, Springfield, Virginia, 22161.

19. Security Classif. (of this report)	20. Security Classif. (of this page)	21. No. of Pages	22. Price
Unclassified	Unclassified	233	

Form DOT F 1700.7 (8-72) Reproduction of completed page authorized

FOREWORD

This report is one of four manuals prepared under Contract Number DOT-FH-11-8265 for the Federal Highway Administration, U.S. Department of Transportation for the purpose of summarizing and upgrading documentation of the Highway-Vehicle-Object Simulation Model (HVOSM). The HVOSM had been previously developed for the Federal Highway Administration (FHWA) by the Calspan Corporation (formerly Cornell Aeronautical Laboratory) under Contract Number CPR-11-3988 during the period from 1966 to 1971 and extended under this contract. Contained in this report is a description of the experimental validation procedures employed in determining the degree and range of validity of the HVOSM.

Complete documentation of the HVOSM is contained in the following manuals:

- Highway-Vehicle-Object Simulation Model
  Volume 1 - Users Manual
- Highway-Vehicle-Object Simulation Model
  Volume 2 - Programmers Manual
- Highway-Vehicle-Object Simulation Model
  Volume 3 - Engineering Manual - Analysis
- Highway-Vehicle-Object Simulation Model - Volume 4 - Engineering Manual - Validation

This report has been reviewed and is approved by:

Edwin A. Kidd

Edwin A. Kidd, Head
Transportation Research Department

TABLE OF CONTENTS

		Page No.
	FOREWORD	ii
	LIST OF FIGURES	vi
	LIST OF TABLES	xi
1.0	INTRODUCTION	1
	1.1 Background	1
	1.2 HVOSM Documentation	2
2.0	HVOSM VALIDATION TESTS	4
	2.1 Sinusoidal Steering Tests - HVOSM-SMI1	4
	2.1.1 Test Vehicle and Instrumentation	4
	2.1.1.1 Vehicle Parameters	5
	2.1.1.2 Instrumentation	10
	2.1.2 Data Acquisition and Reduction	16
	2.1.3 Test Procedure	16
	2.1.4 Comparison of Predicted and Experimental Results	19
	2.1.5 Vehicle Response Sensitivity	26
	2.2 Ramp Traversal Tests - HVOSM-SMI1	26
	2.2.1 Test Vehicle and Instrumentation	26
	2.2.2 Data Acquisition and Reduction	27
	2.2.3 Test Procedure	28
	2.2.4 Comparison of Predicted and Experimental Results	30
	2.2.5 Vehicle Response Sensitivity	62
	2.3 Skidding Tests - HVOSM-SMI1	66
	2.3.1 Test Vehicle and Instrumentation	66
	2.3.2 Data Acquisition and Reduction	66
	2.3.3 Test Procedure	66
	2.3.4 Comparison of Predicted and Experimental Results	69
	2.3.5 Vehicle Response Sensitivity	86

TABLE OF CONTENTS (continued)

		Page No.
2.4	Bridge Rail Impact Test - HVOSM-SMI1	87
2.4.1	Test Vehicle and Instrumentation	87
2.4.1.1	Vehicle Parameters	88
2.4.1.2	Instrumentation	90
2.4.2	Data Acquisition and Reduction	93
2.4.3	Test Procedure	94
2.4.4	Comparison of Predicted and Experimental Results	96
2.4.5	Vehicle Response Sensitivity	98
2.5	Straight Ahead Braking - HVOSM-VD1	100
2.5.1	Test Vehicle and Instrumentation	100
2.5.1.1	Vehicle Parameters	102
2.5.1.2	Instrumentation	125
2.5.2	Data Acquisition and Reduction	133
2.5.3	Test Procedure	134
2.5.4	Comparison of Predicted and Experimental Results	136
2.5.5	Vehicle Response Sensitivity	159
2.5.5.1	Variation of Lining Fade Coefficient	159
2.5.5.2	Effective Push-Out Pressure for the Brake System	160
2.5.5.3	Rolling Radius of the Tires	165
2.6	Braking in a Turn - HVOSM-VD1	170
2.6.1	Test Vehicle and Instrumentation	170
2.6.2	Data Acquisition and Reduction	170

TABLE OF CONTENTS (continued)

			Page No.
	2.6.3	Test Procedure	170
	2.6.4	Comparison of Predicted and Experimental Results	170
	2.6.5	Vehicle Response Sensitivity	191
3.0	HVOSM GENERAL COMPARISONS		192
3.1	General Motors Bridge Parapet Comparison		192
3.2	Astro Spiral Jump		194
3.3	Embankment Comparisons		196
4.0	REFERENCES		221

LIST OF FIGURES

Figure No.	Description	Page No.
2.1-1	Lateral Force vs. Slip Angle and Vertical Load	11
2.1-2	Instrumentation and Equipment Installed in Test Vehicle	12
2.1-3	Inputs for Test 3 Simulation	20
2.1-4	Inputs for Test 9 Simulation	21
2.1-5	Measured and Simulated Responses of Vehicle with ± 5° - 0.5 cps Steer	22
2.1-6	Measured and Simulated Responses of Vehicle with ± 10° - 0.7 cps Steer	24
2.2-1	Inputs for Test 5 Simulation	31
2.2-2	Inputs for Test 6 Simulation	32
2.2-3	Inputs for Test 7 Simulation	33
2.2-4	Inputs for Test 13a Simulation	34
2.2-5	Inputs for Test 13b Simulation	36
2.2-6	Inputs for Test 14 Simulation	38
2.2-7	Measured and Simulated Responses of Vehicle Traversing 7.1° - 6.75" High Ramp	40
2.2-8	Measured and Simulated Responses of Vehicle Traversing 9.2° - 8.5" High Ramp with Left Side Wheels Only	42
2.2-9	Measured and Simulated Responses of Vehicle Traversing 7.1° - 6.75" High Ramp while Cornering at 0.4 G	44
2.2-10	Measured and Predicted Responses of Vehicle Traversing 3.6° - 21.5" High Ramps Alternately with Right and Left Wheels (Test 13a)	49

LIST OF FIGURES (continued)

Figure No.	Description	Page No.
2.2-11	Measured and Predicted Responses of Vehicle Traversing 3.6° - 21.5" High Ramps Alternately with Right and Left Wheels (Test 13b)	52
2.2-12	Alternate Ramp Traversal at 30 MPH	57
2.2-13	Measured and Predicted Responses of Vehicle Jump from Take-off Ramp	59
2.2-14	Ramp Jump at 44 MPH	63
2.2-15	Effects of Change of Vehicle Parameters on Predicted Responses for Alternate Ramp Traversal Simulation	64
2.3-1	Inputs for Test 10 Simulation	70
2.3-2	Inputs for Test 11 Simulation	71
2.3-3	Inputs for Test 12 Simulation	72
2.3-4	Measured and Predicted Responses of Vehicle in Forward Skid on Wet Pavement	73
2.3-5	Photographic and Computer Graphic Display of Skidding Vehicle	77
2.3-6	Measured and Predicted Responses of Vehicle in Forward Skid on Dry Pavement	78
2.3-7	Measured and Predicted Responses of Vehicle in Reverse Skid on Dry Pavement	82
2.4-1	Bridge Railing Installation for Test No. 1	89
2.4-2	Instrumentation and Equipment Installed in Test Vehicle	92
2.4-3	Sequence Photos of Test No. 1 Impact	95
2.4-4	Vehicle and Bridge Railing Responses - Test No. 1	97

Figure No.	Description	Page No.
2.4-5	HVOSM Impact Comparison Inputs	100
2.5-1	Test Vehicle	101
2.5-2	Comparison Carpet Plots of Measured Tire Data and Analytical Fit	106
2.5-3	Experimental Set-Up for Measuring the Rear Wheel and Driveline Moments of Inertia	109
2.5-4	Oscilliscope Patterns of the Forced Response vs. the Shaking Torque	111
2.5-5	Definition of Brake Measurements	115
2.5-6	Variation of Lining Fade Coefficient with Temperature for Test Vehicle	119
2.5-7	Lining Fade Coefficient Variation with Brake Temperature	120
2.5-8	Brake Torque vs. Hydraulic Pressure	121
2.5-9	Brake Output Torque vs. Temperature (Left Rear Wheel) Constant Speed and Pressure	124
2.5-10	Vehicle Instrumentation System	127
2.5-11	Computer Program Inputs for Straight Ahead Stops	137
2.5-12	Experimental Time Histories of Vehicle Responses to Straight Ahead Braking Maneuver	144
2.5-13	Sequence of Events Relative to Trajectory Marking	151
2.5-14	Comparison of Measured and Computed Vehicle Responses - Straight Ahead Braking Maneuver	153
2.5-15	Lining Face Coefficient Variation with Brake Temperature	161

Figure No.	Description	Page No.
2.5-16	Influence of Lining Fade Variation on Vehicle Longitudinal Acceleration	162
2.5-17	Design Relative Front/Rear Brake Capacity	163
2.5-18	Illustration of Measured Brake Capacity	163
2.5-19	Influence of a Change in the Rolling Radius	169
2.6-1	Experimental Time Histories of Vehicle Responses to a Combination Cornering and Braking Maneuver	171
2.6-2	Measurement Definitions for Trajectories of Cornering Stops	176
2.6-3	Computer Program Inputs for Cornering Stops	178
2.6-4	Comparison of Measured and Computed Vehicle Responses - Cornering and Braking Maneuver	185
2.6-5	Measured and Computed Stopping Positions	190
3.1-1	Experimental and Predicted Vehicle Responses for a 50 MPH - 12° Collision with the General Motors Bridge Parapet	193
3.2-1	Experimental and Predicted Responses in Astro Spiral Jump	195
3.3-1	Right Front Tire Track, Test No. 1	199
3.3-2	HVOSM vs. Test Results, Test No. 1, Camera No. 1	200
3.3.3	Vertical Acceleration vs. Time, Test No. 1	205
3.3-4	Right Front Tire Track, Test No. 2	207
3.3-5	Vertical Acceleration vs. Time, Test No. 2	208

Figure No.	Description	Page No.
3.3-6	Right Front Tire Track, Test No. 3	210
3.3-7	Vertical Acceleration vs. Time, Test No. 3	211
3.3-8	Right Front Tire Track, Test No. 4	214
3.3-9	Right Front Tire Track, Test No. 5	215
3.3-10	Vertical Acceleration vs. Time, Test No. 5	217
3.3-11	Right Front Tire Track, Test No. 6	218
3.3-12	Vertical Acceleration vs. Time, Test No. 6	219

LIST OF TABLES

Table No.	Description	Page No.
2.1-1	Test Vehicle Parameter Values - 1963 Ford Galaxie Four-Door Sedan	6
2.1-2	Tire Parameter Data	9
2.1-3	Summary of Instrumentation Transducers	13
2.1-4	Summary of Sinusoidal Steering Test Program	18
2.2-1	Tire Parameter Data	27
2.2-2	Summary of Experimental Program	29
2.3-1	Summary of Experimental Program	67
2.4-1	Summary of Instrumentation Transducers	91
2.5-1	Basic Parameter Values of Test Vehicle - 1963 Ford Galaxie Four-Door Sedan	103
2.5-2	Tire Parameter Data for Inflation Pressure = 28 PSI	105
2.5-3	Moments of Inertia	107
2.5-4	Brake Parameters	113
2.5-5	Summary of Instrumentation Transducers	126
2.5-6	Measured Stopping Distances Straight Ahead Braking Maneuver	150
2.6-1	Measurements of Trajectory for Combined Cornering and Braking Maneuver	176
3.3-1	Test Conditions	197

1. INTRODUCTION

In 1966 Calspan Corporation (formerly Cornell Aeronautical Laboratory, Inc.) began development of a general mathematical model and computer simulation of the dynamic responses of an automobile in accident situations under Contract CPR-11-3988 with the Bureau of Public Roads.

The mathematical model of vehicle dynamics developed in the first year of that effort included the general three-dimensional motion resulting from vehicle control inputs, traversal of irregular terrain, or from collisions with simple roadside barriers. The model was subsequently named the Highway-Vehicle-Object Simulation Model (HVOSM). Later, the model was further developed and a comprehensive validation program was carried out including a series of repeatable full-scale tests with an instrumented vehicle in order to objectively assess the degree of validity of the vehicle model. Extensive measurements of the vehicle parameters required for input to the HVOSM were made under a subcontract with the Ford Motor Company as a part of the validation procedure. This effort was reported in Reference 1 and the model as described therein has been referred to as the V-3 version of the HVOSM.

Modifications were subsequently made to the simulation in order to study the effects of terrain (specifically, railroad grade crossings) on vehicle control ability. The impact routines were removed and extended terrain definition capabilities were added along with a more realistic model of suspension properties. This program version (Reference 2) has been informally referred to as the V-4 version of the HVOSM and has since been used extensively for study of roadway and roadside geometrics.

Further developments of HVOSM aimed at providing a simulation model suitable for the study of the complex dynamics resulting from pre-collision evasive maneuvers were reported in Reference 3. This version, informally called the V-7 version of the HVOSM, includes a detailed model of the braking and driving systems and an empirically based definition of the relationships between longitudinal and lateral tire forces through the inclusion of rotational degrees of freedom of the four vehicle wheels.

During development of the HVOSM, documentation efforts primarily fulfilled the objectives of maintaining communication within the program development structure, ensuring quality control of the development and providing a historical reference. It was, however, recognized early in the development of the HVOSM, that this state-of-the-art advance in the modeling of a vehicle and its environment could be put to best use through its widespread distribution to organizations interested in its application to highway safety. As a result, distribution of the HVOSM was begun before its development was complete and before instructional documentation could be provided.

Recognizing the need to bring documentation of the several HVOSM versions together and to provide the highway safety community with an effective description of the programs and their use, the Federal Highway Administration (FHWA) awarded Calspan Corporation contract number DOT-FH-11-8265 for the purpose of providing such documentation for the HVOSM.

Three versions of the HVOSM were covered by this documentation. They were, the HVOSM-SM11 (Sprung Mass Impact) version (formerly known as the V-3 version), the HVOSM-RD1 (Road Design) version (formerly known as the V-4 version) and the HVOSM-VD1 (Vehicle Dynamics) version (formerly known as the V-7 version). Under the first phase of that effort, only those versions as developed by Calspan were covered by the documentation.

The second phase of contract number DOT-FH-11-8265 called for extension of the capabilities of the HVOSM by adding new features, including some additional modifications made by other research organizations, and providing additional ease of use features.

The documentation provided now covers the two program versions: the HVOSM-RD2 Version (Roadside Design) and the HVOSM-VD2 Version (Vehicle Dynamics). It is intended to be a base to which further developments and modifications to the HVOSM can be added, thus providing a uniform reporting format and centralized source of information for the many HVOSM users. It consists of four volumes, each describing a separate aspect of the HVOSM. Two volumes are directed toward the engineer/analyst containing the analysis (derivation of governing equations, assumptions, and development of controlling logic) and experimental validation. Another volume is directed toward the general program user and contains analysis/program symbology, descriptions of the models and solution procedures, descriptions of input requirements and program application examples. The fourth volume of documentation is intended for use by those interested in the detailed computer programs. This volume contains descriptions of the computer code including a discussion of subroutine functions, annotated flowcharts and program listings.

Validation of the HVOSM is summarized in this report. Section 2.0 describes the rigorous tests of validity applied to the model including a description of the test vehicle and instrumentation, vehicle parameter data, data acquisition and reduction, test procedure and comparisons of experimental and predicted responses. Section 3.0 contains general comparisons between the HVOSM and experimental responses that are not considered to be rigorous evidence of validity either because the experiments were not fully defined or shown to be repeatable, or the vehicle data used in the simulation were based on estimates.

2.0 HVOSM VALIDATION TESTS

2.1 Sinusoidal Steering Tests

2.1.1 Test Vehicle and Instrumentation

The vehicles employed in the tests to secure data for validation of the computer simulation were 1963 Ford Galaxie four-door sedans formerly used by the New York State Police. All of the dynamic tests were conducted with a single automobile. Detailed measurements of the vehicle physical characteristics required as inputs to the simulation model (e.g., sprung and unsprung masses, c.g. position, moments of inertia, ride and roll rates of the suspension, etc.) were made by the Ford Motor Company and are reported in Section 2.1.1.1.

Aside from the installation of instrumentation and control equipment, the only changes to the vehicle from the as-received condition were the installation of new shock absorbers and, for some tests, a set of new wheels and tires. These tires were provided to Calspan by the General Motors Corporation (GM), along with test data which GM had measured for these tires (8.25-14) mounted on 14"-6JK wheels. Similar wheels were mounted on the test automobile so it would be equipped with wheels and tires matching those used for the tire test measurements.

Each test vehicle came equipped with a power steering system which was adapted to provide for two modes of steering, i.e., (1) normal manual steering or (2) an electronic command steer mode. For the latter method, a special hydraulic unit consisting of an electrohydraulic servo valve, solenoid operated flow control valves, pressure regulating valves, pressure gauge and associated hydraulic lines was installed in the engine compartment. When the electronic steer option was in use, hydraulic fluid from the vehicle power steering pump to the mechanical servo valve (actuated by the steering

wheel) was shut off and redirected to the electrohydraulic servo valve, which then controlled the flow of oil to the power steering actuator cylinder in response to electrical signals from the electronic guidance system. Measurement of the magnitude of the steer angle for closed-loop control was obtained by means of a position feedback potentiometer attached to the power steering actuator.

The electronic steer mode provided rapid and highly repeatable steering inputs. These steering inputs included sinusoidal steering in response to signals from a low frequency oscillator, step inputs and automatic tracking of a wire laid on the ground along the desired vehicle trajectory.

The use of an electrohydraulic servo valve required that the power steering pump be continuously operated against a high discharge pressure when the electronic guidance mode was selected. For this reason, this mode was used for only relatively short periods of time to avoid excessive heating of the hydraulic fluid and possible damage to the system components.

2.1.1.1 Vehicle Parameters

Identical values for the vehicle parameters were employed in all of the simulation runs. A tabulation of parameter values that were used to obtain the simulation responses is presented in Table 2.1-1. Also shown in the table are values measured by the Ford Motor Company for an identical automobile with 300 lbs. in the front seat to simulate a driver and passenger, but without the instrumentation installed (Reference 1). Values in the last column of the table are the "final best estimates" for the actual instrumented test vehicle based on (1) the Ford measured data corrected for the different weight and weight distribution, (2) Calspan measurements of the total vehicle weight (with passengers and instruments) and the weight on the front and rear wheels, and (3) certain available measured data for other makes of automobiles.

Table 2.1-1

TEST VEHICLE PARAMETER VALUES
1963 FORD GALAXIE FOUR-DOOR SEDAN

Parameter		1 Value Used in Simulation Comparisons	2 Measured Values of 2nd Car by Ford Motor Company	3 "Best Estimate" Values for Simulation
M_S	$(lb\text{-}sec^2)/in.$	10.818	10.218[1]	10.818
M_{uF}	$(lb\text{-}sec^2)/in.$	0.608	0.407[2]	0.608
M_{uR}	$(lb\text{-}sec^2)/in.$	0.945	0.845[3]	0.945
I_x	$lb\text{-}sec^2\text{-}in.$	6000.0	8742.5	6000.0
I_Y	$lb\text{-}sec^2\text{-}in.$	30000.0	36167.5	35477.0
I_Z	$lb\text{-}sec^2\text{-}in.$	36000.0	36406.3	35800.0
I_{XZ}	$lb\text{-}sec^2\text{-}in.$	-192.0	-439.8	-192.0
I_R	$lb\text{-}sec^2\text{-}in.$	600.0	435.6	435.6
a	in.	54.517	52.81	54.63
b	in.	64.483	66.44	64.62
T_F	in.	61.0	61.2	61.2
T_R	in.	60.0	60.5	60.5
T_S	in.	46.5	46.52	46.52
Z_F	in.	10.138	9.67	9.05
Z_R	in.	12.088	11.35	10.95
e	in.	-2.0	----	-2.0
R_W	in.	14, 15	----	14, 15
K_F	lb/in.	131.0	131.0	131.0
K_R	lb/in.	192.0	194.0	194.0
C_F	(lb-sec)/in.	3.50	1.30[4]	1.30
C_R	(lb-sec)/in.	3.90	1.75[4]	1.75
C'_F	lb	55.0	58.0[5]	58.0
C'_R	lb	50.0	97.0[5]	97.0
Ω_F	in.	3.0 (Jounce and Rebound)	2.9 Jounce 4.3 Rebound	3.0
Ω_R	in.	4.0 (Jounce and Rebound)	4.3 Jounce 4.5 Rebound	4.25

(Table 2.1-1 Continued)

Parameter	1 Values Used in Simulation Comparisons	2 Measured Values of 2nd Car by Ford Motor Company	3 "Best Estimate" Values for Simulation
R_F (lb-in)/rad	266000	266000(6)	266000
R_R (lb-in)/rad	61900	59244(7)	59244
K_{RS} ----	0.07	0.059	0.059
$\phi_1 = \phi_2$ deg for $\delta_1 = \delta_2$ = -5 in.	-3.55	-5.70(8)	-5.70
-4 in.	-2.55	-3.90(8)	-3.90
-3 in.	-1.80	-2.45	-2.45
-2 in.	-1.30	-1.30	-1.30
-1 in.	-0.95	-0.40	-0.40
0	-0.55	0.30	0.30
1 in.	-0.30	0.60	0.60
2 in.	-0.30	0.65	0.65
3 in.	-0.40	0.30	0.30
4 in.	-0.55	-0.40(8)	-0.40
5 in.	-0.80	-1.30(8)	-1.30

(1) Determined from measured weights of total vehicle (full fuel, 300 lb simulated passengers, no instrumentation) and unsprung masses.

(2) Front wheel and brake assemblies only. Does not include fractions of suspension arms, springs, shocks, steering knuckles, spindles, etc.

(3) Rear wheels, brake assemblies, drive shaft and axle assembly. Springs not included.

(4) From average slopes of shock absorber force vs. velocity data for jounce and rebound velocities between 20 and 55 in/sec and approximate installation ratio.

(5) From hysteresis loops of ride and roll rate measurements for each wheel and estimated average shock absorber "blow-off" force in jounce and rebound.

(6) From roll rate measurements with and without stabilizer bar.

(7) From measured average roll rate and theoretical roll rate computed from measured ride rate.

(8) Extrapolated from measured data.

Some of the measured data for the vehicle physical characteristics unfortunately became available too late to be used in the generation of predicted responses for comparison with the actual vehicle responses that were measured in the various tests. It was necessary, therefore, to estimate the values of those parameters for which specific data were lacking, the estimates being based on available data, both published and unpublished, from various sources (e.g., Reference 2).

From Table 2.1-1, it may be observed that most of the estimated values for the vehicle parameters used in obtaining the simulation results are very close to the "best estimate" values that are derived from the measured data shown in column 2 of the table. Also, where there are substantial differences between the original estimates (column 1) and the measured values (column 2), the latter have generally been accepted as "best estimate" values since the original estimates were, in some instances, based on rather meager data. Two exceptions, however, are the values measured for the roll moment of inertia, I_x, and the product of inertia, I_{xz}. For I_x, sufficient data were available from independent measurements of several other similar automobiles to indicate that the value measured by the Ford Motor Company (approximately 46% greater than the estimated value) is probably in error. The original estimate was, therefore, used as the "best estimate" value.

With regard to I_{xz}, it is to be noted that this parameter was not measured directly but rather was computed from

$$I_{xz} = \frac{I_K - I_x \sin^2\theta - I_z \cos^2\theta}{2 \sin\theta \cos\theta}$$

where I_K is the measured moment of inertia about a vertical axis through the sprung mass center of gravity with the vehicle in a pitched attitude of θ degrees. Inasmuch as I_{xz} so determined is dependent upon I_x, which as stated above is believed to be in error, the value of I_{xz} is

also likely to be erroneous. For this reason, despite the fact that not a large amount of data are available on which to base an estimate of a "typical" value for I_{xz}, the original estimate was retained as the "best estimate" value. Note also that a smaller value of I_x would result in closer agreement between the measured and estimated values for I_{xz}.

Unfortunately, Reference 1 does not include adequate descriptions of the test equipment and procedures to determine the cause of the assumed measurement error for I_x. In view of the fact that basically the same procedures and equipment were undoubtedly used for measurement of both I_x and I_y, and both are larger than the respective estimates for these parameters, it is possible that these tests included some type of systematic error in measurements.

Values of the tire parameters used in obtaining the presented simulation results are summarized in Table 2.1-2.

Table 2.1-2 TIRE PARAMETER DATA
8.25-14 Bias Ply Tire on 6K Rim

Parameter		Inflation Pressure
		28 psi
K_T	lb/in.	1098.0
σ_T	in.	3.0
λ_T		10.0
A_0		4400.0
A_1		8.276
A_2		2900.0
A_3		1.78
A_4		3900.0
Ω_T		1.00

A comparison of the mathematical representation of the tire characteristics with data measured by the General Motors Engineering Staff for the tires used in the tests is depicted in Figure 2.1-1. It may be seen that generally good agreement is achieved throughout the complete ranges of tire slip angle and vertical load for which data are available, and that the agreement is particularly good within the normal operating region. The fit to the experimental data could probably be improved by adjustment of the constants; however, the displayed fit is considered adequate for the present purposes.

2.1.1.2 Instrumentation

Extensive instrumentation was installed in the test vehicle to provide comprehensive and detailed measurements of the motions of the sprung mass and individual unsprung masses in each test. Specifically, provisions were made for recording (1) yaw, pitch and roll attitudes of the sprung mass, (2) longitudinal, lateral and vertical accelerations of the sprung mass at each of two locations, (3) suspension deflections at each of the four wheels, (4) steer angle of the front wheels and (5) vehicle speed. Most of this instrumentation and the associated power supplies, recording oscillograph and signal conditioning equipment were mounted on a rigid aluminum plate securely fastened in the rear of the passenger compartment from which the seat and seat back were removed. Photographs of some of the instrumentation installed in the vehicle are shown in Figure 2.1-2. Instrumentation characteristics are summarized in Table 2.1-3.

Attitude Measurements

A pair of two-degree-of-freedom, free gyroscopes were used to measure the yaw, pitch and roll angular displacements of the vehicle axes with respect to a space fixed reference axis system. Both gyros, together with a printed circuit board with solid state operational amplifiers and other miniaturized components for signal conditioning, were

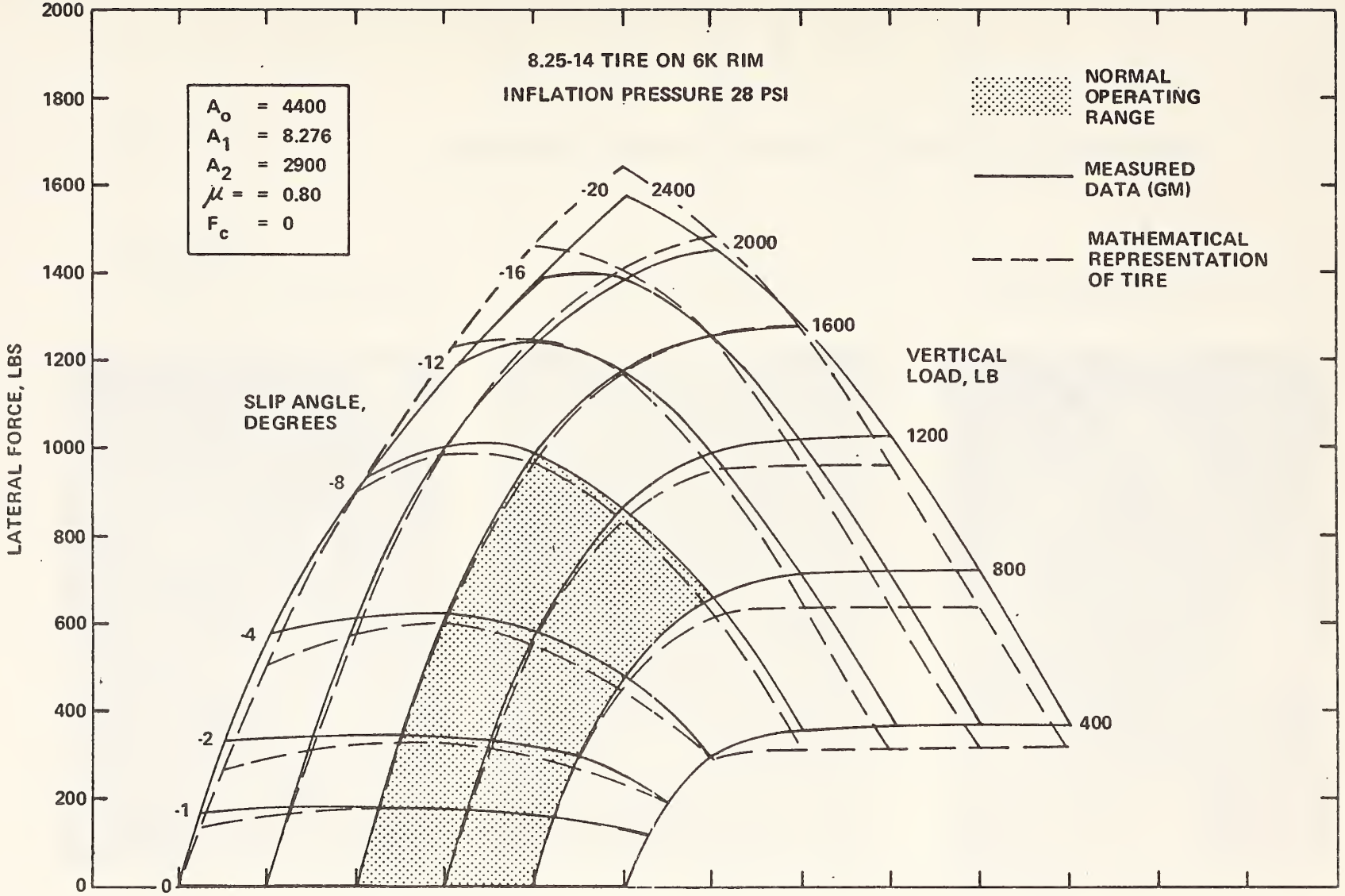

Figure 2.1-1 LATERAL FORCE VS. SLIP ANGLE AND VERTICAL LOAD

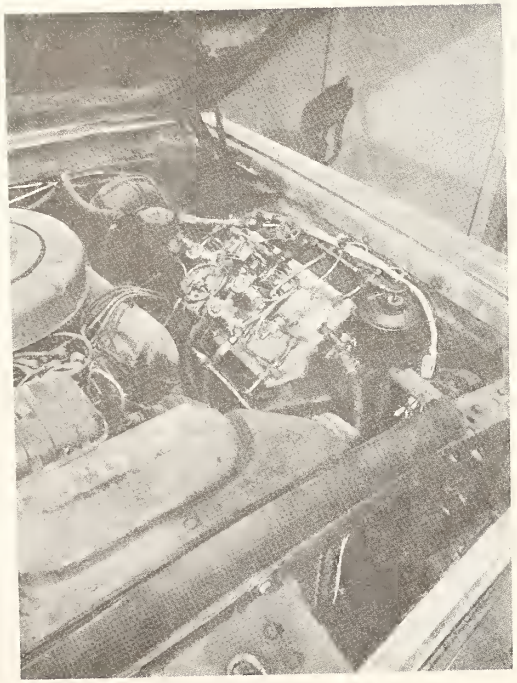

(a) AUTOMATIC STEERING SYSTEM HYDRAULIC PACKAGE IN ENGINE COMPARTMENT

(b) VIEW OF REAR PASSENGER COMPARTMENT AREA

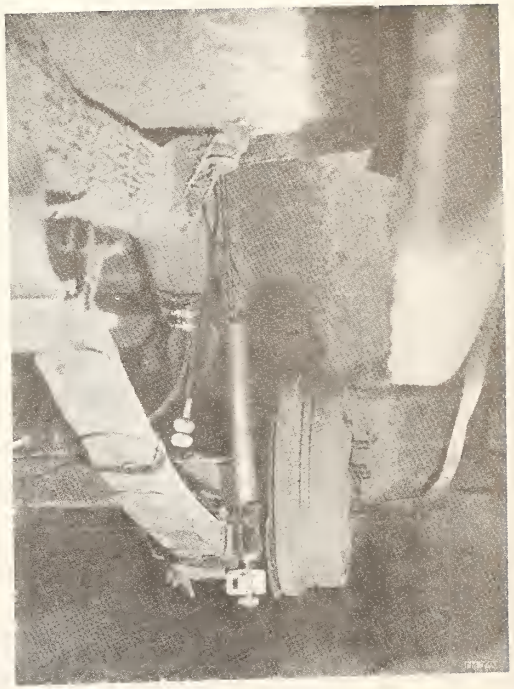

(c) REAR SUSPENSION DEFLECTION POTENTIOMETER

Figure 2.1-2 INSTRUMENTATION AND EQUIPMENT INSTALLED IN TEST VEHICLE

Table 2.1-3 SUMMARY OF INSTRUMENTATION TRANSDUCERS

Trace	Transducer
Pitch and roll attitude	Humphrey FG23-3101-1 free gyro pitch on inner gimbal, roll on outer gimbal
Yaw attitude	Humphrey FG23-3101-1 free gyro yaw on outer gimbal
Front wheel suspension deflections	Amphenol Borg Electronics Corp. 80962 linear potentiometers, 5" stroke, 2500 ohms
Rear wheel suspension deflections	Pacific Scientific 4101119-0 linear potentiometers, 10" stroke, 3000 ohms
Steer angle	Pacific Scientific 4101119-0 linear potentiometer, 10" stroke, 3000 ohms
Longitudinal acceleration	Pace CA19 DC-DC variable reluctance type accelerometers, ±5 G, flat within 5% 0-30 cps
Lateral acceleration	Palomar 5415 DC-DC variable reluctance type accelerometers, ±5 G, flat within 5% 0-30 cps
Vertical acceleration	Palomar 5414 (±5 G), Donner 5100-186F (±15 G), Donner 5100-228F (±20 G) DC-DC variable reluctance type accelerometers ±5 G flat within 5% 0-30 cps ±15 G flat within 5% 0-30 cps ±20 G flat within 5% 0-200 cps

Notes:

(1) Nexus USL-1 operational amplifiers used in each channel.

(2) All channels recorded Consolidated Electrodynamic Corp. oscillograph with CEC Type 7-315 galvanometers.

(3) All channels filtered with external filter having 15 cps corner frequency.

contained in a compact package and are capable of operating under an impact environment of 40 G. Special attention was given to their orientation so as to minimize "contamination" of the signals due to cross-coupling effects of combined motions. One gyro is used in a vertical mode (spin axis parallel to vehicle vertical or Z axis) with the inner gimbal (axis crosswise) measuring pitch and the outer gimbal measuring roll motions. The other gyro had its spin axis aligned parallel to the longitudinal axis of the vehicle and is used to measure heading, i.e., yaw, on the outer gimbal. With the gyros so oriented, the gimbal pickoff signals were direct measurements of the Euler angular coordinates of the sprung mass relative to the space-fixed axis system as defined in the computer simulation program, except for yaw. The "contamination" of the yaw signals is minor because of the small magnitudes of the pitching and rolling motions experienced in the tests but corrections were easily made in the process of reducing the test data.

Sprung Mass Accelerations

Linear accelerations of the vehicle along each of the three orthogonal vehicle-fixed axes were measured by two accelerometer packages; one package was located in the aft passenger compartment and the other at a rearmost location in the trunk of the vehicle. Each package consisted of three orthogonally mounted accelerometers with associated electronic circuits and encapsulated solid state operational amplifiers. Three separate accelerometers, instead of a single tri-axial accelerometer, were purposely employed in each package for the versatility and ease afforded in the interchangeability of accelerometers having ranges best suited to the acceleration magnitudes experienced for each test condition.

Suspension Deflections

Jounce and rebound deflections of each wheel of the vehicle from the static ride positions were measured by linear potentiometers attached between the sprung mass and a moving element of the suspension systems. A typical installation at one of the rear wheels is shown in the photographs of Figure 2.1-2. To guard against excessive rebound of the rear wheels, which had no travel stops other than the shock absorbers and so might damage the potentiometers by exceeding the limit of their available stroke, rebound of the rear axle was limited by cables attached between the rear axle and the frame of the vehicle as may be seen in the photograph. Since the cables permitted rebound deflections of approximately four inches, their effects on vehicle response are considered to have been negligible.

Front Wheel Steer Angle

Steer angles of the front wheels were measured by recording signals from a linear potentiometer attached to the hydraulic actuator of the vehicle power steering system.

Speed

Vehicle speed was measured, whenever possible, by means of a standard fifth-wheel trailed behind the vehicle, which produced a pulse signal for each revolution of the wheel. The speed at the start of each test maneuver was determined from the known distance traversed by the fifth wheel in one revolution and the timing lines recorded on the oscillograph record.

2.1.2 Data Acquisition and Reduction

A 14-channel light-beam oscillograph was used to record the amplified signals from each sensor and instrument. An attenuator unit was also provided to enable adjustment of the overall sensitivity of each data channel. Because of excessive undesirable high frequency noise which tended to obscure the significant characteristics of the oscillograph traces of the low g range accelerometers, the signals of every data channel were passed through filters having a roll-off frequency of approximately 15 cps. All channels were provided with identical filters to avoid phase shift errors that would be introduced if filters were employed in only some of the data channels.

Power for the various instrumentation equipment was supplied partly by the 12-volt electrical system of the vehicle and partly by two 24-Volt DC rechargeable battery power packs. Two converters (12 VDC to 24 VDC and 12 VDC to 110 VAC) were also necessary in the vehicle to provide the specific requirements of some of the equipment.

Controls and meters required for operating and monitoring the various instrumentation and control equipment were mounted on the dash panel convenient to the driver and instrumentation operator. These controls included switches and potentiometers for starting the oscillograph, applying calibration signals, caging and uncaging of the gyroscopes, transferring to the electronic steer mode, adjustment and application of steer input commands, etc.

2.1.3 Test Procedure

Because the purpose of the reported tests has been to provide a basis for a rigorous validation of the simulation model, it was important to determine the reliability of the actual measured responses. For this reason, reported test runs were conducted for each condition to establish the validity and repeatability of the actual measured responses of the vehicle with which the analytical results were to be compared.

Precautions were taken to minimize random errors that would contribute to the variability of the measured responses. For example, an attempt was made to conduct all runs in a test series with the vehicle on an identical approach path, at the same speed, and with the same steer input. In most cases, the tests were repeated five or six times, and three runs showing the best repeatability were selected for comparison with the predicted responses.

The general test procedure for all tests was to position the vehicle several hundred feet from the test area and, with the vehicle stationary, record the "zero reference" and "calibrate" signals of all data channels on the oscillograph record. The automobile was then accelerated to the desired test speed. During the constant speed approach to the test area, the instrumentation operator started the oscillograph recorder, uncaged the gyroscopes, and the electronic steering hydraulic system was also activated. The driver then closed a switch applying the external steering input commands when the vehicle reached a reference marker so that at time "zero", the vehicle would be, as closely as possible, at the same location for each test.

Two motion picture cameras, each operating at a nominal speed of 50 frames per second, were used for documentary photographic coverage of the vehicle responses for each test run.

A summary of the experimental program is presented in Table 2.1-4.

Two series of sinusoidal steering response tests were conducted. In one case (test series 3), the steering input was approximately $\pm$ 5 degrees amplitude at 0.5 cps; for the second (test series 9), the amplitude was increased to $\pm$ 10 degrees, and the frequency was increased to about 0.7 cps. The vehicle speed for both series of tests was nominally 25 MPH. To achieve repeatability of the time history of the steer angle, it was necessary to control the time, within a sinusoidal input cycle, when the steering

Table 2.1-4 SUMMARY OF SINUSOIDAL STEERING TEST PROGRAM

TEST CONDITION	NO. OF TESTS REPORTED	DESCRIPTION	NOMINAL SPEED	TEST SERIES NO.
SINUSOIDAL STEERING	3	±5 degrees of steer at 0.5 cycles per second	25 MPH	3
	3	±10 degrees of steer at 0.7 cycles per second	25 MPH	9

command signals were applied to the electrohydraulic servo control valve. This was done by employing a "trigger" circuit which applied the output of the sine wave generator to the servo valve when the voltage was zero and changing from negative to positive.

2.1.4 Comparison of Experimental and Predicted Results

Before discussing the comparisons of simulated and measured responses, a clarification of the inputs used for the computer simulations should be made. Because of unavoidable slight differences in the speed and the time history of the steer angle among the test runs shown in the comparisons, the average of the measured values for these parameters was used in the simulations. For the sinusoidal steer tests, "zero" time corresponded to the initiation of steering.

It was necessary to use estimated values for some of the physical characteristics of the vehicle in the presented response predictions. Actual measured data from tests performed by the Ford Motor Company did not become available until relatively late in the performance period of the reported research. Where specific data were lacking, the estimated values that were used represent "typical" data for automobiles as obtained from several published and unpublished reference sources. The HVOSM inputs used for this series of comparisons are shown in Figures 2.1-3 and 2.1-4.

The simulated and measured responses of the vehicle for the two series of sinusoidal steering tests are presented in Figures 2.1-5 and 2.1-6. Peak lateral acceleration for the lower frequency, smaller steer input tests was about 0.3 g, whereas for the other test series, accelerations somewhat greater than 0.4 g were experienced as measured by the accelerometer located in the passenger compartment. The distorted sine wave of the steer angle for the 0.4 g test (Figure 2.1-6) is believed to have been caused by fluid flow limitations of the electrohydraulic servo valve installed in the power steering system. With the exception of the yaw angle responses,

SINGLE VEHICLE ACCIDENT SIMULATION
RUN TEST 3 COMPARISON (0.5 CPS STEER)

```
    0.0     3.30     .010              .010     70.      0.0      0.0      0.0      1
   1.0                                                                             2
 10.818    .608     .945     386.4   6000.0   30000.   36000.    -192.     600.    3
 54.517  64.483     61.0      60.0    10.25    12.14     -2.0     14.0     4400.    4
   131.    25.0     3.50      3.50     55.0    0.001   266000.                      5
  192.0    25.0      4.0      3.90     50.0    0.001    61900.   46.50    0.070    6
 1098.0    3.00    10.00     8.276   2900.     1.78     0.80    0.750     3900.    7
    0.0     0.0      0.0       0.0      0.0      0.0      0.0      0.0              8
    0.0     0.0    -23.0     431.0      0.0      0.0                               9
    0.0     0.0      0.0       0.0      0.0      0.0      0.0      0.0              10
 -34.48     0.0      4.0   -112.48     -15.     -.5                               11
   -5.0     5.0      1.0                                                          12

PHIC(I),I=1,   11
   -3.550   -2.550   -1.800   -1.300   -0.950   -0.550   -0.300   -0.300   -0.400   -0.550   -0.800

    0.0      3.5      0.1      0.0      0.0      0.0                               13

PSIF(I),I=1,  36
    0.0     -1.624   -3.036   -4.250   -5.016   -5.240   -5.161   -4.567   -3.604   -2.244   -0.805    0.739    2.310
   3.854     4.818    5.240    5.240    4.778    3.907    2.746    1.333    0.0     -1.624   -3.023   -4.316   -5.029
  -5.227    -5.174   -4.409   -3.472   -2.165   -0.620    0.884    2.468    3.875    4.875

TOE(I),I=1,  36
    0.0      0.0      0.0      0.0      0.0      0.0      0.0      0.0      0.0      0.0      0.0      0.0      0.0
    0.0      0.0      0.0      0.0      0.0      0.0      0.0      0.0      0.0      0.0      0.0      0.0      0.0
    0.0      0.0      0.0      0.0      0.0      0.0      0.0      0.0      0.0      0.0

TCR(I),I=1,  36
    0.0      0.0      0.0      0.0      0.0      0.0      0.0      0.0      0.0      0.0      0.0      0.0      0.0
    0.0      0.0      0.0      0.0      0.0      0.0      0.0      0.0      0.0      0.0      0.0      0.0      0.0
    0.0      0.0      0.0      0.0      0.0      0.0      0.0      0.0      0.0      0.0

   0.0     -1.0      1.0      0.0     -1.0      1.0      1.0      1.0      0.0      14

XBDRY(I),I=1,  1          YBDRY(I),I=1,  1
 10000.000 10000.000

                                                                                   9999
```

Figure 2.1-3 INPUTS FOR TEST 3 SIMULATION

SINGLE VEHICLE ACCIDENT SIMULATION
RUN TEST 9 COMPARISON (0.7 CPS STEER)

```
     0.0     3.50     .010              .010      70.      0.0      0.0      0.0        1
  1.0                                                                                   2
 10.818    .608     .945     386.4   6000.0   30000.   36000.    -192.     600.       3
 54.517   64.483    61.0     60.0     10.25    12.14    -2.0      14.0     4400.       4
  131.     25.0     3.50     3.50     55.0    0.001   266000.                          5
  192.0    25.0     4.0      3.90     50.0    0.001   61900.   46.50    0.070         6
 1098.0     3.00    10.00    8.276    2900.    1.78     0.80    0.750    3900.       7
    0.0      0.0      0.0      0.0      0.0      0.0      0.0      0.0                 8
    0.0      0.0    -23.0     459.0     0.0      0.0                                  9
    0.0      0.0      0.0      0.0      0.0      0.0      0.0      0.0                10
 -34.48      0.0      4.0   -112.48    -16.     -.5                                   11
   -5.0      5.0      1.0                                                            12

PHIC(I),I=1,   11
   -3.550   -2.550   -1.800   -1.300   -0.950   -0.550   -0.300   -0.300   -0.400   -0.550   -0.800

    0.0      3.5      0.1      0.0      0.0      0.0                                 13

PSIF(I),I=1,  36
    0.0      2.000    4.700    7.950   11.400   10.950    6.950    1.700   -3.300   -5.900   -7.300   -8.800   -9.300
   -7.200   -3.550    1.400    6.200    9.200   10.700   10.700    8.200    5.000    1.000   -2.000   -5.600   -7.800
   -8.600   -7.200   -4.600   -1.100    2.200    5.200    8.500   10.200    8.600    5.700

TQF(I),I=1,   36
    0.0      0.0      0.0      0.0      0.0      0.0      0.0      0.0      0.0      0.0      0.0      0.0      0.0
    0.0      0.0      0.0      0.0      0.0      0.0      0.0      0.0      0.0      0.0      0.0      0.0      0.0
    0.0      0.0      0.0      0.0      0.0      0.0      0.0      0.0      0.0      0.0

TQR(I),I=1,   36
    0.0      0.0      0.0      0.0      0.0      0.0      0.0      0.0      0.0      0.0      0.0      0.0      0.0
    0.0      0.0      0.0      0.0      0.0      0.0      0.0      0.0      0.0      0.0      0.0      0.0      0.0
    0.0      0.0      0.0      0.0      0.0      0.0      0.0      0.0      0.0      0.0

  0.0     -1.0      1.0      0.0     -1.0      1.0      1.0      1.0      0.0        14

XBDRY(I),I=1,   1          YBDRY(I),I=1,   1
 10000.000 10000.000

                                                                   9999
```

Figure 2.1-4 **INPUTS FOR TEST 9 SIMULATION**

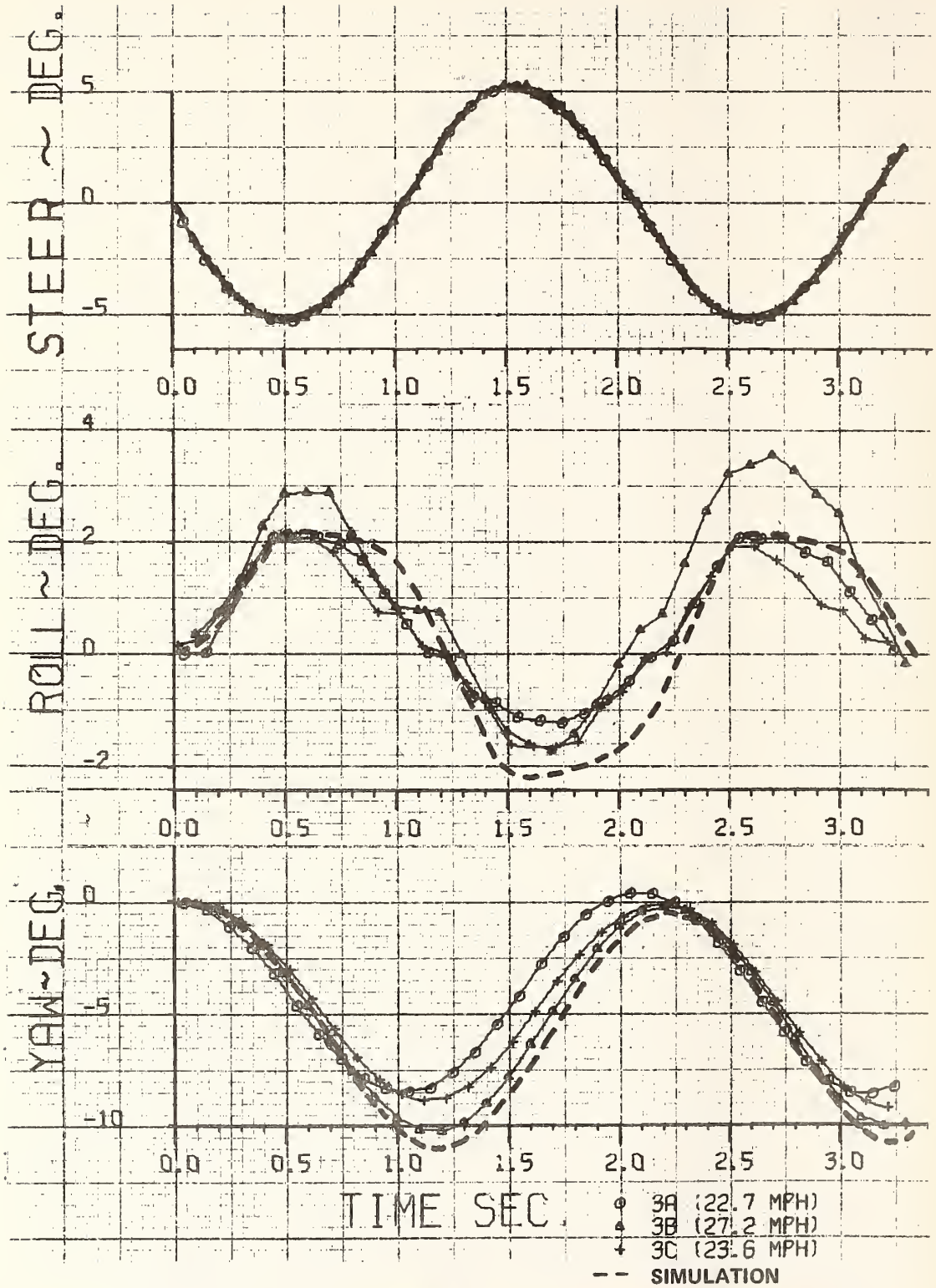

Figure 2.1-5 **MEASURED AND SIMULATED RESPONSES OF VEHICLE WITH ±5° — 0.5 CPS STEER**

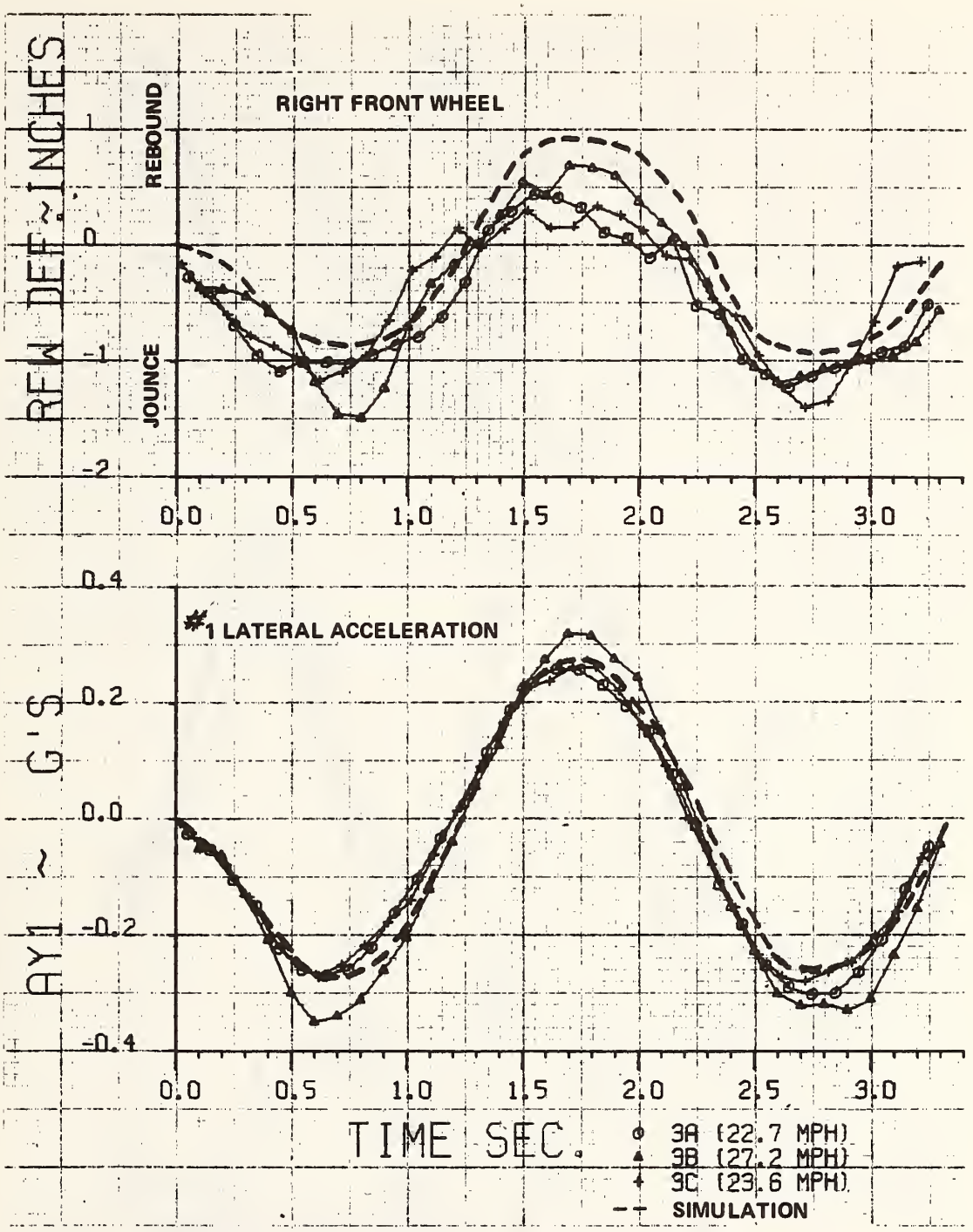

Figure 2.1-5 **MEASURED AND SIMULATED RESPONSES OF VEHICLE WITH ±5° – 0.5 CPS STEER (Continued)**

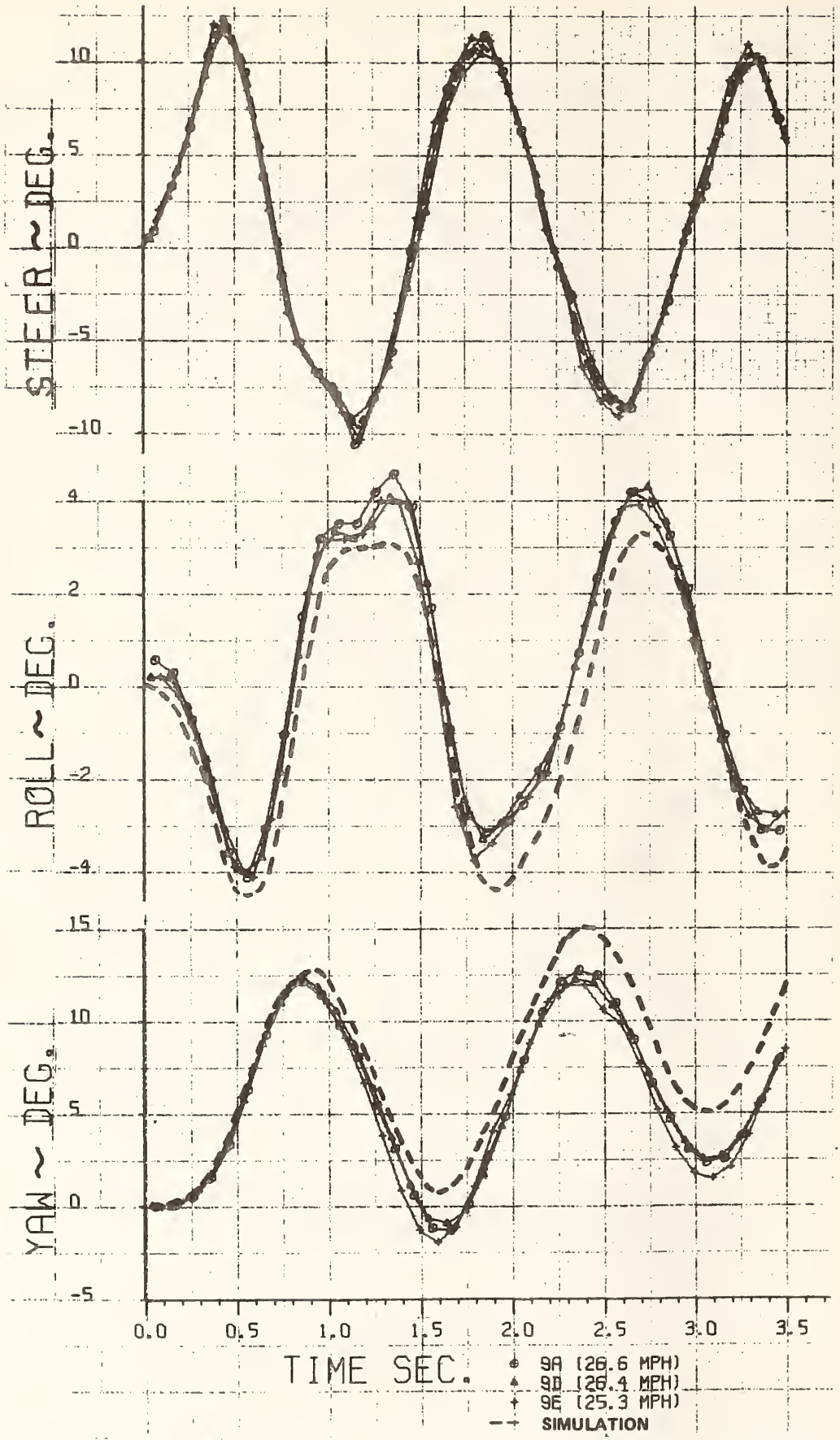

Figure 2.1-6 **MEASURED AND SIMULATED RESPONSES OF VEHICLE WITH ±10° — 0.7 CPS STEER**

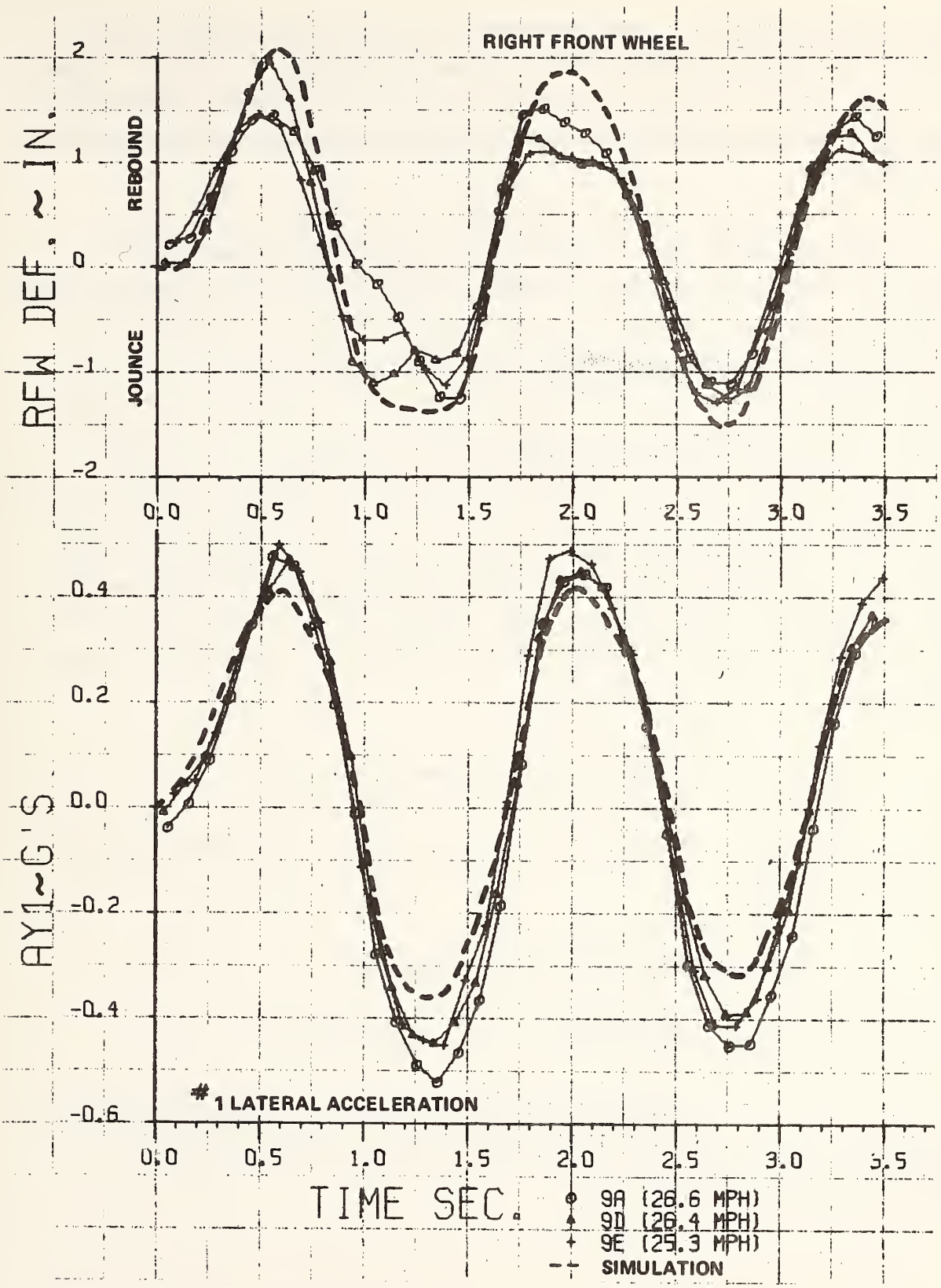

Figure 2.1-6 **MEASURED AND SIMULATED RESPONSES OF VEHICLE WITH ±10° — 0.7 CPS STEER (Continued)**

particularly for the 0.4-g test, the simulated vehicle responses correlate well with the measured data, which were quite repeatable. The deviations in the test results are probably largely due to differences in vehicle speed among the tests in each series which, for the 0.3-g tests, was as much as 4.5 MPH.

Both the phase and the peak-to-peak amplitude changes of the simulated vehicle yaw oscillations are in agreement with the measured data, but the predicted yaw response of the simulated vehicle is slightly more divergent than the measured vehicle response of the vehicle for the 0.4-g case. Factors that may have caused this deviation include: unequal steer angles of the test vehicle front wheels which, combined with the large lateral weight transfer that occurred in the tests, could have acted to produce cornering forces at the individual wheels significantly different from those of the simulated vehicle, in which the steer angles of the front wheels are assumed to be equal; roll steer effects in the front suspension which are neglected in the simulation; a slight bias of the steer angle, i.e., "zero" steer on the test record may have actually corresponded to a small steer angle.

2.1.5 Vehicle Response Sensitivity

No vehicle response sensitivity runs were made for this test series.

2.2 Ramp Traversal Tests HVOSM-SMI1

2.2.1 Test Vehicle and Instrumentation

The vehicle and instrumentation packages employed in the ramp test series were identical to those reported in Section 2.1.1 with the following exceptions.

Two of the ramp test series were made with 15" tires inflated to 65 psig. The tire parameters used to model these tires is shown in Table 2.2-1 and were based on extrapolations from meager data on the effects of small changes in inflation pressure on tire lateral force properties.

In addition, the fifth wheel was removed in the two higher speed tests to avoid possible damage. For these tests, the vehicle speed was obtained from either the vehicle speedometer or from photographic reduction.

2.2.2 Data Acquisition and Reduction

Data acquisition and reduction for this test series was identical to that reported in Section 2.1.2.

Table 2.2-1 TIRE PARAMETER DATA
8.25x14 Bias Ply Tire on 6K Rim

Parameter		Inflation Pressure 65 psi
K_T	lb/in.	2200.0
σ_T	in.	3.0
λ_T		10.0
A_0		11500.0
A_1		7.53
A_2		4000.0
A_3		3.47
A_4		5400.0
Ω_T		1.00

2.2.3 Test Procedure

Vehicle responses during traversal of ramps were measured for five different conditions as summarized in Table 2.2-2. In the first series (tests 5), the automobile was driven straight with all four wheels passing over the ramp. The ramp, of plywood construction, had a slope of 7.1 degrees and was 6.75 inches high at the rear edge. For the second series of tests (tests 6), the ramp height was increased to 8.5 inches (9.2 degree slope), but only the wheels on the left side of the automobile traversed the ramp to induce some rolling response. The ramp for the third series of tests (tests 7) was the same as for the first case, but this time a step input of steer angle of about 6 degrees was applied when the vehicle was approximately 20 feet from the ramp. Thus, the vehicle was undergoing a transient cornering maneuver of about 0.4 g as it traversed the ramp, with each wheel subsequently becoming airborne and striking the ground surface at different times upon passing over the elevated rear edge of the ramp. The first three series of ramp tests were each performed at a nominal speed of 25 MPH.

For the last two series of ramp traversal tests, the services of professional stunt drivers were obtained. In the first of these (tests 13), the vehicle was alternately driven over two ramps; the wheels on the right side of the car traversing the first ramp and the left-side wheels passing over the second ramp, which began about 63 feet further down the roadway. Each ramp was 21.5 inches high at the rear edge (3.6 degree slope) and hence, produced a considerable amount of vehicle roll in each direction. The driver attempted to maintain a constant speed of 30 MPH throughout each test and found it necessary to introduce substantial steering inputs to align the vehicle for proper traversal of the second ramp.

Table 2.2-2 SUMMARY OF EXPERIMENTAL PROGRAM

TEST CONDITION	NO. OF TESTS REPORTED	DESCRIPTION	NOMINAL SPEED	TEST SERIES NO.
RAMP TRAVERSAL	3	Four wheels over 7.1 degree, 6.75 inch high ramp	25 MPH	5
	3	Two left wheels over 9.2 degree, 8.5 inch high ramp	25 MPH	6
	3	Step input of 6 degree steer, 20 feet ahead of ramp. Four wheels over 7.1 degree, 6.75 inch high ramp	25 MPH	7
	2	Right and left wheels alternately over 3.6 degree, 21.5 inch high ramps	30 MPH	13
	1	Four wheels over 3.5 ft. high "takeoff" ramp	44 MPH	14

The fifth ramp test (test 14) was one in which the vehicle was driven over a 3.5 ft. high "takeoff" ramp and became completely airborne for a distance of approximately 65 feet. The landing was to have been made on a downward sloping "receiving" ramp. However, because the driver was apprehensive about the use of an unfamiliar vehicle and wanted to reduce the risks of falling short and crashing into the elevated end of the receiving ramp, he elected to perform the jump at a speed of 44 MPH, which was about 4 MPH greater than the speed he normally would employ. Unfortunately, the increased speed was excessive, causing the vehicle to overshoot the receiving ramp. The landing was, therefore, unintentionally hard, with the front end of the automobile (and subsequently the aft end of the sprung mass) striking the roadway with a force sufficient to bend the frame and body. Except for bending of the shafts of each of the suspension deflection potentiometers, the instrumentation equipment was undamaged and good oscillograph data records were obtained up to the time of impact with the ground.

2.2.4 Comparison of Predicted and Experimental Results

HVOSM input data used for comparisons with this test series are shown in Figures 2.2-1 through 2.2-6. Time histories of the measured and simulated vehicle responses for the first three conditions of ramp traversal are displayed in Figures 2.2-7, 2.2-8 and 2.2-9, respectively. The excellent repeatability of the measured data in each of these three cases adds confidence to the validity of the measurements. The final two conditions of ramp traversals were performed using skilled stunt drivers under conditions that made the control and measurement of repeatability more difficult.

SINGLE VEHICLE ACCIDENT SIMULATION
RUN TEST 5 COMPARISON

```
     0.0     2.20     .005                .010     70.     0.0     0.0     0.0      1
  1.0                                                                               2
10.818     .608     .945     396.4   6000.0   30000.   36000.   -192.    600.     3
54.517   64.483    61.0     60.0    10.138   12.038    -2.1     14.0    4400.     4
  131.     25.0     3.00     3.50    55.0     0.001   266000.                     5
192.0      25.0     4.0      3.90    50.0     0.001   61900.   46.50   0.070      6
1098.0     3.00    10.00     8.276   2900.    1.72     0.90    0.750   3900.      7
   0.0      0.0      0.0      0.0     0.0      0.0      0.0     0.0               8
-188.0      0.0    -23.0     447.0    0.0      0.0                                9
   0.0      0.0      0.0      0.0     0.0      0.0      0.0     0.0              10
-34.48      0.0      4.0    -112.48  -16.      -.5                               11
  -5.0      5.0      1.0                                                        12

PHIC(I),I=1,    11
  -3.550   -2.550   -1.800   -1.300   -0.950   -0.550   -0.300   -3.300   -3.400   -0.550   -3.100

   0.0      4.0      1.0      0.0      0.0      0.0                              13

PSIF(I),I=1,    5
   0.0      0.0      0.0      0.0      0.0

TCF(I),I=1,     5
   0.0      0.0      0.0      0.0      0.0

TCR(I),I=1,     5
   0.0      0.0      0.0      0.0      0.0

 -48.0      0.0      0.0    -96.0     96.0     96.0     2.0      2.0      2.0      14

XROBY(I),I=1,   2          YROBY(I),I=1,   2
 -48.000     0.0      -96.000   96.000

     1        2
ZRG
-0.75000  -1.75000  -2.75000  -3.75000  -4.75000  -5.75000  -6.75000
-0.75000  -1.75000  -2.75000  -3.75000  -4.75000  -5.75000  -6.75000
-0.75000  -1.75000  -2.75000  -3.75000  -4.75000  -5.75000  -6.75000

THG
 0.12435   0.12435   0.12435   0.12435   0.12435   0.12435   0.12435
 0.12435   0.12435   0.12435   0.12435   0.12435   0.12435   0.12435
 0.12435   0.12435   0.12435   0.12435   0.12435   0.12435   0.12435
```

Figure 2.2-1 INPUTS FOR TEST 5 SIMULATION

```
     0.0     2.20     .005              .010      70.      0.0      0.0      0.0        1
    1.0                                                                               2
   10.818    .608    .945     386.4   6000.0   30000.   36000.    -192.     600.     3
   54.517  64.483    61.0      60.0    10.138   12.038    -2.0     14.0     4400.     4
    131.     25.0     3.00      3.50    55.0    0.001   266000.                       5
    192.0    25.0     4.0       3.90    50.0    0.001    61900.  46.50    0.070      6
   1098.0     3.00    10.00     8.276  2900.     1.78     0.80    0.750    3900.     7
      0.0      0.0      0.0       0.0     0.0      0.0      0.0      0.0              8
   -187.0    108.0    -23.0     438.0     0.0      0.0                               9
    0.0      0.0      0.0       0.0     0.0      0.0      0.0      0.0              10
   -34.48    0.0      4.0     -112.48  -16.     -.5                                 11
   -5.0      5.0      1.0                                                           12

PHIC(I),I=1,    11
    -3.550    -2.550    -1.800    -1.300    -0.950    -0.550    -0.300    -0.300    -0.400    -0.550    -0.900

      0.0      4.0      1.0       0.0       0.0       0.0                           13

PSIF(I),I=1,    5
      0.0       0.0       0.0       0.0       0.0

TQF(I),I=1,     5
      0.0       0.0       0.0       0.0       0.0

TQR(I),I=1,     5
      0.0       0.0       0.0       0.0       0.0

   -48.0    0.0      8.0     -96.0     96.0     96.0     2.0      2.0      2.0       14

XBDRY(I),I=1,   2          YBDRY(I),I=1,   2
   -48.000    0.0     -96.000    96.000

      1        2
ZPG
    -0.75000   -2.04167   -3.33334   -4.62501   -5.91668   -7.20835   -8.50002
    -0.75000   -2.04167   -3.33334   -4.62501   -5.91668   -7.20835   -8.50002
    -0.75000   -2.04167   -3.33334   -4.62501   -5.91668   -7.20835   -8.50002

THG
     0.16008    0.16008    0.16008    0.16008    0.16008    0.16008    0.16008
     0.16008    0.16008    0.16008    0.16008    0.16008    0.16008    0.16008
     0.16008    0.16008    0.16008    0.16008    0.16008    0.16008    0.16008

                                                                                  9999
```

Figure 2.2-2 **INPUTS FOR TEST 6 SIMULATION**

```
   0.0    2.50    .005          .010    70.     0.0     0.0     0.0     1
-443.0    48.0   -23.0   442.0   0.0     0.0                             2
   0.0     2.5     0.1     0.0   0.0     0.0                            13

PSIF(I),I=1,  26
   0.0     0.0    -0.600  -2.450  -5.000  -6.200  -6.200  -6.100  -6.000  -6.000  -6.000  -6.000  -6.000
  -6.000  -6.000  -6.000  -6.000  -6.000  -6.000  -6.000  -6.000  -6.000  -6.000  -6.000  -6.000  -6.000

TQF(I),I=1,  26
   0.0     0.0     0.0     0.0     0.0     0.0     0.0     0.0     0.0     0.0     0.0     0.0     0.0
   0.0     0.0     0.0     0.0     0.0     0.0     0.0     0.0     0.0     0.0     0.0     0.0     0.0

TQR(I),I=1,  26
   0.0     0.0     0.0     0.0     0.0     0.0     0.0     0.0     0.0     0.0     0.0     0.0     0.0
   0.0     0.0     0.0     0.0     0.0     0.0     0.0     0.0     0.0     0.0     0.0     0.0     0.0

-48.0   0.0     8.0    -96.0    96.0    96.0    2.0     2.0     2.0    14

XBDRY(I),I=1,  2          YBDRY(I),I=1,  2
  -48.000    0.0        -96.000    96.000

    1       2
ZPG
  -0.75000  -1.75000  -2.75000  -3.75000  -4.75000  -5.75000  -6.75000
  -0.75000  -1.75000  -2.75000  -3.75000  -4.75000  -5.75000  -6.75000
  -0.75000  -1.75000  -2.75000  -3.75000  -4.75000  -5.75000  -6.75000

THG
   0.12435   0.12435   0.12435   0.12435   0.12435   0.12435   0.12435
   0.12435   0.12435   0.12435   0.12435   0.12435   0.12435   0.12435
   0.12435   0.12435   0.12435   0.12435   0.12435   0.12435   0.12435

9999
```

Note: Other inputs same as for Test 6 simulation

Figure 2.2-3 **INPUTS FOR TEST 7 SIMULATION**

SINGLE VEHICLE ACCIDENT SIMULATION
RUN TEST 13A COMPARISON (ALTERNATE RAMPS)

```
  0.0     5.0     0.005              .010      70.0      0.0      0.0      0.0          1
  1.0                                                                                  2
 10.818  0.608    0.945    386.4     6000.    30000.    36000.   -192.     600.        3
 54.517 64.483   61.       60.      10.138   12.088    -2.0     15.      11500.       4
131.0   25.0     3.0       3.5      55.0      0.001   266000.0                        5
192.0   25.0     4.0       3.9      50.0      0.001    61900.0 46.50    0.070        6
2200.    3.00   10.00     7.53     4000.     3.47       0.800      1.00 5400.        7
  0.0     0.0    -2.0      0.0       0.0      0.0        0.0       0.0               8
-55.0     0.0   -24.57   528.0       0.0      0.0                                    9
  0.0     0.0     0.0      0.0       0.0      0.0        0.0       0.0               10
-34.48    0.0     4.0    -112.48   -16.0     -0.5                                   11
 -5.0     5.0     1.0                                                               12

PHIC(I),I=1,   11
   -3.550   -2.550   -1.800   -1.300   -0.950   -0.550   -0.300   -0.300   -0.400   -0.550   -0.800


  0.0     4.9     0.1     0.0     0.0     0.0                                        13

PSIF(I),I=1,  50
     0.0      0.900    0.500    1.250    1.800    1.900    2.000    1.500    1.200    1.450    1.400    1.000   -0.500
    -0.100    1.000    1.900    1.250    0.950    1.050    1.000    0.0     -2.500   -2.100   -3.700   -4.000   -3.900
    -3.750   -3.400   -2.500   -2.000   -0.500    1.100    1.800    1.800    1.500    1.500    1.800    2.400    3.350
     3.500    2.950    2.300    2.000    1.800    1.600    1.500    1.450    1.350    1.150    0.950


TQF(I),I=1,   50
     0.0      0.0      0.0      0.0      0.0      0.0      0.0      0.0      0.0      0.0      0.0      0.0      0.0
     0.0      0.0      0.0      0.0      0.0      0.0      0.0      0.0      0.0      0.0      0.0      0.0      0.0
     0.0      0.0      0.0      0.0      0.0      0.0      0.0      0.0      0.0      0.0      0.0      0.0      0.0
     0.0      0.0      0.0      0.0      0.0      0.0      0.0      0.0      0.0      0.0      0.0


TQR(I),I=1,   50
     0.0      0.0      0.0      0.0      0.0      0.0      0.0      0.0      0.0      0.0      0.0      0.0      0.0
     0.0      0.0      0.0      0.0      0.0      0.0      0.0      0.0      0.0      0.0      0.0      0.0      0.0
     0.0      0.0      0.0      0.0      0.0      0.0      0.0      0.0      0.0      0.0      0.0      0.0      0.0
     0.0      0.0      0.0      0.0      0.0      0.0      0.0      0.0      0.0      0.0      0.0


  0.0    1950.    150.    -54.    36.     18.      4.      2.      2.          14

XBDRY(I),I=1,  4          YBDRY(I),I=1,  2
     0.0      325.000  1079.000  1403.000   -24.000    12.000


    1     2
ZPG
     0.0       0.0       0.0       0.0       0.0       0.0       0.0
     0.0      -8.70000 -18.26999   0.0       0.0       0.0       0.0
     0.0       0.0       0.0       0.0       0.0       0.0       0.0
     0.0      -8.70000 -18.26999   0.0       0.0       0.0       0.0
     0.0       0.0       0.0       0.0       0.0       0.0       0.0
     0.0       0.0       0.0       0.0       0.0       0.0       0.0
     0.0       0.0       0.0       0.0       0.0       0.0       0.0
     0.0       0.0       0.0       0.0       0.0       0.0       0.0
```

Figure 2.2-4 **INPUTS FOR TEST 13a SIMULATION**

```
      -1.00000  -10.57000  -20.12999   0.0   0.0   0.0   0.0
       0.0        0.0        0.0      0.0   0.0   0.0   0.0
      -1.00000  -10.57000  -20.12999   0.0   0.0   0.0   0.0
       0.0        0.0        0.0      0.0   0.0   0.0   0.0

 THG
       0.0        0.0        0.0      0.0   0.0   0.0   0.0
       0.0        0.06299    0.06299  0.0   0.0   0.0   0.0
       0.0        0.0        0.0      0.0   0.0   0.0   0.0
       0.0        0.06299    0.06299  0.0   0.0   0.0   0.0
       0.0        0.0        0.0      0.0   0.0   0.0   0.0
       0.0        0.0        0.0      0.0   0.0   0.0   0.0
       0.0        0.0        0.0      0.0   0.0   0.0   0.0
       0.0        0.0        0.0      0.0   0.0   0.0   0.0
       0.06299    0.06299    0.06299  0.0   0.0   0.0   0.0
       0.0        0.0        0.0      0.0   0.0   0.0   0.0
       0.06299    0.06299    0.06299  0.0   0.0   0.0   0.0
       0.0        0.0        0.0      0.0   0.0   0.0   0.0

                                                          9999
```

Figure 2.2-4 (Continued)

```
  0.0      5.0     0.005              .010      70.0      0.0      0.0      0.0        1
  1.0                                                                                 2
 10.818  0.608    0.945    386.4    6000.    30000.    36000.   -192.     600.       3
 54.517 64.483    61.      60.      10.138   12.088    -2.0      15.    11500.       4
131.0   25.0      3.0      3.5      55.0      0.001  266000.0                        5
192.0   25.0      4.0      3.9      50.0      0.001   61900.0  46.50    0.070       6
2200.    3.00    10.00    7.53     4000.     3.47       0.800    1.00  5400.       7
  0.0    0.0     -2.0      0.0      0.0       0.0       0.0      0.0                 8
-55.0    0.0    -24.57   498.0      0.0       0.0                                   9
  0.0    0.0      0.0      0.0      0.0       0.0       0.0      0.0                10
-34.48   0.0      4.0    -112.48   -16.0     -0.5                                  11
 -5.0    5.0      1.0                                                              12

PHIC(I),I=1,   11
    -3.550    -2.550    -1.800    -1.300    -0.950    -0.550    -0.300    -0.300    -0.400    -0.550    -0.800

  0.0      4.9      0.1      0.0      0.0       0.0                                 13

PSIF(I),I=1,   50
      0.0       1.000     0.800     1.150     1.600     2.200     2.650     3.050     2.600     2.300     1.000     0.300    -1.400
     -2.800    -2.500    -1.300    -0.700    -0.550    -0.200     1.500     3.700     3.200     2.200     0.500    -0.800    -2.800
     -4.000    -4.450    -4.600    -4.550    -3.900    -2.450    -0.300     1.200     2.100     2.200     3.000     2.900     2.550
      2.900     3.100     3.300     3.300     3.300     3.300     3.250     3.000     2.750     2.350     2.050

TQF(I),I=1,   50
      0.0       0.0       0.0       0.0       0.0       0.0       0.0       0.0       0.0       0.0       0.0       0.0       0.0
      0.0       0.0       0.0       0.0       0.0       0.0       0.0       0.0       0.0       0.0       0.0       0.0       0.0
      0.0       0.0       0.0       0.0       0.0       0.0       0.0       0.0       0.0       0.0       0.0       0.0       0.0
      0.0       0.0       0.0       0.0       0.0       0.0       0.0       0.0       0.0       0.0       0.0

TQR(I),I=1,   50
      0.0       0.0       0.0       0.0       0.0       0.0       0.0       0.0       0.0       0.0       0.0       0.0       0.0
      0.0       0.0       0.0       0.0       0.0       0.0       0.0       0.0       0.0       0.0       0.0       0.0       0.0
      0.0       0.0       0.0       0.0       0.0       0.0       0.0       0.0       0.0       0.0       0.0       0.0       0.0
      0.0       0.0       0.0       0.0       0.0       0.0       0.0       0.0       0.0       0.0       0.0

  0.0    1950.    150.    -54.    36.      18.       4.      2.       2.            14

XBORY(I),I=1,  4          YBORY(I),I=1,  2
      0.0      325.000  1078.000  1403.000   -24.000    12.000

    1        2
ZPG
      0.0        0.0        0.0        0.0        0.0        0.0        0.0
      0.0       -8.70000  -18.26999   0.0        0.0        0.0        0.0
      0.0        0.0        0.0        0.0        0.0        0.0        0.0
      0.0       -8.70000  -18.26999   0.0        0.0        0.0        0.0
      0.0        0.0        0.0        0.0        0.0        0.0        0.0
      0.0        0.0        0.0        0.0        0.0        0.0        0.0
      0.0        0.0        0.0        0.0        0.0        0.0        0.0
      0.0        0.0        0.0        0.0        0.0        0.0        0.0
```

Figure 2.2-5 **INPUTS FOR TEST 13b SIMULATION**

SINGLE VEHICLE ACCIDENT SIMULATION
RUN TEST 13B COMPARISON (ALTERNATE RAMPS) CONTINUED

-1.00000	-10.57000	-20.12999	0.0	0.0	0.0	0.0
0.0	0.0	0.0	0.0	0.0	0.0	0.0
-1.00000	-10.57000	-20.12999	0.0	0.0	0.0	0.0
0.0	0.0	0.0	0.0	0.0	0.0	0.0

THG

0.0	0.0	0.0	0.0	0.0	0.0	0.0
0.0	0.06299	0.06299	0.0	0.0	0.0	0.0
0.0	0.0	0.0	0.0	0.0	0.0	0.0
0.0	0.06299	0.06299	0.0	0.0	0.0	0.0
0.0	0.0	0.0	0.0	0.0	0.0	0.0
0.0	0.0	0.0	0.0	0.0	0.0	0.0
0.0	0.0	0.0	0.0	0.0	0.0	0.0
0.0	0.0	0.0	0.0	0.0	0.0	0.0
0.06299	0.06299	0.06299	0.0	0.0	0.0	0.0
0.0	0.0	0.0	0.0	0.0	0.0	0.0
0.06299	0.06299	0.06299	0.0	0.0	0.0	0.0
0.0	0.0	0.0	0.0	0.0	0.0	0.0

9999

2-5

SINGLE VEHICLE ACCIDENT SIMULATION
RUN TEST 14 COMPARISON (RAMP JUMP)

```
  0.0     4.0    0.005              .010     70.0     0.0      0.0      0.0          1
  1.0                                                                                2
 10.818 0.608   0.945    386.4    6000.    30000.  36000.  -192.    600.             3
 54.517 64.483  61.      60.      10.138   12.088  -2.0     15.     4400.            4
 131.0  25.0    3.0      3.5      55.0     0.001   266000.0                          5
 192.0   25.0    4.0      3.9      50.0     0.001   61900.0 46.50    0.070           6
 2200.    3.00    10.00  8.276    2900.0    1.780  0.800     1.00   3900.0           7
  0.0     0.0      0.0   0.0       0.0      0.0     0.0      0.0                     8
 -70.0   0.0     -24.57  774.0     0.0      0.0                                      9
  0.0     0.0     0.0     0.0      0.0      0.0     0.0      0.0                     10
 -34.48  0.0     4.0     -112.48  -16.0   -0.5                                       11
  -5.0    5.0     1.0                                                                12

 PHIC(I),I=1,    11
     -3.550    -2.550    -1.800    -1.300    -0.950    -0.550    -0.300    -0.300    -0.400    -0.550    -0.800

  0.0     4.0     1.0     0.0     0.0     0.0                                        13

 PSIF(I),I=1,    5
      0.0       0.0       0.0       0.0       0.0

 TQF(I),I=1,     5
      0.0       0.0       0.0       0.0       0.0

 TQR(I),I=1,     5
      0.0       0.0       0.0       0.0       0.0

  0.0    1200.    60.    -100.    100.    100.     7.      2.     2.0               14

 XBDRY(I),I=1,   7               YBDRY(I),I=1,   2
      0.0      180.000    321.000    750.000    897.000  1039.000  1182.500  -100.000   100.000

       1      2
 ZPG
       -1.00000   -5.33330   -9.66660  -14.00000  -26.01599  -38.78189    0.0
        0.0        0.0        0.0        0.0        0.0        0.0      -46.00000
      -46.00000  -44.20599  -33.32570  -22.44539  -12.28570   -7.58200    0.0
       -1.00000   -5.33330   -9.66660  -14.00000  -26.01599  -38.78189    0.0
        0.0        0.0        0.0        0.0        0.0        0.0      -46.00000
      -46.00000  -44.20599  -33.32570  -22.44539  -12.28570   -7.58200    0.0
       -1.00000   -5.33330   -9.66660  -14.00000  -26.01599  -38.78189    0.0
        0.0        0.0        0.0        0.0        0.0        0.0      -46.00000
      -46.00000  -44.20599  -33.32570  -22.44539  -12.28570   -7.58200    0.0

 THG
        0.07210    0.07210    0.07210    0.07210    0.20964    0.20964    0.0
        0.0        0.0        0.0        0.0        0.0        0.0        0.0
        0.0       -0.17939   -0.17939   -0.17939   -0.07824   -0.07824    0.0
        0.07210    0.07210    0.07210    0.07210    0.20964    0.20964    0.0
        0.0        0.0        0.0        0.0        0.0        0.0        0.0
```

Figure 2.2-6 INPUTS FOR TEST 14 SIMULATION

SINGLE VEHICLE ACCIDENT SIMULATION
RUN TEST 14 COMPARISON [illegible] (RAMP JUMP) CONTINUED

```
  0.0       -0.17939   -0.17939   -0.17939   -0.07824   -0.07824    0.0
  0.07210    0.07210    0.07210    0.07210    0.20964    0.20964    0.0
  0.0        0.0        0.0        0.0        0.0        0.0        0.0
  0.0       -0.17939   -0.17939   -0.17939   -0.07824   -0.07824    0.0

9999
```

Figure 2.2-6 (Continued)

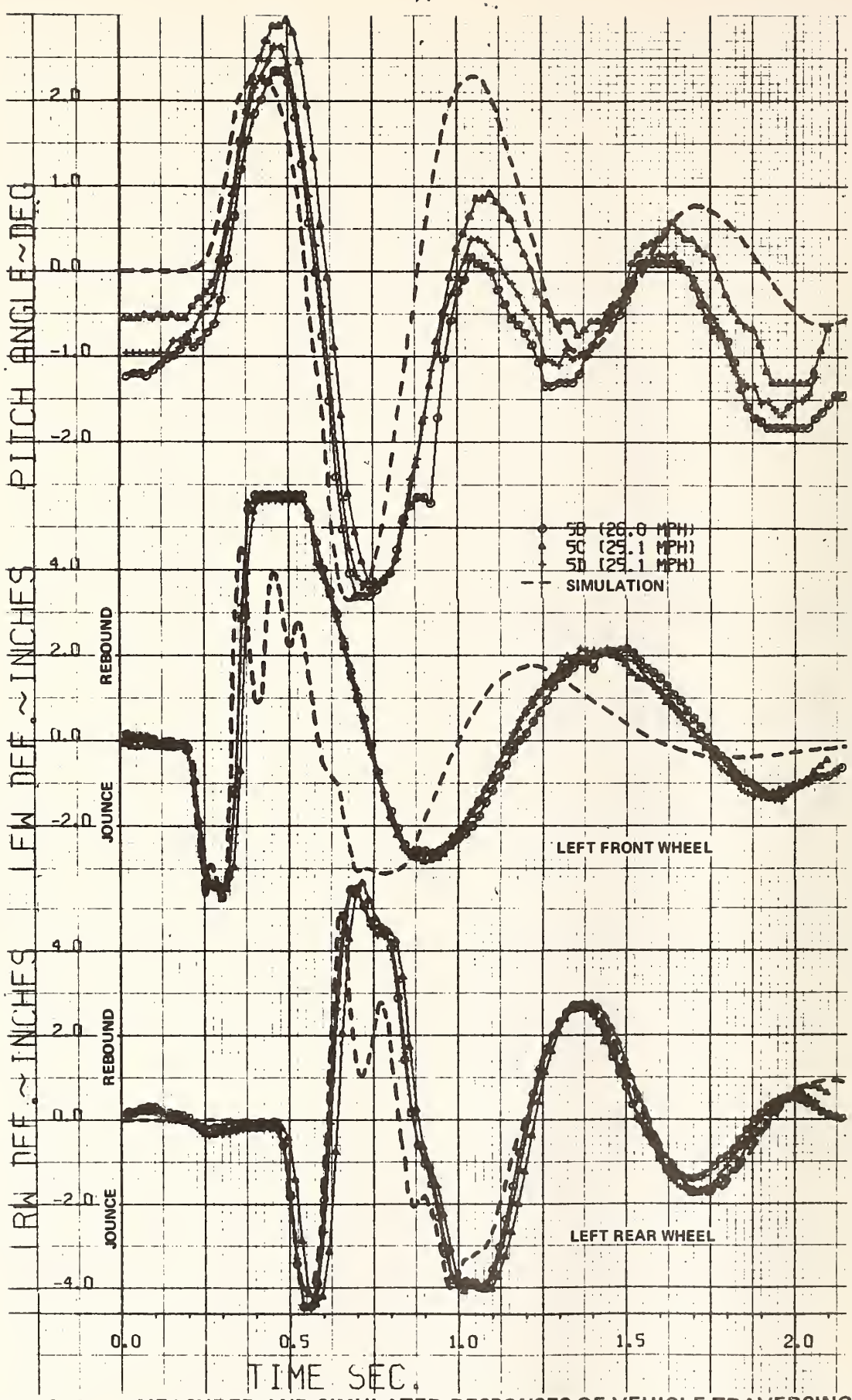

Figure 2.2-7 **MEASURED AND SIMULATED RESPONSES OF VEHICLE TRAVERSING 7.1° — 6.75" HIGH RAMP**

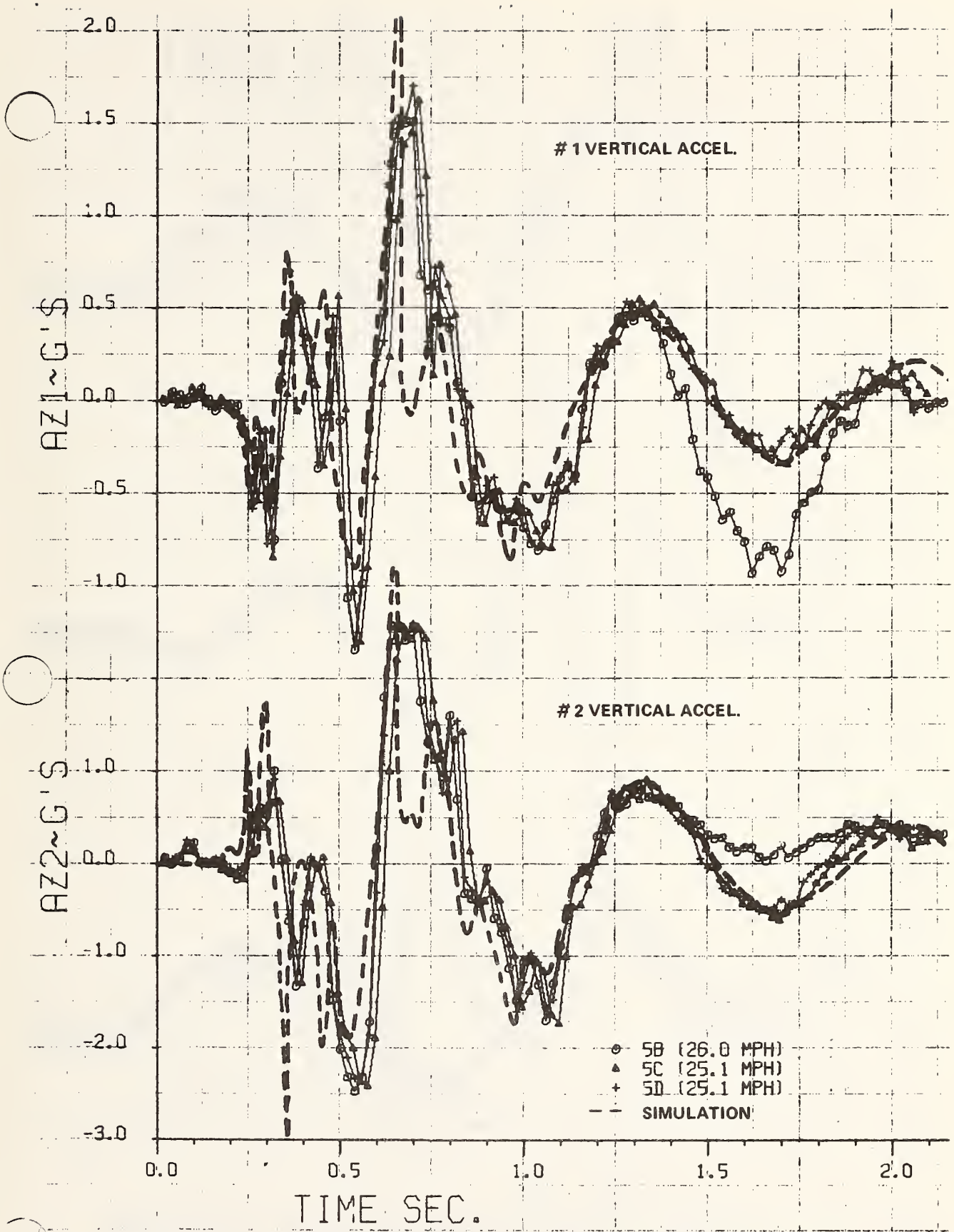

Figure 2.2-7 MEASURED AND SIMULATED RESPONSES OF VEHICLE TRAVERSING 7.1° — 6.75" HIGH RAMP (Continued)

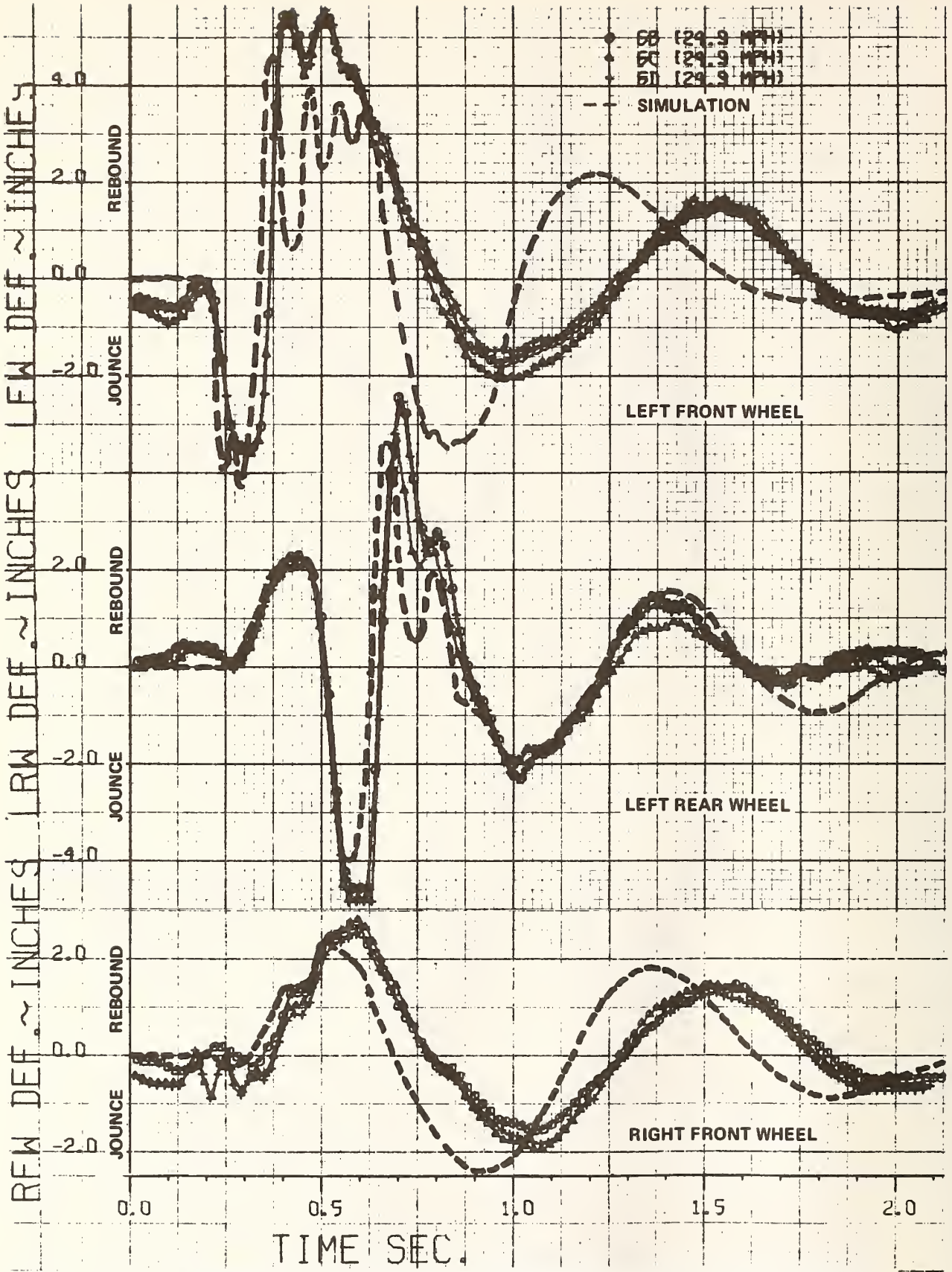

Figure 2.2-8 MEASURED AND SIMULATED RESPONSES OF VEHICLE TRAVERSING 9.2° — 8.5" HIGH RAMP WITH LEFT SIDE WHEELS ONLY

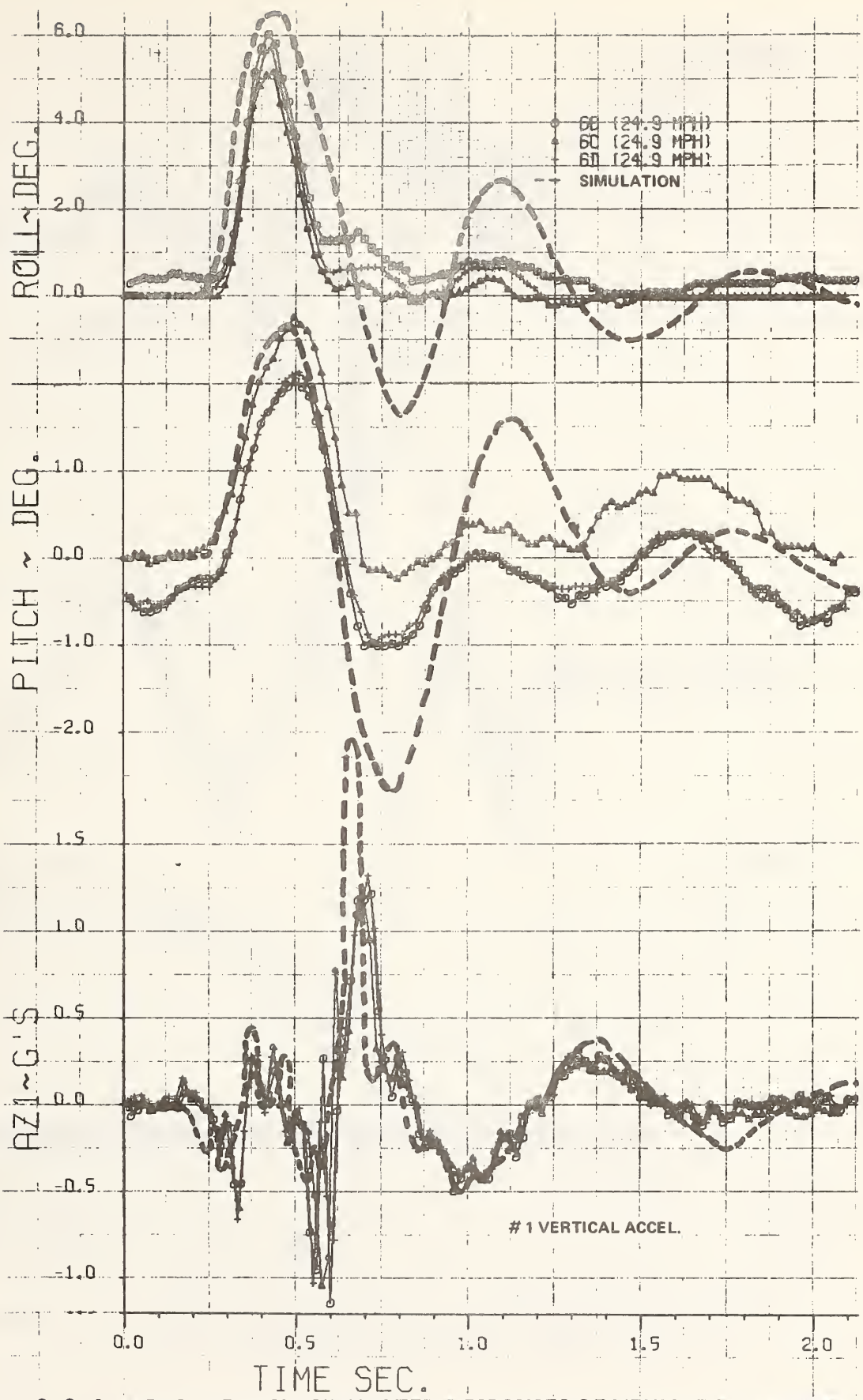

Figure 2.2-8 MEASURED AND SIMULATED RESPONSES OF VEHICLE TRAVERSING 9.2° — 8.5" HIGH RAMP WITH LEFT SIDE WHEELS ONLY (Continued)

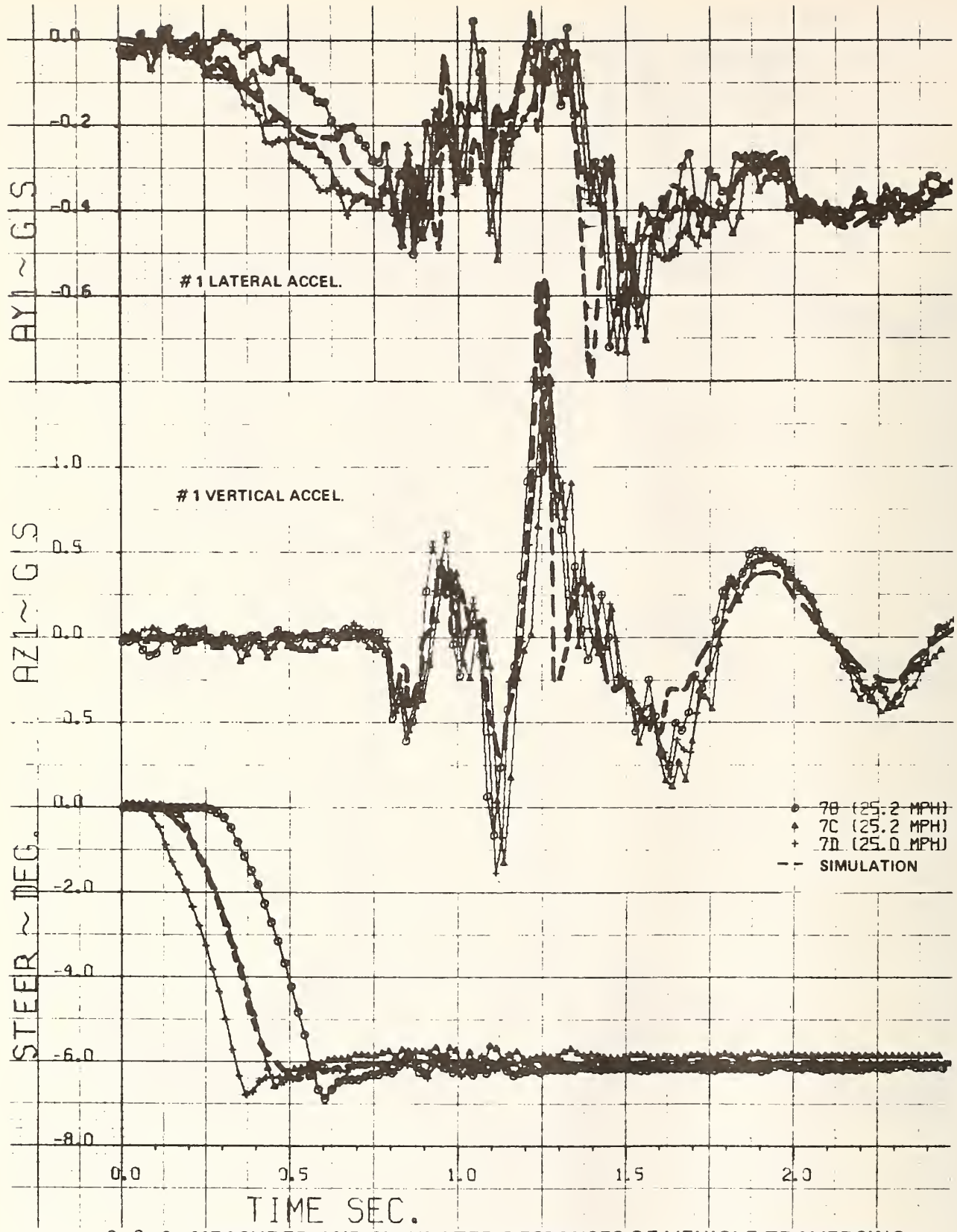

Figure 2.2-9 MEASURED AND SIMULATED RESPONSES OF VEHICLE TRAVERSING 7.1° — 6.75" HIGH RAMP WHILE CORNERING AT 0.4G

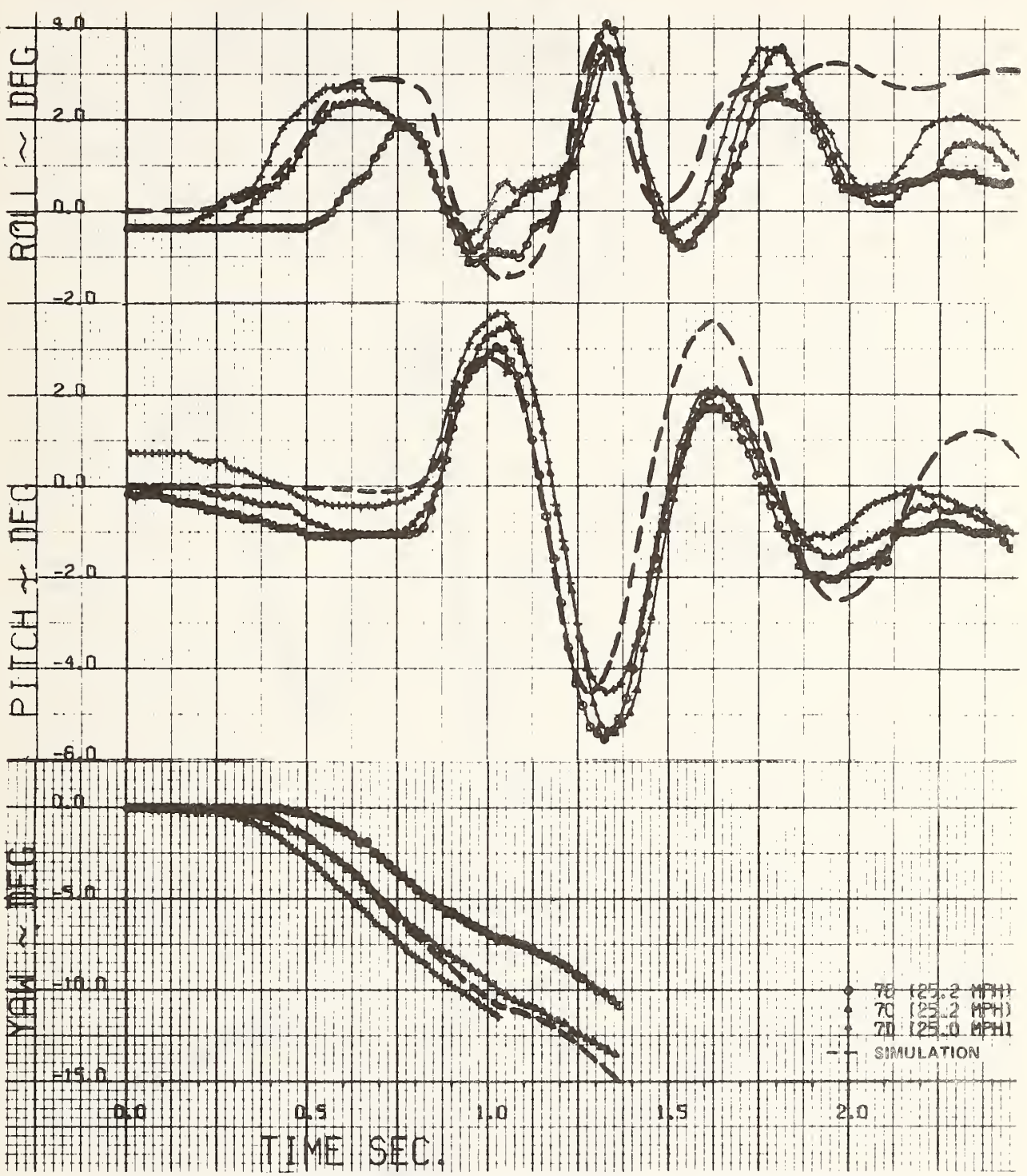

Figure 2.2-9 MEASURED AND SIMULATED RESPONSES OF VEHICLE TRAVERSING 7.1° — 6.75" HIGH RAMP WHILE CORNERING AT 0.4G (Continued)

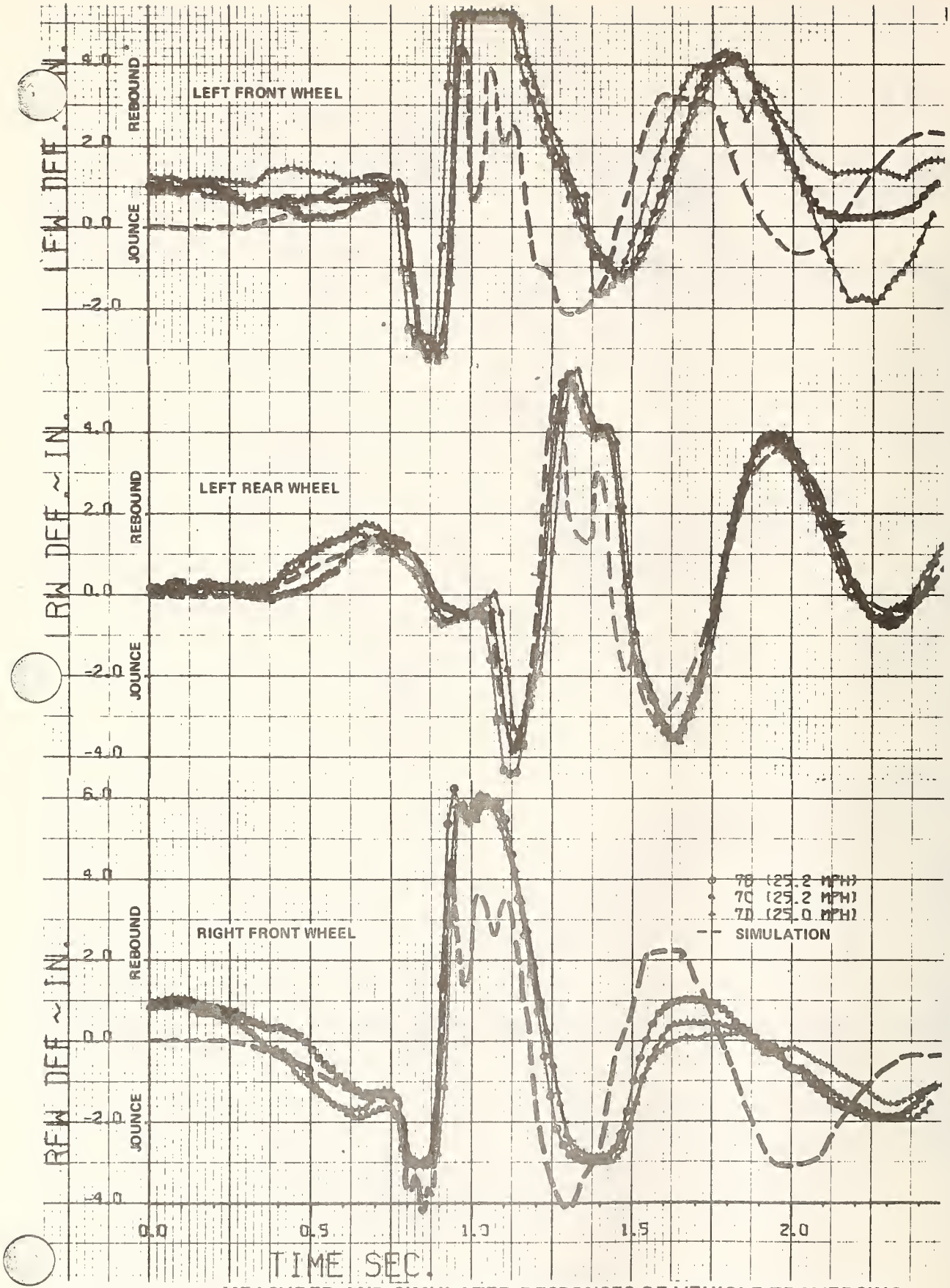

Figure 2.2-9 MEASURED AND SIMULATED RESPONSES OF VEHICLE TRAVERSING 7.1° — 6.75" HIGH RAMP WHILE CORNERING AT 0.4G (Continued)

In the case of the straight approach with all wheels passing over the small ramp (test series 5, Figure 2.2-7), it may be noted that the simulated responses, in general, agree well with the experimental results. The largest differences occur in the comparisons of pitch angle and left front wheel suspension deflections. The simulated pitch response shows a larger peak at about t = 1.1 sec and a slightly reduced damped-oscillation frequency after leaving the ramp. The deviation of the computed suspension response from the experiments is seen to be primarily a phase shift after the suspension strikes the rebound travel stop, although the shapes of the curves are very similar. Note that the magnitude of maximum rebound in the simulation is limited by the assumption of equal jounce and rebound travel limits. Also, filtering of the predicted acceleration responses could improve the correlation with the measured responses by reducing the "spikes" in the simulation results. Unevenness of the roadway approach to the test area resulted in non-zero values for some of the measured variables at time "zero" of the plots.

Most of the above comments apply as well to the comparisons shown in Figure 2.2-8 for the vehicle on a straight approach with only the wheels on the left side passing over a slightly higher ramp (test series 6). From the comparisons of both the pitch and roll angle time histories, it is seen that these responses of the actual vehicle are more heavily damped than those of the simulated automobile. Note that the experimental roll data show no negative overshoot during the return from the initial peak of 6° positive roll. This unexpected behavior results from a "tuning" effect, which did not occur in the simulation because of slightly different timing of the sequence of events. Examination of the movies of the test indicates that the rear wheel passes over the ramp at just the right moment during the recovery from the initial roll, caused by front wheel traversal of the ramp, to effectively cancel the negative rolling velocity and prevent the vehicle from subsequently assuming negative roll attitudes. The different simulated vehicle response may be caused, in part, by the assumption of point contact with the ground in the analytical representation of the tires.

In Figure 2.2-9, the measured and simulated vehicle responses for the case of cornering while traversing the small ramp (test series 7) are displayed. Good repeatability of the measured variables for the three test runs is evident; most of the variability probably results from the different times at which the steering input command was applied. Unfortunately, in these tests, the yaw angle oscillograph trace was improperly positioned on the record so these data were lost approximately 1 second after initiation of steering.

The simulation results agree extremely well with the measured data, even in the details of the several responses. Note that the right front suspension strikes the jounce bumper twice, viz., when the wheel goes over the ramp and again upon recontact with the ground. The reduced cornering force when the front wheels leave the ramp and the subsequent development of large cornering forces produced by recontact of the steered wheels with the ground surface are manifested in both the measured and simulated vehicle lateral acceleration responses in the time period between approximately 0.9 and 1.5 seconds. The data show that the steady state lateral acceleration of the vehicle in the turn was about 0.4 g. The magnitude of the pitch oscillations of the simulated vehicle are somewhat greater and the suspension deflections slightly out of phase in comparison with the measured data.

The discrepancies between predicted and measured rebound deflections of the suspension appear to have been produced primarily by the assumption of symmetrically located and completely elastic deflection-limiting stops in the suspensions.

The measured and predicted time histories of vehicle motions during the alternate ramp traversal tests (test series 13) are shown for comparison in Figures 2.2-10 and 2.2-11. Although the characteristics of the responses for each test are very similar, separate comparisons are presented because the steer inputs by the driver were not as repeatable and the time histories of the other measured variables were significantly different due to the slight difference in speeds for the two tests.

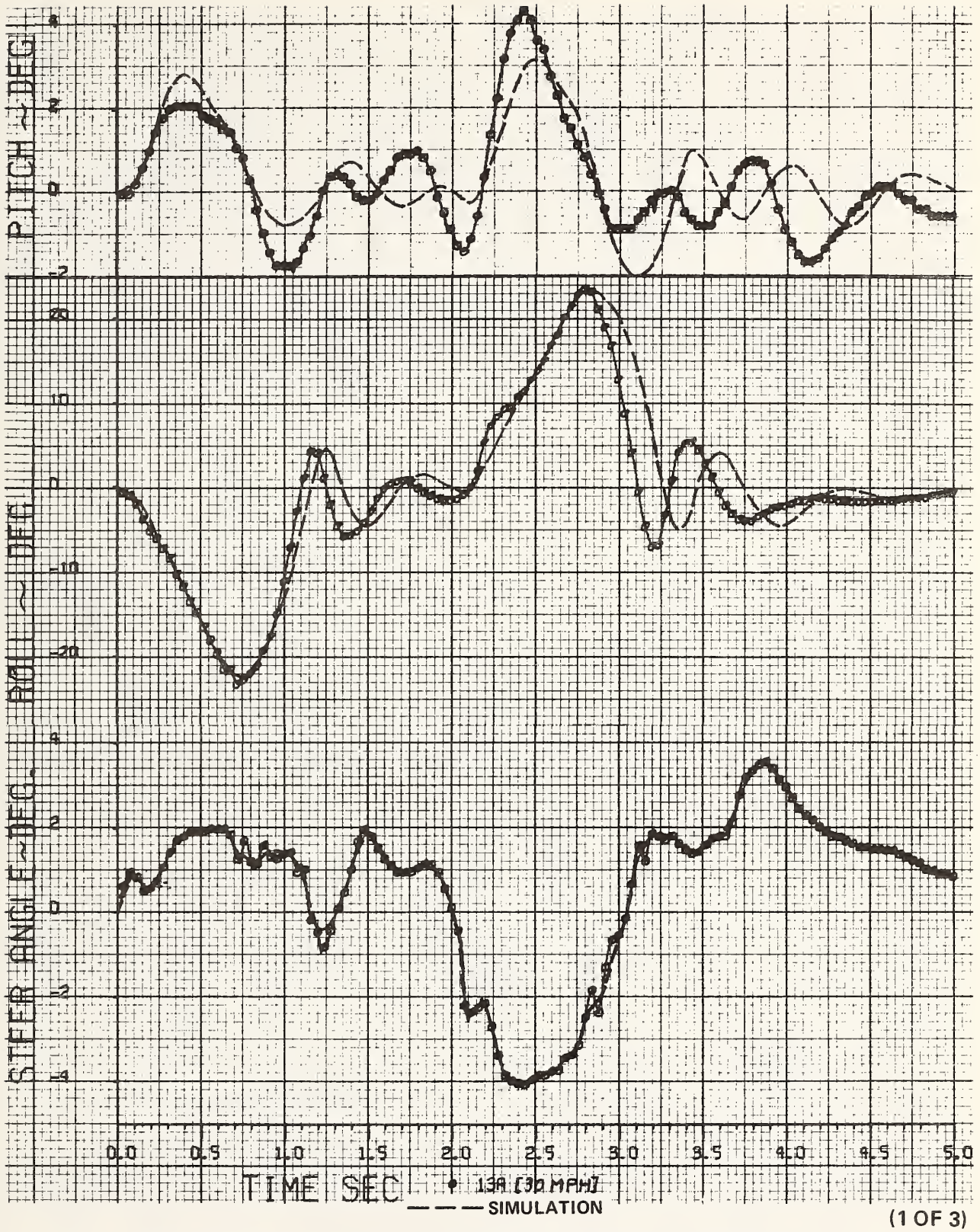

(1 OF 3)

Figure 2.2-10 MEASURED AND PREDICTED RESPONSES OF VEHICLE TRAVERSING 3.6° - 21.5" HIGH RAMPS ALTERNATELY WITH RIGHT AND LEFT WHEELS (TEST 13a)

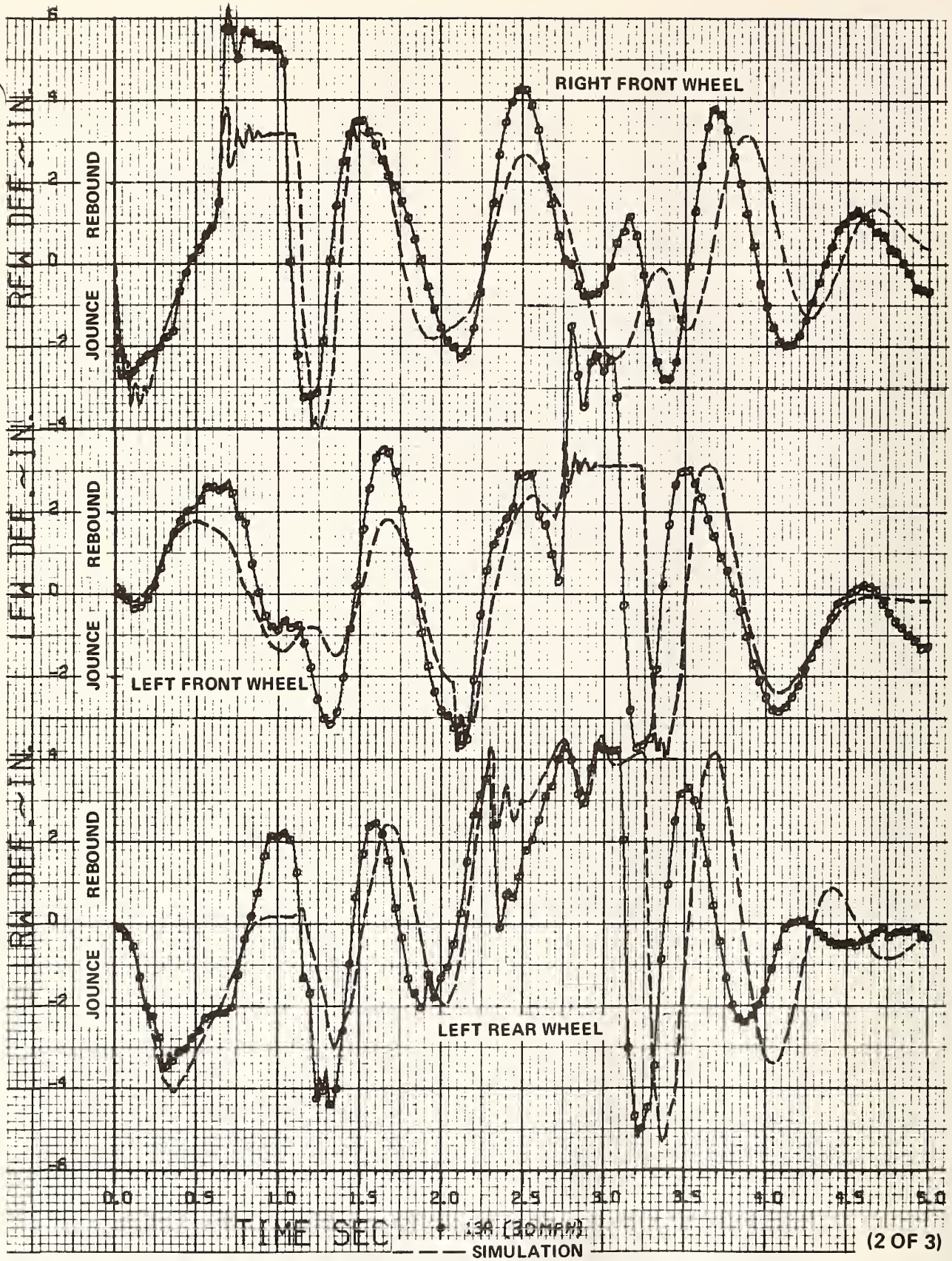

Figure 2.2-10 MEASURED AND PREDICTED RESPONSES OF VEHICLE TRAVERSING 3.6° - 21.5" HIGH RAMPS ALTERNATELY WITH RIGHT AND LEFT WHEELS (TEST 13a) (continued)

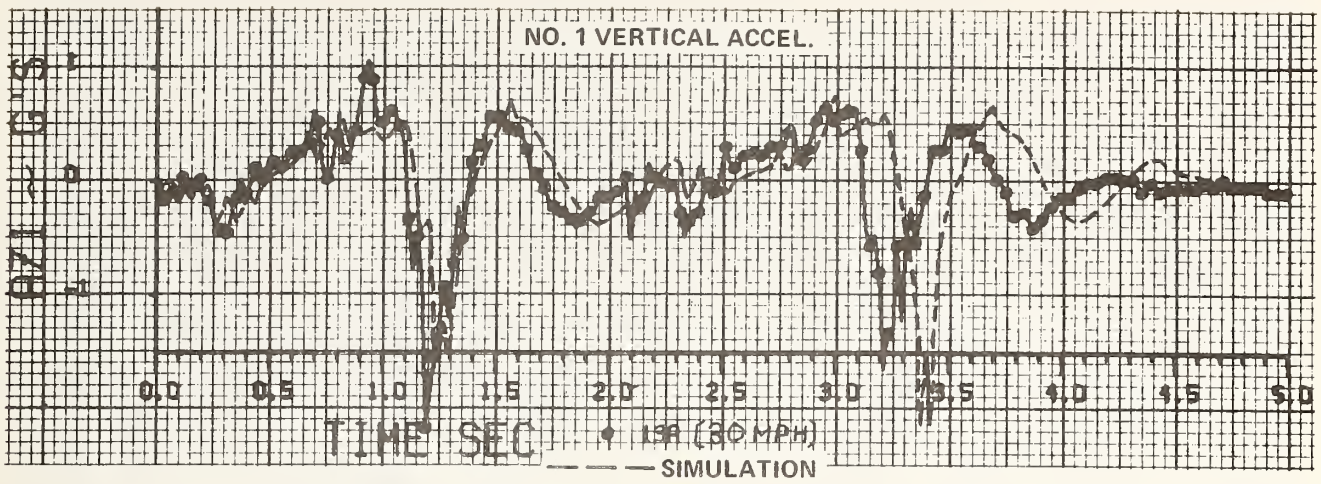

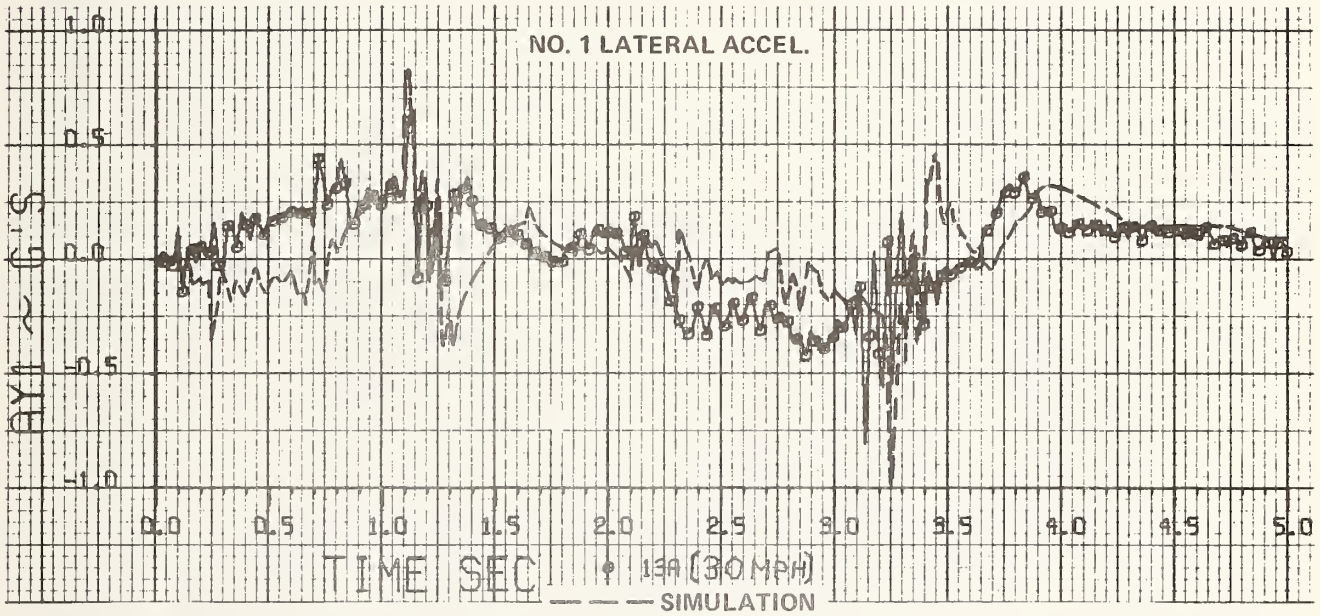

(3 OF 3)

Figure 2.2-10 MEASURED AND PREDICTED RESPONSES OF VEHICLE TRAVERSING 3.6° - 21.5" HIGH RAMPS ALTERNATELY WITH RIGHT AND LEFT WHEELS (TEST 13a) (continued)

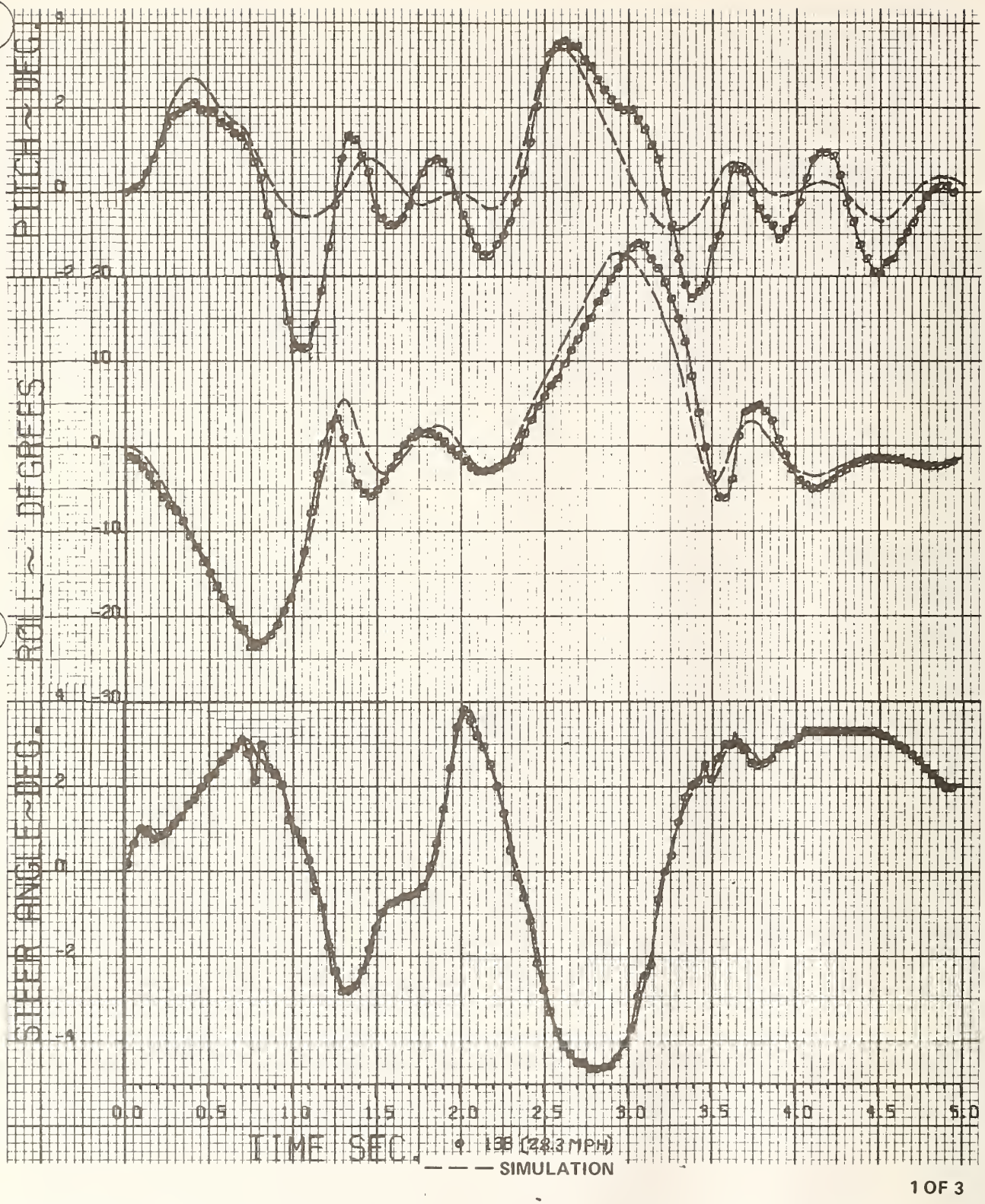

1 OF 3

ure 2.2-11 MEASURED AND PREDICTED RESPONSES OF VEHICLE TRAVERSING 3.6° - 21.5" HIGH RAMPS ALTERNATELY WITH RIGHT AND LEFT WHEELS (TEST 13b)

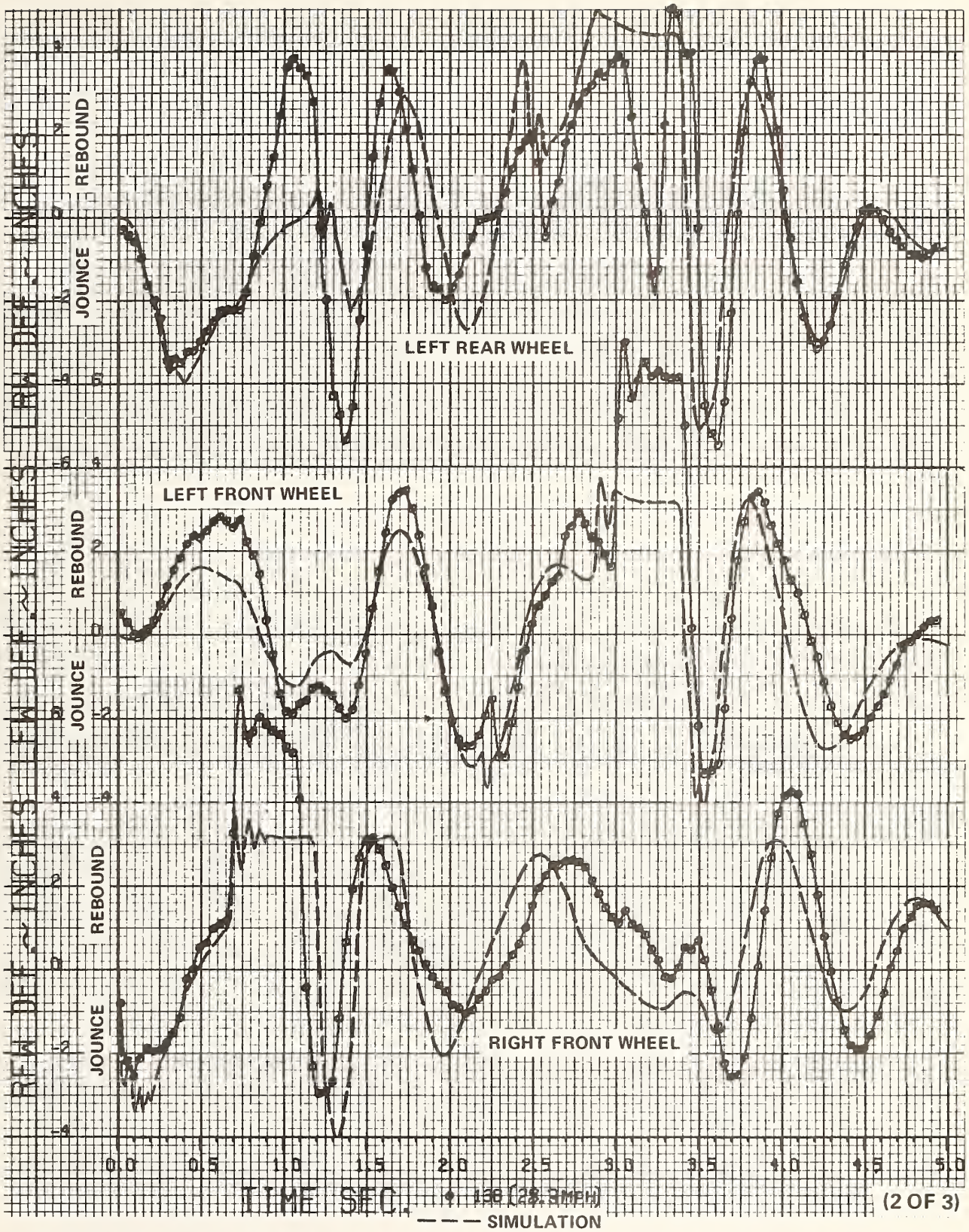

Figure 2.2-11 MEASURED AND PREDICTED RESPONSES OF VEHICLE TRAVERSING 3.6° - 21.5" HIGH RAMPS ALTERNATELY WITH RIGHT AND LEFT WHEELS (TEST 13b) (continued)

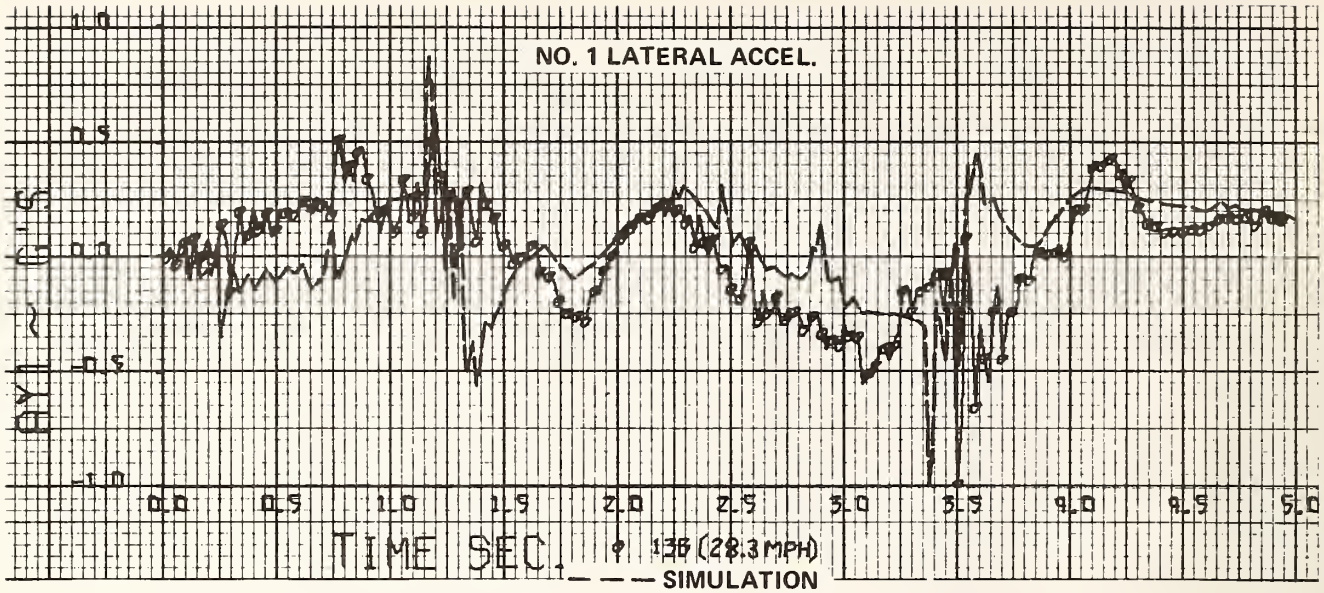

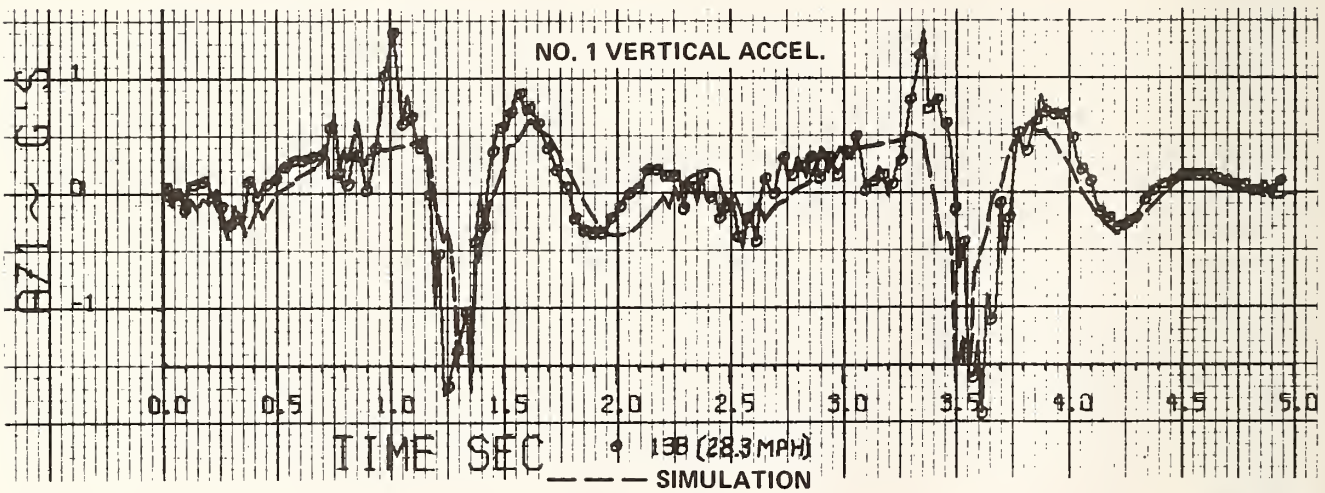

(3 OF 3)

Figure 2.2-11 MEASURED AND PREDICTED RESPONSES OF VEHICLE TRAVERSING 3.6° - 21.5" HIGH RAMPS ALTERNATELY WITH RIGHT AND LEFT WHEELS (TEST 13b) (continued)

Because the two ramps were narrow with a considerable distance between them (down the roadway), some difficulty was experienced in the simulation in achieving a vehicle path that resulted in the left-side wheels of the vehicle properly traversing the downstream ramp, for reasonable lateral spacing of the ramps (the exact lateral distance between ramps for these tests was inadvertently not recorded, but could be approximately determined from the documentary films). Among factors that contributed to this difficulty were: (1) unknown tractive torques applied to the rear wheels in the tests, (2) unknown initial heading angle of the vehicle with respect to the length axis of the ramps (small steering corrections were made just prior to reaching the beginning of the ramp), and (3) unknown tire characteristics at the 65 psi inflation pressure and for the high camber angles experienced in the test.

For the simulation results shown, estimated tire properties extrapolated from meager data on the effects of small changes in inflation pressure in the 25-35 psi range were used. Also, an initial heading angle of -2 degrees was found necessary to produce a vehicle path that would allow the second ramp to be traversed properly. Movies of both tests show that the left rear wheel of the automobile went off the inside edge of the second ramp, rather than the end, a condition that also was obtained in the simulation results.

It may be seen from Figures 2.2-10 and 2.2-11 that the time histories of the various detailed predicted responses correlate well with the measurements of the tests. Note that the large roll angles of approximately $\pm$ 24 degrees experienced in the tests are almost exactly predicted by the simulation model. The slight lag in the peaks of some of the predicted responses for test 13a may be caused by slight speed differences since the simulated vehicle was "coasted", whereas the actual test vehicle probably had varying amounts of power applied by the driver in attempting to maintain a constant speed throughout the tests. The substantial accelerations of the passenger compartment, as the vehicle wheels strike the ground and the suspensions deflect to full

jounce during the recovery from the maximum roll angles, are evident in the plots of the vertical and lateral accelerations and are predicted reasonably well.

That the predicted vehicle trajectories are very close to the actual path of the vehicle in the tests is evident from Figure 2.2-12 which shows a computer-graphics display of the predicted motions of the automobile (test 13a) for comparison with time-matched movie frames from one of the documentary cameras. However, a readily noticeable difference in the appearance of the automobile is apparent in comparing the last picture of the sequences shown. This is partly caused by differences in panning of the actual and simulated cameras. The documentary camera was, of course, manually controlled and the position of the vehicle within the film frame was, therefore, variable and dependent upon the manner in which the operator kept the approaching vehicle within the camera field of view. The simulated "camera", on the other hand, automatically pans in a horizontal plane to keep the vehicle c.g. centered with respect to the sides of the picture but does not pan vertically. Hence, as the car approaches the elevated "camera", its image moves toward the bottom edge of the picture. Automatic vertical panning was not included in the auxiliary computer-graphics program to avoid the "jitter" effect that would be evident in a computer-generated motion picture due to the "camera" following the sometimes very rapid vertical motions of the simulated vehicle.

Of greater concern, perhaps, is the disparity in the roll attitude of the vehicle. However, from the plots of measured and predicted time history of the roll angle presented in Figure 2.2-10, it is clear that this difference is, in fact, attributable to the slight phase shift between the two responses. At the time shown (3.35 sec), the simulated vehicle is at the maximum negative roll angle during the recovery from traversal of the second ramp, whereas the actual vehicle has already passed through this peak and is at the maximum positive roll angle that immediately follows. Obviously, a much more favorable pictorial comparison would have resulted if matching frames at t = 3.28 or 3.5 seconds had been selected for presentation.

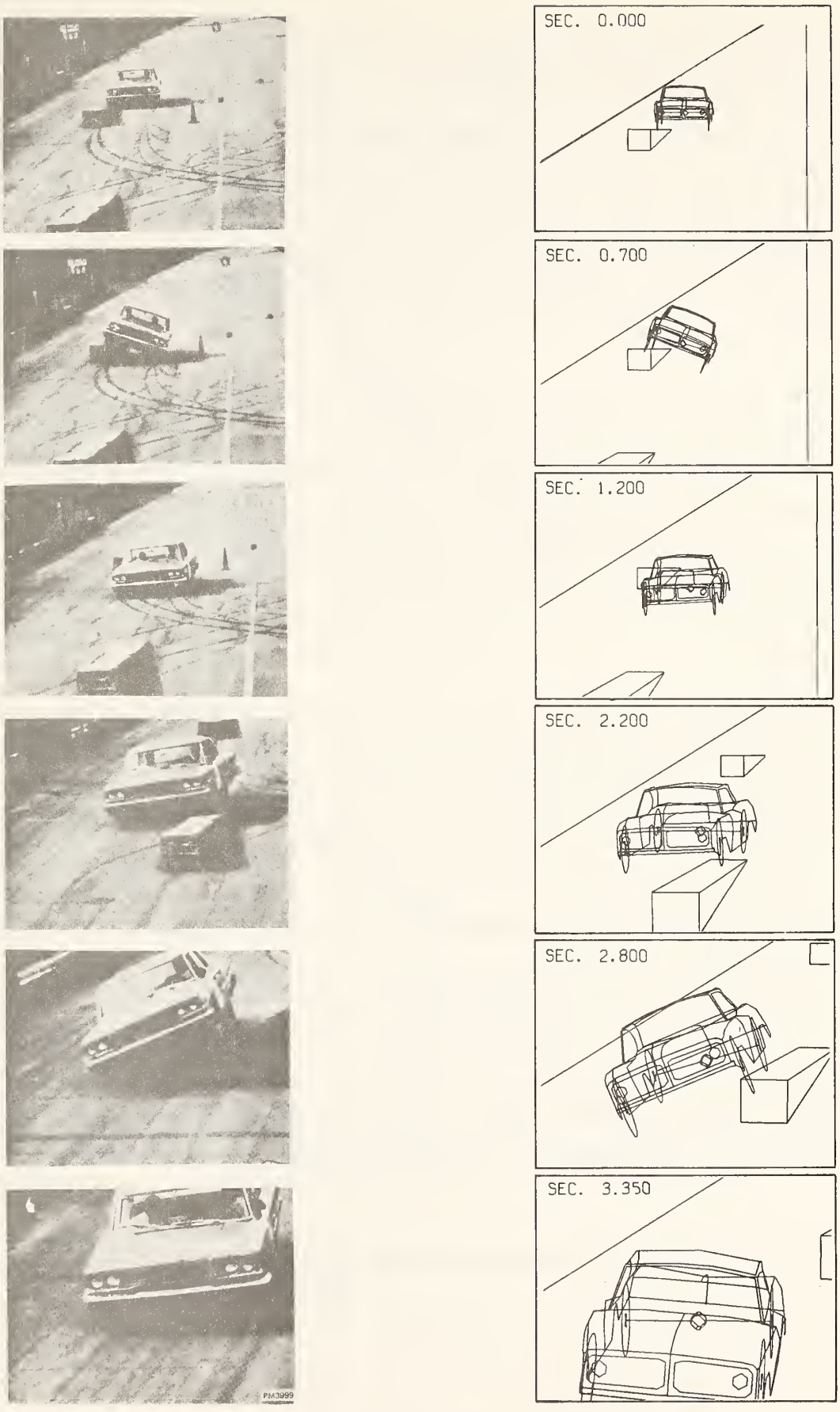

Figure 2.2-12 ALTERNATE RAMP TRAVERSAL AT 30 MPH

Predicted and measured results for the ramp jump test (test 14) are presented in Figure 2.2-13. As previously noted, the speed of the vehicle was excessive and the car overshot the receiving ramp onto which it was intended to land after being completely airborne for a distance of about 50 feet. As a consequence of the violent landing in which the sprung mass struck the ground, both at the front and rear and with sufficient force to bend the frame, some test data were lost and are of doubtful validity after impact. The time period during which the oscillograph traces were unreadable are indicated on the plots.

At the present time, the analytical model lacks the capability of simulating energy-dissipating sprung mass impacts with the ground. In addition, because much of the energy of the vehicle is absorbed and subsequently released by the linear, completely elastic suspension deflection-limiting stops assumed in the model, the vehicle rebounds several times after the first impact in the simulated results. For these reasons, the predicted responses are not in good agreement with the measured results after impact.

It may be seen that the predicted responses of the pitch angle and the suspension deflections agree well with the measured test data up to the point of impact at approximately 1.7 sec. Note also that the actual automobile rolled during the free-flight portion of its trajectory, reaching a maximum value of about -10 degrees. This may have been caused by several factors, including (1) slightly unequal elevations of the takeoff ramp for the right and left pairs of wheels, (2) unequal spring rates for the suspensions on each side of the vehicle, or (3) the center of gravity not on the vehicle longitudinal center line as a result, perhaps, of the absence of a passenger on the right side to counteract the weight of the driver. For the simulation results, mirror symmetry on either side of the vertical plane containing the vehicle longitudinal axis was assumed, thereby resulting in no roll motions.

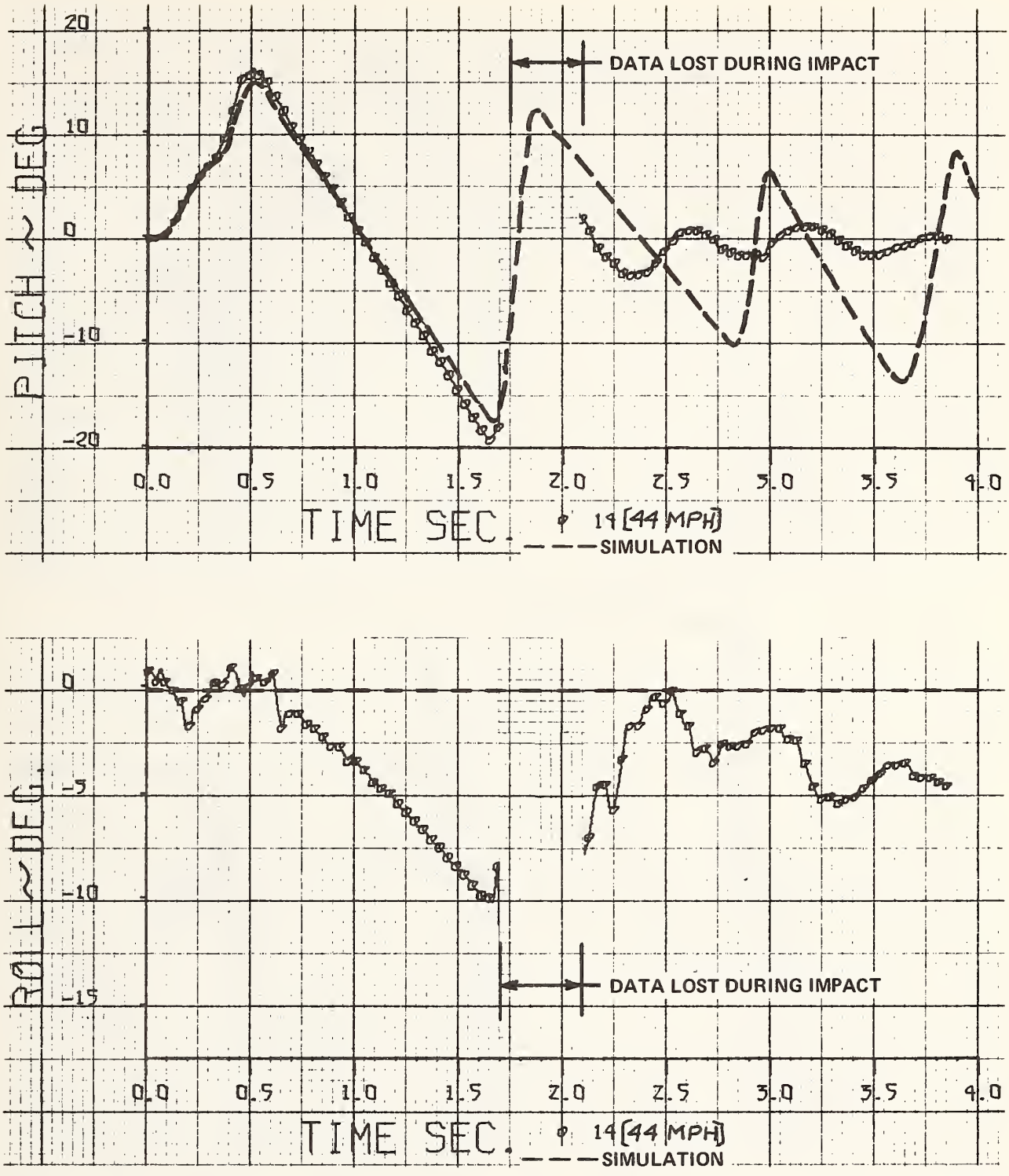

(1 of 3)

Figure 2.2-13 MEASURED AND PREDICTED RESPONSES OF VEHICLE JUMP FROM TAKE - OFF RAMP

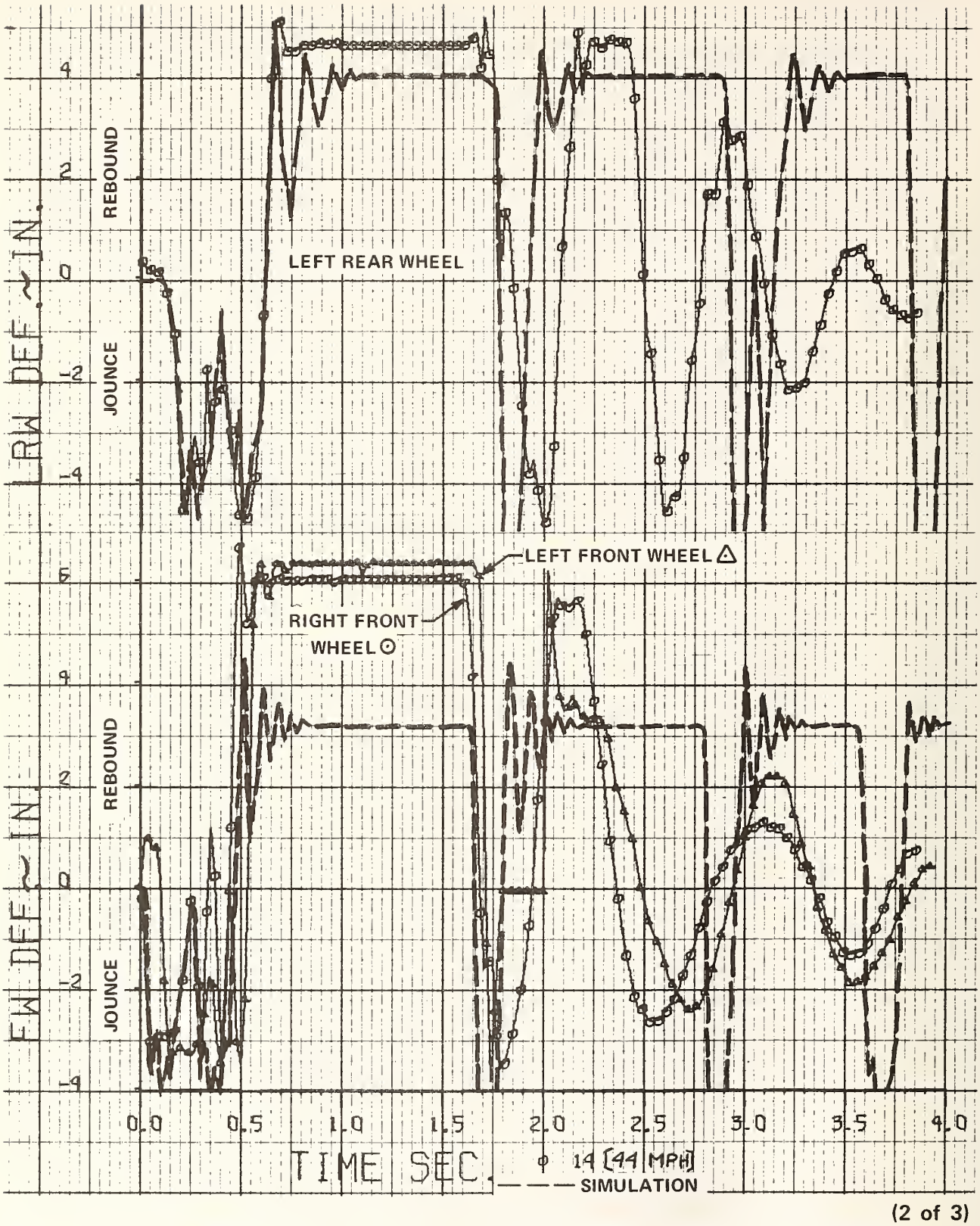

(2 of 3)

Figure 2.2-13 MEASURED AND PREDICTED RESPONSES OF VEHICLE JUMP FROM TAKE - OFF RAMP (continued)

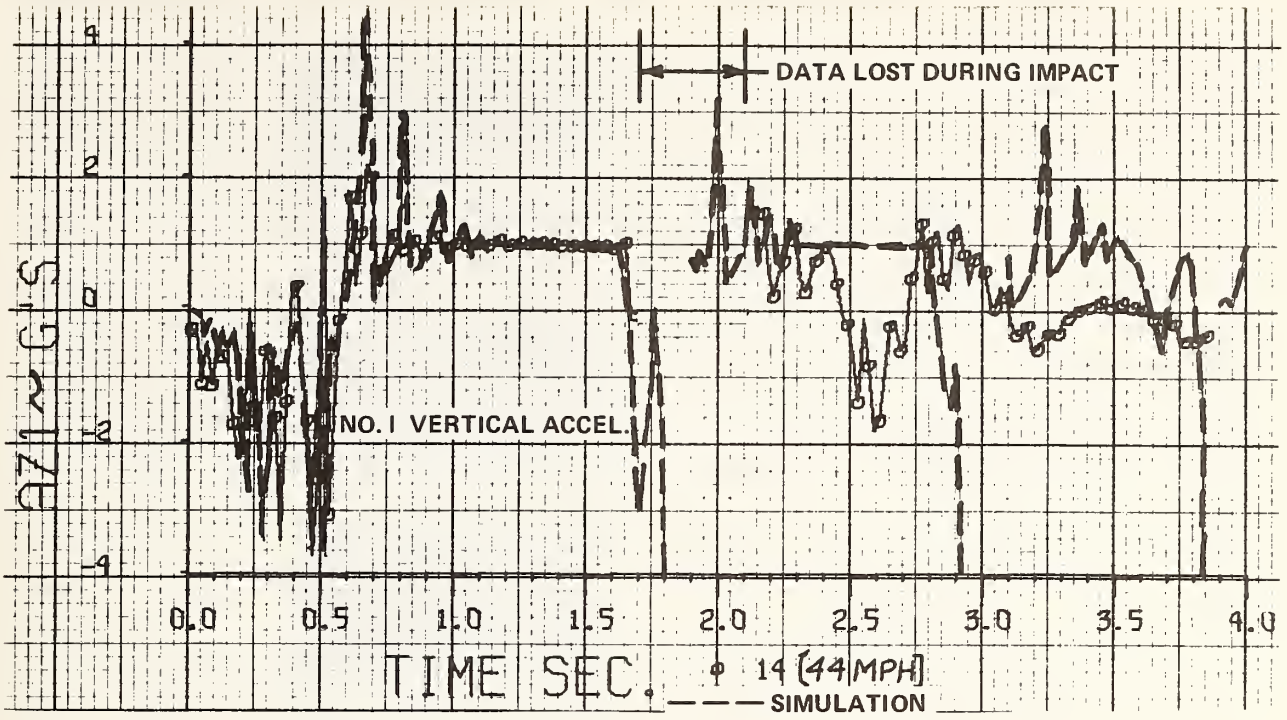

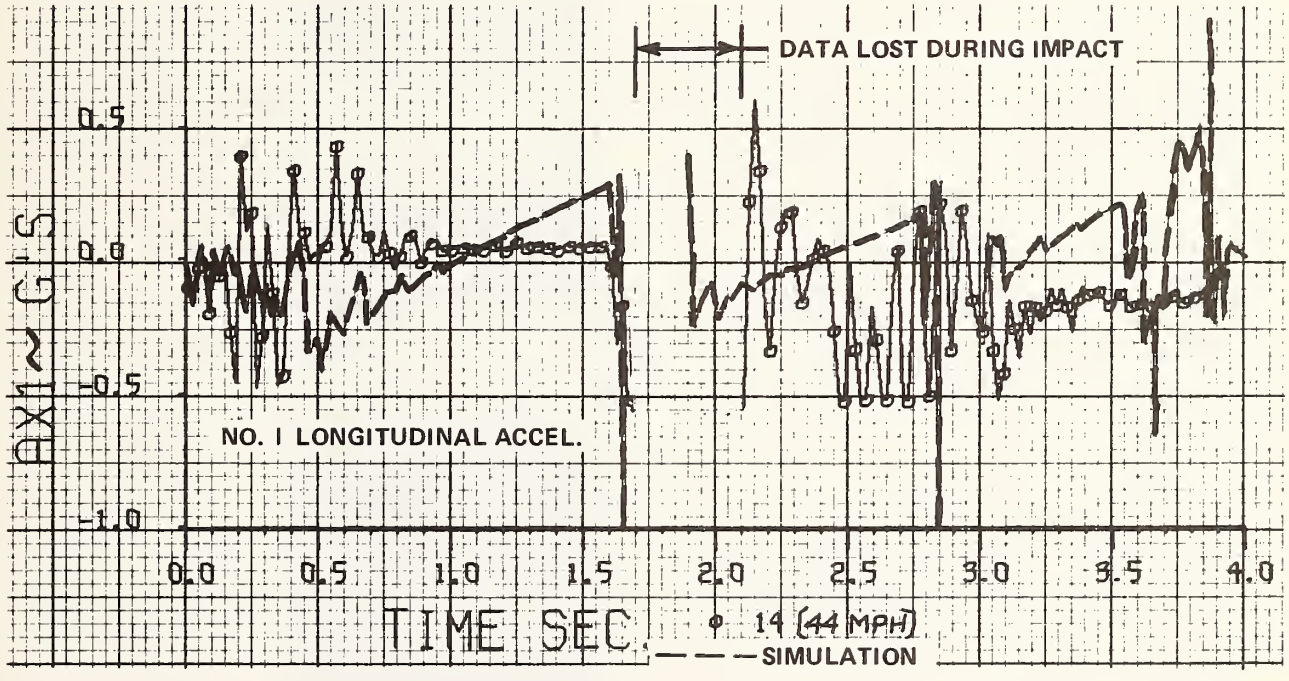

(3 of 3)

Figure 2.2-13 MEASURED AND PREDICTED RESPONSES OF VEHICLE JUMP FROM TAKE - OFF RAMP (continued)

Pictures from movies of the ramp jump test and computer-generated graphic displays of the predicted trajectory at corresponding times are shown for comparison in Figure 2.2-14. The close similarity, up to the time of impact, of the predicted trajectory and attitude of the automobile with those shown in the photographs is clearly evident. At the highest point of the trajectory, the vehicle center of gravity was nearly 10 feet above the ground. Excessive pitch and bounce of the simulated vehicle after the landing impact may be noted in the last of the sequence of pictures. As indicated earlier, this results primarily from the lack, in the present model, of a capability for simulating sprung mass impacts with the ground and the attendant dissipation of energy in the vehicle structure that occurred in the test.

2.2.5 Vehicle Response Sensitivity

Additional computer simulations of the first of the alternate ramp traversal tests (test 13a) were performed to determine whether the predicted vehicle responses would be significantly altered by use of the "best estimate" values for the vehicle parameters and also by increasing I_x by approximately 50%. This test condition was selected because the large roll angles experienced make it the most suitable for demonstrating the effects of changes of the vehicle roll moment of inertia.

Predicted responses of the left front and left rear wheels using (1) original parameter values (column 1 of Table 2.1-1) and (2) "best estimates" (column 3 of Table 2.1-1) are depicted in Figure 2.2-15 for comparison. Also shown in Figure 2.2-15 are predicted roll responses for the two cited cases and for the case of "best estimates" with I_x increased to 8800 lb-sec^2-in. These plots show that only small changes occurred in the responses when "best estimate" values were substituted for the originally estimated vehicle parameters. For the most part, these changes would appear to improve the correlation with the responses measured in the test, e.g., the larger rebound deflections of the front wheel at t = 0.5 sec and t = 1.65 sec (see Figure 2.2-10).

EXPERIMENT

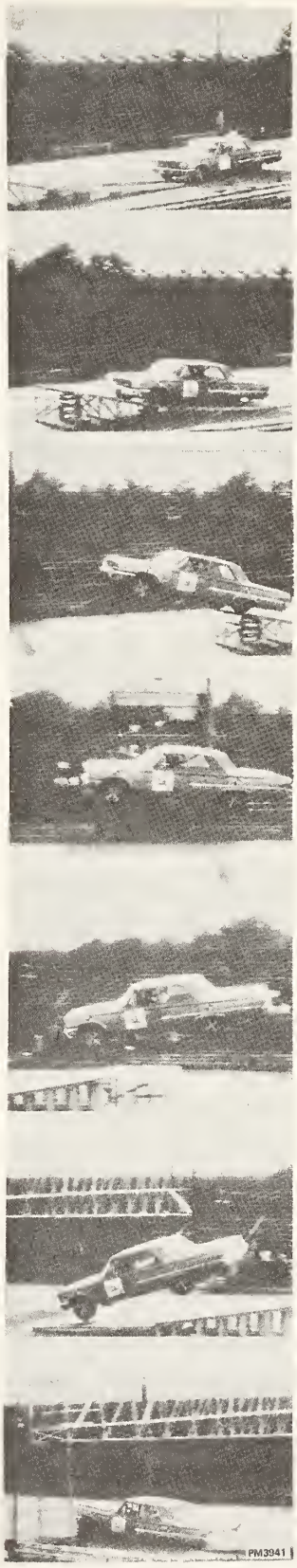

COMPUTER PREDICTION

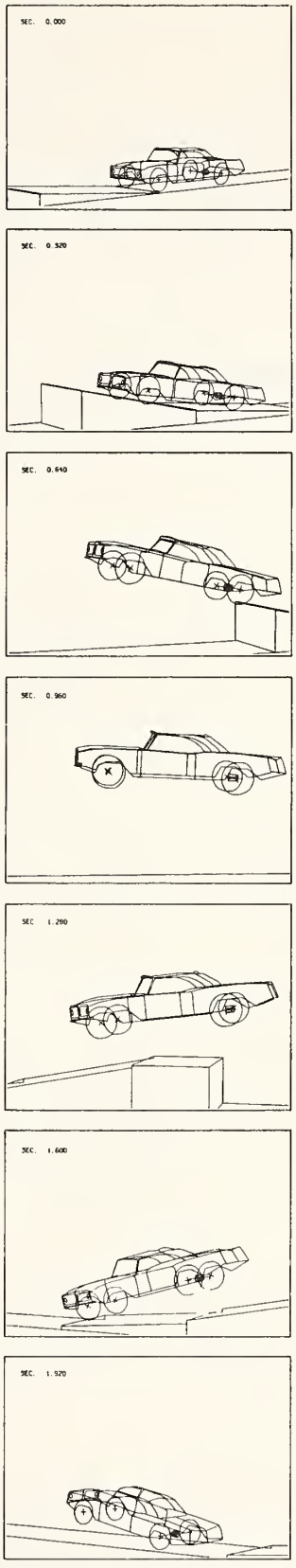

Figure 2.2-14 RAMP JUMP AT 44 MPH

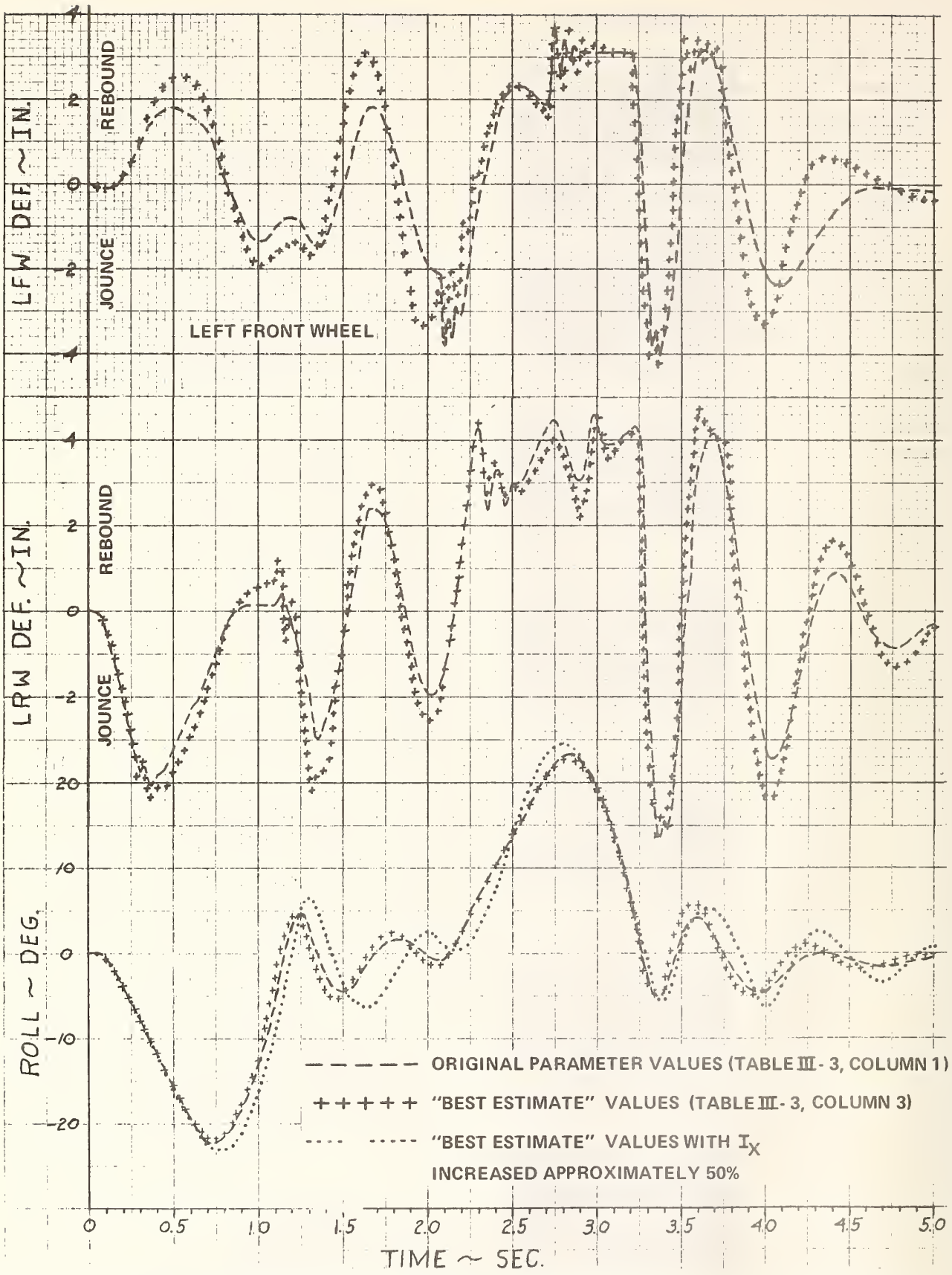

Figure 2.2-15 EFFECTS OF CHANGE OF VEHICLE PARAMETERS ON PREDICTED RESPONSES FOR ALTERNATE RAMP TRAVERSAL SIMULATION

Increasing the roll moment of inertia by nearly 50% also had only a relatively small effect on the roll response, resulting in only a slightly higher peak amplitude and a generally lagging response. For that simulation run, the left rear wheel went off the inside edge of the second ramp at a lower height than for the other two simulation runs, because the change of roll moment of inertia had a slight effect on the vehicle trajectory. Had this not occurred, the maximum positive roll angle would have been delayed slightly and would also have been increased somewhat over that shown at approximately t = 2.8 sec. Again, the response obtained with the "best estimate" values for the vehicle parameters most nearly matches that measured in the test, adding strength to the conclusion that the measured value for I_x listed in column 2 of Table 2.1-1 is incorrect.

2.3 Skidding Tests HVOSM-SMI1

2.3.1 Test Vehicle and Instrumentation

The test vehicle and instrumentation used for this test series were identical to those reported in Section 2.1.1. However, for test series 11 and 12, the tire parameters reflected estimates of 65 psi inflation pressure, and the fifth wheel was not used for speed measurement for fear of damage. Speed estimates were obtained either from the vehicle speedometer or from photographic reduction.

2.3.2 Data Acquisition and Reduction

Data acquisition and reduction procedures used were identical to those reported in Section 2.1.2.

2.3.3 Test Procedure

Three series of repeated tests involving vehicle skidding were performed as summarized in Table 2.3-1. Two of the series were forward skid tests in which the skids were induced by quickly locking only the rear wheels by means of the parking brake and almost simultaneously applying a large steer angle of the front wheels. The other series were reverse skids in which the vehicle, initially traveling backwards, was caused to spin around by appropriate steering and throttle control inputs so as to reverse its heading and continue down the roadway without stopping or application of brakes.

In the first series of forward skids (tests 10), a switch applying a step steer command signal was closed by movement of the parking brake pedal to assure good repeatability in the timing of the brake and steering control inputs. These tests were performed at an initial speed of 25 MPH on a sealed asphalt surface that was thoroughly wetted. Measurements of

Table 2.3-1 SUMMARY OF EXPERIMENTAL PROGRAM

TEST CONDITION	NO. OF TESTS REPORTED	DESCRIPTION	NOMINAL SPEED	TEST SERIES NO.
SKIDDING	3	Rear wheels locked, large steer input on wet asphalt, 180 degree yaw.	25 MPH	10
	2	Rear wheels locked, large steer input on dry asphalt, 180 degree yaw.	35 MPH	12
	2	Reverse skid, induced by steer and traction on dry asphalt, 180 degree yaw.	30 MPH	11

the coefficient of sliding friction of the wetted surface were attempted, using both a Penn State Skid Resistance Tester ("Drag Tester") and a British Portable Skid Resistance Tester. However, these devices provided more of a qualitative indication of the surface skid resistance, rather than an accurate, quantitative measurement of the sliding coefficient of the actual tires over the speed range of 25 to 0 MPH experienced in the tests.

Both the second and third series of skid tests were performed by a professional stunt driver on a dry asphalt pavement. For these tests (and the previously described ramp tests using professional drivers), the vehicle was equipped with 15 inch tires that were inflated to 65 psi. Also, the electronic command steer mode was not employed in these tests, so the repeatability of the steering input was not as good as in the first series.

For the dry pavement forward skids (test series 12), the rear wheels were locked by the parking brake shortly after the front wheels were steered to the left. In each of the two tests, the driver reversed the steer angle of the front wheels as the vehicle spun around and came to a stop. Nominal speed for these tests was 35 MPH.

Execution of the reverse skid tests (test series 11) required considerable skill by the driver and involved some control inputs that could not be directly measured. Briefly, the following technique was employed: the vehicle was accelerated in reverse to a speed of approximately 30 MPH and the front wheels then steered as rapidly as possible to the limit of negative steer angle. During this time, the automatic transmission was also shifted from reverse to low gear, which decreased the speed as a result of engine braking. At the proper moment, approximately after the vehicle had rotated through 90 degrees change in heading angle, full, or nearly full throttle was applied, and the front wheels returned to essentially zero steer angle. The net result was to cause the vehicle to spin clockwise approximately 180 degrees, so as to continue down the roadway with a (now) forward velocity without having come to a complete halt during the course of the maneuver. Both reverse skid tests were performed on a dry asphalt surface.

2.3.4 Comparison of Predicted and Experimental Results

The HVOSM inputs used for comparison with the skidding tests are shown in Figures 2.3-1 through 2.3-3. Experimental and simulated responses of the vehicle for the first series of skids (tests 10), performed on wet roadway, are presented in Figure 2.3-4. Simulation results are shown for two assumed values of the tire-ground friction coefficient (i.e., 0.3 and 0.4), to show the effects on the various responses of changes in this variable, for which the value in the tests is not accurately known.

Correlation between simulation and experiment is again considered to be very good. The comparison indicates that the average friction coefficient in the tests was probably close to a value of 0.4. Comparison of the predicted and experimental time histories of yaw angle indicates that the simulated vehicle follows the response of the actual vehicle up to about 90 degrees of yaw but does not quite reach the full 180 to 185 degree turnaround attitude experienced in the tests. This difference might indeed be attributable to a non-constant coefficient of friction of the wetted asphalt surface which was not of uniform roughness, whereas, in the computer model, a constant coefficient of friction is assumed. Also, the effects of velocity on the tire-ground friction coefficient are neglected in the simulation. During the performance of each test, a vibration or chattering of the wheels occurred, which could be heard and was felt by the occupants as the rear end of the automobile swung rapidly around. This phenomenon would be expected to produce the effect of a reduced friction coefficient at the affected wheels and hence, might have caused the vehicle to spin around to a larger yaw angle.

```
   0.0     5.00     .010              .020      70.      0.0      0.0      0.0        1
  1.0                                                                               2
 10.818    .608     .945     386.4   6000.0   30000.   36000.    -192.    600.      3
 54.517  64.483    61.0     60.0     10.25    12.14     -2.0     14.0     4400.     4
  131.     25.0     3.00     3.50     55.0    0.001   266000.                       5
  192.0    25.0     4.0      3.90     50.0    0.001    61900.   46.50    0.070     6
 1098.0     3.00    10.00    8.276   2900.     1.78     0.40    0.750    3900.     7
    0.0      0.0      0.0      0.0      0.0      0.0      0.0      0.0              8
    0.0      0.0    -23.0    440.0      0.0      0.0                               9
   0.0      0.0      0.0      0.0      0.0      0.0      0.0      0.0              10
 -34.48     0.0      4.0    -112.48   -16.     -.5                                11
  -5.0      5.0      1.0                                                          12

PHIC(II,I=1,    11
   -3.550   -2.550   -1.800   -1.300   -0.950   -0.550   -0.300   -0.300   -0.400   -0.550   -0.800

    0.0      4.9      0.1      0.0      0.0      0.0                              13

PSIF(I),I=1,   50
    0.0      0.0      1.170    3.730    7.170   11.970   16.270   17.930   18.000   18.000   18.000   18.000   18.000
  18.100   18.200   18.400   18.530   18.800   19.000   19.230   19.500   19.770   20.030   20.330   20.500   20.630
  20.800   20.850   20.900   20.950   21.000   21.000   21.000   21.000   21.000   21.000   21.000   21.000   21.000
  21.000   21.000   21.000   21.000   21.000   21.000   21.000   21.000   21.000   21.000   21.000

TQF(I),I=1,   50
    0.0      0.0      0.0      0.0      0.0      0.0      0.0      0.0      0.0      0.0      0.0      0.0      0.0
    0.0      0.0      0.0      0.0      0.0      0.0      0.0      0.0      0.0      0.0      0.0      0.0      0.0
    0.0      0.0      0.0      0.0      0.0      0.0      0.0      0.0      0.0      0.0      0.0      0.0      0.0
    0.0      0.0      0.0      0.0      0.0      0.0      0.0      0.0      0.0      0.0      0.0

TQR(I),I=1,   50
    0.0  -5000.000 -5000.000 -5000.000 -5000.000 -5000.000 -5000.000 -5000.000 -5000.000 -5000.000 -5000.000 -5000.000 -5000.000
-5000.000 -5000.000 -5000.000 -5000.000 -5000.000 -5000.000 -5000.000 -5000.000 -5000.000 -5000.000 -5000.000 -5000.000 -5000.000
-5000.000 -5000.000 -5000.000 -5000.000 -5000.000 -5000.000 -5000.000 -5000.000 -5000.000 -5000.000 -5000.000 -5000.000 -5000.000
-5000.000 -5000.000 -5000.000 -5000.000 -5000.000 -5000.000 -5000.000 -5000.000 -5000.000 -5000.000 -5000.000

    0.0     -1.0      1.0      0.0     -1.0      1.0      1.0      1.0      0.0      14

XBDRY(I),I=1,   1          YBDRY(I),I=1,   1
   10.000     0.001

                                                                                  9999
```

Figure 2.3-1 **INPUTS FOR TEST 10 SIMULATION**

SINGLE VEHICLE ACCIDENT SIMULATION
RUN TEST 11 COMPARISON (REVERSE SKID)

```
  0.0     4.3    C.010          .020     7C.C      0.0      0.0      0.0          1
  1.0                                                                            2
 10.818  C.608   0.945   386.4   600C.   3000C.   36000.   -192.    600.         3
 54.517  64.483  61.     60.     10.138  12.088   -2.0     15.      11500.       4
131.0    25.0    3.C     3.5     55.C    0.001   266000.0                        5
192.0    25.0    4.0     3.9     50.0    0.001    61900.0  46.50   C.07C        6
2200.     3.C    10.00   7.53C   4000.   3.47     0.85     1.00    5400.        7
  0.0     0.0     0.0     0.0     0.0     0.0      0.0      0.0                  8
  0.C     0.0   -24.57  -563.     0.0     0.0                                   9
  0.0     0.C     0.0     C.0     0.0     0.0      C.0      0.0                  10
-34.48    0.0     4.0   -112.48  -16.0   -0.5                                   11
 -5.C     5.0     1.0                                                          12

PHIC(I),I=1,    11
   -3.550    -2.550    -1.800    -1.300    -C.950    -0.55C    -0.300    -0.300    -0.400    -0.550    -0.800

  0.0     4.3     C.1     C.C     0.C     0.C                                   13

PSIF(I),I=1,  44
     0.0      -0.020    -0.050    -1.600    -4.30C    -7.000   -10.000   -12.80C   -15.500   -18.300   -21.200   -24.000   -27,000
   -28.000    -28.000   -28.000   -28.000   -28.00C   -28.000   -28.000   -28.000   -28.000   -28.000   -28.000   -28.000   -28.000
   -26.500    -24.700   -23.C0C   -21.000   -19.50C   -16.800   -12.900    -9.80C    -5.200    -3.200    -1.500     0.0       0.0
     0.0        0.0       0.0       0.0       0.0

TQF(I),I=1,   44
     0.0       0.C       0.0       C.0       0.0       0.0       0.0       0.0       0.0       0.0       0.0       0.0       0.0
     0.0       0.0       0.0       0.0       0.0       0.0       0.0       0.0       0.0       0.0       0.0       0.0       0.0
     C.0       0.0       0.C       C.0       0.0       0.0       0.0       0.0       0.0       0.0       0.0       0.0       0.0
     0.0       0.0       C.0       C.0       0.0

TQR(I),I=1,   44
     0.0       0.0       0.0       0.0       C.0       0.0       0.0    -108.00C  -216.000  -324.000  -432.000  -344.000  -258.000
  -172.000   -86.000     0.0       0.0     350.000   700.000  1050.000  720.00C   720.000   720.000   720.000   720.000   720.000
   72C.000   720.000   720.000   580.000   580.000   580.000   580.000   580.000   580.000   580.000   580.000   580,000   580.000
   580.000   580.000   580.0C0   580.000   580.000

  0.0    -1.0     1.0     0.0    -1.0     1.0      1.0      1.C      0.0          14

XBDRY(I),I=1,   1          YBDRY(I),I=1,   1
 1000C.00C 10000.000

                                                                                9999
```

Figure 2.3-2 **INPUTS FOR TEST 11 SIMULATION**

SINGLE VEHICLE ACCIDENT SIMULATION
RUN TEST 12 COMPARISON (FORWARD SKID)

```
  0.0      3.5     0.010              .020      70.0      0.0      0.0      0.0          1
  1.0                                                                                   2
 10.818  0.608    0.945    386.4    6000.    30000.   36000.   -192.    600.          3
 54.517 64.483   61.      60.      10.138   12.088   -2.0     15.      4400.          4
 131.0   25.0     3.0      3.5     55.0      0.001  266000.0                         5
 192.0   25.0     4.0      3.9     50.0      0.001   61900.0  46.50    0.070         6
 2200.    3.0    10.00     8.276  2900.0    1.780    0.85     1.00    3900.0         7
   0.0    0.0     0.0      0.0      0.0      0.0      0.0      0.0                    8
   0.0    0.0   -24.57   613.0      0.0      0.0                                     9
   0.0    0.0     0.0      0.0      0.0      0.0      0.0      0.0                    10
 -34.48   0.0     4.0    -112.48  -16.0     -0.5                                    11
  -5.0    5.0     1.0                                                               12

 PHIC(I),I=1,   11
    -3.550    -2.550    -1.800    -1.300    -0.950    -0.550    -0.300    -0.300    -0.400    -0.550    -0.800

  0.0      3.5      0.1      0.0      0.0      0.0                                   13

 PSIF(I),I=1,  36
      0.0      -0.400    -1.100    -2.400    -4.200    -6.200    -8.000    -8.300    -8.500    -8.200    -7.500    -6.500    -5.000
     -3.500    -2.000    -0.500     1.100     2.200     3.400     4.700     5.900     6.500     6.700     7.000     7.200     8.000
      8.900     9.000     9.400    10.100    10.300    10.800    10.900    11.000    10.900    10.500

 TQF(I),I=1,   36
      0.0       0.0       0.0       0.0       0.0       0.0       0.0       0.0       0.0       0.0       0.0       0.0       0.0
      0.0       0.0       0.0       0.0       0.0       0.0       0.0       0.0       0.0       0.0       0.0       0.0       0.0
      0.0       0.0       0.0       0.0       0.0       0.0       0.0       0.0       0.0       0.0

 TQR(I),I=1,   36
      0.0       0.0       0.0       0.0    -300.000 -5000.000 -5000.000 -5000.000 -5000.000 -5000.000 -5000.000 -5000.000 -5000.000
 -5000.000 -5000.000 -5000.000 -5000.000 -5000.000 -5000.000 -5000.000 -5000.000 -5000.000 -5000.000 -5000.000 -5000.000 -5000.000
 -5000.000 -5000.000 -5000.000 -5000.000 -5000.000 -5000.000 -5000.000 -5000.000 -5000.000 -5000.000

  0.0     -1.0      1.0      0.0     -1.0      1.0      1.0      1.0      0.0          14

 XBDRY(I),I=1,  1          YBDRY(I),I=1,  1
  10000.000 10000.000

                                                                                      9999
```

Figure 2.3-3 **INPUTS FOR TEST 12 SIMULATION**

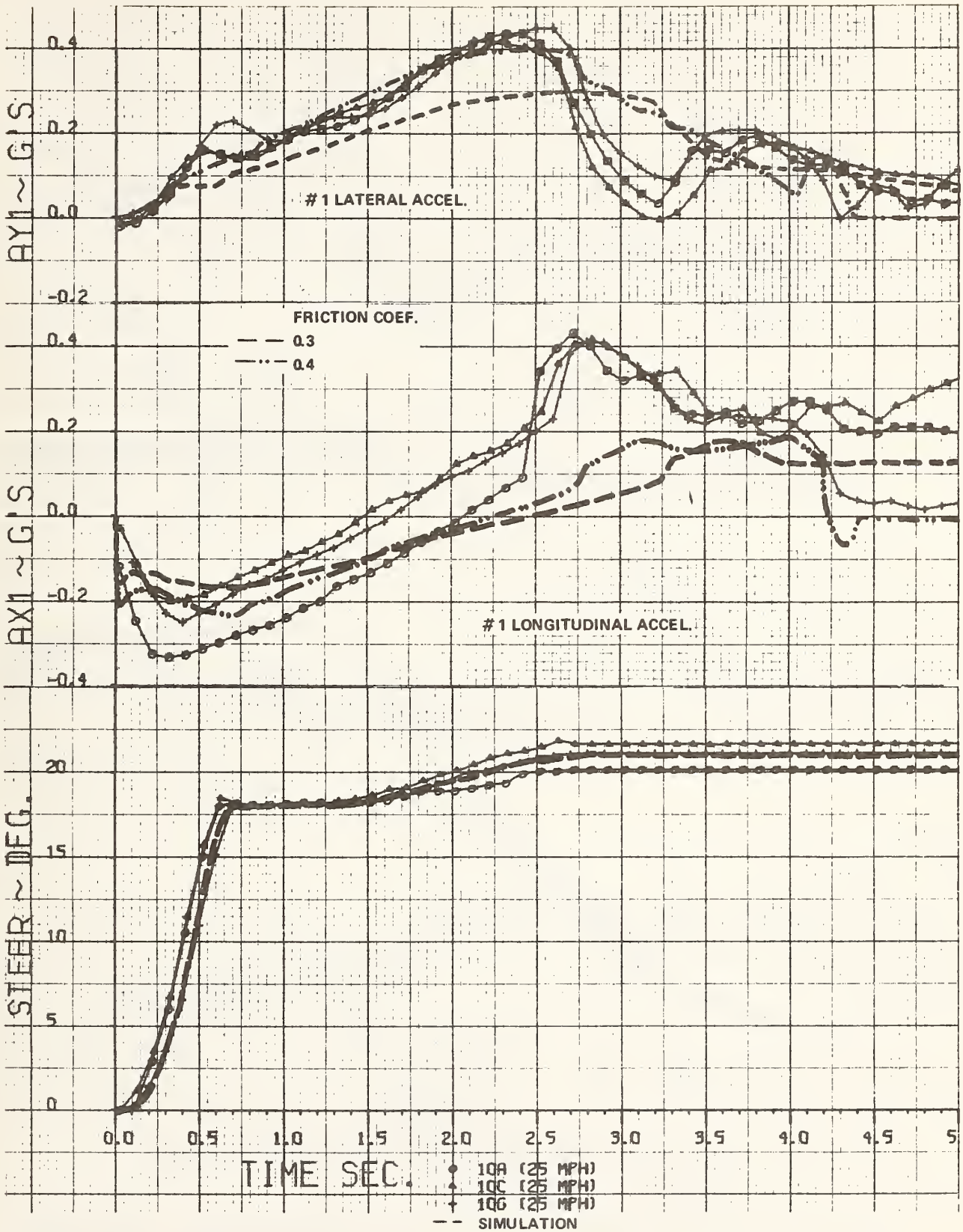

Figure 2.3-4 MEASURED AND PREDICTED RESPONSES OF VEHICLE IN FORWARD SKID ON WET PAVEMENT

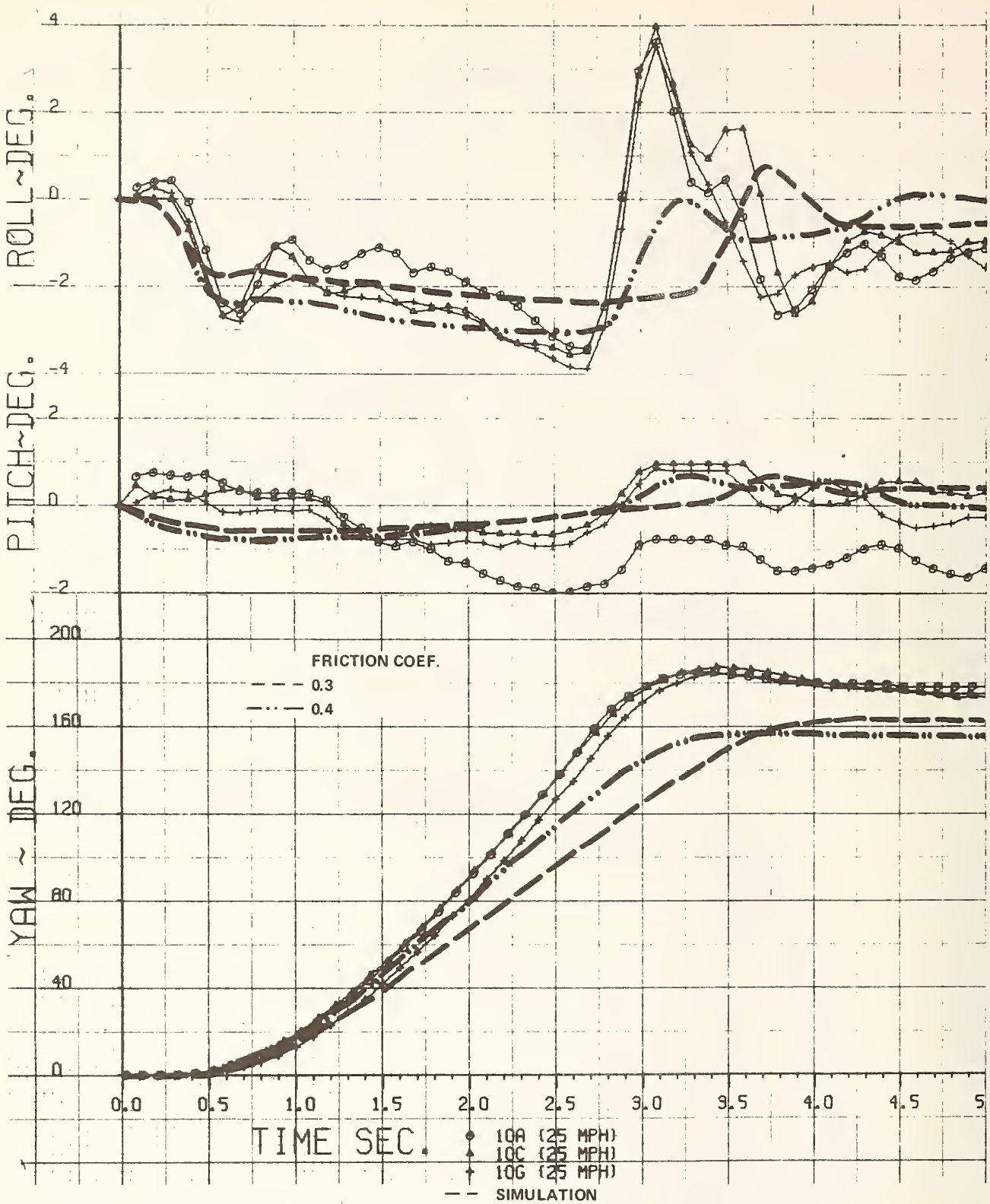

Figure 2.3-4 MEASURED AND PREDICTED RESPONSES OF VEHICLE IN FORWARD SKID ON WET PAVEMENT (continued)

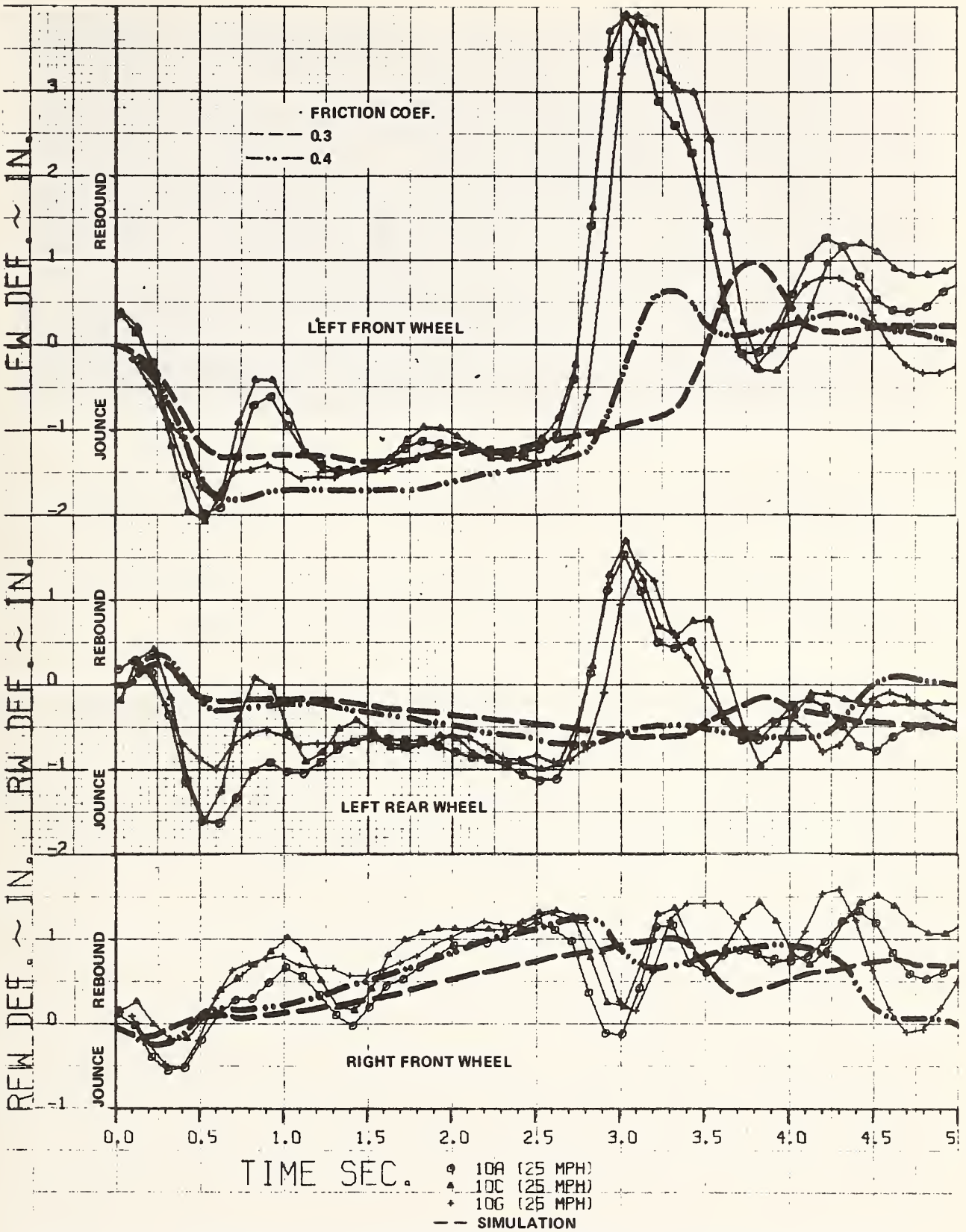

Figure 2.3-4 MEASURED AND PREDICTED RESPONSES OF VEHICLE IN FORWARD SKID ON WET PAVEMENT (continued)

It may be seen that the changes of amplitude of each measured response, and the times at which these changes occur, are duplicated by the simulation (for a friction coefficient of 0.4), although the predicted magnitudes of the changes are generally smaller. Of particular interest, perhaps, are the sudden and large excursions in the measured test responses at about t = 2.7 seconds, the occurrence of which are also predicted by the simulation model. A review of the tabular output of the simulation program revealed that these excursions coincide with the time at which the right front wheel stops sliding and the side force of that tire reverses in sign (becomes negative), while shortly thereafter, the left front wheel stops sliding and its tire side forces (positive) are greatly reduced. This explanation of the probable underlying reason for the noted excursions illustrates one advantage of a validated computer model in that sufficiently detailed output information can be provided to enable an understanding of phenomena observed in experiments which otherwise could not be explained.

A pictorial display of the predicted response is presented in Figure 2.3-5 along with time-matched frames from a movie of the test.

Measured and predicted results for the dry pavement forward skid tests (test series 12) are displayed in Figure 2.3-6. Good repeatability of the detailed responses were obtained even though the driver steered the vehicle somewhat differently in the two tests. Simulated results are shown for two assumed values of the tire-ground friction coefficient, vis., 0.75 and 0.85, to show the effects of variations of this parameter. The actual value is unknown but believed to have been within this range.

The agreement between the predictions and measurements is generally better than that achieved for the skid on wet pavement, particularly for the yaw and roll angle responses. It may be seen that the simulated vehicle closely followed the measured change in heading angle throughout the entire rotation of approximately 180 degrees. The test vehicle actually turned slightly more than 180 degrees but the yaw angle could not be measured beyond this value because the polarity of the gyro pickoff signal reversed at

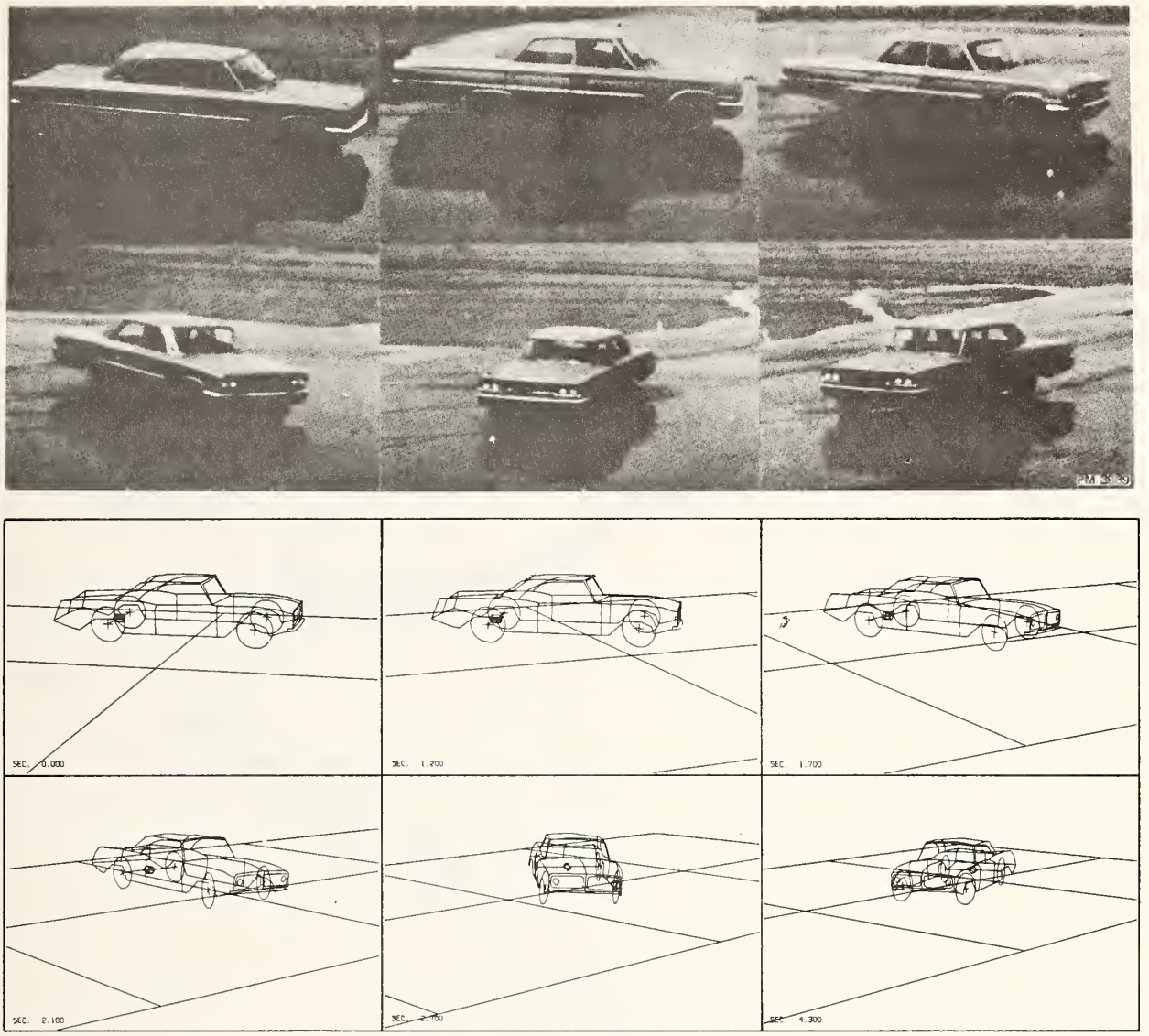

Figure 2.3-5 PHOTOGRAPHIC AND COMPUTER GRAPHIC DISPLAY OF SKIDDING VEHICLE

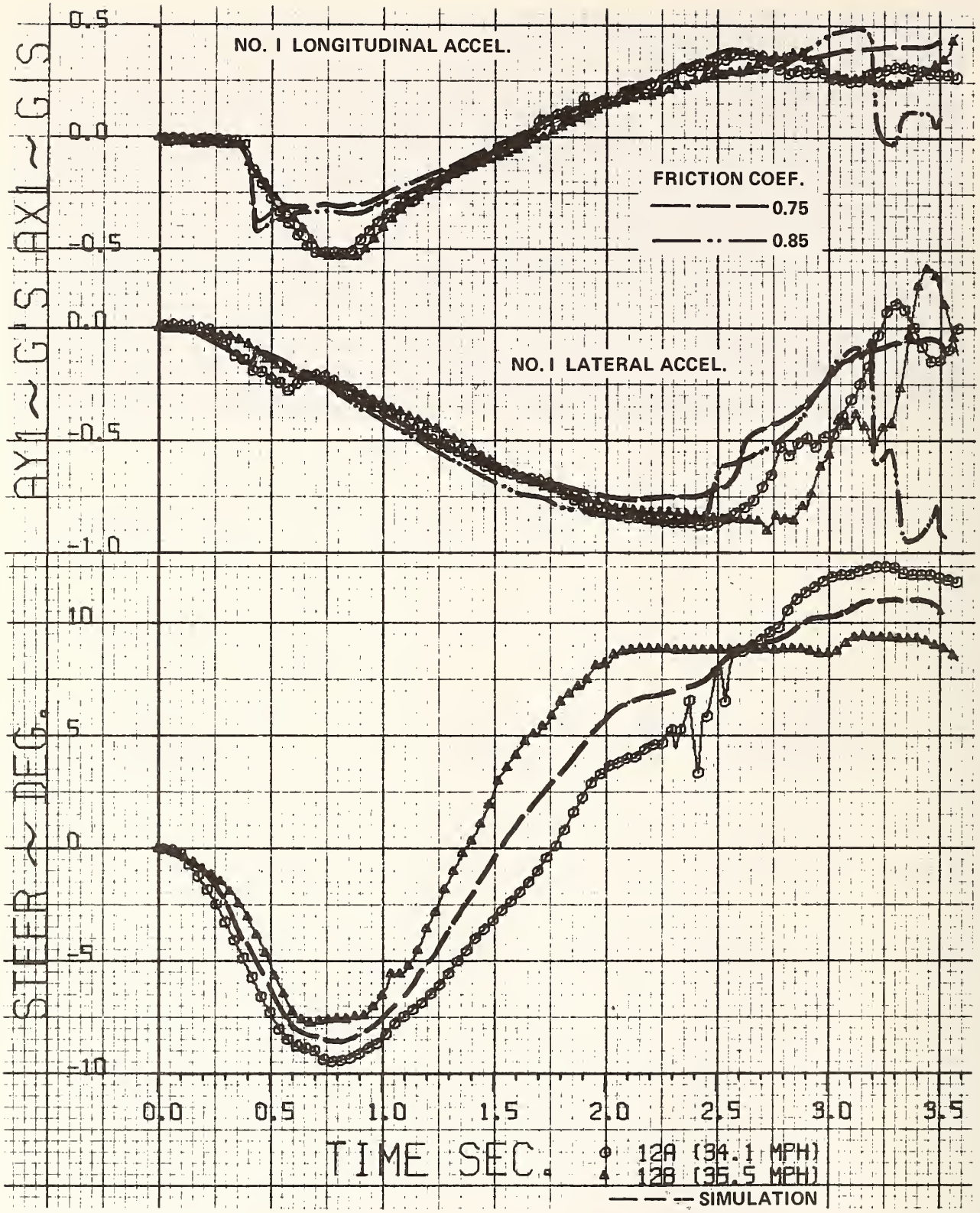

(1 of 3)

Figure 2.3-6 MEASURED AND PREDICTED RESPONSES OF VEHICLE IN FORWARD SKID ON DRY PAVEMENT

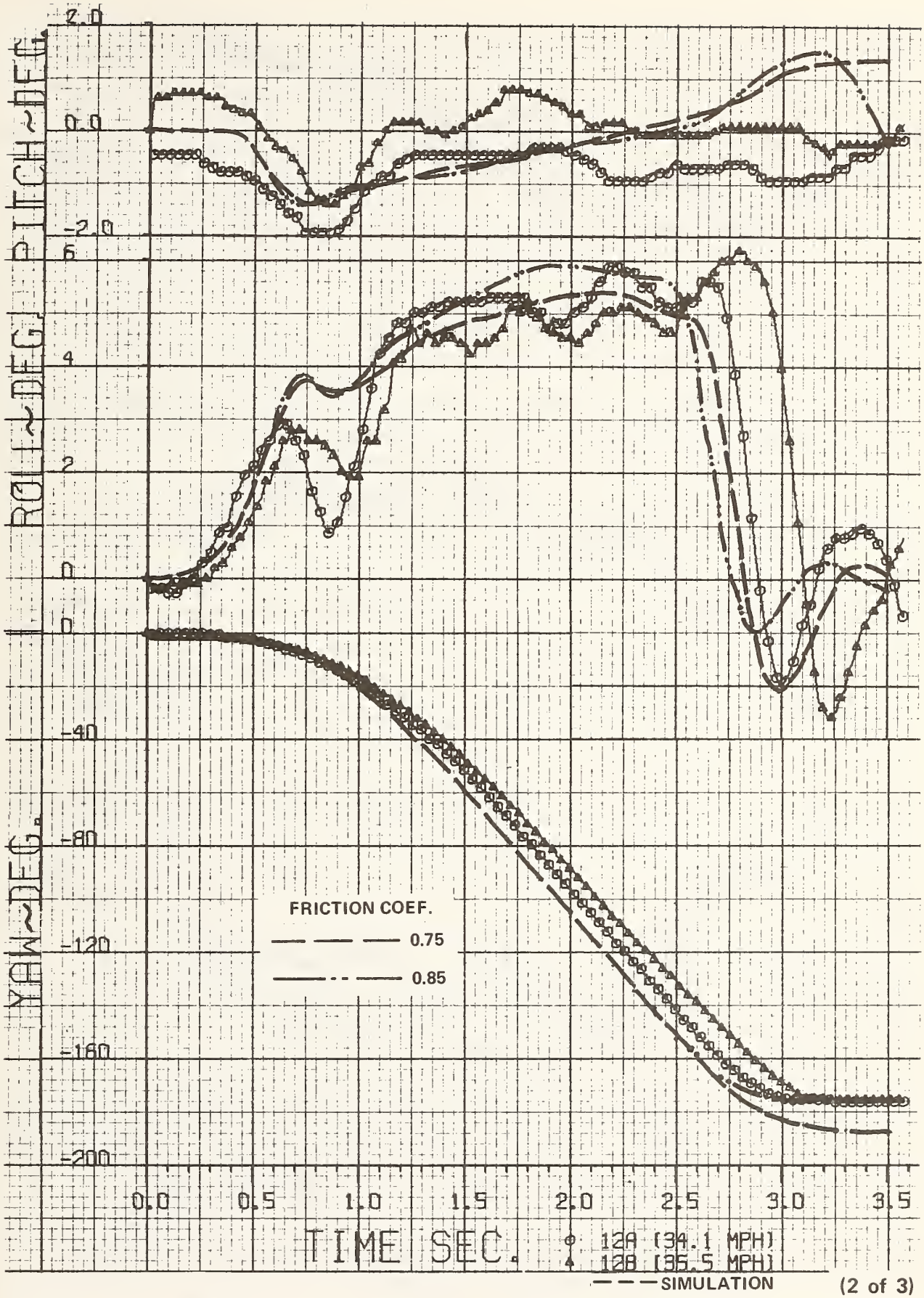

(2 of 3)

Figure 2.3-6 MEASURED AND PREDICTED RESPONSES OF VEHICLE IN FORWARD SKID ON DRY PAVEMENT (continued)

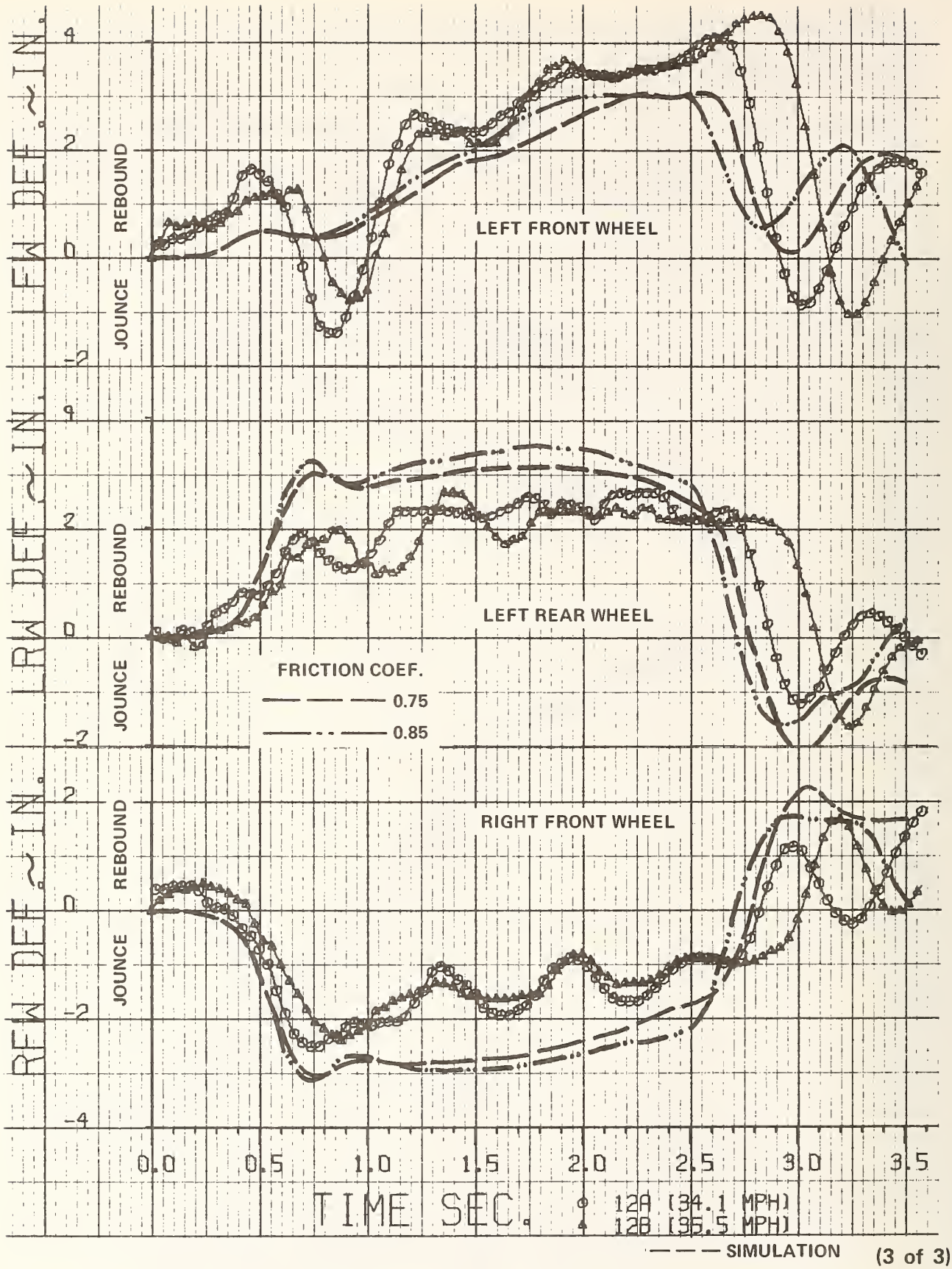

Figure 2.3-6 MEASURED AND PREDICTED RESPONSES OF VEHICLE IN FORWARD SKID ON DRY PAVEMENT (continued)

this point and caused the oscillograph galvanometer trace to be driven off the record. The principal difference between the predicted and measured results appears in the plot of the right front wheel suspension deflection, which shows a slightly higher sustained jounce deflection for the simulated vehicle. Recovery from the maximum value of positive 6 degrees of roll occurs slightly earlier in the predictions, which action is also reflected in the plots of each of the suspension deflections. The accelerations of the passenger compartment are accurately predicted.

The reverse skid test (test series 11) measurements and computer simulation results are presented in Figure 2.3-7. Considering the complexity of the driver control inputs required to execute the maneuver, the repeatability of the responses measured in these tests is indeed surprisingly good.

Part of the data for the front wheel steer angle for these tests are lacking because of inadvertent improper positioning of the oscillograph trace on the record. Estimates of the steer angles were, therefore, made by extrapolating to the limiting steer angle, with the assumption that the steering rates were constant and equal to those immediately preceding and following the region in which the recording trace was missing (steer angles less than -15 degrees). The magnitudes and times of application of other control inputs that could not be directly recorded (engine braking resulting from shifting from reverse to low gear and subsequent tractive torques from throttle application) that were used in the computer simulation of this test were also estimated from the measured time history of longitudinal acceleration (AX1) and the documentary movie films.

Excellent correlation with the test measurements was obtained with the computer simulation, particularly the results shown for an assumed tire-ground friction coefficient of 0.85. It is interesting to note that the larger value of friction coefficient resulted in the vehicle rotating more rapidly and through a slightly greater change in heading angle. In addition, the measured sudden change in lateral acceleration at approximately t = 2.6 sec. is much more closely matched.

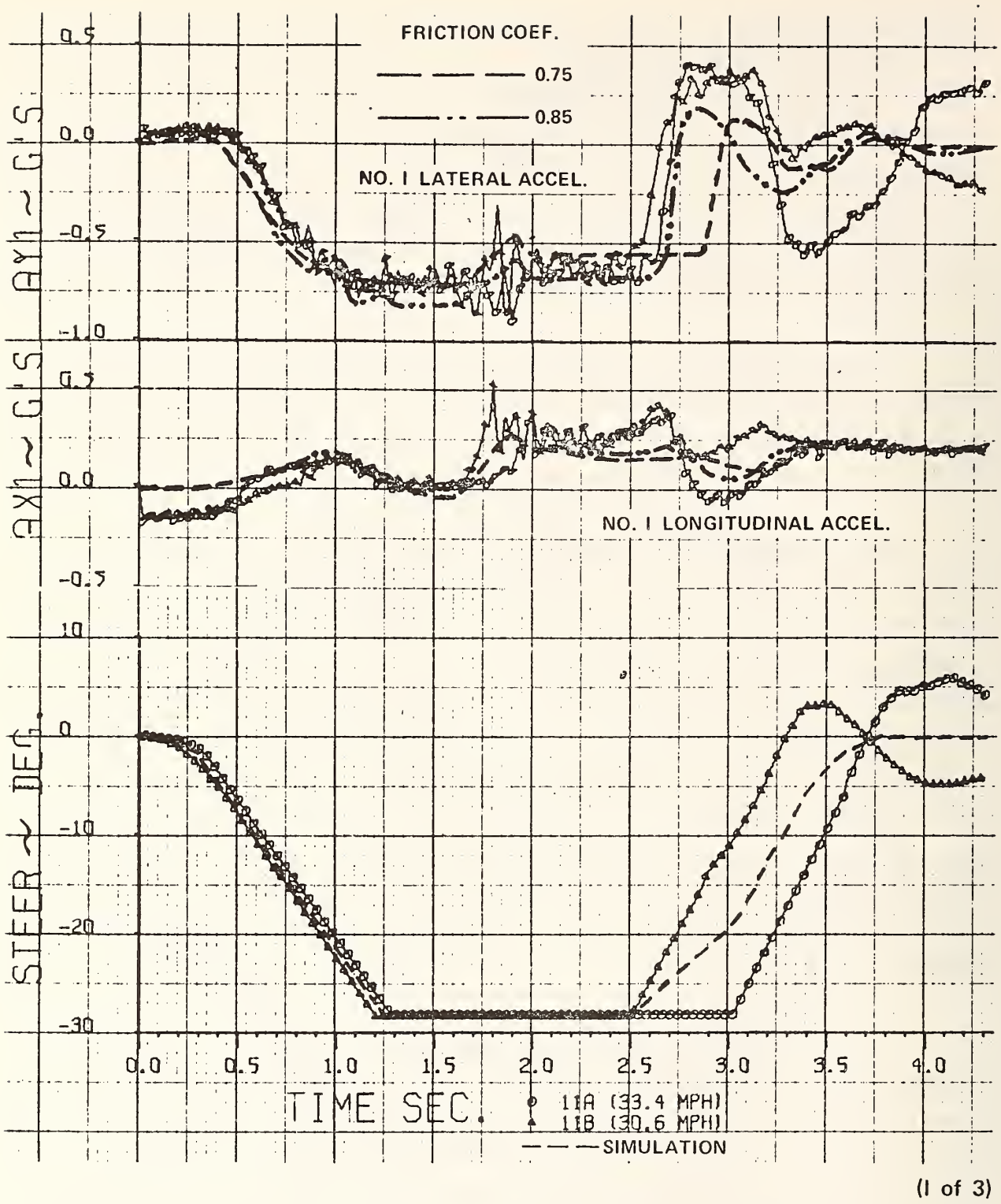

Figure 2.3-7 MEASURED AND PREDICTED RESPONSES OF VEHICLE IN REVERSE SKID ON DRY PAVEMENT

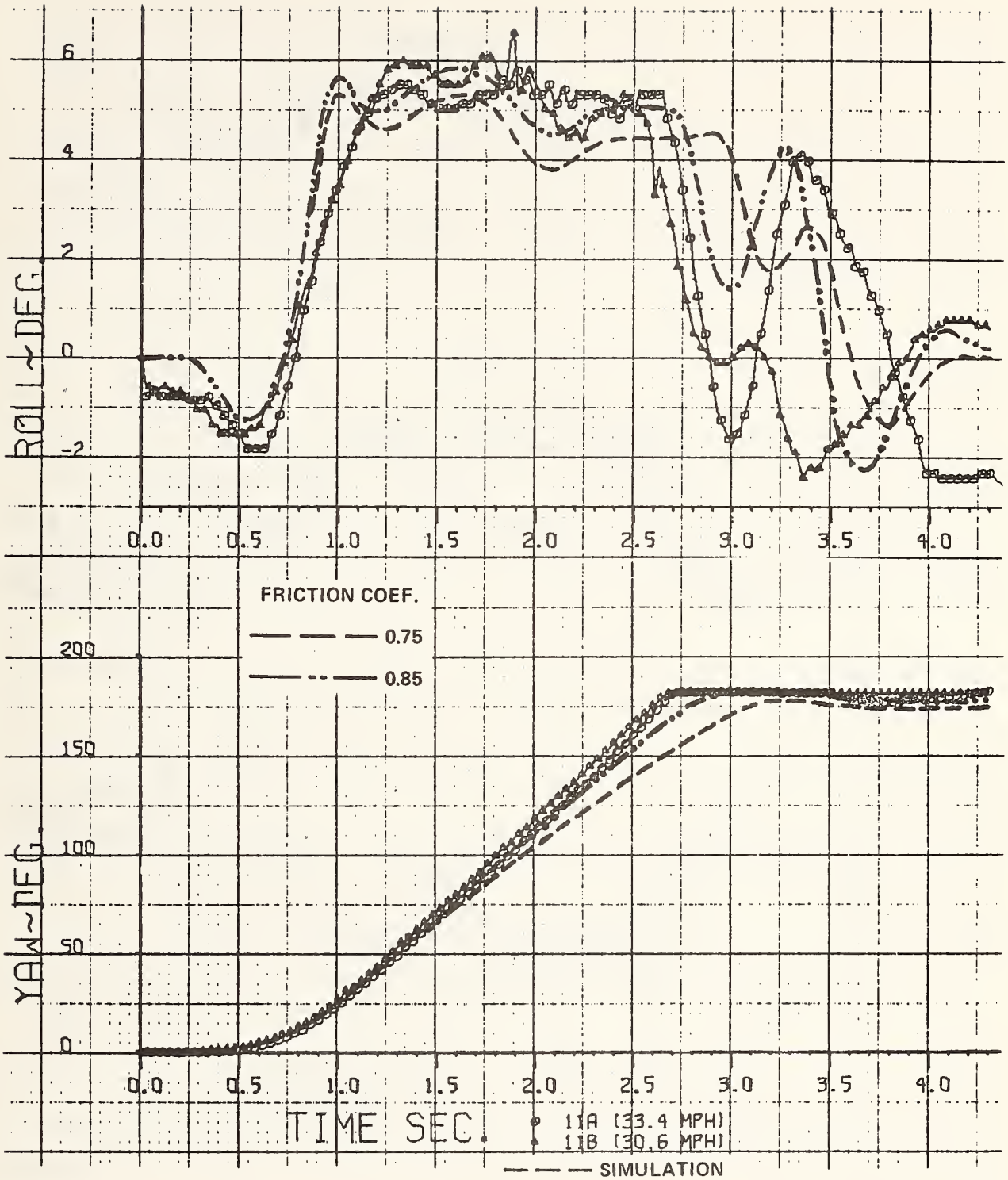

(2 of 3)

Figure 2.3-7 MEASURED AND PREDICTED RESPONSES OF VEHICLE IN REVERSE SKID ON DRY PAVEMENT (Continued)

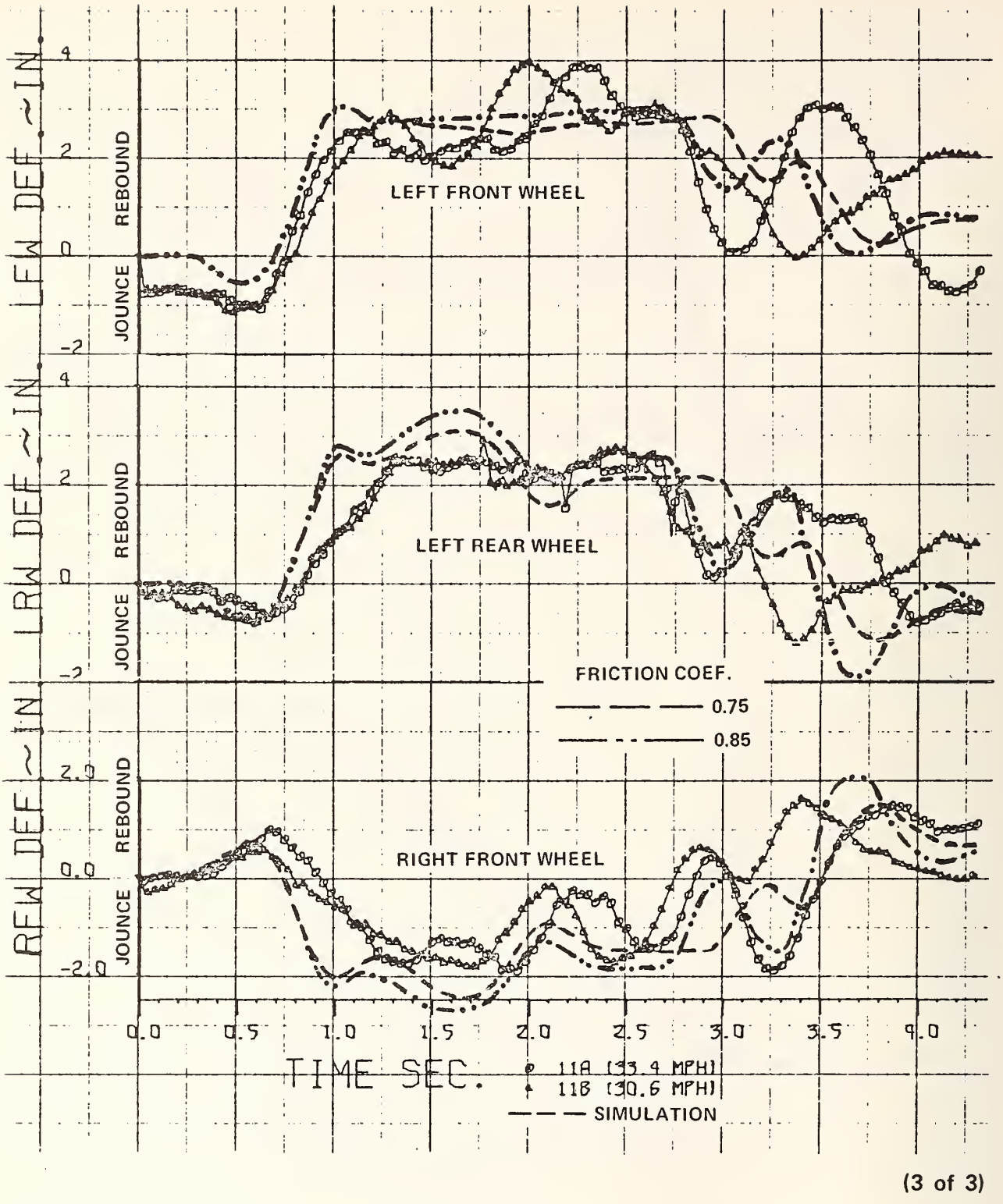

Figure 2.3-7 MEASURED AND PREDICTED RESPONSES OF VEHICLE IN REVERSE SKID ON DRY PAVEMENT (Continued)

From the measurement plots of the longitudinal acceleration, it is evident that the vehicle was accelerating backwards at approximately 0.15 g during the first half-second of the test. The present analytical model does not have the capability of simulating a vehicle accelerating in reverse (negative tractive torques). For this reason, no wheel torques were used in the simulation runs for this period. Furthermore, the average of the vehicle speeds at "time zero" for the tests, as determined from film data, was assumed for the initial velocity, i.e., no velocity change due to accelerating in reverse was considered.

The large change in yaw attitude of the vehicle in the skidding tests created some difficulty in achieving an accurate measurement of the true pitch and roll motions, partly because of the test procedure employed. If the spin axis of the pitch-roll gyro is misaligned with the true vertical at the time of uncaging the gimbals, subsequent pure yaw rotations about the vehicle yaw (vertical) axis will produce erroneous pitch and roll signals, which vary with the yaw angle.

That this indeed was the case during the first series of skidding tests was evidenced by the pitch attitude oscillograph record which indicated that the vehicle, when completely stopped after rotating 180 degrees in yaw, was in about a 4 degree nose down attitude. Since this was obviously an instrumentation error, the alignment of the gyro package in the vehicle was checked and found to be 2 degrees off the vertical under the loading condition of the test. This inclination would produce an erroneous indicated pitch change of 4 degrees with a 180 degree change in the vehicle heading. The error in the indicated roll attitude varies as the sine of the yaw angle and would have a maximum value of 2 degrees.

The experimental pitch and roll data that are shown in Figure 2.3-4 are corrected data for an assumed misalignment of the gyro spin axis of 2 degrees. Because the gyros were uncaged while the vehicle was in motion and pitching slightly during the approach to the skid area, the actual misalignment of the spin axis from the vertical could vary slightly depending

upon the instantaneous attitude of the vehicle at uncaging. This is believed to be the principal reason for the pitch and roll angle deviations that occurred in some of the test runs.

2.3.5 Vehicle Response Sensitivity

No vehicle response sensitivity analysis was conducted for this test series.

2.4 Bridge Rail Impact Test HVOSM-SM11

2.4.1 Test Vehicle and Instrumentation

The test vehicle for the bridge rail impact test was a 1963 Ford Galaxie four-door sedan formerly used by the New York State Police. The automobile was self-powered and equipped with automatic control systems for accelerating up to speed and for steering during the approach to the point of impact with the bridge railing.

The automatic guidance system consisted of a pair of coils mounted on the front bumper which sensed lateral displacements from a signal wire embedded along the center line of the approach roadway. Unbalanced electrical signals from the coil pickups, when the vehicle is not in the center of the roadway, are amplified and applied to an electrohydraulic servo valve which controls the flow of oil to the vehicle power steering actuator cylinder to steer the car back on the desired path.

The speed control system was an adaptation of an automatic speed control unit for automobiles that is available commercially. The system was adjusted so that the vehicle would accelerate from zero speed to maximum throttle opening. Vehicle speed was measured by a sensor driven by the speedometer cable, and the throttle setting was reduced as the speed approached the desired preset terminal impact speed.

A manually controlled brake application system was also installed in the vehicle, for reasons of safety, to provide an abort capability during the approach to the bridge railing and for braking the vehicle after the impact.

2.4.1.1 Vehicle Parameters

The vehicle employed in the impact test was a 1963 Ford, similar to the one used in prior validation experiments. Consequently, the basic vehicle parameters used in the simulation were the same as reported in Section 2.1.1.1 with minor differences to account for total weight and weight distribution.

Bridge Rail Configuration

The experimental bridge rail for the first test, shown in the photographs of Figure 2.4-1, consisted of two continuous, horizontal beam rails connected by means of lever arms to tabular torsion posts that support the entire structure. Flexibility of the barrier was achieved through twisting of the torsion posts, allowing the relatively stiff rails to deflect laterally up to 10 inches before reaching the yield stress of the post material.

The ground clearance of the lower of the two 8" x 6" x 1/4" rails was 10 inches; overall height of the bridge railing was 34 inches. The calculated effective overall lateral bridge railing stiffness was approximately 4000 lbs/in.

The design of the bridge rail for the second full-scale test was similar to the first configuration, the major difference being in the design of the torsion tube lever arms. The stiff rectangular tube lever arms were replaced by a leaf spring arrangement which would bend under the applied impact loads to increase the elastic deflection range of the bridge railing. The modified lever arms were designed to provide an additional 10 inches of elastic deflection (20" total), thereby effectively doubling the elastic range of the first test configuration. The effective lateral stiffness of the bridge railing was, therefore, halved to a value of approximately 2000 lbs/in.

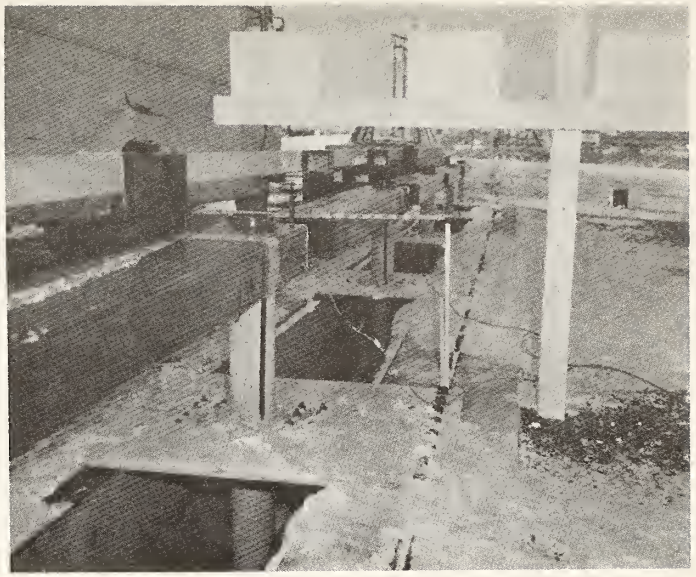

Figure 2.4-1 BRIDGE RAILING INSTALLATION FOR TEST NO. 1

2.4.1.2 Instrumentation

Instrumentation mounted on the vehicle to measure its dynamic responses during impact included a pair of two-degree-of-freedom, free gyroscopes and three accelerometers. These instruments, along with associated power supplies and signal conditioning electronics were mounted on a rigid aluminum plate securely fastened in the rear of the passenger compartment. The gyroscopes were used to measure the yaw, pitch and roll angular displacements of the vehicle with respect to a space-fixed reference axis system. The three accelerometers, located on the vehicle center line and approximately three feet aft of the center of gravity, measured passenger compartment accelerations in the longitudinal, transverse and vertical directions, respectively.

All signals from the on-board instrumentation were transmitted to recorders in an instrumentation van via an umbilical cable attached to and trailing the rear of the test vehicles. Photographs showing some of the instrumentation and equipment installed in the test vehicles are presented in Figure 2.4-2. Instrumentation characteristics are summarized in Table 2.4-1.

The bridge railings were instrumented with strain gauges to provide a measure of the dynamic loads and stresses applied to the structure during impact. For the first test, strain gauges were attached to the lever arms of post assemblies Nos. 4 and 5, i.e., on the arm closest to the point of impact (No. 4) and the adjacent arm in the upstream direction.* These strain gauges, which were located 12 inches from the centers of the posts, permitted calculation of the lateral loads transmitted by the arms and the resulting torsional moments applied to the posts.

*Post-arm assemblies are numbered 1 through 7 beginning at the downstream end of the bridge railing.

Table 2.4-1

SUMMARY OF INSTRUMENTATION TRANSDUCERS

TRANSDUCERS	DESCRIPTION	AMPLITUDE RANGE	FLAT FREQUENCY RESPONSE RANGE, Hz
VEHICLE PITCH AND ROLL ATTITUDE	HUMPHREY FG23-3191-1 FREE GYRO	PITCH (INNER GIMBAL) ±80° ROLL (OUTER GIMBAL) ±177°	- -
YAW ATTITUDE	HUMPHREY FG23-3101-1 FREE GYRO	OUTER GIMBAL ±177°	-
PASSENGER COMPARTMENT LONGITUDINAL ACCELERATION	STATHAM F50-350 S/N 1134	±50 g	0 TO ≈ 1500
PASSENGER COMPARTMENT TRANSVERSE ACCELERATION	STATHAM A39-TC-50-350 N S/N 1211	±50 g	0 TO ≈ 1500
PASSENGER COMPARTMENT VERTICAL ACCELERATION	STATHAM A39-TC-50-350 S/N 998	±50 g	0 TO ≈ 1500
DUMMY-CHEST FORE-AFT DUMMY CHEST TRANSVERSE DUMMY CHEST VERTICAL	CONSOLIDATED ELECTRODYNAMIC CORPORATION TRIAXIAL ACCELEROMETER S/N 1494	±100 g ±60 g ±60 g	0 TO ≈ 700
BRIDGE RAIL STRAINS	BALDWIN SR4-350 BONDED STRAIN GAUGE	3%*	0-50,000*
BRIDGE RAIL DEFLECTION (TEST 1)	TRANSDUCER CONTROLS CORPORATION MODEL TCC-PT-101-508 STRING POT. S/N 088-103	50 INCHES	-
ZERO TIMING SIGNAL	CAL BUILT STRIP SWITCH	-	-

*TYPICAL CHARACTERISTIC

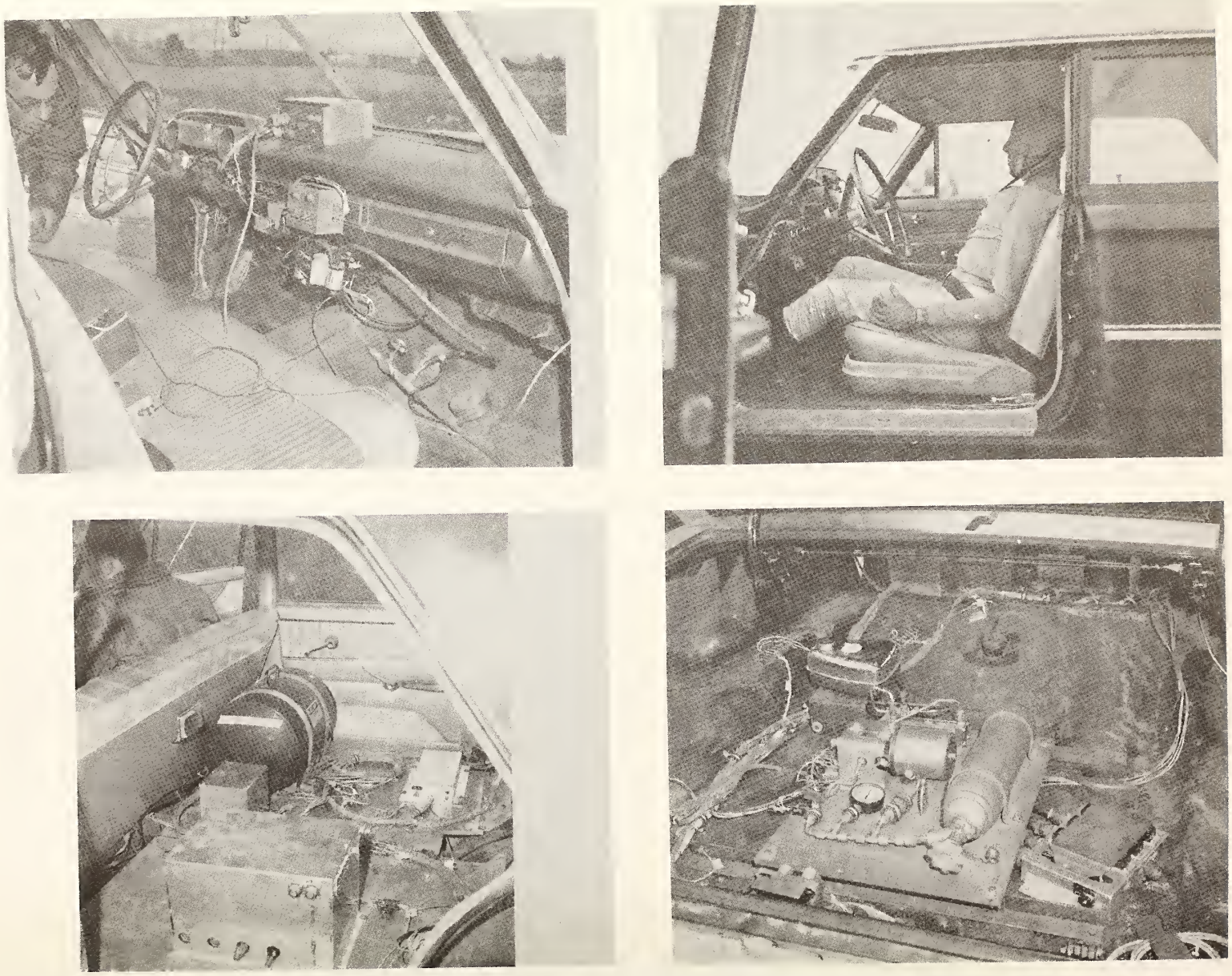

Figure 2.4-2 INSTRUMENTATION AND EQUIPMENT INSTALLED IN TEST VEHICLE

In the test of the second bridge railing configuration, three of the torsion posts were instrumented with strain gauges. A three-gauge rosette was used on post No. 4 whereas single gauges oriented 45 degrees to the axis of the torsion tubes were mounted on each of the two adjacent posts (Nos. 3 and 5).

Graduated scales attached to the ends of the torsion tube lever arms were photographed with high speed cameras to obtain time histories of bridge railing deflection. Only the deflection of post arm No. 4, which was also measured with a string potentiometer, was obtained in the first test. For the second test, the displacements of arm Nos. 3, 4 and 5 were recorded photographically.

Five high speed movie cameras using 16 mm color film and operating at frame speeds between 400 and 1500 frames per second were employed to obtain a visual record of the impacts. Cameras were located to view the car and bridge railing from both directions along the rail at ground level as well as one camera which provided an end view from an elevated position. Data cameras were also positioned behind the bridge rail to photograph graduated scales attached to the ends of the torsion post arms for determining time histories of deflection from a frame by frame analysis. All high speed data cameras were equipped with neon lamps that were triggered by a Red Lake Laboratory timing light generator for recording timing pulses on the films at 0.010 second intervals.

Documentary photographic coverage was obtained with another movie camera operated at a nominal speed of 50 frames per second and by still photos of the vehicle and bridge railing before and after the tests.

2.4.2 Data Acquisition and Reduction

Signals from the various instrumentation transducers were amplified by Nexus USL-1 solid state operational amplifiers which, for vehicle instruments, were mounted in the test cars along with the

necessary power supplies and associated electronic circuitry. The amplified signals were transmitted through an umbilical cable and recorded on two Consolidated Electrodynamic Corporation light beam oscillographs. Several data channels were also recorded on a Precision Instrument 7 channel FM magnetic tape recorder.

Two strip switches spaced 8 ft. apart were placed across the approach roadway a short distance ahead of the bridge railing. Closure of the switches upon traversal by the wheels of the test car produced pulses which were recorded on the oscillographs for determination of impact speed. The redundancy provided by this system, which allowed two independent calculations of the speed based either on the known spacing between the switches or on the wheelbase of the test vehicle, was a safeguard against possible malfunction of one of the switches.

Another strip switch attached to the face of the bridge railing at the point of impact closed circuits to fire flashbulbs strategically located in the field of view of all data cameras for correlation of "time zero" at initial contact in the film and oscillograph records.

2.4.3 Test Procedure

In the test of the first experimental torsion post bridge railing design, the 1963 Ford weighing 4312 lbs. impacted at a speed of 52 MPH and at angle of approach of 25 degrees. The bridge railing successfully contained the vehicle and redirected it smoothly without violent pitching or rolling motions or spin-out due to snagging. A photographic sequence of the impact is shown in Figure 2.4-3.

The vehicle departed from the railing on essentially a straight path at an angle of 12.5 degrees as measured from the tire tracks on the pavement. The brakes were automatically applied when the umbilical cable was torn loose from the car at 0.3 seconds after impact, and the vehicle came to rest approximately 142 feet downstream from the impact point

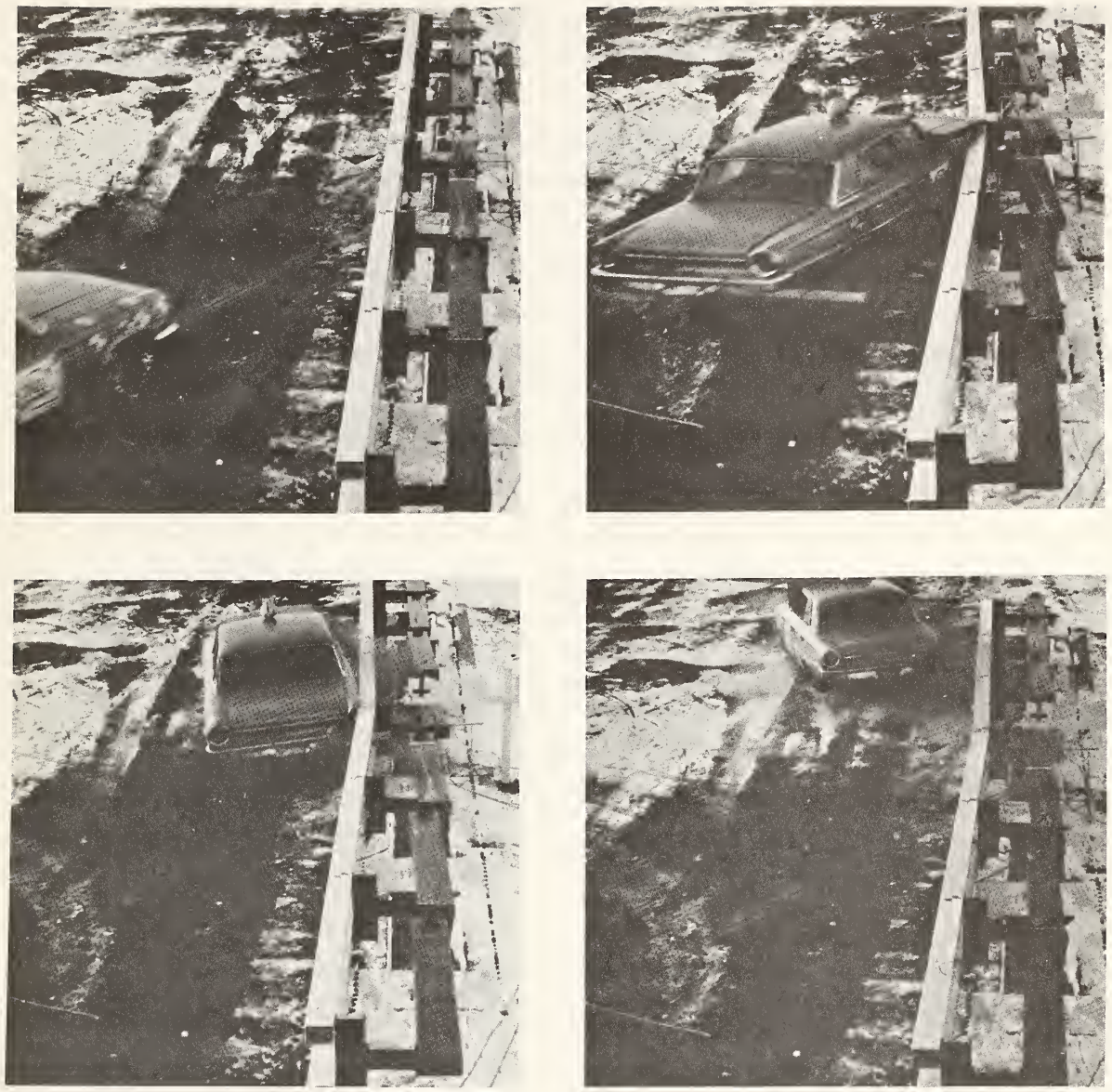

Figure 2.4-3 SEQUENCE PHOTOS OF TEST NO. 1 IMPACT

near the center of the railing and 33 feet laterally onto the roadway from the rail. Scratches on the face of the rails indicated that the vehicle was in contact with the bridge railing for a distance of approximately 14 feet.

2.4.4 Comparison of Predicted and Experimental Results

The measured responses of the vehicle and the bridge railing are presented in Figure 2.4-4 along with results from computer simulations of the impact. The lateral acceleration measured in the passenger compartment was generally between 4 and 5 g's except for some short duration higher accelerations that occurred when the vehicle was in broadside contact with the rails. Note that the deflected railing was returning from the maximum deflected position at the same time that the rear of the car swung rapidly around to impact the railing which probably contributed to the increased lateral acceleration at that time. Also, because the accelerometer was located approximately 3 feet aft of the center of gravity, the measured accelerations include effects of the angular acceleration of the vehicle about the yaw axis. Hence, the accelerations shown are initially less than those at the vehicle c.g. and later greater as the effective point of application of the impact force moves aft of the center of gravity.

Data for all on-board instrumentation was terminated when the umbilical cable became disconnected from the vehicle at 0.3 seconds after initial contact with the railing. No data were obtained for the longitudinal and vertical accelerations of the car because of a failure in the power supply for these instruments. Although pitch and roll data were obtained, these data are not presented since the maximum values in each case were only approximately 3.5 degrees.

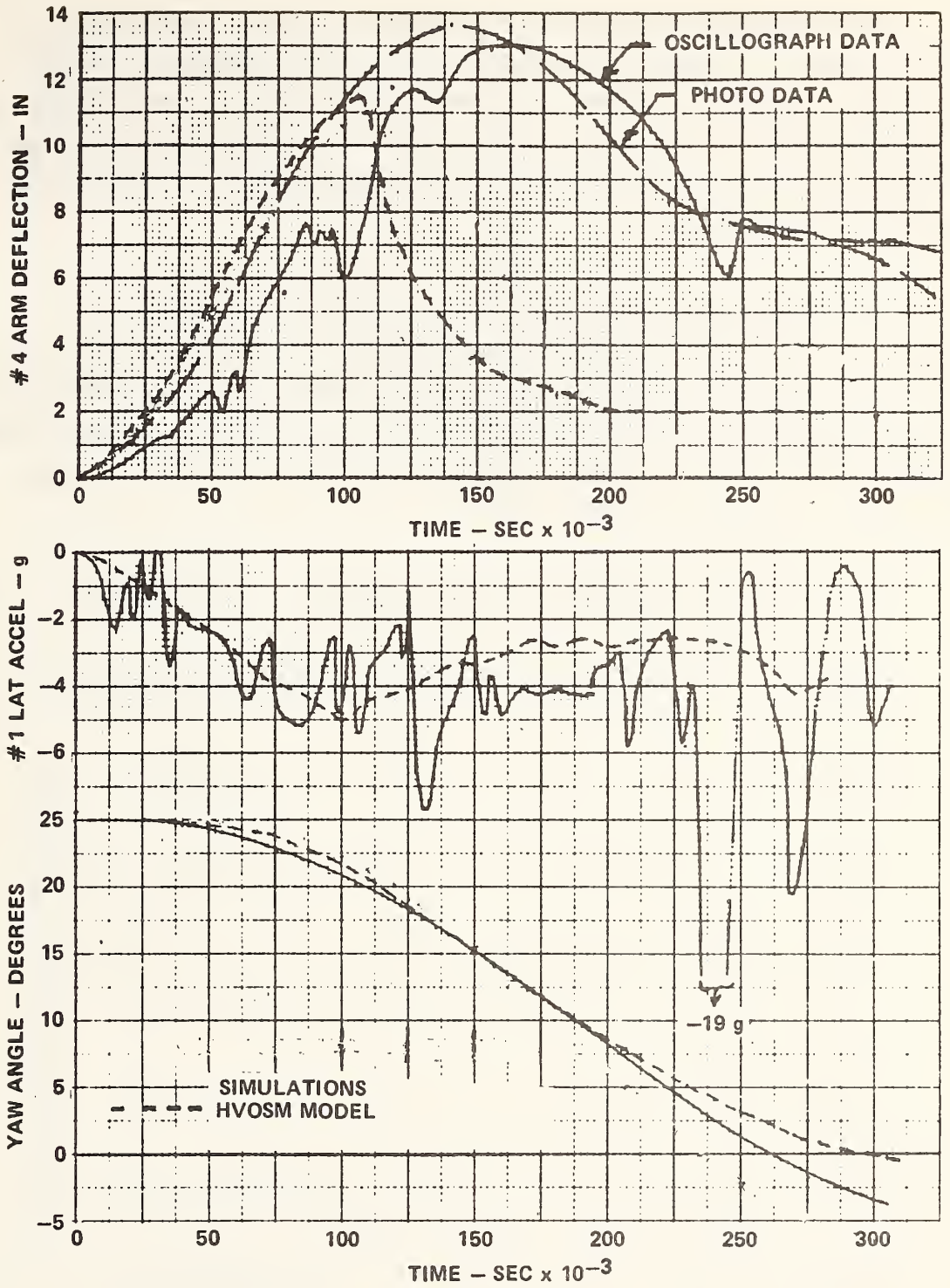

Figure 2.4-4 VEHICLE AND BRIDGE RAILING RESPONSES – TEST NO. 1

The simulation results shown in Figure 2.4-4 compare favorably with the measured responses except for the barrier deflection during unloading. However, it should be noted that the effective spring rate of the actual bridge railing decreased markedly when the torsion post nearest the point of impact (No. 4) failed at 100 milliseconds which resulted in greater rail deflections.

The inputs used in the simulation comparison are shown in Figure 2.4-5. It should be noted that difficulties in the logic associated with determining the vehicle-to-barrier interface were encountered when significant roll of the vehicle took place. Consequently, it was necessary to artificially increase the roll moment of inertia in order to suppress vehicle roll response to obtain a solution.

2.4.5 Vehicle Response Sensitivity

No response sensitivity analysis was conducted.

```
SINGLE VEHICLE ACCIDENT SIMULATION
RUN D.C. BRIDGE RAIL TEST 1 COMPARISON

  0.0     0.4     0.005                   0.002    70.0     0.0       0.0     -1.0                    1
  1.0                                                                                               2
  9.6066  0.608   0.945    386.4  599999.0  33500.  33800.   -192.   435.6                        3
 52.04    67.21   61.2      60.5    9.1193  10.8078  -2.0     15.0    4400.                        4
131.0     25.0    3.0        1.3   58.0      0.001  266000.                                       5
194.0     25.0    4.25       1.75  97.0      0.001  59244.0  46.52   0.059                        6
1098.     3.00    10.00      8.276 2900.0    1.780   0.500    1.00   3900.0                       7
  0.0     0.0     25.0       0.0     0.0     0.0     0.0     0.0                                   8
  0.0     0.0    -22.0     915.2     0.0     0.0                                                   9
  0.0     0.0     0.0        0.0     0.0     0.0     0.0     0.0                                  10
-36.96    0.0     4.0      -50.      0.0     0.0                                                  11
 -5.0     5.0     1.0                                                                            12

PHIC(I),I=1,   11
 -5.700   -3.900   -2.450   -1.300   -0.400    0.300    0.600    0.650    0.300   -0.400   -1.300

  0.0     0.5     0.05      1.0      0.0       0.0                                                13

TOF(I),I=1,   11
  0.0     0.0      0.0      0.0      0.0       0.0      0.0   -5000.000 -5000.000 -5000.000 -5000.000

TOR(I),I=1,   11
  0.0     0.0      0.0      0.0      0.0       0.0      0.0   -5000.000 -5000.000 -5000.000 -5000.000

  0.0    -1.0      1.0      0.0     -1.0       1.0      1.0      1.0      0.0                       14

XBDRY(I),I=1,   1          YBDRY(I),I=1,   1
 10000.000 10000.000

 492.0   600.0    0.4   3000.0    0.075    1.5                                                     17
  80.0    0.50  -34.0   -10.0     84.0   -125.     38.0    -16.0    14.0                          18
   4.0    0.0     1.0     0.4      1.0     500.     0.002    3.0                                   19
   0.0 4000.0     0.0     0.0      0.0      0.0      0.0      0.0      0.0                        20
   0.0    0.0
                                                                                                  9999
```

Figure 2.4-5 HVOSM IMPACT COMPARISON INPUTS

2.5 Straight Ahead Braking HVOSM-VD1

2.5.1 Test Vehicle and Instrumentation

The test vehicle which was instrumented and used to obtain the braking dynamics validation data was a 1963 Ford Galaxie four-door sedan (Figure 2.5-1) equipped with power steering and power brakes. This vehicle is identical to that used in earlier validation efforts (Sections 2.1.2.4) and thus eliminated the need to remeasure all the vehicle parameters. The basic vehicle parameters as previously measured and reported were appropriately modified to account for the instrumentation which was installed for the present tests. Additional parameters were required to define the vehicle drive-line and brake system. The procedures used to measure these parameters and the results obtained are presented in Section 2.5.1.1.

Inspection of the brakes on the car as received, revealed significant scoring of the drums and shoes and one leaking wheel cylinder which had saturated the shoes of that wheel. To assure that the braking system would perform in a uniform and predictable manner for the tests, a complete brake system overhaul was performed. Two of the brake drums were replaced, and all four drums were machined to remove taper, scoring and out-of-round. The wheel cylinders were rebuilt and all the brake linings replaced and cam ground match the drums. The car was driven for a period of time on the test track in a manner so as to "wear in" the linings prior to the brake calibration measurements and the validation tests.

The only other modification to the vehicle, other than installation of the instrumentation system, was the installation of a new set of tires and wheels to match those for which tire data was obtained. The tire data was supplied by General Motors for "current" model tires. This data was for Uniroyal G78-14 bias-belted, polyester-fiber glass tires (product/size number 3781-143) mounted on six inch rims.

Figure 2.5-1 **TEST VEHICLE**

2.5.1.1 Vehicle Parameters

Except for small modifications to account for the installed instrumentation system, the basic vehicle parameters defining its component masses, dimensions, suspension system, etc., were the same as those used in Section 2.1.1, because the two test vehicles were identical. These basic parameters for the vehicle in the test configuration (i.e., including instrumentation and data recording system, full fuel tank, driver -- 130 lbs. and front seat passenger -- 190 lbs.) are summarized in Table 2.5-1.

The tire data were supplied by General Motors. An analytical fit to these experimental data for use in the computer simulation was made. The tire parameters resulting from this fit are summarized in Table 2.5-2. The radial stiffness, K_T, of the tire in its linear range was determined from the measured change in tire radius between the no load condition and its nominal static load condition. The parameters (σ_T and λ_T) defining the change in radial tire stiffness for large loads are estimates based on very limited available data. The parameter AMU is used to establish the level of the tire/ground locked wheel friction coefficient, μ. The RATIO table is the means by which the variation of μ with speed and vertical tire load is implemented in the simulation.

The computer simulation includes the wheel and drive-line equations of motion and thus requires that the respective moments of inertia be specified. These moments of inertia were measured as part of this effort and are summarized in Table 2.5-3. The procedures by which these inertias were measured are described in the following paragraphs.

Table 2.5-1

BASIC PARAMETER VALUES OF TEST VEHICLE
1963 FORD GALAXIE FOUR-DOOR SEDAN
(with Driver and Front Seat Passenger)

Parameter		Value Used
M_s	$(lb\text{-}sec^2)/in.$	11.05
M_{uF}	$(lb\text{-}sec^2)/in.$	0.608
M_{uR}	$(lb\text{-}sec^2)/in.$	0.945
I_x	$in\text{-}lb\text{-}sec^2$	6000
I_y	$in\text{-}lb\text{-}sec^2$	40000
I_z	$in\text{-}lb\text{-}sec^2$	40000
I_{xz}	$in\text{-}lb\text{-}sec^2$	-192
I_R	$in\text{-}lb\text{-}sec^2$	453.6
a	in.	58.5
b	in.	60.75
T_F	in.	61.2
T_R	in.	60.5
$\overline{l_s}$	in.	46.52
z_F	in.	9.05
z_R	in.	10.95
ρ	in.	-2.0
R_W	in.	13.46
K_F	lb/in.	131.0
K_R	lb/in.	194.0
C_F	(lb-sec)/in.	1.30
C_R	(lb-sec)/in.	1.75
C'_F	lb	58.0
C'_R	lb	97.0
Ω_{FC}	in.	-2.9
Ω_{FE}	in.	4.3

Table 2.5-1 (Continued)
BASIC PARAMETER VALUES OF TEST VEHICLE
1963 FORD GALAXIE FOUR-DOOR SEDAN
(with Driver and Front Seat Passenger)

Parameter			Value Used
Ω_{RC}			-4.3
Ω_{RE}			4.5
R_F	(lb-in/rad)		266000
R_R	(lb-in/rad)		59244
K_{RS}			0.059
$\phi_1 = \phi_2$	degrees		
	for $\delta_1 = \delta_2$	= -5 in.	-5.70
		4 in.	-3.90
		3 in.	-2.45
		2 in.	-1.30
		1 in.	-0.40
		0 in.	0.30
		1 in.	0.60
		2 in.	0.65
		3 in.	0.30
		4 in.	-0.40
		5 in.	-1.30

Table 2.5-2
TIRE PARAMETER DATA FOR
INFLATION PRESSURE = 28 PSI

Parameter		Value
K_T	lb/in.	1300.0
σ_T	in.	3.0
λ_T		10.0
A_0		4000.0
A_1		8.4
A_2		3000.0
A_3		1.71
A_4		4200.0
A_5		0.941
A_6		-1.783×10^{-4}
A_7		3.33×10^{-8}
Ω_T		1.0
AMU		0.987

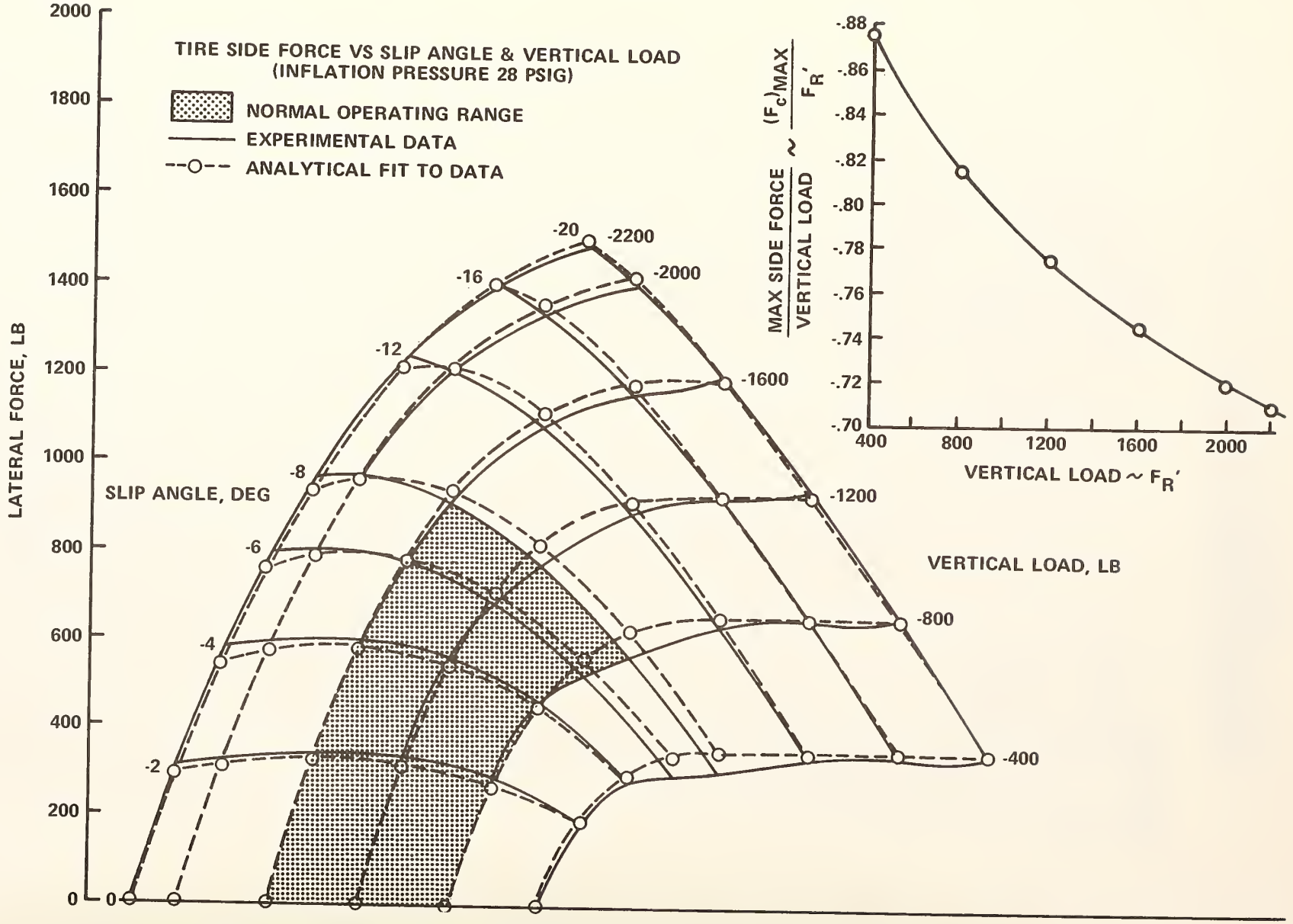

Figure 2.5-2 COMPARISON CARPET PLOTS OF MEASURED TIRE DATA AND ANALYTICAL FIT

Table 2.5-3

MOMENTS OF INERTIA

Front Wheel	12.2 in-lb-sec^2
Rear Wheel	13.6 in-lb-sec^2
Drive Line	6.5 in-lb-sec^2

The measurement of the front wheel (including brake drums, etc.) moment of inertia was accomplished by suspending the wheel (from a 10 ft. length of 1/4 inch drill rod) as a torsional pendulum. The torsional spring rate of the drill rod and the natural frequency of the resulting torsional pendulum were measured. From these measurements and the equation for the undamped natural frequency of a simple second order system, the moment of inertia of the wheel was computed. The "effective" moment of inertia of the rear wheel includes the inertia of the wheel, tire, brake drum, rear axle and those gears in the differential which can move with either wheel while the drive shaft is stationary. The effective moment of inertia of the drive line includes the inertia of the drive shaft, universal joints, transmission output shaft, differential drive pinion and shaft plus the "effective" inertia at the drive shaft of the transmission and differential gearing which moves with the drive shaft when the transmission is in neutral.

Because of the complexity and the number of components contributing to the moment of inertia of the rear wheels and drive line, it was not practical to remove them from the vehicle and disassemble them to measure the inertias of the individual component parts in the manner used for the front wheels. Instead, the "effective" moments of inertia of the rear wheels and drive line were indirectly measured by use of a forced oscillation method. In this method, the "effective" moments of inertia of the system can be indirectly determined by adding springs (of known spring rate) to the system and then measuring the system undamped natural frequency. From the undamped natural frequency and spring rate, the system effective inertia

can be computed. The undamped natural frequency of a damped system obviously cannot be obtained from free oscillation tests. It can, however, be determined by forced oscillation tests as that frequency at which the forced response of the system lags the applied shaking torque by 90 degrees. This phase relationship can be readily observed on an oscilloscope where the vertical deflection of the beam is proportional to the system response and the horizontal deflection of the beam is proportional to the applied shaking torque. The proportionality of these signals to the physical parameters need not be known -- all that is required is that each signal must be in phase with the variation of the corresponding physical quantity. The resulting "scope" patterns will become symmetric about the vertical axis when the phase lag becomes equal to 90 degrees. The shaking frequency for which this occurs is the desired undamped natural frequency.

The experimental setup used for making the rear wheel and driveline moment of inertia measurements is shown in the photographs in Figure 2.5-3. An oscillating torque of controlled amplitude and frequency was applied to one wheel by an electromagnetic shaker via a force rod, lever arm and wheel fixture as shown in the photographs.

The elastic restoring torques for the wheels were provided by a torsion bar attached to each wheel via the wheel fixtures. The end restraint for each torsion bar was provided by a simple "A" frame clamped to it which reacted the loads to the floor. The torsional stiffness of the bars could be adjusted by moving the location of the "A" frame end restraints and thereby changing the length of the bars. The elastic restoring torque for the drive shaft was provided by a cantilever leaf spring attached to it via a "U" bolt.

A signal proportional to the applied shaking torque was obtained from a pair of strain gauges mounted on the root-end of the lever arm. Signals proportional to the displacements in the system were obtained from accelerometers attached to each tire and the drive shaft. The torque and angular displacement signals were applied, respectively, to the horizontal

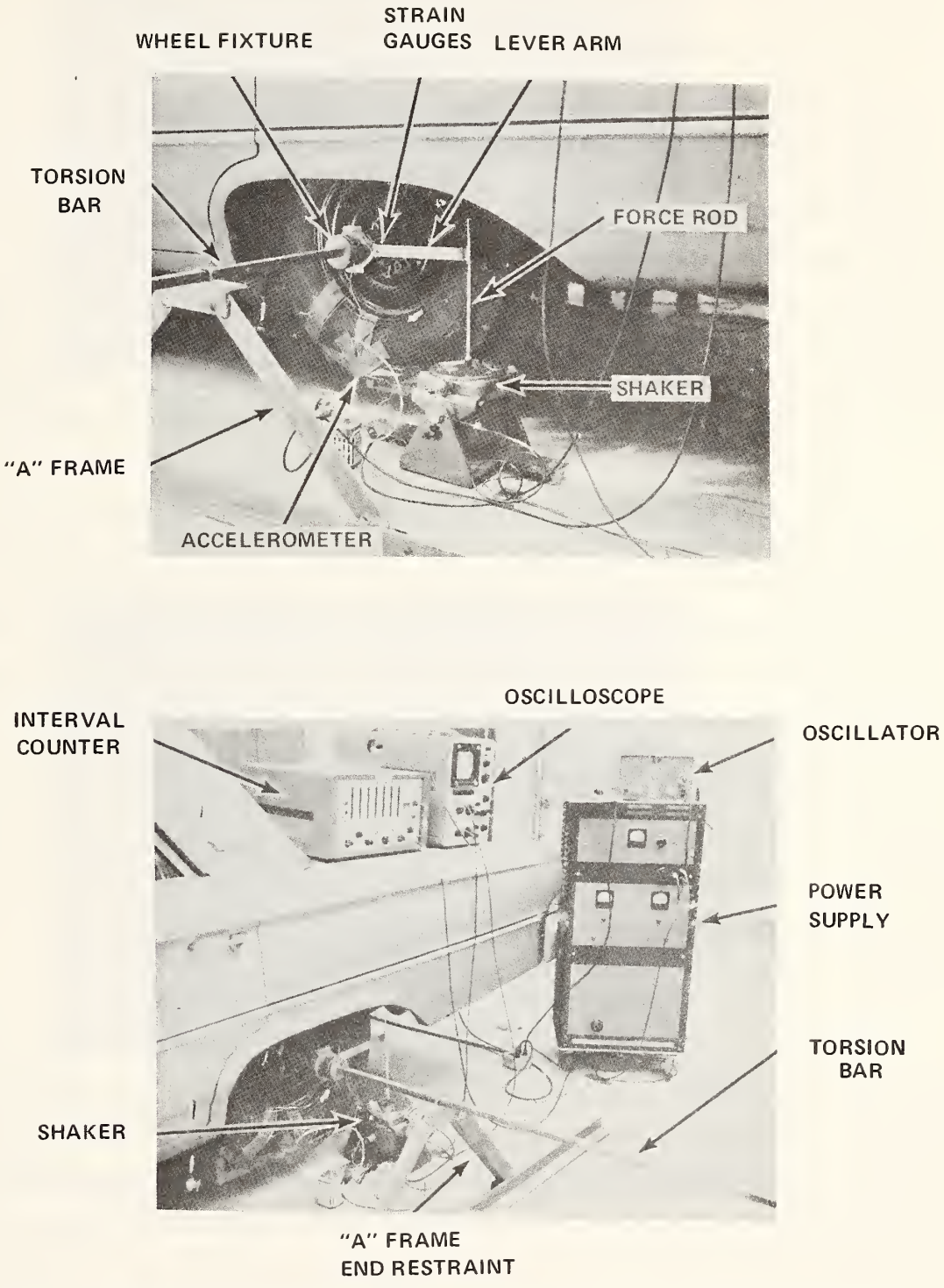

Figure 2.5-3 EXPERIMENTAL SET-UP FOR MEASURING THE REAR WHEEL AND DRIVE-LINE MOMENTS OF INERTIA

and vertical axes of an oscilloscope. The shaker was driven with a low frequency oscillator and power supply. The shaking frequency was determined from its period which was measured with an interval counter.

To determine the "effective" moment of inertia of the rear wheels, the drive shaft degree of freedom was locked out by placing the transmission in "park", and the torsion bars were used to apply a preload torque to the differential gears. The natural frequency of the rigid body mode of this system was then adjusted via the torsion bar stiffness (i.e., length variation) to be sufficiently below the natural frequency of the first elastic mode (that mode where the rear axles are elastically responding to the excitation) so as to eliminate any significant interaction between them. The torsional stiffness of the torsion bars was measured by static loading.

The natural frequency of the system was determined as that shaking frequency which resulted in a 90 degree phase lag of the response (displacements) relative to the applied shaking torque. The 90 degree phase relation is accurately identified on the oscilloscope by symmetry of the Lissajous pattern about the vertical axis. The sensitivity of the pattern symmetry to changes in the shaking frequency in the neighborhood of the natural frequency is evident in the photographs of the oscilloscope patterns presented in Figure 2.5-4. The shaking frequency which resulted in the pattern of the upper photo is judged to be the natural frequency of the system. A reduction of only 1-1/2 percent in the shaking frequency from this natural frequency resulted in the pattern of the lower photo of Figure 2.5-4.

The procedure used for determining the "equivalent" drive-line inertia follows that described above except that the transmission was in neutral and the rear wheel torsion bars were preloaded against the drive shaft spring to eliminate differential gear backlash. The "equivalent" drive-line inertia includes the inertias of the transmission output shaft and those gears that move with drive shaft while transmission is in neutral, the drive shaft itself, the universal joints, and the differential shafts and gears which move only with the drive shaft.

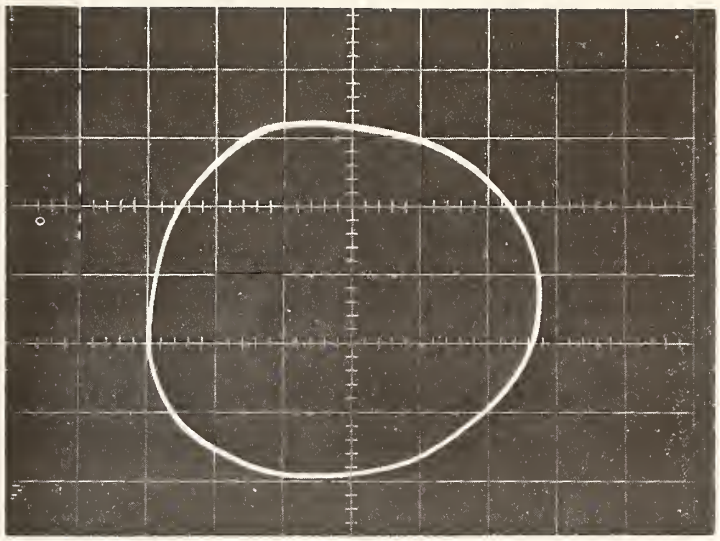

SHAKING FREQUENCY ≃ NATURAL FREQUENCY

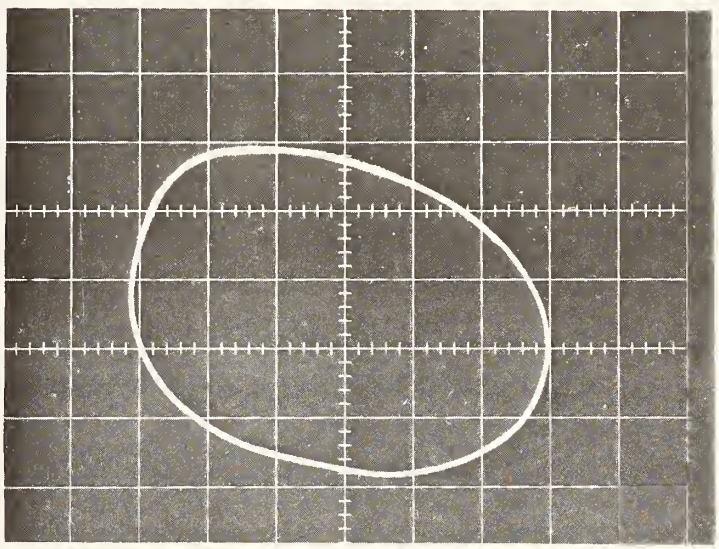

SHAKING FREQUENCY 1-1/2% BELOW NATURAL FREQUENCY

Figure 2.5-4 OSCILLOSCOPE PATTERNS OF THE FORCED RESPONSE VERSUS THE SHAKING TORQUE

The computer simulation predicts the individual wheel brake torque as a linear function of the specified time history of the brake hydraulic pressure (minus an input push-out pressure). The proportionality (brake torque coefficient) between the brake torque and the effective hydraulic pressure is a function of up to sixteen constants (G_1 through G_{16}) describing the brake, a lining fade coefficient and the brake temperature. This functional form of the brake torque coefficient is based on an analysis presented in Reference 3. The motivation for using this functional form for the brake torque coefficient was to conveniently accommodate the brake fade characteristics in the simulation as a variation of the torque coefficient with temperature.

The brake torque coefficients and push-out pressures for the test vehicle brakes were measured at room temperature. The variation of the brake torque coefficient with temperature was also measured; from this information, the variation of lining fade coefficient with temperature was derived. With the exception of G_3 , G_{12} , G_{14} , G_{15} and G_{16} , all of the constants, G_i , describing the brakes are either direct dimensional measurements or they are derived from these measurements. The constants G_3 and G_{12} (which are not measured) are the "effective" shoe/drum friction coefficients for the primary and secondary shoes, respectively. These "effective" friction coefficients are chosen so as to yield the measured brake torque coefficient at room temperature. The constants G_{14} , G_{15} and G_{16} describe the brake capacity to absorb and dissipate heat. The values used in the computations are engineering estimates based on information in Reference 4. The test vehicle is equipped with Bendix Duo-Servo brakes on the front and rear wheels.

The values of the brake parameters used in the simulation of these brakes are summarized in Table 2.5-4. The methods and equations used for determining these values for the brake parameters from the measurements are described below.

Table 2.5-4
BRAKE PARAMETERS

Parameter	Value	
	Front Brakes	Rear Brakes
Brake Torque Coefficient - $\frac{\text{in.-lbs}}{\text{psi}}$	44.50	32.00
Push-Out Pressure - psi	110.00	192.00
G_1 - inches	7.62	7.62
G_2 - ND*	1.40	1.40
G_3 - ND	0.480	0.476
G_4 - square inches	0.942	0.691
G_6 - inches	3.12	3.12
G_7 - inches	6.21	6.21
G_8 - inches	6.43	6.43
G_9 - inches	4.62	4.62
G_{10} - ND	1.00	1.00
G_{11} - inches	9.25	9.25
G_{12} - ND	0.384	0.381
G_{14} - BTU/hr/ft^2/°F	0.02	0.02
G_{15} - BTU/lb/°F	0.125	0.125
G_{16} - lbs	5.00	5.00

* ND denotes nondimensional.

NOTE: 1. The missing parameters (G5 and G13) are not required for description of the Duo-Servo brake.

2. Definitions of the individual parameters are given in Appendix I.

The following are the definitions of and equations for the brake input parameters used in the simulation. Figure 2.5-5 illustrates the required measurements of the brake assembly

G_1 — measured

$G_2 = Q$ — actuation constant for secondary shoe

$$Q = \left[\frac{G_8}{G_9} + \cos\beta_s\right] / \sin\beta_s$$

(the subscript " $_s$ " indicates secondary shoe)

$G_3 \equiv \mu_p$ — "effective" friction coefficient of primary shoe

G_4 — brake actuator cylinder area obtained from measurement of diameter

G_6 — measured

$G_7 \equiv L_p$ — for primary shoe; distance from wheel center to location of "effective" drag force; computed as follows

$$L_p = \frac{(\text{DRUM RADIUS})(4)\sin\beta_p(\cos\alpha_1 - \cos\alpha_2)_p}{(2)(\alpha_2 - \alpha_1)_p + (\sin 2\alpha_1 - \sin 2\alpha_2)_p}$$

Note all quantities are for primary shoe and α_1 and α_2 are respectively the heel and toe angles of primary shoe lining as shown in Figure 2.5-5. β_i is defined as follows (i = p or s for primary or secondary shoe)

$$\beta_i = \frac{\sin\alpha_{2i} - \alpha_{2i}\cos\alpha_{2i} - \sin\alpha_{1i} + \alpha_{1i}\cos\alpha_{1i}}{\cos\alpha_{1i} - \cos\alpha_{2i}}$$

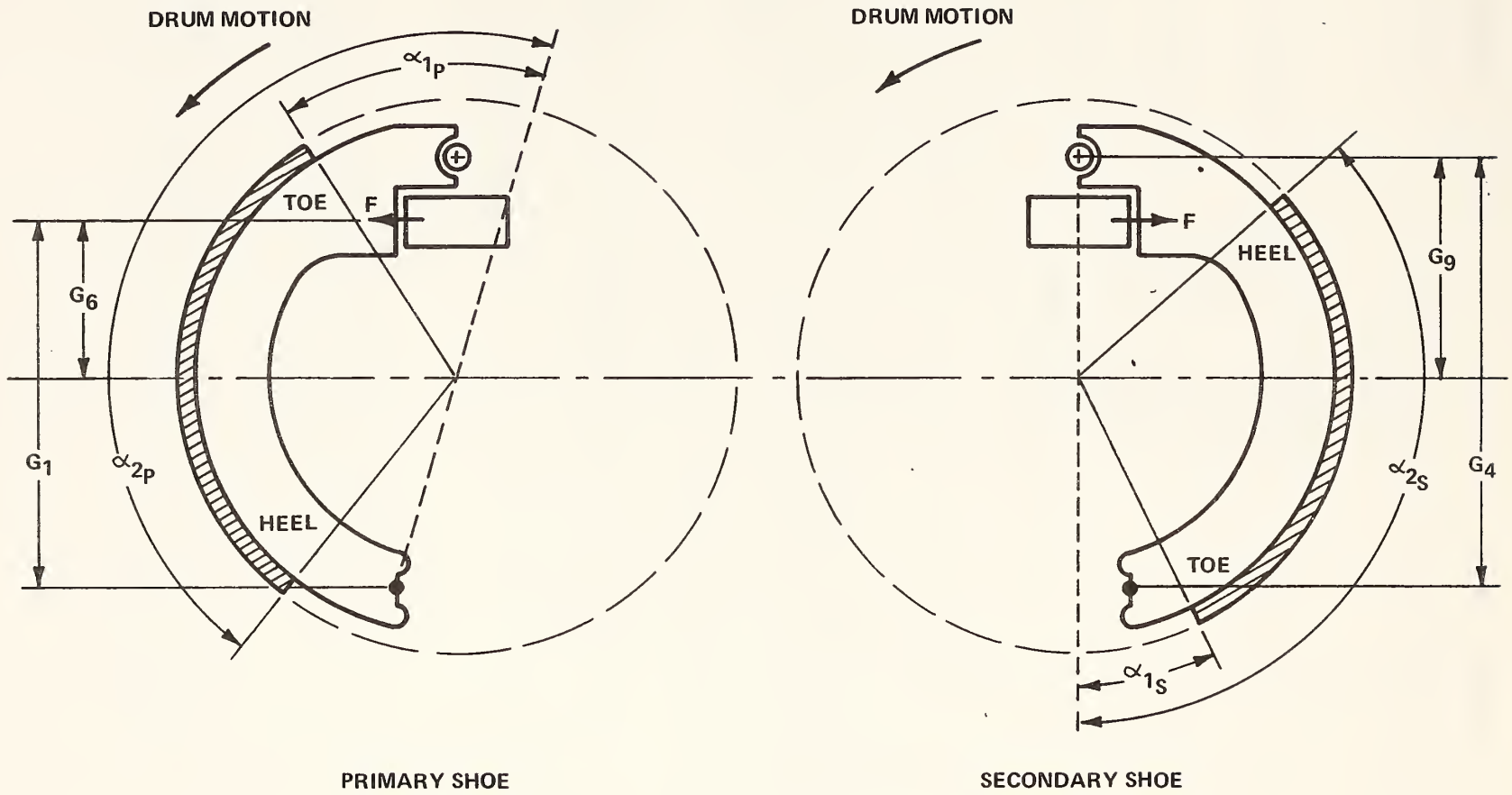

Figure 2.5-5 DEFINITION OF BRAKE MEASUREMENTS

$G_8 \equiv L_S$	same as G_7 except for secondary shoe
G_9	measured
G_{10}	$\sin \beta_S$
G_{11}	measured
$G_{12} \equiv \mu_S$	"effective" friction coefficient of secondary shoe
G_{14}	coefficient of convection heat loss - BTU/hr/ft^2/F°
G_{15}	specific heat of brake "effective" mass - BTU/lb/°F
G_{16}	effective thermal mass of brake assembly - lbs

Values for all of the above parameters were measured or derived from the measurements except the "effective" shoe friction coefficients. They were chosen so that the following equation for the Duo-Servo brake yielded the measured brake torque coefficient.

$$(1)\quad T/p = G_4 \left[\left(1 + \frac{G_6 + G_7 \sin\xi}{G_1 - G_6 - G_7 \sin\xi} \right) \left(G_7 \sin\xi + \frac{G_8 G_{11} G_{12}(LF)}{G_9 G_{10}[1 - G_2 G_{12}(LF)]} \right) - \frac{G_1 G_8 G_{12}(LF)}{G_9 G_{10}[1 - G_2 G_{12}(LF)]} \right]$$

where ξ = arctan $[G_3(LF)]$

and LF = fade coefficient of the brake.

This was accomplished most easily by using Equation (1) to compute the variation of T/p as a function of μ_p for several values of the ratio of $k = \mu_s/\mu_p$. The resulting curves are of the following form.

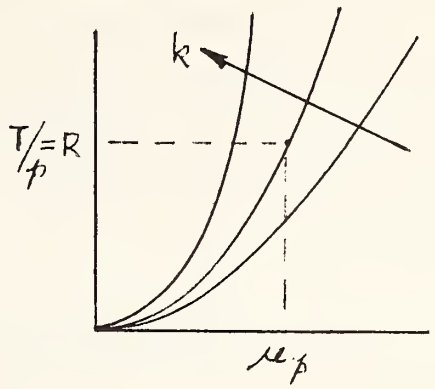

Thus, for the measured value of the torque coefficient, $R = T/p$, the required value of μ_p is read off the curve for an assumed ratio $k = \mu_s/\mu_p$. Typically, the linings for Duo-Servo brakes are high coefficient on the primary shoe and low coefficient for the secondary shoe (Reference 3).

The objective of representing the brake torque coefficient in this manner and then forcing it to match the measured value is to realistically accommodate the effects of lining fade through the use of the variation of lining fade coefficient with brake temperature. The brake temperature is computed as a function of the work done by the brake and the thermal parameters representing it.

The variation of the lining fade coefficient with brake temperature cannot be measured directly. However, the variation of the brake output torque with temperature at a constant applied hydraulic pressure can be measured, and this result then transformed into the variation of fade coefficient with temperature. In doing this, it is assumed that the variation of fade coefficient with temperature is independent of pressure, and the measured variation of torque is used for a constant pressure in the desired

operating range. The transformation of the measured torque variation into the lining fade coefficient variation is accomplished by the use of a curve of torque coefficient versus lining fade coefficient which can be computed by the use of Equation (1). These curves for the test vehicle brakes are presented in Figure 2.5-6. For each temperature, the measured torque is divided by the applied pressure (minus the effective push-out pressure) to obtain the torque coefficient, and this value is used to read the corresponding lining fade coefficient from the above curve (Figure 2.5-6). The resulting variation of lining fade coefficient with temperature is presented in Figure 2.5-7.

The measurement of the brake torque as a function of the applied hydraulic pressure was made at a very low wheel angular velocity (approximately one-quarter of a revolution per second). The wheel was turned at a constant rate with a large torque wrench, while the applied pressure (up to 600 psi) was held constant. These measurements were made for each individual wheel and are presented in Figure 2.5-8. It should be noted that for low applied hydraulic pressures, the experimentally obtained variation of brake torque with pressure is nonlinear. This is believed to be due to nonuniform initial contact of the shoes with the drums. As the pressure is increased, the shoe contact area would progressively increase, and thus, the resulting self-actuation would vary as the magnitude, direction and point of application of the "effective" shoe friction force (Reference 3) varied due to continual readjustment of the shoe/drum friction (shear) force distribution. A possible reason for the high degree of nonlinearity ascribed to this effect is that these brakes were not sufficiently worn in prior to the tests and measurements.

This nonlinearity is approximated in the simulation by using an "effective" push-out pressure of sufficient magnitude to shift the predicted linear variation of brake torque with pressure such that is closely matched the measured variation over the linear range as indicated in Figure 2.5-8.

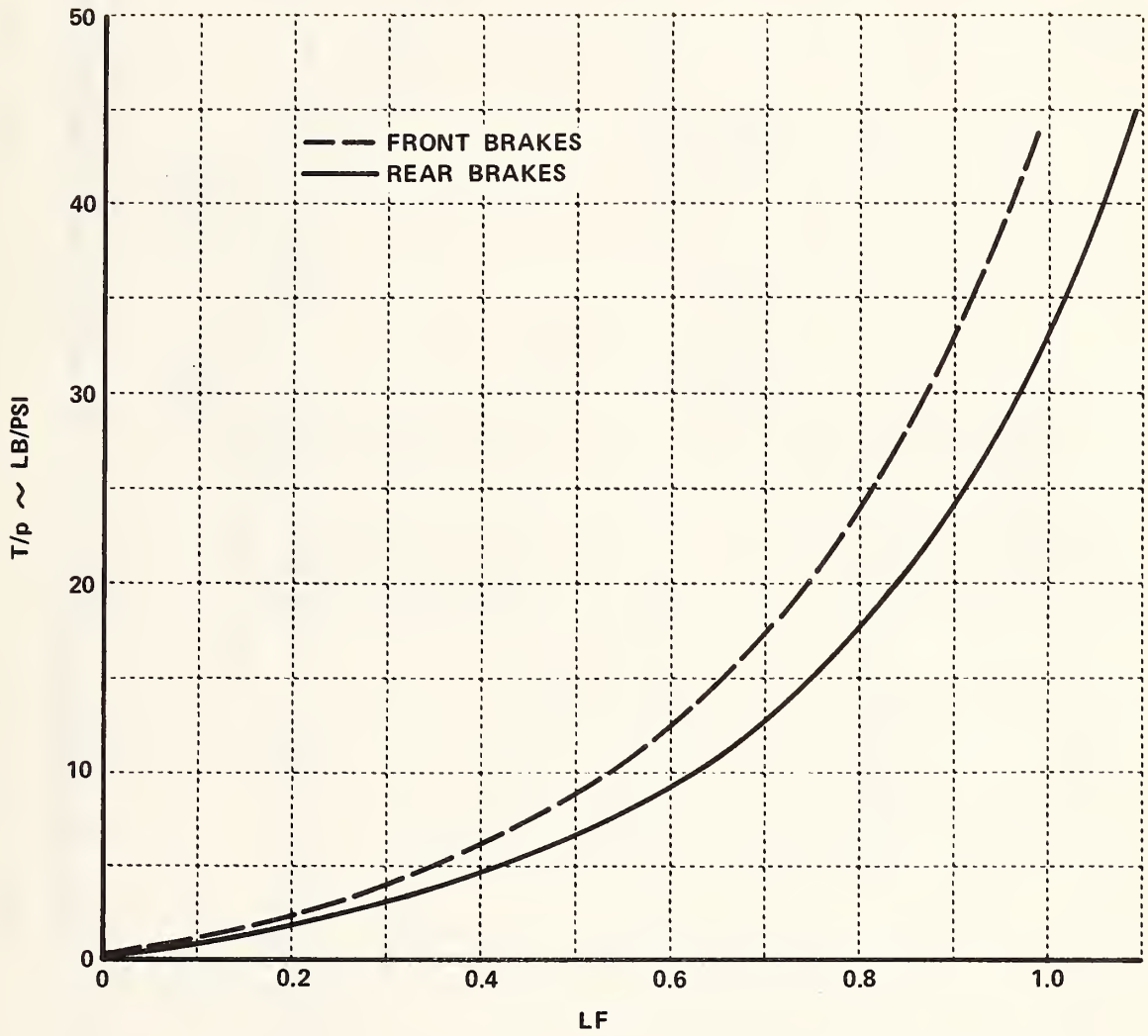

Figure 2.5-6 VARIATION OF LINING FADE COEFFICIENT WITH TEMPERATURE FOR TEST VEHICLE

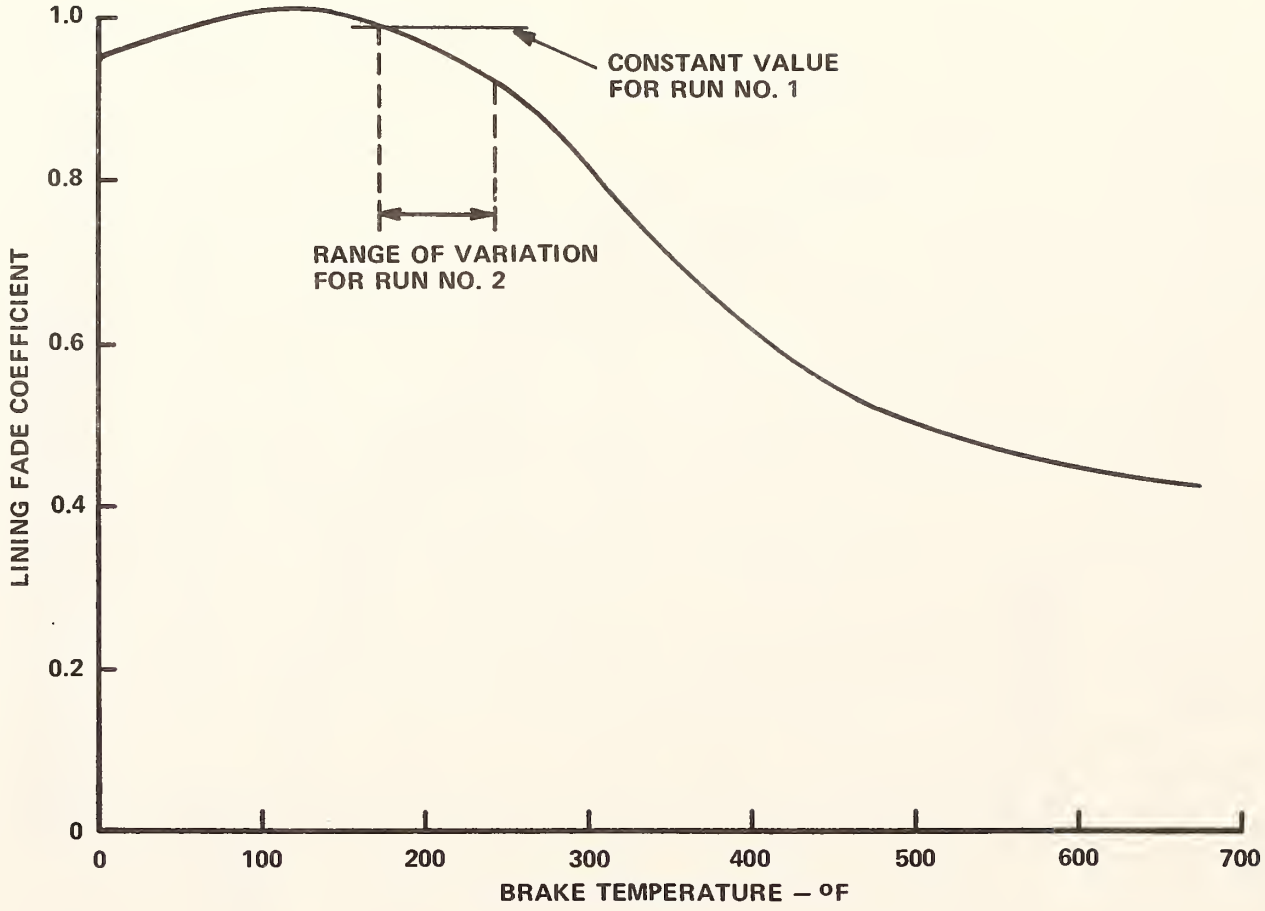

Figure 2.5-7 LINING FADE COEFFICIENT VARIATION WITH BRAKE TEMPERATURE

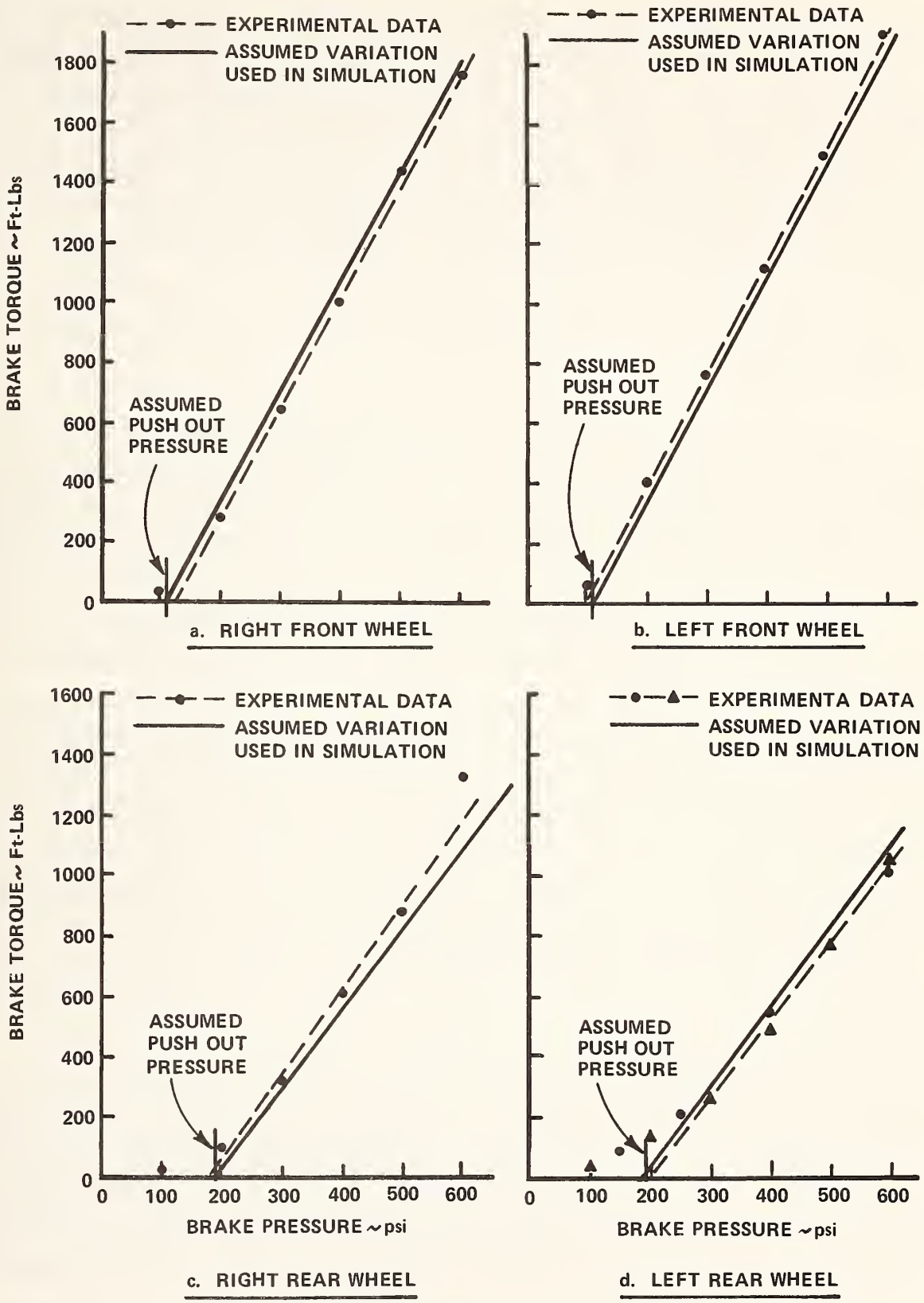

Figure 2.5-8 BRAKE TORQUE VS HYDRAULIC PRESSURE

The error introduced into the predicted braking torque at the low pressures is of consequence only for relatively light braking. Thus, this approximation should not significantly influence the correlation, because the validation tests were conducted close to incipient wheel lockup (400-500 psi). Furthermore, in the validation tests, the brakes were applied suddenly so that the pressure passed rapidly through the nonlinear range (rise time approximately 200 milliseconds). Thus, it would be expected that this nonlinearity may have a significant influence on the very short-term transient response but very little effect on the relatively long-term event of interest herein.

It should be noted that there is a characteristic difference of this nonlinear region between the front and rear wheel brakes which results in different effective push-out pressures for the front and rear brakes. This effect and its influence on the results is discussed in Section 2.5-5.

The variation of wheel braking torque with temperature was measured experimentally for one of the rear wheels; this characteristic variation with temperature was assumed to hold for all four wheels. These measurements were made over the temperature range between 70°F and 300°F and at constant wheel speeds corresponding to about 15-20 MPH for several constant brake system pressures. The procedure used to make these measurements utilized the vehicle's own engine and drive line, required no special equipment and capitalized on one of the characteristics of rear axle differentials -- i.e., for constant speed operation equal torque is supplied to each wheel axle even though their individual angular velocities may differ. With both rear wheels off the ground, the brake drum of one rear wheel was disconnected from its axle by cutting out the bolt circle portion of the brake drum which connects it to the axle (a spare drum was used). The drum was left installed to restrain the brake shoes on this disabled wheel, and its axle was thus free to turn when the brakes were applied. This "free" axle was restrained from turning by a lever arm and load cell. Thus, with the transmission in gear, the engine could be used to drive the opposite wheel at any desired constant speed with the desired

brake system pressure applied. Because the torque supplied to both axles is equal, the braking torque supplied to the driven wheel was read at the restrained axle. With one axle restrained, the "speed" of the driven wheel is twice the speedometer indication. The temperatures of the primary and secondary brake shoe linings were measured with thermocouples. The installation of the thermocouples, which was consistent with SAE J843 Recommended Procedure (Reference 5), is described in Section 2.5.1.2.6 of this report.

The test procedure was to first nominally set the brake pressure with the wheel nonrotating and then apply about 50 percent of the expected torque by setting the throttle and putting the automatic transmission in low gear (low gear used to develop high torque and prevent shifting). Application of the torque "winds up" the brake mechanism, and the system pressure was then readjusted to the desired value as the torque was further increased (via the throttle) up to the break-away value. When the wheel began rotating, the speed was quickly adjusted to the desired value by use of the throttle because the temperature of the brake immediately begins to increase.

At the higher brake pressures, the higher rate of energy dissipation by the brake caused the temperature to increase very rapidly to the self-imposed temperature limit of 300°F (chosen for protection of the brake lining from heat damage). Because it was very difficult to get the speed stabilized before reaching the temperature limit for these short duration runs, there was some variation of the wheel speed which may have reduced the accuracy of the results as compared with those obtained for the lower temperature range.

For each brake pressure level, the data were plotted as brake output torque versus brake temperature (of the primary shoe) as shown in Figure 2.5-9. Attempts were made to repeat each run, but it was difficult to closely match the desired wheel speed; thus, the presented results reflect the inability to precisely repeat the test conditions as well as the influence of wheel speed. Because the validation tests were conducted at

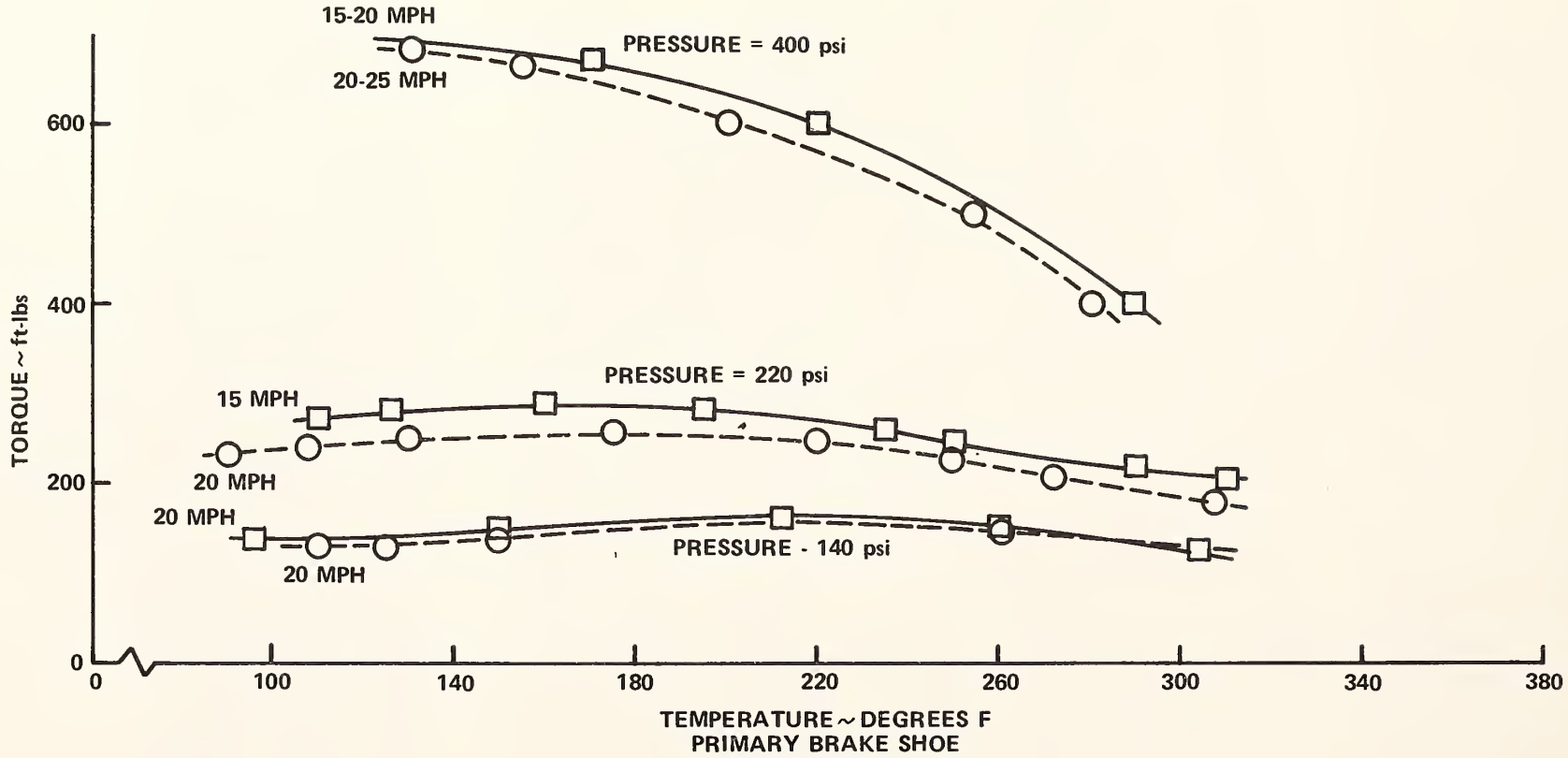

Figure 2.5-9 BRAKE OUTPUT TORQUE VS. TEMPERATURE (LEFT REAR WHEEL) CONSTANT SPEED AND PRESSURE

the higher brake system hydraulic pressures, the lining fade variation with temperature is based on the results obtained at 400 psi. This fade variation was obtained by first extrapolating the 400 psi torque versus temperature curve up to 1000°F and down to 0°F and then transforming these results into the variation of lining fade with temperature through the use of a curve of torque versus lining fade for this brake. Although the temperature range experienced during the tests (and thus required for computation) is 170°F-230°F, the computer program requires tabular inputs for the 0°F-1000°F temperature range.

2.5.1.2 Instrumentation

Instrumentation was installed on the vehicle to measure fourteen channels of information describing the vehicle response during braking maneuvers. A Sangamo Model 3500, 14-channel tape recorder was carried on board the vehicle to obtain continuous analog records of the data on magnetic tape. The fourteen vehicle response parameters and the transducers used to measure them are summarized in Table 2.5-5. Photographs of the installed instrumentation and recording system are presented in Figure 2.5-10.

As can be seen in the photographs, the instrumentation, signal conditioning and recording system are mounted in the rear of the passenger compartment and the trunk compartment, while all the controls for the system are in the front of the passenger compartment. The tape recorder, accelerometer package, gyro attitude package, amplifier package and instrumentation battery package are all mounted on a single platform attached to the floor of the rear compartment. The terminal boards, system control relays, rear wheel potentiometers and brake temperature monitoring meter are all mounted in the rear passenger compartment on the rear seatback support structure. The battery power for the tape recorder, DC to AC converter, tire air supply for trajectory markers and fluid reservoir for the rear bumper trajectory marker are all mounted in the trunk compartment.

Table 2.5-5

SUMMARY OF INSTRUMENTATION TRANSDUCERS

	Measured Parameter	Transducer
1.	Sprung Mass Longitudinal Acceleration	CEC Type 4-202-001 Strain Gauge Accelerometer; ±5 g's; Response Flat ±1 db to 1000 cps
2.	Sprung Mass Lateral Acceleration	CEC Type 4-202-001 Strain Gauge Accelerometer; ±5 g's; Response Flat ±1 db to 1000 cps
3.	Pitch Attitude	Humphrey FG 23-3101-1 Free Gyro; Pitch on Inner Gimbal; Roll on Outer Gimbal
4.	Roll Attitude	Humphrey FG 23-3101-1 Free Gyro; Pitch on Inner Gimbal; Roll on Outer Gimbal
5.	Yaw Attitude	Humphrey FG 23-3101-1 Free Gyro; Yaw on Outer Gimbal
6.	Steer Angle	Pacific Scientific 4101119-0 Linear Potentiometer; 10" Stroke; 3000 Ohms
7.	Front Wheel Suspension Deflection (Left)	Pacific Scientific 4101119-0 Linear Potentiometer; 10" Stroke; 3000 Ohms
8.	Rear Wheel Suspension Deflection (Left)	Pacific Scientific 4101119-0 Linear Potentiometer; 10" Stroke; 3000 Ohms
9.	Brake System Hydraulic Pressure	CEC Type 4-326 Pressure Transducer; 2500 psi Range
10.	Temperature-Brake Lining	Chromel-Alumel Thermocouple
11.	Angular Displacement of Each Wheel About Axle	Helipot Model 6651; 1000 Ohms, 2.5 Watts; Single Turn, Continuous Rotation, Conductive Plastic Potentiometer
12.		
13.		
14.		

Note: (1) Nexus USL-1 operational amplifiers used in each channel.
(2) All channels recorded on Sangamo Model 3500, 14-channel tape recorder.

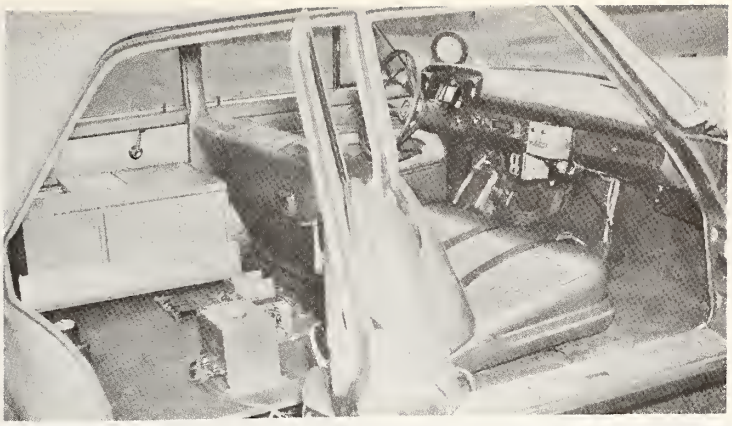

(a) OVERALL VIEW – FRONT AND REAR PASSENGER COMPARTMENTS

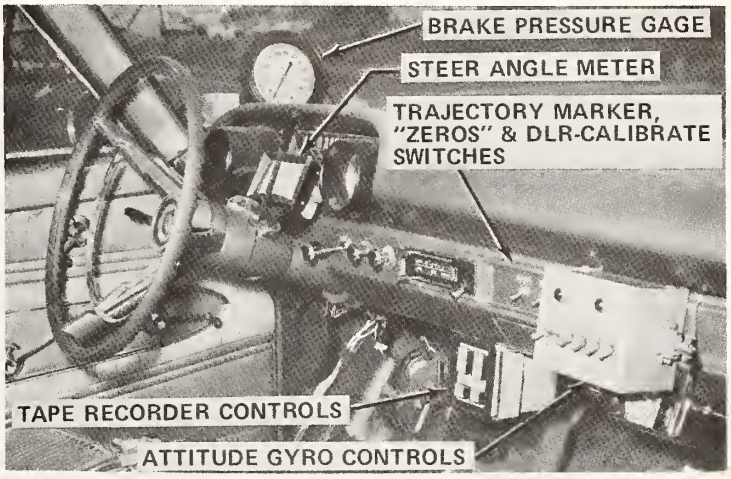

(b) EQUIPMENT IN FRONT COMPARTMENT

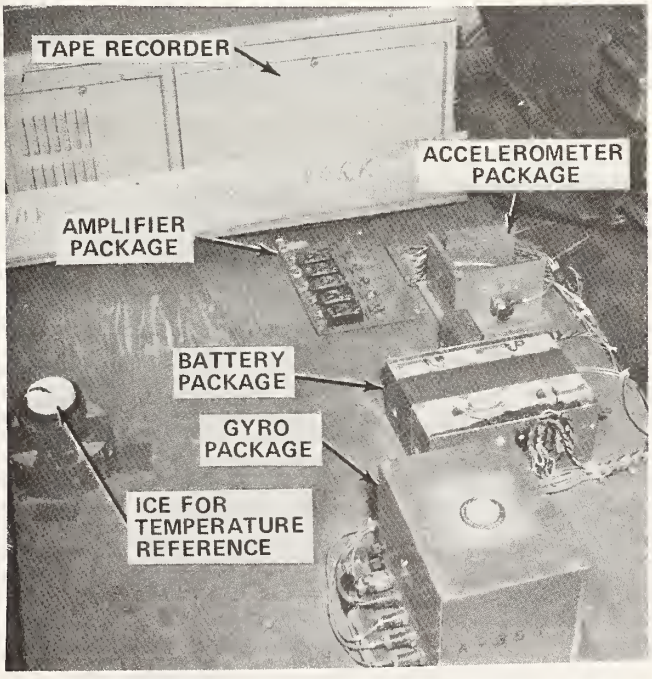

(c) EQUIPMENT ON FLOOR – REAR COMPARTMENT

Figure 2.5-10 VEHICLE INSTRUMENTATION SYSTEM

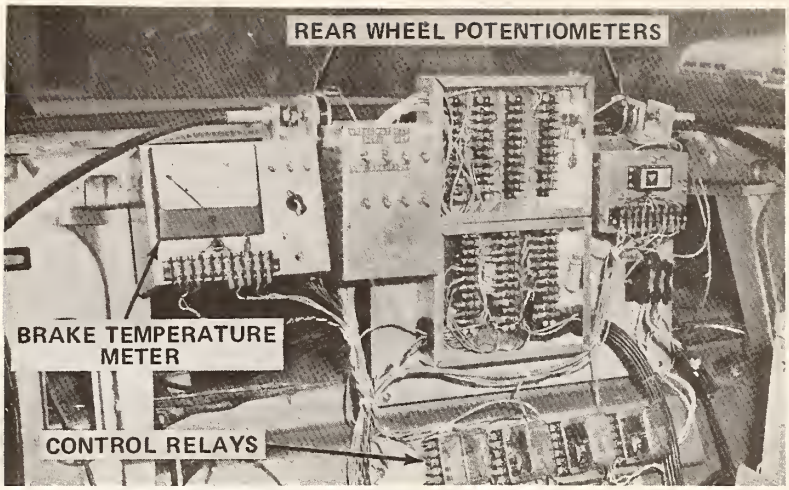

(d) EQUIPMENT ON SEAT BACK – REAR COMPARTMENT

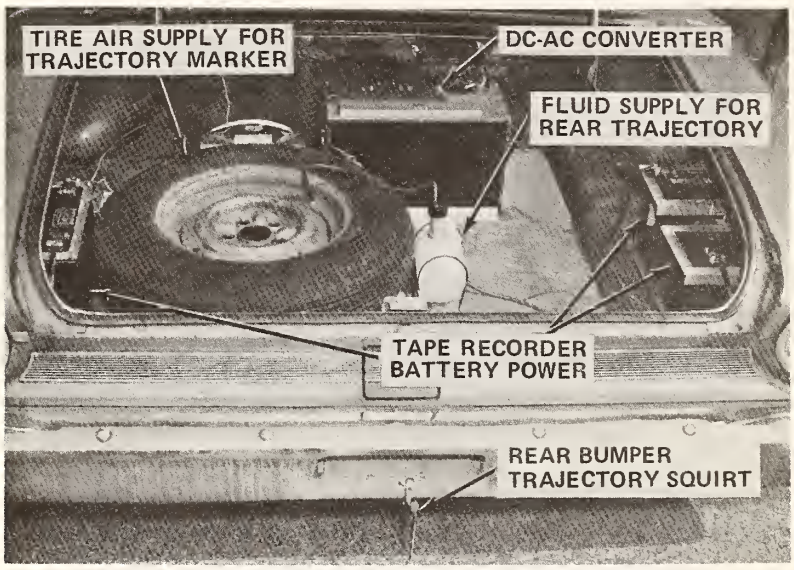

(e) EQUIPMENT IN TRUNK COMPARTMENT

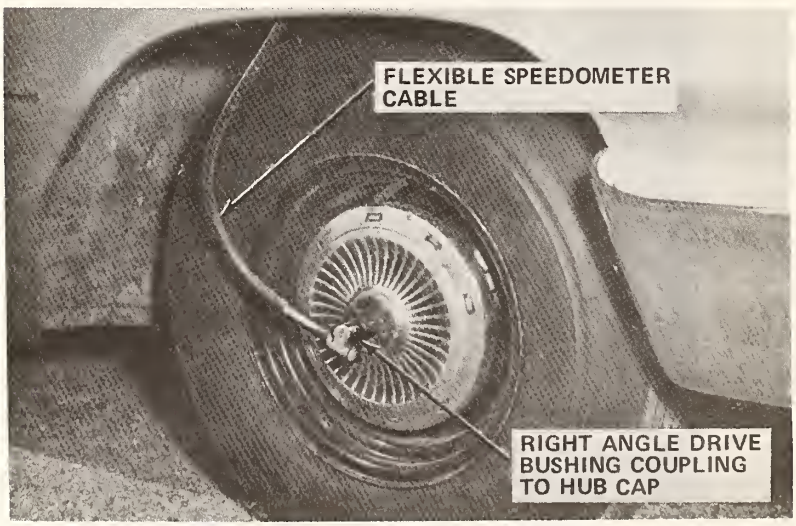

(f) INSTRUMENTATION COUPLING TO WHEELS

Figure 2.5-10 VEHICLE INSTRUMENTATION SYSTEM (Cont.)

The instrumentation system and installation was designed to facilitate the gathering and reduction of the data. The recording of "zeros" and "DLR-Calibration" of all channels prior to each run (as required by the automated data reduction and plotting systems) was made possible by a single switch operating a series of relays. A time zero signal was generated for the computerized data reduction system by using the brake light switch to remove a DC bias signal from the left rear wheel suspension deflection signal. The brake light switch closes at about 20-50 psi which is (for practical purposes) the initiation of the brake pressure rise.

Sprung Mass Accelerations

Linear accelerations of the vehicle along the X and the Y vehicle-fixed axes were measured by an accelerometer package mounted at the approximate location of the sprung mass c.g. Actually, the package was about 2.5 inches below sprung mass c.g. and in the simulation, the sprung mass acceleration at this location was computed.

Sprung Mass Attitude Measurement

A pair of two-degree-of-freedom, free gyroscopes were used to measure the yaw, pitch and roll angular displacements of the vehicle axes with respect to a space-fixed reference axis system. Both gyros, together with a printed circuit board with solid state operational amplifiers and other miniaturized components for signal conditioning, are contained in a compact package and are capable of operating under an impact environment of 40 g's. Special attention was given to their orientation so as to minimize "contamination" of the signals due to cross-coupling effects of combined motions. One gyro is used in a vertical mode (spin axis parallel to vehicle vertical or Z axis) with the inner gimbal (axis athwartwise) measuring pitching and the outer gimbal measuring roll motions. The other gyro has its spin axis aligned parallel to the longitudinal axis of the vehicle and is used to measure heading, i.e., yaw, on the outer gimbal.

With the gyros so oriented, the gimbal pickoff signals are direct measurements of the Euler angular coordinates of the sprung mass relative to the space-fixed axis system as defined in the computer simulation program, except for yaw. The "contamination" of the yaw signals is minor because of the small magnitudes of the pitching and rolling motions experienced in the tests, but corrections are easily made in the process of reducing the test data.

Front Wheel Steer Angle

Steer angles of the front wheels were measured by recording signals from a linear-stroke potentiometer attached to the hydraulic actuator of the vehicle power steering system and calibrating the output signal in terms of wheel steer angle.

Suspension Deflections

Jounce and rebound deflections of the left front and rear wheels from the static ride positions were measured by linear-stroke potentiometers attached between the sprung mass and a point on the respective suspension systems.

Brake System Hydraulic Pressure

The hydraulic pressure in the brake system was measured by a pressure transducer installed on the master cylinder in parallel with the brake light switch.

Temperature of the Brake Lining

Thermocouples were chosen for this temperature measurement because of their fundamental linearity and simplicity of application. The installation of the thermocouples followed the SAE J843 Recommended Procedure. For each thermocouple, a small clearance hole (just sufficient to accept the active junction) was drilled radially through the brake shoe and the brake lining to the braking surface of the lining material. The thermocouples were installed in these holes such that the end of the active junction was within 1/64 inch of the braking surface. Each thermocouple was secured in place (i.e., potted in the small clearance hole) by the use of epoxy cement. To avoid the possibility of a local "hot spot" due to the presence of the epoxy, a small flat about 1/8 to 1/4 inch in diameter was formed on the surface at the location of each thermocouple by grinding off a few thousandths of the material. A small container with a mixture of crushed ice and water is used to provide a constant known reference temperature. The thermocouples were calibrated in a heated oil bath over the expected temperature range.

Thermocouples were installed in the above manner in the primary shoe of the left front wheel and in both the primary and secondary shoes of the left rear wheel. Only the temperature of the primary shoe of the left front wheel was recorded during the tests because of the limited recording capacity. However, all three could be visually monitored directly on a meter installed in the vehicle. During these tests, the temperature difference between the instrumented shoes was always less than 50°F. The temperature of the two instrumented shoes on the left rear wheel were monitored and recorded during the measurement of the variation of brake torque with temperature.

Wheel Angular Velocity

The angular rotation of each wheel is used to drive (via a flexible cable) a precision rotary potentiometer. With a constant voltage across the potentiometer, the output signal at the wiper arm is proportional to wheel angular position, and the rate of change of the signal is proportional to the wheel angular velocity.

The system is mechanically quite simple. The potentiometers are mounted inside the vehicle and driven by a flexible speedometer cable to each wheel (see photographs of Figure 2.5-10). Each cable is attached to a wheel via a right-angle cable drive assembly which has been adapted to the wheel hub cap. This allows the cable housing to accommodate the wheel rotation, steer and suspension deflections while the cable itself transmits the wheel rotary motion to the potentiometer.

Trajectory Marking System

A trajectory marking system was installed on the instrumented vehicle. It consists of pneumatically powered "squirts" attached to the mid-point of each bumper which are controlled by solenoid valves; for these tests, the system was actuated by a signal from a switch on the brake pedal. A different colored water paint is used in each to differentiate the front from rear. The air pressure to drive the fluid was supplied by a spare tire. In operation, each unit squirts a fine stream of colored paint onto the pavement and thereby trace out the trajectory of the mid-point of each bumper. This system also has the potential of not only recording the trajectory but also the time history of it by simply pulsing the solenoid valves at a known rate.

2.5.2 Data Acquisition and Reduction

The total data acquisition system includes the vehicle instrumentation, the on-board analog tape recorder, an analog-to-digital conversion system, a computerized data reduction program and a data plotting system. The instrumentation segment of the system is described in Section 2.5.1.2. The analog signals proportional to the time variation of the individual measured physical parameters were recorded on a Sangamo Model 3500 tape recorder. As required by the data reduction program, the sequence of data records composing a run file consists of a calibration zeros record, a "dummy load resistance" (DLR) calibration record, a data zeros record and last, an event data record. All the data was recorded at a tape speed of 30 inches per second. Recording of the event data was commenced a sufficient time piror to the beginning of the event to allow the recorder to get up to speed and to record enough pre-event data to establish the initial values of the event parameters. A time zero marker is superimposed on the recorded data by a pressure switch in the hydraulic brake system which closes at approximately 50 psi.

The digitizing of the analog data was performed on the Calspan developed COREC hardware/software system which is a general purpose data collection facility. This A/D conversion was performed at a scanning rate of 300 samples per second and results in a digital tape of the data. However, the data records on this digital tape exceed the maximum allowable record length for data input to the Calspan IBM-360 Mod. 65 Computer Facility. Thus, an intermediate operation was required to subdivide these long records into records of acceptable length. This operation also reordered the data into continuous data streams for each data channel. This reordering was necessary, because the scanning process of the A/D conversion is across channels and results in a sequential interleafing of the data, once per scan.

The data reduction program computes the calibration factors for each channel from the information on the calibration zeros record and DLR-Calibration record. These calibration factors are applied to "raw" digitized data to obtain the reduced data which can then be numerically filtered (use of the filter optional for each channel). The reduction program employs a Martin-Graham digital filter (Reference 12). The filter characteristics of principle interest are: (1) flat response out to cutoff frequency, ω_{co} , possible to within one percent, (2) a $(\cos)^2$ form for the rolloff characteristic beyond ω_{co} , (3) filter introduces no phase shift. The acceleration and brake temperature data were filtered with ω_{co} = 15 cps, and the wheel angular velocity data was filtered with ω_{co} = 2 cps.

The data reduction program derives the wheel angular velocities from the slope of the measured wheel angular displacement time histories. This process utilizes the digital filter to minimize the influence on the derivative of noise in the displacement data.

The final reduced data from each channel is computer plotted as a time history beginning at 0.5 seconds prior to the initiation of the maneuver as defined by the time zero marker.

2.5.3 Test Procedure

Validation data for straight ahead braking maneuvers were obtained using moderately heavy braking, which was just short of wheel lockup.

In preparation for a series of tests, a mixture of crushed ice and water was put in the thermocouple reference temperature container, and the reservoir for the trajectory markers was filled with the marking fluid. The marking fluid, which was a diluted solution of poster paint in water, had to be drained from the system after the testing each day to prevent the solenoid valves from sticking. The gas tank was kept full so as to maintain the vehicle mass and moments of inertia at constant known values.

Before a data run, the brake pressure level was set to the desired test value by adjusting a variable stop on the brake pedal and monitoring the resulting pressure level during several trial braking stops with the brake temperature in the desired test range. Next, a calibration zeros record and a DLR-Calibration record were taken. Just prior to the run, the brake temperature, as monitored on the primary shoe of the left front wheel, was brought to an equilibrium temperature of 180°F. If the temperature was below 180°F, it was increased by mild braking; if greater than 180°F, it was lowered by driving the vehicle around the test area. The high initial test temperature of 180°F was chosen as a convenience to facilitate the testing; that is, a larger brake temperature differential relative to the outside ambient temperature increases the heat dissipation rate and thus the brakes cool down to the test temperature faster -- this shortens the run turnaround time.

A data run for the straight ahead stops was initiated by accelerating the vehicle to a steady-state velocity about 2-3 MPH greater than the desired maneuver initial speed. The attitude gyros were then uncaged, and the transmission shifted into neutral when about 50 ft. from the test area on the skid pad. During the acceleration period and prior to uncaging the gyros, the tape recorder was turned on. When the vehicle speed had decreased to the desired initial maneuver speed, the driver depressed the brake pedal to its stop as fast as possible and firmly held it there until the vehicle came to a stop. The initial motion of the brake pedal turned on the trajectory marking squirt system, and operated a switch for time zero indication when the hydraulic pressure reached a value of 40-50 psi. After the car stopped, the trajectory markers were manually turned off and the stopping distance indicated by the squirt trace on the ground was measured with a steel tape.

In order to assess the repeatability of the physical system being tested, repeat runs were made. This requires that it be possible to repeat the control inputs and the initial conditions for the system which include the vehicle initial velocity, initial brake temperature, the time history of

the brake pressure, the time history of the steering, and the time interval between the initiation of the braking and steering inputs. If the initial conditions and inputs were absolutely identical for several repeat runs, then any differences in the resulting responses could be ascribed to the lack of perfect repeatability in the physical system and would be a measure of it. However, in reality, it is not possible to exactly repeat the initial conditions and inputs, so that the differences between the resulting responses are the result of both the lack of repeatability and the variation in the inputs and initial conditions.

To allow the magnitude of the brake pressure to be easily set and repeated, an adjustable stop was installed on the brake pedal. This resulted in repeatable pressure levels when the brake system was allowed several minutes to return to an equilibrium condition prior to reactuation of the system. For the validation tests of this effort, the driver applied the brakes as rapidly as possible by depressing the pedal to its stop with his foot and holding it there; this resulted in repeatable time histories of the pressures.

2.5.4 Comparison of Predicted and Experimental Results

The HVOSM inputs used in the comparisons are shown in Figure 2.5-11 and the time histories of responses measured in the repeated straight ahead braking maneuver are presented in the graphs of Figure 2.5-12. The time zero pulse (40-50 psi of brake pressure) was used to register the time histories of the three repeat runs. It is observed that the input brake pressures, the vehicle initial velocity as depicted by the initial wheel angular velocity, and the vehicle responses repeat very well.

A repeatable variation of the brake pressure over the duration of the event may be noted in Figure 2.5-12 (a). The pressure increases rapidly to a relative peak value when the brakes are applied and then gradually diminishes throughout the event until the vehicle has stopped; whereupon, it increases to, and briefly oscillates about, a value somewhat greater

```
BV13   BRAKING DYNAMICS VALIDATION - STRAIGHT STOPS - RUNS 35-37
                  VEHICLE DYNAMICS SIMULATION
  0.0      4.5     0.005            0.01     70.       1.3     60.0      0.0          1
 1.0                                                                                  2
 11.05    .608     .945     386.4  6000.0   40000.   40000.    -192.    453.6        3
 58.50   60.75    61.2     60.5     7.83     9.73     -2.0     14.68     4000.       4
 131.      0.5              1.3     58.0     0.10   266000.                          5
194.0     0.5              1.75     97.0     0.10   59244.0  46.52     0.059        6
 1300.     3.0     10.       8.4   3000.     1.71     .987      1.0     4200.       7
    0.0      0.0      0.0      0.0      0.0      0.0      0.0      0.0               8
    0.0      0.0   -21.52    737.       0.0      0.0                                 9
.0.0       0.0      0.0      0.0      0.0      0.0      0.0      0.0               10
  0.0      0.0      2.52     -97.      0.0      0.0                                11
 -5.0      5.0      1.0                                                           12
-5.70  -3.90  -2.45  -1.30  -0.40   0.30   0.60   0.65   0.30  -0.40  -1.30
  0.0      4.0      1.0      1.0                                                   13
  0.0      6.0      0.25                                                          16
0.1079   0.1053   0.1030   0.1011   0.0994   0.0981   0.0971   0.0964   0.0959    21
0.0959   0.0960   0.0965   0.0973   0.0984   0.0998   0.1015   0.1035   0.1058
0.1085   0.1114   0.1147
 .092     .092     .092     .092     .092     .092     .092     .092     .092
 .092     .092     .092     .092     .092     .092     .092     .092     .092
 .092     .092     .092
 300.0    2.0     -2.9      300.0    2.0      4.3                                  23
 300.0    2.0     -4.3      300.0    2.0      4.5                                  24
  0.0     12.2     1.0                                                           25
  6.5     13.6     3.00                                                  0.001    26
  29.     2.0      0.0      100000.                                               27
 0.0   .01   .02   .03   .04   .05   .06   .07   .08   .09   .10   .11   .12
 .13   .14   .15   .16   .17   .18   .19   .20   .30   .40   .50   .60   .70
 .80   .90  1.0
  0.0      0.17     0.30     0.48     0.65     0.75     0.83
  0.92     0.97     1.04     1.09     1.13     1.17     1.18
  1.19     1.23     1.25     1.23     1.20     1.19     1.17
 1.08     1.04     1.01     1.0      1.0      1.0      1.0
  1.0
  0.0      0.17     0.30     0.48     0.65     0.75     0.83
  0.92     0.97     1.04     1.09     1.13     1.17     1.18
  1.19     1.23     1.25     1.23     1.20     1.19     1.17
 1.08     1.04     1.01     1.0      1.0      1.0      1.0
```

```
      FORMAT(13F6.3), PHIC(I),I=  1, 11
      FORMAT(9F8.0,I8), APF(I),I=  1, 9
      FORMAT(9F8.0),    APF(I),I= 10, 18
      FORMAT(9F8.0),    APF(I),I= 19, 21
      FORMAT(9F8.0),    APR(I),I=  1, 9
      FORMAT(9F8.0),    APR(I),I= 10, 18
      FORMAT(9F8.0),    APR(I),I= 19, 21
      FORMAT(9F8.0,I8),NO.SLIP,NO.UGW,(UGW(I) 1,3 )
      FORMAT(13F6.3), SLIP(J),J=  1, 13
      FORMAT(13F6.3), SLIP(J),J= 14, 26
      FORMAT(13F6.3), SLIP(J),J= 27, 29
      FORMAT(7F10.5),     RHOS(J,  1),J=  1,  7
      FORMAT(7F10.5),     RHOS(J,  1),J=  8, 14
      FORMAT(7F10.5),     RHOS(J,  1),J= 15, 21
      FORMAT(7F10.5),     RHOS(J,  1),J= 22, 28
      FORMAT(7F10.5),     RHOS(J,  1),J= 29, 29
      FORMAT(7F10.5),     RHOS(J,  2),J=  1,  7
      FORMAT(7F10.5),     RHOS(J,  2),J=  8, 14
      FORMAT(7F10.5),     RHOS(J,  2),J= 15, 21
      FORMAT(7F10.5),     RHOS(J,  2),J= 22, 28
```

Figure 2.5-11 **COMPUTER PROGRAM INPUTS FOR STRAIGHT AHEAD STOPS – CARD IMAGE FORMAT**

(1 of 7)

BV13 BRAKING DYNAMICS VALIDATION - STRAIGHT STOPS - RUNS 35-37
VEHICLE DYNAMICS SIMULATION
13JUL'71

INERTIAL DATA

MS	= 11.0500	LB.-SEC.**2/IN	
MUF	= 0.6080	"	
MUR	= 0.9450	"	
IX	= 6000.0	LB.-SEC.**2-IN	
IY	= 40000.0	"	
IZ	= 40000.0	"	
IXZ	=-192.000	"	
TR	= 453.60	"	
G	= 386.400	IN/SEC.**2	

DIMENSIONS

A	= 58.5000	INCHES	
B	= 60.7500	"	
TF	= 61.2000	"	
TR	= 60.5000	"	
ZF	= 7.8300	"	
ZR	= 9.7300	"	
RHO	= -2.0000	"	
RW	= 14.6800	"	

SUSPENSION DATA

KF	= 131.000	LB./IN.	
KR	= 194.000	LB./IN.	
CF'	= 59.000	LBS.	
CR'	= 97.000	LBS.	
EPSILONF	= 0.100	IN./SEC.	
EPSILONR	= 0.100	IN./SEC.	
CF	= 1.300	LB-SEC/IN	
CR	= 1.750	LB-SEC/IN	

LAMBDAF	= 0.500		
LAMBDAR	= 0.500		
OMEGAF	= 0.0	INCHES	
OMEGAR	= 0.0	INCHES	
TS	= 46.520	INCHES	
RR	= 59244.0	LB-IN/RAD	
RF	= 266000.0	LB-IN/RAD	
KRS	= 0.059	ROLL STEER COEFF.	

INITIAL CONDITIONS

PHI0	= 0.0	DEGREES	XC0'	= 0.0	INCHES	P0	= 0.0	DEG/SEC	U0	= 737.000	IN/SEC
THETA0	= 0.0	"	YC0'	= 0.0	"	Q0	= 0.0	"	V0	= 0.0	"
PSI0	= 0.0	"	ZC0'	= -21.520	"	R0	= 0.0	"	W0	= 0.0	"
PHIR0	= 0.0	"	DELTA1	= 0.0	"	D(PHIR)/DT	= 0.0	"	D(DEL1)/DT	= 0.0	"
PSIF0	= 0.0	"	DELTA2	= 0.0	"	D(PSIF)/DT	= 0.0	RAD/SC	D(DEL2)/DT	= 0.0	"
			DELTA3	= 0.0	"				D(DEL3)/DT	= 0.0	"

ACCELEROMETER POSITIONS

X1	= 0.0	INCHES	
Y1	= 0.0	"	
Z1	= 2.520	"	
X2	= -97.000	"	
Y2	= 0.0	"	
Z2	= 0.0	"	

DRIVER STEER CONTROL TABLE

T	PSIF	T	PSIF	T	PSIF	T	PSIF	T	PSIF	T	PSIF	T	PSIF
0.0	0.0	1.00	0.0	2.00	0.0	3.00	0.0	4.00	0.0				

TIRE DATA

KT	1300.000	LB/IN
SIGMAT	= 3.000	INCHES
LAMBDAT	= 10.000	
A0	=4000.000	
A1	= 8.400	
A2	=3000.000	
A3	= 1.710	
A4	=4200.000	
AMU	= 0.987	
OMEGT	= 1.000	

TERRAIN TABLE ARGUMENTS

XR(BEGIN)	= 0.0	0.0	0.0	0.0	0.0	INCHES
XF(END)	= 0.0	0.0	0.0	0.0	0.0	"
X(INCR)	= 0.0	0.0	0.0	0.0	0.0	"
YR(BEGIN)	= 0.0	0.0	0.0	0.0	0.0	"
YF(END)	= 0.0	0.0	0.0	0.0	0.0	"
Y(INCR)	= 0.0	0.0	0.0	0.0	0.0	"
NO.X BOUNDS	= 0	0	0	0	0	
NO.Y BOUNDS	= 0	0	0	0	0	
AMUG	= 0.0	0.0	0.0	0.0	0.0	

NO.TERR.TAB. = 0

PROGRAM CONTROL DATA

START TIME	= 0.0	SEC
END TIME	= 4.500	"
INCR FOR INTEGRATION	= 0.0050	"
PRINT INTERVAL	= 0.010	"
THETA MAX (TO SWITCH)	= 70.000	DEG
UVWMIN(STOP)	= 1.300	
PQRMIN(STOP)	= 60.000	
INDCRB	= 0	
(=0.NO CURB,=1 CURB, =-1 STEER DEG. OF FREEDOM)		
MODE OF INTEGRATION	= 1	
(=0 VAR.ADAMS-MOULT., =1 RUNGE-KUTTA,=2 FIX.AM)		

Figure 2.5-11 **COMPUTER PROGRAM INPUTS FOR STRAIGHT AHEAD STOPS – TABULAR FORMAT**

(2 of 7)

FRONT WHEEL CAMBER
VS
SPRENSION DEFLECTION

DELTAF INCHES	PHIC DEGREES
-5.000	-5.700
-4.000	-3.900
-3.000	-2.450
-2.000	-1.300
-1.000	-0.400
0.0	0.300
1.000	0.600
2.000	0.650
3.000	0.300
4.000	-0.400
5.000	-1.300

CURB IMPACT DATA

YC1'	=	0.0	INCHES
YC2'	=	0.0	"
ZC2'	=	0.0	"
DELTC	=	0.0	SEC(INTEG.INCR)
PHIC1	=	0.0	DEGREES
PHIC2	=	0.0	"
MUF	=	0.0	
IPSI	=	0.0	LB-SEC**2-IN
CPSI'	=	0.0	LB-IN
OMEGA PST	=	0.0	RAD
KPSI	=	0.0	LB-IN/RAD
EPSILON PST	=	0.0	RAD/SEC
TRATL,FRONT(PT)=		0.0	INCHES

SUSPENSION STOPS, EXTENSION AND COMPRESSION

FRONT		REAR	
COMPRESSION			
KFC =	300.000 LB/IN	KRC =	300.000 LB/IN
KFC' =	2.000 LB/IN**3	KRC' =	2.000 LB/IN**3
OMEGFC =	-2.900 INCHES	OMEGRC =	-4.300 INCHES
EXTENSION			
KFE =	300.000 LB/IN	KRE =	300.000 LB/IN
KFE' =	2.000 LB/IN**3	KRE' =	2.000 LB/IN**3
OMEGFE =	4.300 INCHES	OMEGRE =	4.500 INCHES

BRAKING DYNAMICS

FRONT		
IDJF	=	0.0 LB-SEC**2 IN
TWJF,ROTA=		12.200 "
AXLE RAT=		1.000
REAR		
IDJR	=	6.500 LB-SEC**2-IN
TWJR,ROTA=		13.600 "
AXLE RAT=		3.000

WHEEL RADIUS-RADIAL SPRING FOR TABLE

RWHJR(BEGIN)	=	0.0 INCHES
RWHJE(END)	=	6.000 "
DRWHJ(INCRE.)	=	0.250 "

RW-HJ INCHES	FJR LBS	RW-HJ INCHES	FJR LBS	RW-HJ INCHES	FJR LBS	RW-HJ INCHES	FJR LBS
0.0	0.0	1.75	225.	3.50	0.115E 04	5.25	0.242E 04
0.250	91.0	2.00	211.	3.75	0.142E 04	5.50	0.231E 04
0.500	110.	2.25	253.	4.00	0.164E 04	5.75	0.262E 04
0.750	135.	2.50	234.	4.25	0.144E 04	6.00	0.249E 04
1.00	150.	2.75	283.	4.50	0.194E 04		
1.25	183.	3.00	256.	4.75	0.209E 04		
1.50	179.	3.25	0.105E 04	5.00	0.203E 04		

ANTI-PITCH TABLES FOR CIRCUMFERENTIAL TIRE FORCE

APF=	0.10700	0.10530	0.10300	0.10110	0.09940	0.09810	0.09710	0.09640	0.09590	0.09580	0.09600
	0.09650	0.09730	0.09840	0.09980	0.10150	0.10350	0.10580	0.10850	0.11140	0.11470	
APR=	0.09200	0.09200	0.09200	0.09200	0.09200	0.09200	0.09200	0.09200	0.09200	0.09200	0.09200
	0.09200	0.09200	0.09200	0.09200	0.09200	0.09200	0.09200	0.09200	0.09200	0.09200	

Figure 2.5-11 COMPUTER PROGRAM INPUTS FOR STRAIGHT AHEAD STOPS – TABULAR FORMAT

(3 of 7)

BV13 BRAKING DYNAMICS VALIDATION - STRAIGHT STOPS - RUNS 35-37
VEHICLE DYNAMICS SIMULATION
13JUL'71

RHOS(SLIP,UGW),RATIO OF FRICTION COEFFICIENTS, CIRCUMFERENTIAL TO PEAK SIDE FORCE. UGW(I)=UG(I)*COS(PSIIP(I)) +VG(I)*SIN(PSIIP(I))
NO.OF SLIP= 29, NO.OF UGW= 2 SLIP AND UGW GIVEN AS POSITIVE VALUES

SLIP	UGW(1)IN/SEC 0.0	RHOS UGW(2) 1.000E 05	UGW(3) 0.0	SLIP	UGW(1)IN/SEC 0.0	RHOS UGW(2) 1.000E 05	UGW(3) 0.0	SLIP	UGW(1)IN/SEC 0.0	RHOS UGW(2) 1.000E 05	UGW(3) 0.0
0.0	0.0	0.0	0.0	0.100	1.09000	1.09000	0.0	0.200	1.17000	1.17000	0.0
0.010	0.17000	0.17000	0.0	0.110	1.13000	1.13000	0.0	0.300	1.08000	1.08000	0.0
0.020	0.30000	0.30000	0.0	0.120	1.17000	1.17000	0.0	0.400	1.04000	1.04000	0.0
0.030	0.48000	0.48000	0.0	0.130	1.18000	1.18000	0.0	0.500	1.01000	1.01000	0.0
0.040	0.65000	0.65000	0.0	0.140	1.19000	1.19000	0.0	0.600	1.00000	1.00000	0.0
0.050	0.75000	0.75000	0.0	0.150	1.23000	1.23000	0.0	0.700	1.00000	1.00000	0.0
0.060	0.83000	0.83000	0.0	0.160	1.25000	1.25000	0.0	0.800	1.00000	1.00000	0.0
0.070	0.92000	0.92000	0.0	0.170	1.23000	1.23000	0.0	0.900	1.00000	1.00000	0.0
0.080	0.97000	0.97000	0.0	0.180	1.20000	1.20000	0.0	1.000	1.00000	1.00000	0.0
0.090	1.04000	1.04000	0.0	0.190	1.19000	1.19000	0.0				

RATIO(FR',SPEED), MODIFICATION FACTOR FOR TIRE-TERRAIN FRICTION COEFFICIENTS. SPEED= SQRT(UG(I)**2 + VG(I)**2). FR' =FRCP
NO.OF FRCP= 3, NO.OF SPEED= 3

FRCP,LB	SPEED,IN/SEC 0.0	SPEED,IN/SEC 704.0	SPEED,IN/SEC 1408.0	SPEED,IN/SEC	SPEED,IN/SEC	SPEED,IN/SEC
200.0	1.13800E 00	9.29000E-01	7.19000E-01			
1200.0	1.00000E 00	7.92000E-01	5.82000E-01			
2200.0	9.30000E-01	7.22000E-01	5.13000E-01			

Figure 2.5-11 **COMPUTER PROGRAM INPUTS FOR STRAIGHT AHEAD STOPS – TABULAR FORMAT**

(4 of 7)

BV13 BRAKING DYNAMICS VALIDATION - STRAIGHT STOPS - RUNS 35-37
VEHICLE DYNAMICS SIMULATION
13JUL'71

ENGINE RPM	ENGINE TORQUE WIDE OPEN THROTTLE LB-FT	ENGINE TORQUE CLOSED THROTTLE LB-FT
500.	500.	0.
900.	563.	-120.
1300.	594.	-144.
1700.	618.	-155.
2100.	630.	-180.
2500.	621.	-192.
2900.	600.	-204.
3300.	561.	-216.
3700.	516.	-231.
4100.	480.	-249.
4500.	438.	-267.
4900.	420.	-288.

	BRAKE PARAMETERS FRONT GN(I,1)	REAR GN(I,2)
1	7.62000E 00	7.62000E 00
2	1.40000E 00	1.40000E 00
3	4.80000E-01	4.76000E-01
4	9.42000E-01	6.91000E-01
5	0.0	0.0
6	3.12000E 00	3.12000E 00
7	6.21000E 00	6.21000E 00
8	6.43000E 00	6.43000E 00
9	4.62000E 00	4.62000E 00
10	1.00000E 00	1.00000E 00
11	9.25000E 00	9.25000E 00
12	3.84000E-01	3.81000E-01
13	0.0	0.0
14	1.00000E 01	1.00000E 01
15	9.99999E 10	9.99999E 10
16	9.99999E 10	9.99999E 10

INITIAL BRAKE TEMPERATURE, DEG.F
TAU0(1), RIGHT FRONT = 170.00
TAU0(2), LEFT " = 170.00
TAU0(3), RIGHT REAR = 170.00
TAU0(4), LEFT " = 170.00

TABLE LF VARIES WITH TEMPERATURE
TTAU(J),J=1,51, 0(DEG.F) TO 1000(DEG.F) IN 20 DEGREE INCREMENTS

BRAKE LINING FADE COEFFICIENTS

TTAU DEG.F	LF	TTAU DEG.F	LF	TTAU DEG.F	LF	TTAU DEG.F	LF
0.0	0.9600	260.0	0.9070	520.0	0.4890	780.0	0.4160
20.0	0.9740	280.0	0.8590	540.0	0.4750	800.0	0.4140
40.0	0.9850	300.0	0.8140	560.0	0.4650	820.0	0.4100
60.0	0.9960	320.0	0.7700	580.0	0.4540	840.0	0.4070
80.0	1.0000	340.0	0.7270	600.0	0.4440	860.0	0.4040
100.0	1.0300	360.0	0.6870	620.0	0.4410	880.0	0.4010
120.0	1.0100	380.0	0.6450	640.0	0.4380	900.0	0.3980
140.0	1.0000	400.0	0.6090	660.0	0.4350	920.0	0.3950
160.0	0.9950	420.0	0.5860	680.0	0.4320	940.0	0.3910
180.0	0.9820	440.0	0.5610	700.0	0.4290	960.0	0.3880
200.0	0.9720	460.0	0.5360	720.0	0.4250	980.0	0.3850
220.0	0.9520	480.0	0.5150	740.0	0.4220	1000.0	0.3820
240.0	0.9300	500.0	0.5000	760.0	0.4190		

Figure 2.5-11 COMPUTER PROGRAM INPUTS FOR STRAIGHT AHEAD STOPS – TABULAR FORMAT

(5 of 7)

BV13 BRAKING DYNAMICS VALIDATION - STRAIGHT STOPS - RUNS 35-37
VEHICLE DYNAMICS SIMULATION
13JUL'71

BRAKING SYSTEMS WITH COMPUTED TORQUES

NTTS,(MAX 101),NO.OF PC,TS,TR ENTRIES =	41	TAUA	AMBIENT TEMPERATURE, DEG.F =	170.0	
IBTYP(1) FRONT BRAKE TYPE =	3	PO(1)	FRONT,BRAKE PUSH OUT PRES.,PSIG=	110.00	
IBTYP(2) REAR " " =	3	PO(2)	REAR, " " " " =	192.00	
K1 SLOPE PR/PF (P1,LT.PF,LE.P2) =	1.0000	C1	COEFFICIENT FOR RESISTING FORCE=	9.61100E-05	
K2 " " (PF,GT.P2) =	1.0000	C2	" " " =	2.85300E-02	
P1 BRAKE PRES. FOR PR/PF CHANGE,PSIG=	1.000000E 03	C3	" " " =	6.03360E 01	
P2 " " " " " =	1.000000E 03	ZETAB,THRESHOLD WHEEL SPEED TO LIMIT BRAKE TORQUE,RAD/SEC=		0.10	

TABLES PC,TS,TR VARY WITH TIME
TT(J),J=1,NTTS, 0 TO 10 SECS. IN 0.10 SEC INCREMENTS

SEC TT	BRAKE MASTER CYL PRES.(PSIG) PC	THROTTLE SETTING TS	TRANSMISSION RATIO TR	SEC TT	BRAKE MASTER CYL PRES.(PSIG) PC	THROTTLE SETTING TS	TRANSMISSION RATIO TR	SEC TT	BRAKE MASTER CYL PRES.(PSIG) PC	THROTTLE SETTING TS	TRANSMISSION RATIO TR
0.0	0.	0.0	0.0	1.40	495.	0.0	0.0	2.80	453.	0.0	0.0
0.10	0.	0.0	0.0	1.50	490.	0.0	0.0	2.90	452.	0.0	0.0
0.20	0.	0.0	0.0	1.60	485.	0.0	0.0	3.00	450.	0.0	0.0
0.30	0.	0.0	0.0	1.70	480.	0.0	0.0	3.10	452.	0.0	0.0
0.40	0.	0.0	0.0	1.80	480.	0.0	0.0	3.20	475.	0.0	0.0
0.50	15.	0.0	0.0	1.90	480.	0.0	0.0	3.30	550.	0.0	0.0
0.60	315.	0.0	0.0	2.00	480.	0.0	0.0	3.40	550.	0.0	0.0
0.70	530.	0.0	0.0	2.10	478.	0.0	0.0	3.50	550.	0.0	0.0
0.80	520.	0.0	0.0	2.20	473.	0.0	0.0	3.60	550.	0.0	0.0
0.90	510.	0.0	0.0	2.30	470.	0.0	0.0	3.70	550.	0.0	0.0
1.00	505.	0.0	0.0	2.40	465.	0.0	0.0	3.80	550.	0.0	0.0
1.10	500.	0.0	0.0	2.50	462.	0.0	0.0	3.90	550.	0.0	0.0
1.20	500.	0.0	0.0	2.60	460.	0.0	0.0	4.00	550.	0.0	0.0
1.30	495.	0.0	0.0	2.70	458.	0.0	0.0				

Figure 2.5-11 **COMPUTER PROGRAM INPUTS FOR STRAIGHT AHEAD STOPS – TABULAR FORMAT**

(6 of 7)

```
 1.0
3.0     3.0     0.0      704.     1408.
200.  1200.  2200.
1.138       1.00       .930
 .929        .792       .722
 .719        .582       .513
41.0      3.0      3.0      1.0      1.0     1000.    1000.
 0.0      0.0      0.0      0.0      0.0       15.      315.     530.      520.
 510.     505.     500.     500.     495.     495.     490.     485.      480.
 480.     480.     480.     478.     473.     470.     465.     462.      460.
 458.     453.     452.     450.     452.     475.     550.     550.      550.
 550.     550.     550.     550.     550.
 0.0      0.0      0.0      0.0      0.0      0.0      0.0      0.0       0.0
 0.0      0.0      0.0      0.0      0.0      0.0      0.0      0.0       0.0
 0.0      0.0      0.0      0.0      0.0      0.0      0.0      0.0       0.0
 0.0      0.0      0.0      0.0      0.0      0.0      0.0      0.0       0.0
 0.0      0.0      0.0      0.0      0.0
 0.0      0.0      0.0      0.0      0.0      0.0      0.0      0.0       0.0
 0.0      0.0      0.0      0.0      0.0      0.0      0.0      0.0       0.0
 0.0      0.0      0.0      0.0      0.0      0.0      0.0      0.0       0.0
 0.0      0.0      0.0      0.0      0.0
   500      900     1300     1700     2100     2500     2900     3300      3700
  4100     4500     4900
   500      563      594      618      630      621      600      561       516
   480      438      420
     0     -120     -144     -165     -180     -192     -204     -216      -231
  -249     -267     -288
 7.62     1.40     0.490    0.942              3.12     6.21     6.43      4.62
 1.0      9.25     0.384              10.0     10.E10   10.E10
 7.62     1.40     0.476    0.691             3.12     6.21     6.43      4.62
 1.0      9.25     0.381              10.0     10.E10   10.E10
170.     170.     170.     170.
.960     .974     .985     .996     1.00     1.03     1.01     1.00      .995
.992     .972     .952     .930     .907     .859     .814     .770      .727
.687     .645     .609     .586     .561     .536     .515     .500      .488
.475     .465     .454     .444     .441     .438     .435     .432      .429
.425     .422     .419     .416     .414     .410     .407     .404      .401
.398     .395     .391     .389     .385     .382
170.      110.     192.  .9611E-4  .02853   60.336   0.10
9999
```

```
      FORMAT(7F10.5),     RHOS(J,  2),J= 29, 29
28    FORMAT(9F8.0,I8),NO.FR',NO.SPEED,(SPEED I,6 )
      FORMAT(13F6.3), FRCP(J),J=  1,  3
      FORMAT(7F10.5),     RATIO(J,  1),J=  1,  3
      FORMAT(7F10.5),     RATIO(J,  2),J=  1,  3
      FORMAT(7F10.5),     RATIO(J,  3),J=  1,  3
29    NTTS,IBTYP(1),IBTYP(2),AK1,AK2,PONE,PTWO
30    BRAKE PRES. TPC(I), I=   1,  9
                  TPC(I), I=  10, 18
                  TPC(I), I=  19, 27
                  TPC(I), I=  28, 36
                  TPC(I), I=  37, 41
31    THROTTLE SET TTS(I), I=   1,  9
                  TTS(I), I=  10, 18
                  TTS(I), I=  19, 27
                  TTS(I), I=  28, 36
                  TTS(I), I=  37, 41
32    TRANS. RATIO TTR(I), I=   1,  9
                  TTR(I), I=  10, 18
                  TTR(I), I=  19, 27
                  TTR(I), I=  28, 36
                  TTR(I), I=  37, 41
33    ENGINE RPM,TRPME(I), I=   1,  9
                 TRPME(I), I=  10, 12
34    WIDEOPEN TH.TWOT(I), I=   1,  9
                 TWOT(I), I=  10, 12
35    CLOSED THROT TCT(I), I=   1,  9
                  TCT(I), I=  10, 12
36    BRAKE PARAM.GN(I,1), I=   1,  9
      BRAKE PARAM.GN(I,1), I=  10, 16
36    BRAKE PARAM.GN(I,2), I=   1,  9
      BRAKE PARAM.GN(I,2), I=  10, 16
37    TAUO(I),I=1,4
38    LINING FADE  TLF(I), I=   1,  9
                  TLF(I), I=  10, 18
                  TLF(I), I=  19, 27
                  TLF(I), I=  28, 36
                  TLF(I), I=  37, 45
                  TLF(I), I=  46, 51
39    TAUA,PZERO(1),PZERO(2),CONE,CTWO,CTHREE,ZETAB
```

Figure 2.5-11 **COMPUTER PROGRAM INPUTS FOR STRAIGHT AHEAD STOPS – CARD IMAGE FORMAT**

(7 of 7)

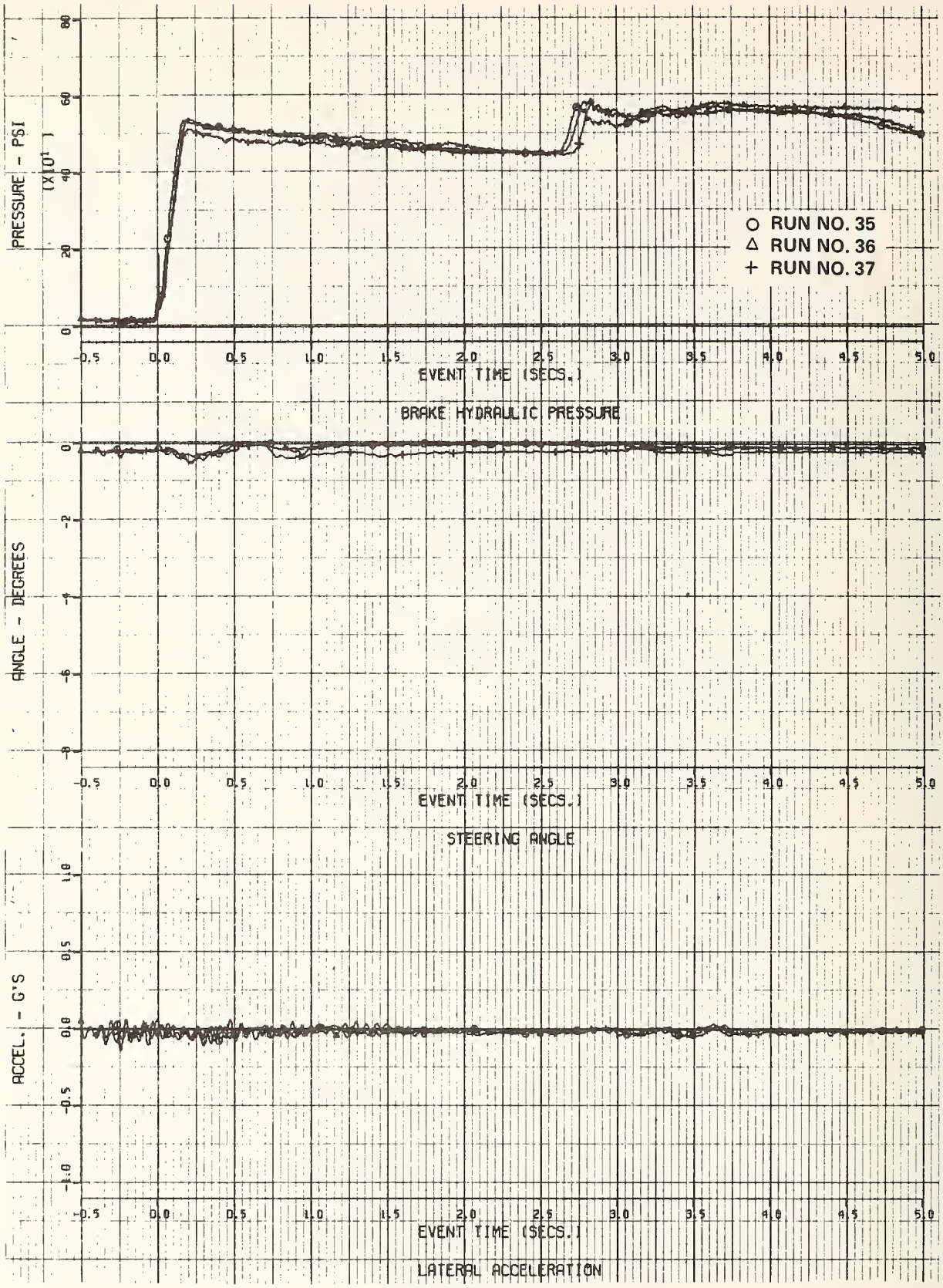

Figure 2.5-12(a) **EXPERIMENTAL TIME HISTORIES OF VEHICLE RESPONSES TO STRAIGHTAHEAD BRAKING MANEUVER**

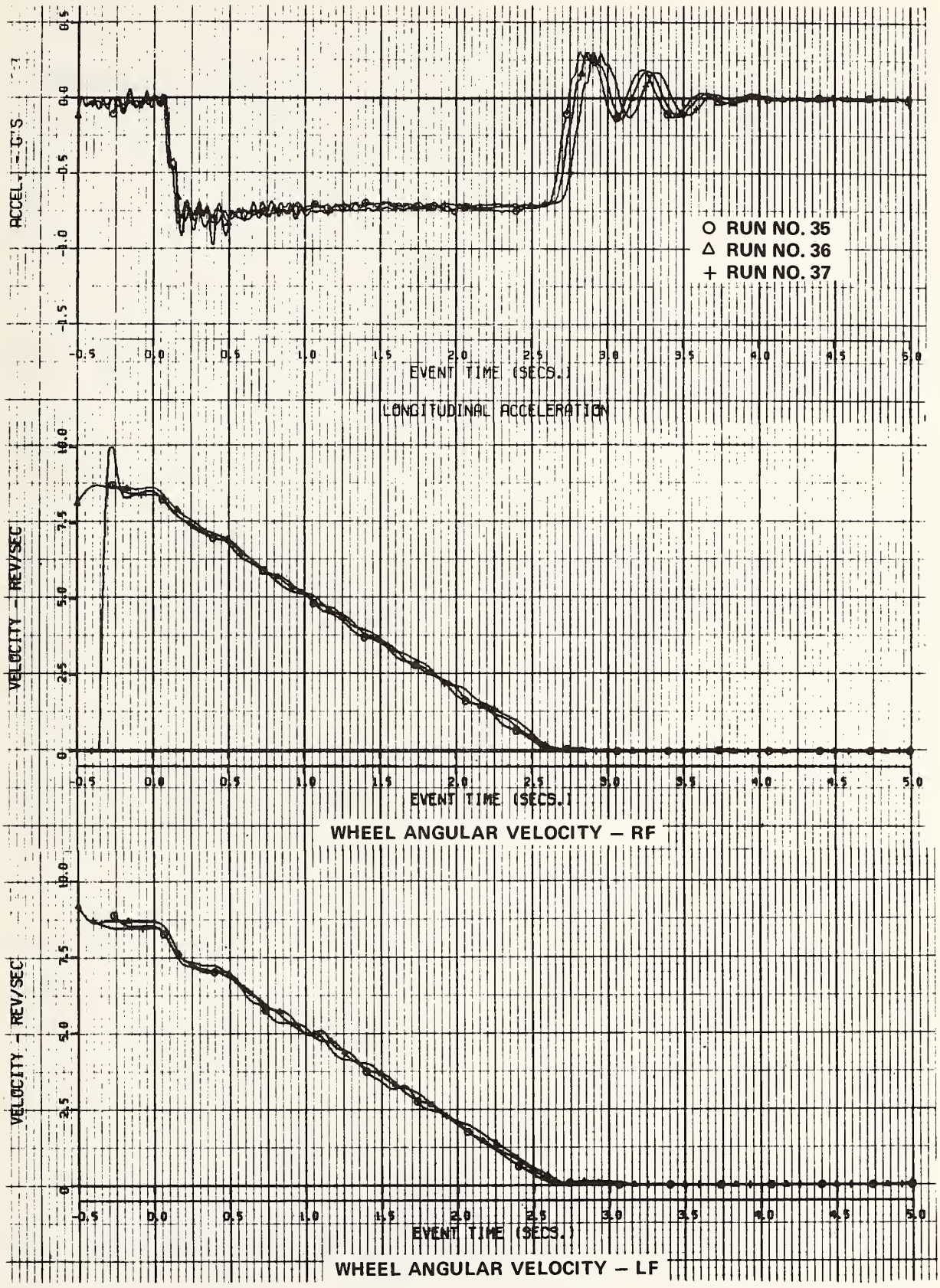

Figure 2.5-12(b)

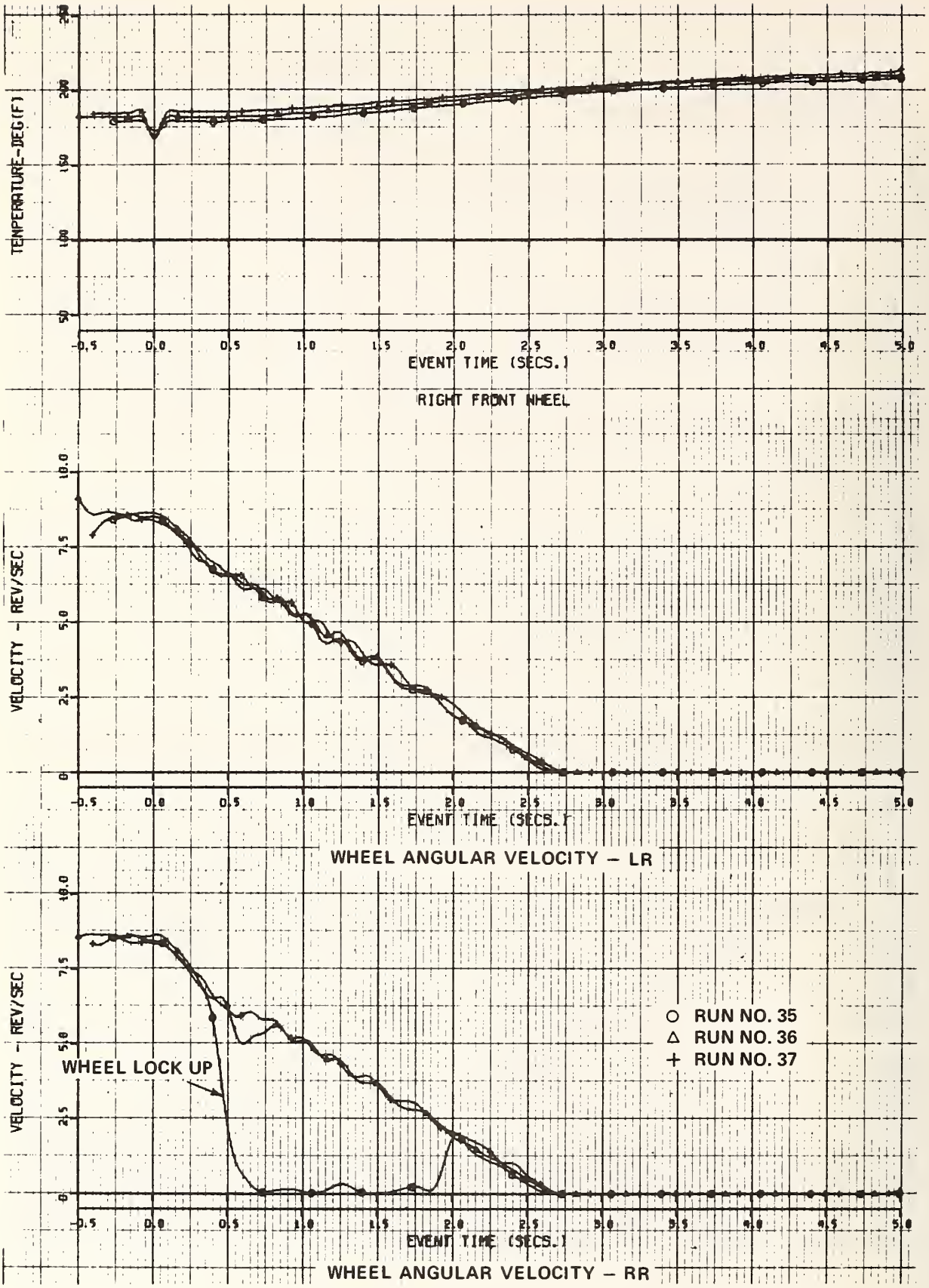

Figure 2.5-12(c)

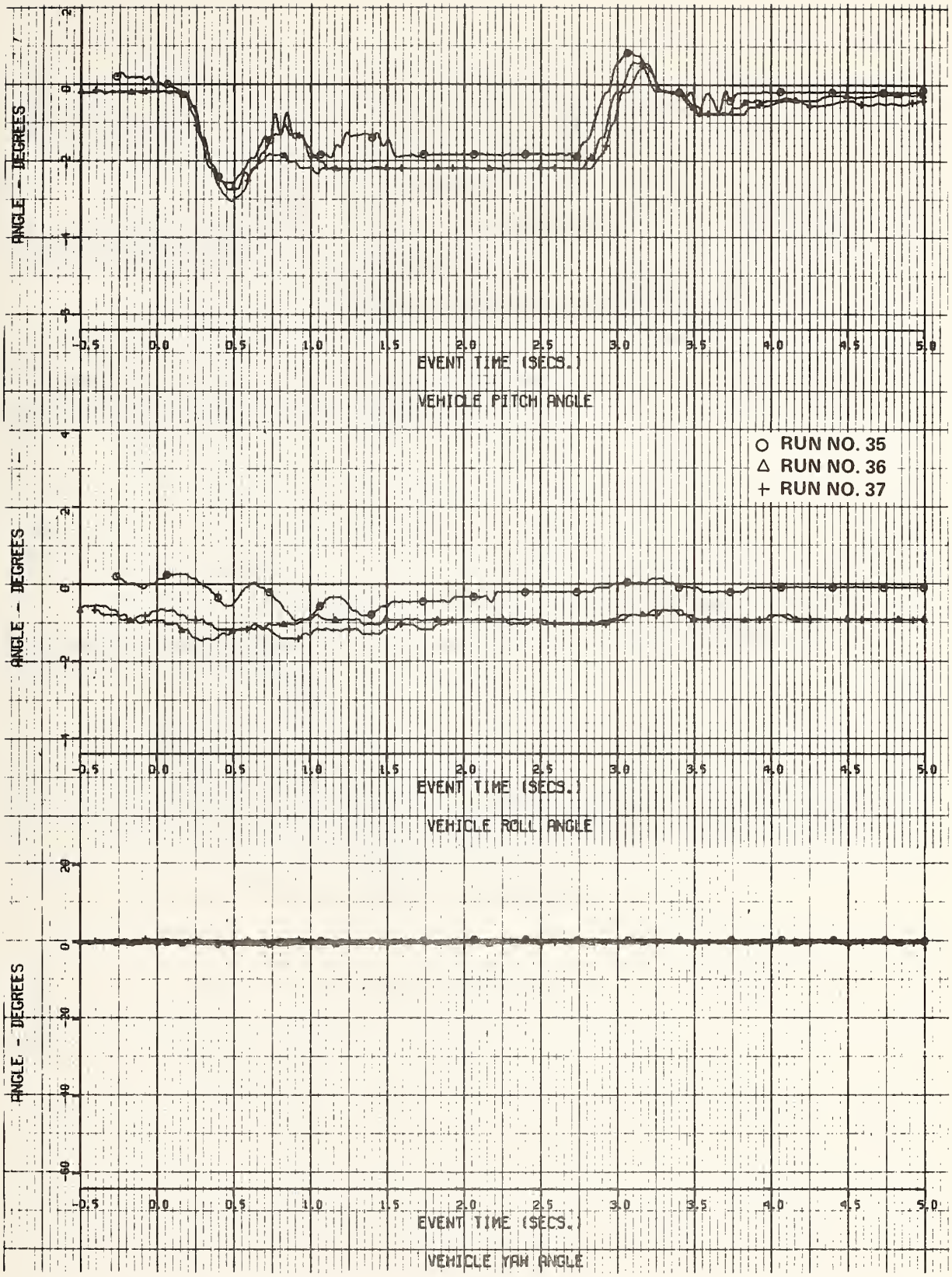

Figure 2.5-12(d)

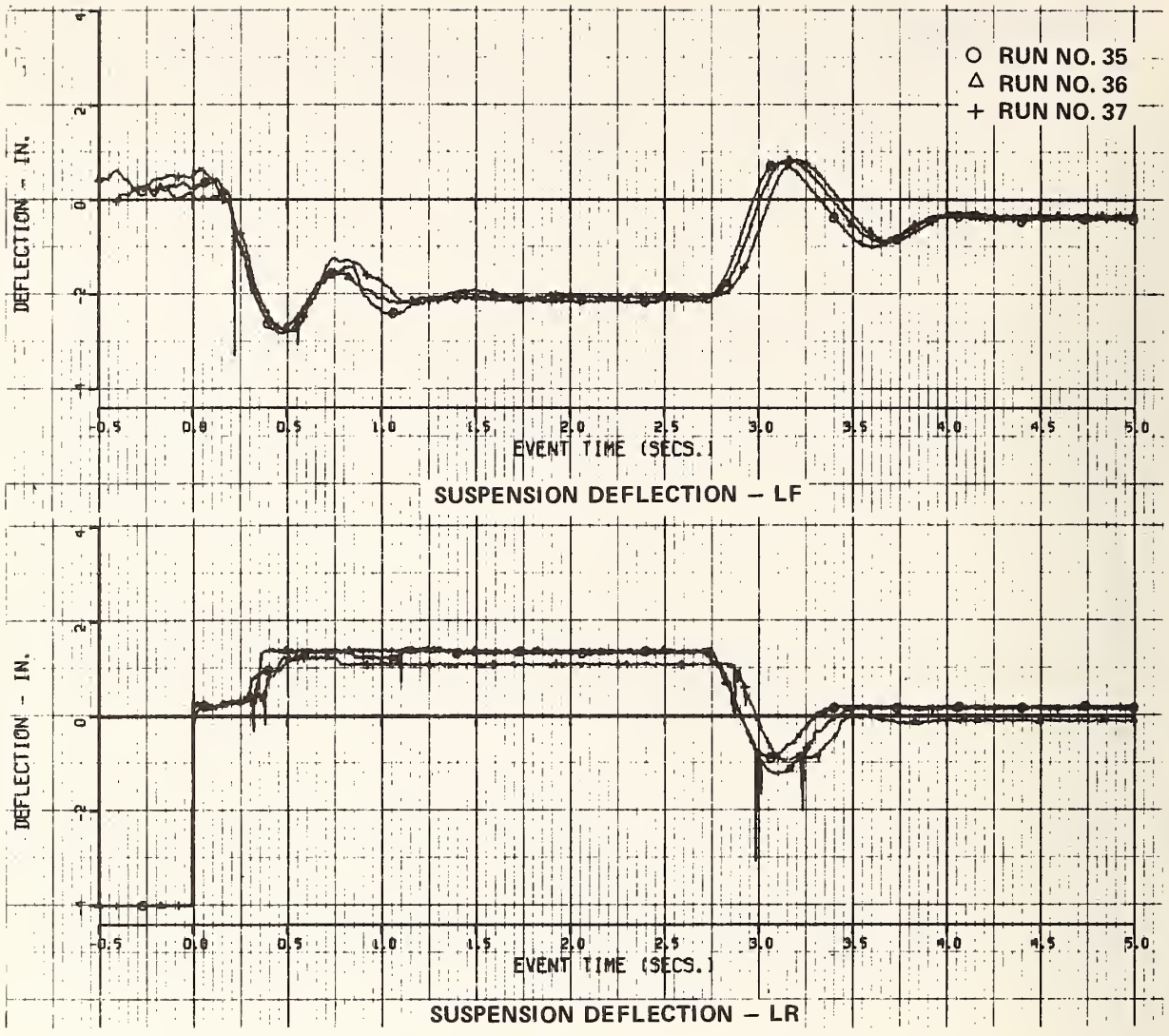

Figure 2.5-12(e)

than the initial peak value. It is believed that the major part of this variation is the result of what is referred to as mechanical wrap-up of the brake system in conjunction with the self-actuation of the duo-servo brake and elastic deformation of the brake drums. The similarity in character of the brake pressure and the longitudinal acceleration time histories suggests another possible factor contributing to the phenomenon. The variation of the brake pressure could result from the variation of the longitudinal acceleration causing a similar variation in the pedal force applied by the driver. Because the adjustable pedal stop assembly is mounted on the vehicle floor, it is possible for the stop, and thus the brake pedal, to move slightly relative to the master cylinder due to an elastic deformation of the floor under the varying pedal force.

In one of the straight ahead stops, the applied brake pressure was slightly low (relative to the other runs) during the early part of the event. This increased the duration of the event for this test as is observed from a comparison of the trailing edge of the longitudinal acceleration time histories. For this run, the event duration is greater than that of one run by 0.1 second and of the other by 0.05 second.

From the plots of rear wheel angular velocity shown in Figure 2.5-12 (c), it may be seen that the right rear wheel locked up for about 1.4 seconds in one of the tests and nearly locked up in another at t = 0.5 seconds. Note from the plots of Figure 2.5-8 that the measured brake torque coefficient for this wheel was slightly greater than that for the other rear wheel. This could account for the difference in the behavior of the two rear wheels for the conditions of the tests in which the right rear wheel operated at incipient lockup, whereas, the left rear wheel braking effort was slightly below this condition.

At the beginning of the wheel angular velocity time histories (t = -0.5 second) a variation of the velocity may be noted, whereas, in fact, these velocities were constant at the initial value, Ω_0 . This indicated variation prior to t = 0 is erroneous and resulted from the way the derivative of the function (in this case angular displacement time history) was evaluated in the computer data reduction process. However, the angular velocities at t = 0 seconds are correct. The values evaluated by the computer data reduction process at time zero were checked by hand calculations using two different methods of operating on the raw data.

A difference of 0.8 degrees of vehicle roll attitude may be observed for one run relative to the others. This is the result of a slight deviation of the vehicle roll attitude at the time the gyros were uncaged.

Table 2.5-6 presents the stopping distances measured for the straight ahead stops. The trajectory marker of the rear bumper was used to determine the stopping distances. The measured distances are the length of the trajectory as marked on the pavement, plus a lag distance described below.

Table 2.5-6
MEASURED STOPPING DISTANCES
STRAIGHT-AHEAD BRAKING MANEUVER

RUN NO.	*STOPPING DISTANCE INCHES
35	976
36	1002
37	996
*INCLUDING LAG DISTANCE = 66 INCHES	

It is estimated that there is about 0.09 second lag between the time the brake pressure reaches 40-50 psi (the time zero mark) and the time the marking fluid reaches the ground. The sequence of events is illustrated in the sketch of Figure 2.5-13. The marker switch closes when the pedal motion begins and time zero is recorded when the pressure reaches 40-50 psi. The solenoid valve controlling the marker fluid is mounted on the bumper, and the end of the fluid nozzle is about two inches off the ground. The lag is the result of the time it takes for the valve to open, and the fluid to reach the ground. The estimated distance the vehicle travels during this lag interval, based on the vehicle initial velocity, is added to the measured stopping distance.

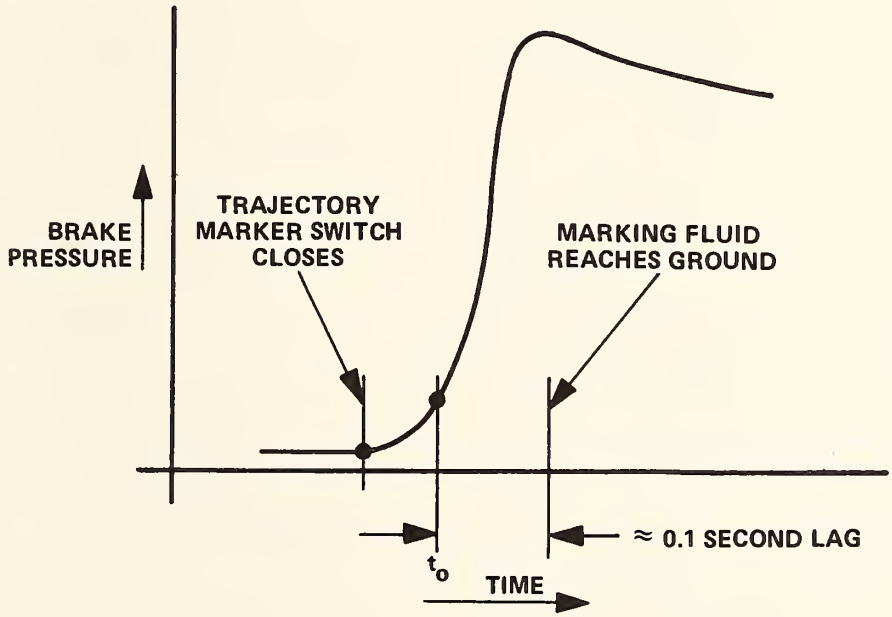

Figure 2.5-13 **SEQUENCE OF EVENT RELATIVE TO TRAJECTORY MARKING**

The computed vehicle responses are presented in Figure 2.5-14 where they are superimposed on the corresponding measured results as presented in Figure 2.5-12. It should be noted that the variation of the brake lining fade was suppressed for these predictions because of the uncertainty of the relevant inputs as discussed in Section 2.5-5. However, the influence of lining fade variation on the results is examined and presented in Section 2.5.5. The constant value of lining fade coefficient which was used in the simulation corresponds to the 170°F measured temperature of the brakes at the beginning of each test run.

In the computed results, it should be noted that there are some spurious responses (especially in the accelerations) at the very end of the event which occur as the vehicle speed approaches zero. This is the result of a numerical instability which occurs only at a very low vehicle velocity. It is of no practical consequence and should be ignored.

The computed stopping distance is 991 inches as compared to the three measured values of 976, 1002 and 996 inches. The correlation of the predicted results with the measured results is seen to be very good, especially with regard to some of the detailed characteristics of the time histories of the individual wheel angular velocities. In particular for the front wheels, it is observed that over the time interval $0 \leq t \leq 0.2$, there is, in both the experimental and predicted results, an initial very rapid decrease of the angular velocity. This corresponds to the time interval when the braking torque is increasing very rapidly to its peak value and thus exceeds (by a relatively large amount) the instantaneous torque generated by the circumferential force of the tire/ground interface, because the wheel has not yet developed sufficient circumferential slip. This large excess of the braking torque over the tire-developed torque decelerates the wheel rapidly. During the interval immediately following, i.e., $0.2 \leq t \leq 0.5$, the rate of change of the angular velocity of the front wheel is observed to be relatively low in both the measured and computed results. During this interval, the brake torque is decreasing

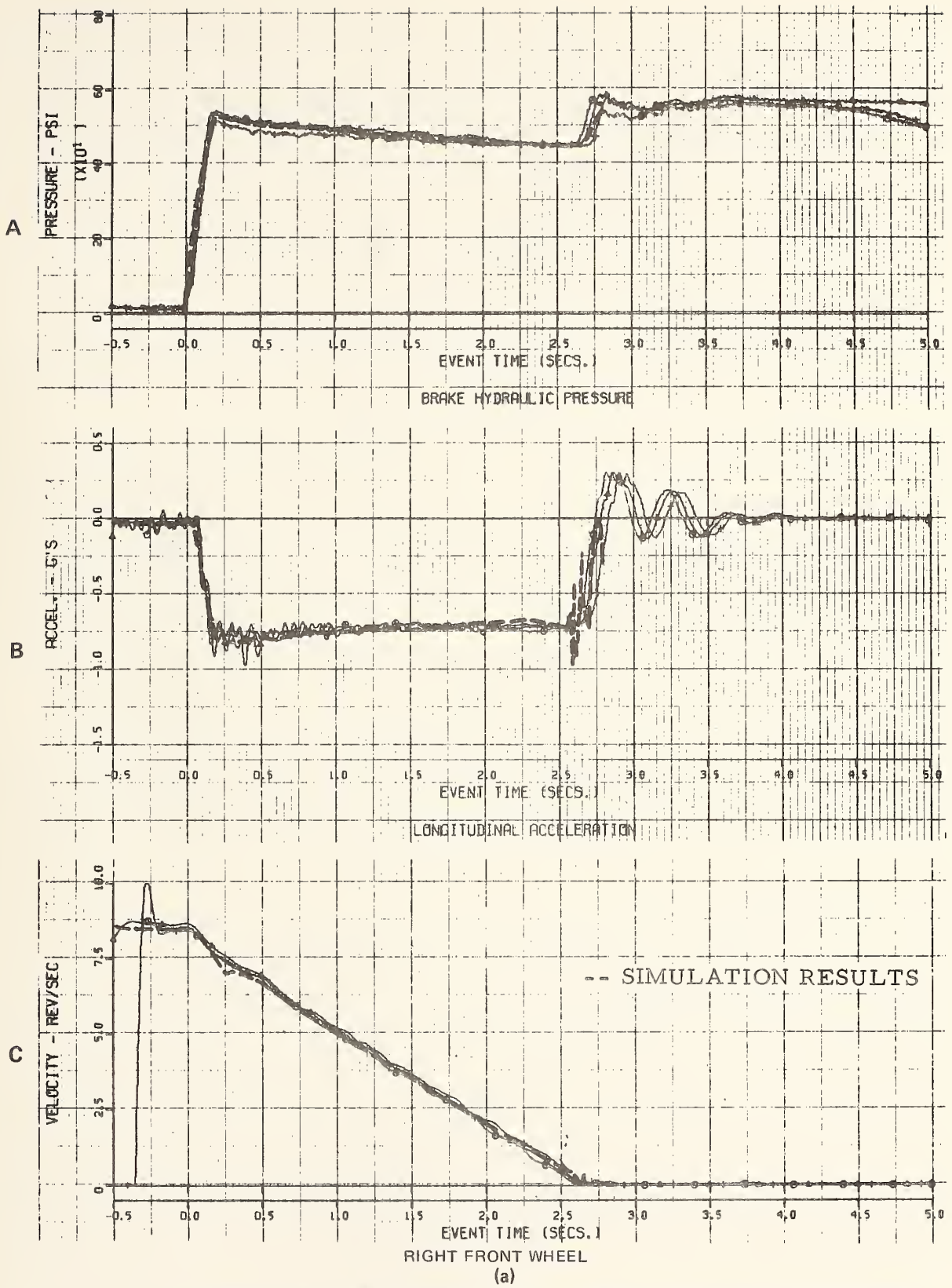

Figure 2.5-14 COMPARISON OF MEASURED AND COMPUTED VEHICLE RESPONSES — STRAIGHT AHEAD BRAKING MANEUVER

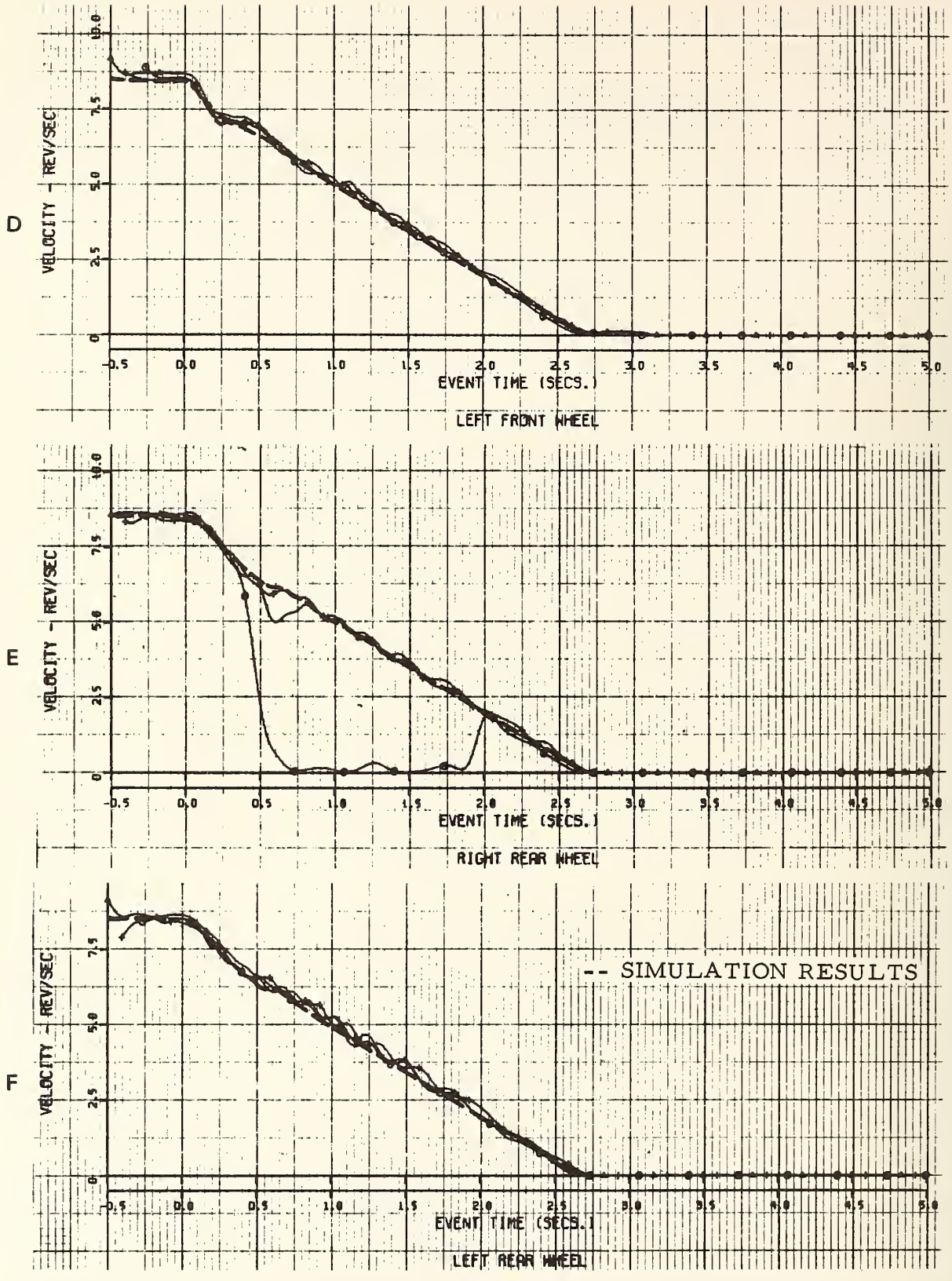

(b)

gure 2.5-14 (Cont.) COMPARISON OF MEASURED AND COMPUTED VEHICLE RESPONSES – STRAIGHT AHEAD BRAKING MANEUVER

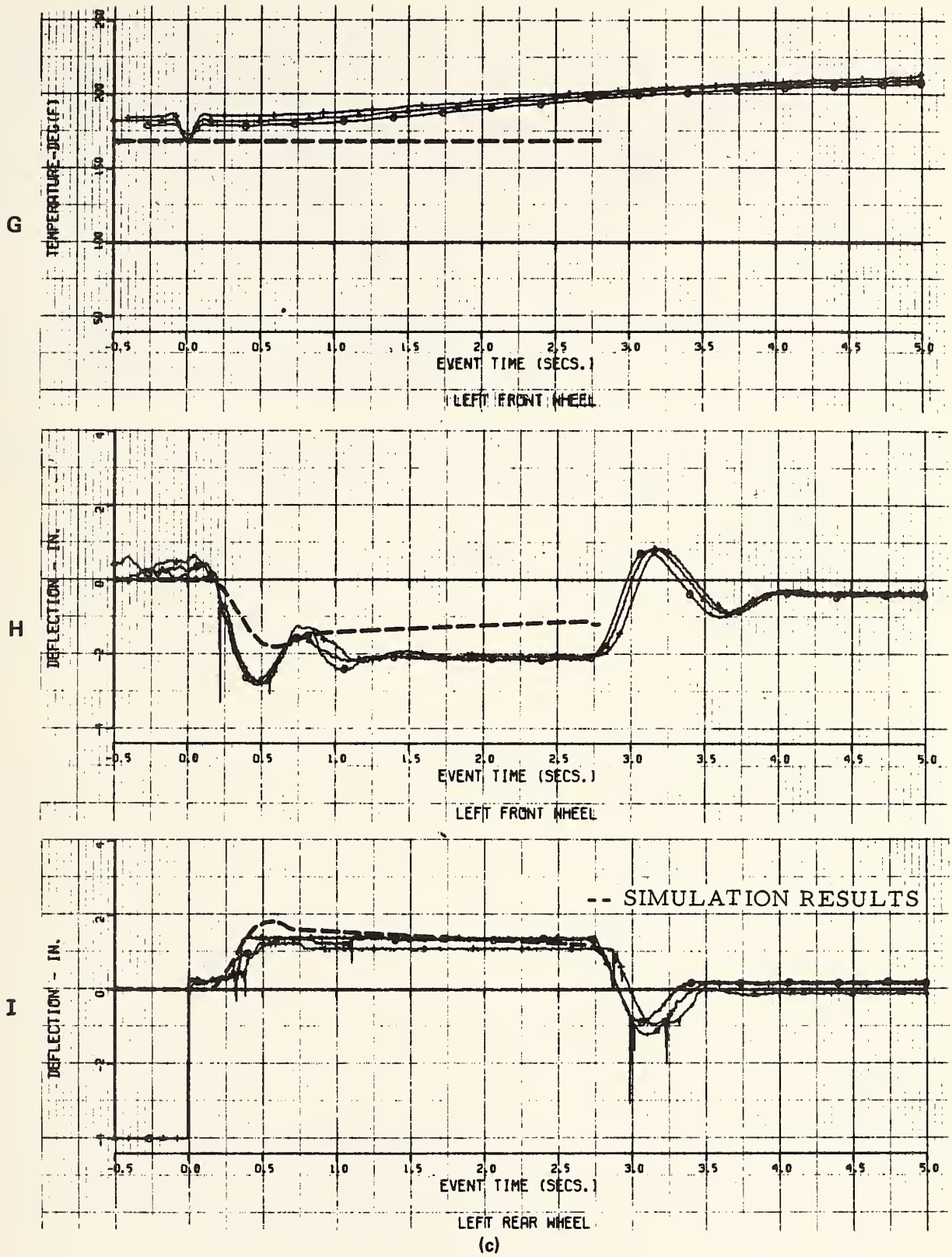

Figure 2.5-14 (Cont.) COMPARISON OF MEASURED AND COMPUTED VEHICLE RESPONSES – STRAIGHT AHEAD BRAKING MANEUVER

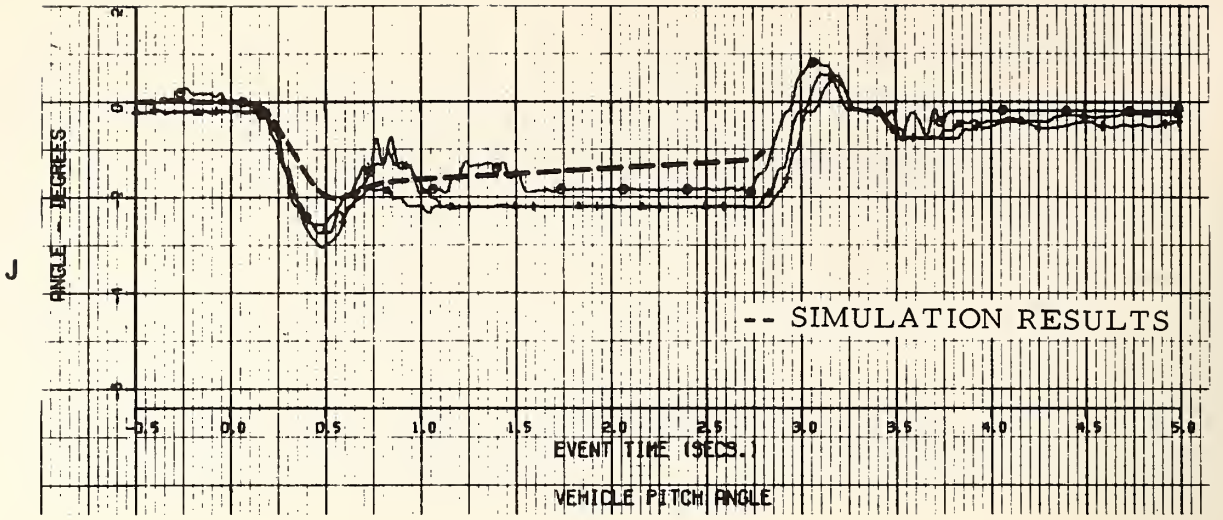

(d)

Figure 2.5-14 (Cont.) COMPARISON OF MEASURED AND COMPUTED VEHICLE RESPONSES – STRAIGHT AHEAD BRAKING MANEUVER

slightly, while at the same time the torque generated by the tire/ground interface is increasing due to the increasing vertical load on the tire which results from the longitudinal weight transfer. Thus, during this interval, the net decelerating torque and the corresponding wheel deceleration are reduced. The time correlation of the longitudinal weight transfer with this interval is observed in the time histories of the vehicle pitch attitude and front wheel suspension deflection.

Similar detailed characteristics are observed in both the measured and predicted time histories of the rear wheel angular velocities. However, in the time interval $0.2 \leq t \leq 0.5$, longitudinal weight transfer has the opposite effect on the rear wheel deceleration; that is, it tends to increase the wheel deceleration during this interval. This is the result of the weight transfer reducing the vertical load on the rear wheels and thus reducing the tire-developed torque. In the experiments, the right rear wheel was operating at incipient lockup, as is described above; this effect of the transient weight transfer was evidently a contributing factor in precipitating lockup of this wheel during one of the test runs.

The correlation of the measured and computed longitudinal acceleration is very good; however, the computed acceleration does decrease slightly throughout the event (i.e., it follows a similar trend in the applied brake pressure) whereas the measured acceleration tends to remain more constant. The specific source of this minor discrepancy is not known; however, the following brief discussion indicates some possibilities. The vehicle decelerating force and resulting deceleration are the direct result of the forces generated at the tire/ground interface, and these are proportional to the brake torque which is, in turn, proportional to the applied brake system hydraulic pressure. Thus, in the sequence of events between the applied brake pressure and the resulting tire generated forces, it is quite possible that there exist physical phenomena which are not included in the simulation but which have a small effect on the resulting tire force variation. For example, the brake lining/drum friction coefficient may

increase with a decrease in their relative velocity, and the tire "deflected" radius may decrease with decreasing vehicle speed; these effects would increase the tire-generated forces throughout the event and thus would tend to make the vehicle deceleration constant by compensating for the decreasing pressure. Note that a variation of tire/ground friction coefficient with speed will not influence these results; this is discussed in Section 2.5.5.

Including the variation of lining fade coefficient with brake temperature in the simulation causes an additional decrease of vehicle deceleration throughout the event. This results from the brake temperature at time zero being greater than that corresponding to the peak value of lining fade coefficient, thus the lining fade coefficient and torque decrease throughout the event as the temperature increases.

While, in general, the correlation between the predicted and measured responses is very good, the correlation obtained for the sprung mass response relative to the unsprung masses is the least satisfactory as may be observed in the pitch attitude and wheel deflection time histories. The source of the observed differences is attributed primarily to the assumed input values used to describe the shock absorber and suspension characteristics. Because the sprung mass responses were not the primary objective of this investigation, effort was not expended to measure these characteristics. Instead, they were assumed to be the same as used in the previous investigation (Reference 6), because the vehicles are identical except for the shock absorbers. The shock absorbers on the previous test vehicle were new, and their characteristics were measured; whereas, those on this test vehicle, while working satisfactorily, were not new and their characteristics were surely somewhat different. It is also quite possible that there were some other small differences in the suspension characteristics of the two vehicles.

2.5.5 Vehicle Response Sensitivity

The validity of the predicted results of any simulation not only depends on the adequacy of the simulation itself but obviously also depends on the inputs used and the sensitivity of the computed results to these inputs. Furthermore, it is not always possible to define all of the values for the input parameters accurately. Thus, it is of interest to at least qualitatively assess the sensitivity of the computed results to some of these inputs whose values are not accurately known. This was done for several of these inputs by changing them individually and rerunning the computation; the results are presented and discussed below.

2.5.5.1 Variation of Lining Fade Coefficient

The brake temperature was measured by use of thermocouples installed in the brake as described in Section 2.5.1.2, and the initial equilibrium temperature of nominally 180°F was obtained as described in Section 2.5.3. It should be noted that these measured brake "lining temperatures" are not the desired surface temperature of the lining/drum interface which determines the brake fade characteristics. Because of the heat transfer properties and thermally effective mass of the brake drum and shoes, the measured brake "lining temperature" variations will be attenuated relative to the surface temperature and lag it in time.

It was intended that the same temperature measurement during the validation tests as was used for the determination of the brake fade characteristics would allow the use of these fade characteristics in the simulation as an approximation. However, the accuracy of this approximation is critically dependent on the proper choice of the "effective" thermal properties of the brake assemblies for use in the simulation. They must be chosen so as to reproduce the brake "lining temperature" and not the surface temperature. The lack of an independent explicit procedure for chosing these "effective" thermal properties degrades the quantitative value of the predicted influence

of the brake fade characteristics. However, the simulation of the phenomenon is correct, and the results which include lining fade are qualitatively believed to be correct.

The variation of lining fade coefficient with brake temperature is presented in Figure 2.5-15. This variation was derived from the measurements described in Section 2.5.1.1. Two computer runs of straight ahead stops were made. In run No. 1 the fade variation was disabled and the fade coefficient held at a constant value corresponding to a brake temperature of 170°F. In run No. 2, the lining fade coefficient was allowed to vary according to the predicted brake temperature variation and the fade characteristic presented in Figure 2.5-15. The range of values experienced in these two runs are indicated on the figure.

The brake temperature time histories and the resulting vehicle longitudinal accelerations obtained from these two runs are presented in Figure 2.5-16. The effect of lining fade variation is observed to progressively reduce the longitudinal deceleration throughout the event as the brake temperature increases. The deceleration is lower by 13 percent at t = 2.25 seconds. Because of the lower decelerations, the stopping distance increased by 8 percent (i.e., from 991 inches to 1069 inches).

2.5.5.2 Effective Push-Out Pressure for the Brake System

As was discussed in Section 2.5.1.1, and presented in Figure 2.5-8, the measured brake output torque did not vary linearly with the pressure for the lower range of pressures; this effect is accommodated in an approximate manner in the simulation by using an "effective" push-out pressure. The front to rear distribution of braking capacity is controlled by designing the front and rear brakes to have the appropriate relative brake torque coefficients (slope of the curves) as illustrated in Figure 2.5-17. The ratio of the front, T_F, to rear, T_R, brake torque at a given pressure is determined only by the relative

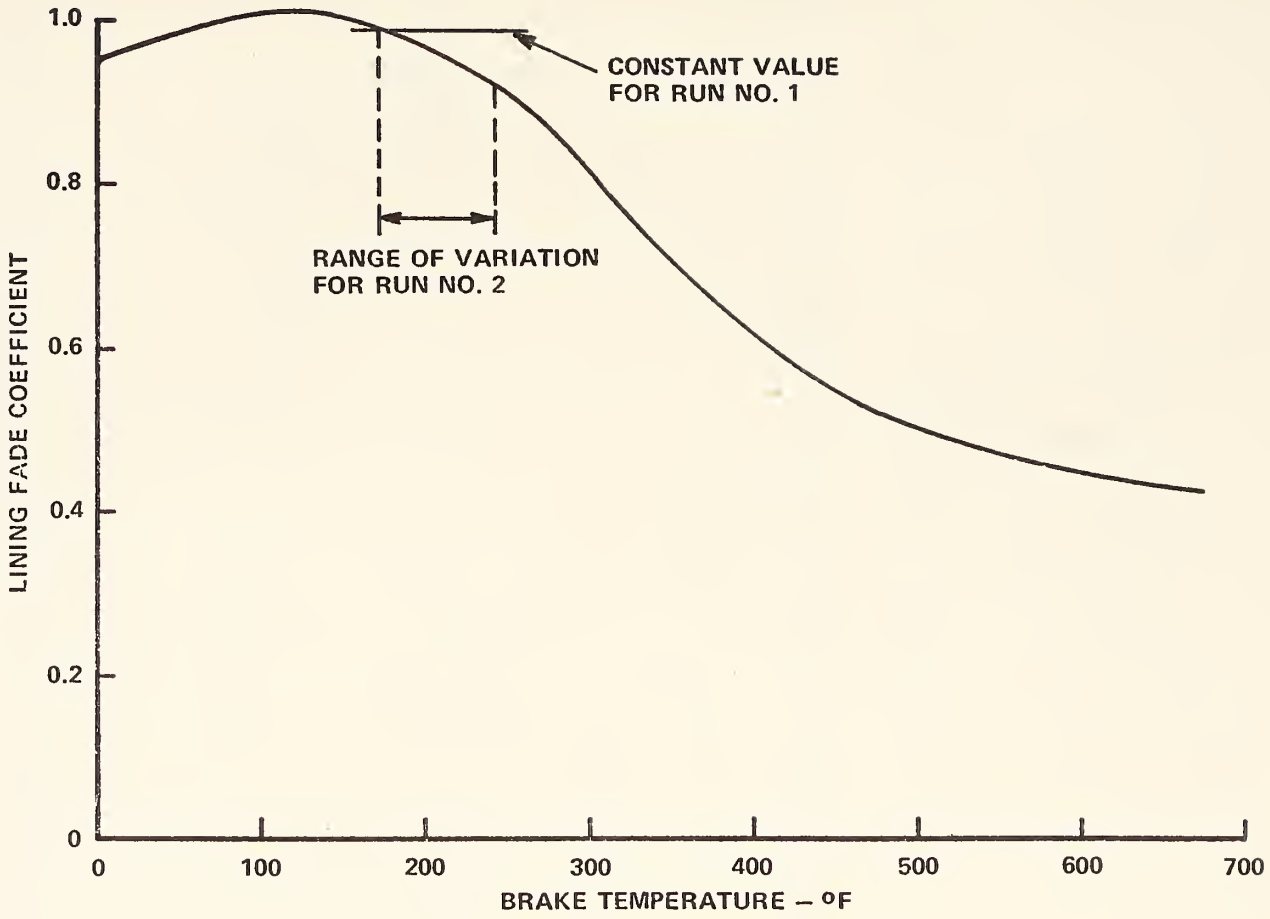

Figure 2.5-15 LINING FADE COEFFICIENT VARIATION WITH BRAKE TEMPERATURE

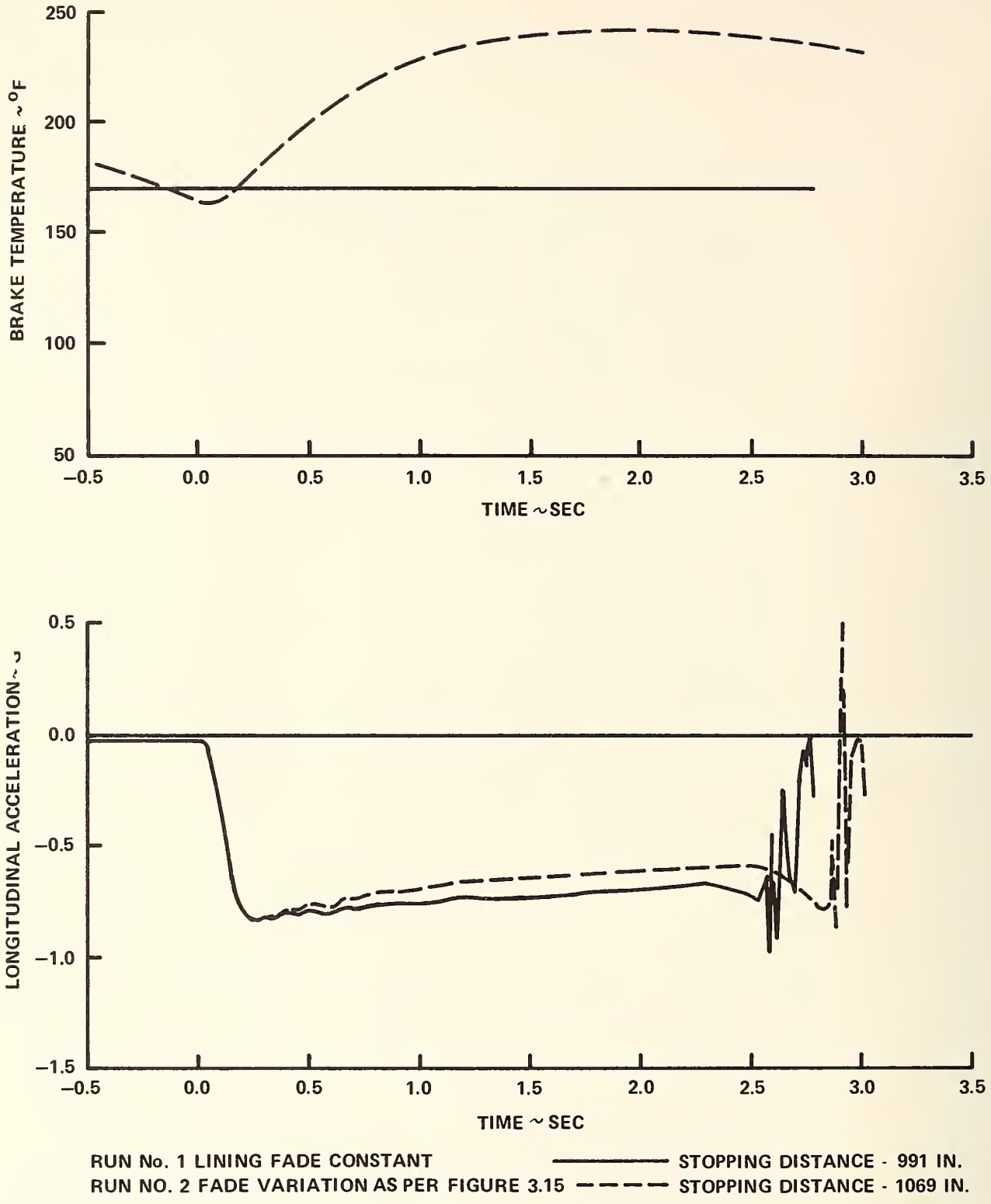

Figure 2.5-16 INFLUENCE OF LINING FADE VARIATION ON VEHICLE LONGITUDINAL ACCELERATION

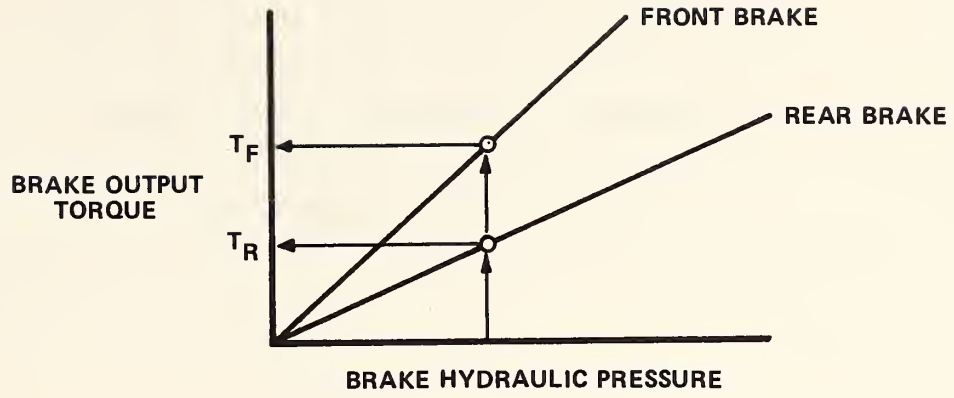

Figure 2.5-17 DESIGN RELATIVE FRONT/REAR BRAKE CAPACITY

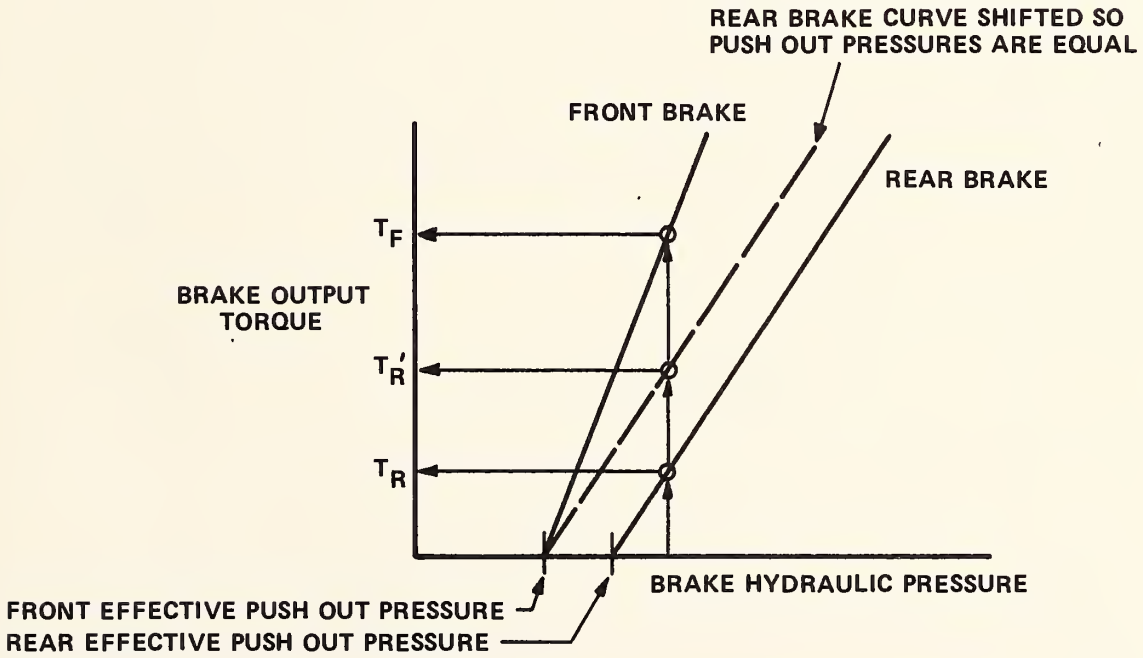

Figure 2.5-18 ILLUSTRATION OF MEASURED BRAKE CAPACITY

slopes. However, for the actual physical system, this ratio is affected by another factor evident from the measured results as illustrated in Figure 2.5-18. (The control measured results are presented in Figure 2.5-8.) Because of the difference in the variation of the front and rear brake output torques over the lower range of pressures, it is clear that the "effective" push-out pressure is different for the front and rear brakes. Thus, as can be observed in the figure, the ratio of front to rear brake torques, T_F/T_R is greater than that which would exist if both the front and rear brakes had the same push-out pressure. That is, the front to rear braking capacity is a function of the "effective" push-out pressures as well as the brake torque coefficients.

It is not known if this difference of effective push-out pressures is common or, if so, if it is consistent from vehicle to vehicle of a given model. However, for the measured results, it is seen to have a sizable effect on the front to rear distribution of braking capacity. Furthermore, it was noted in the computed results using the measured braking characteristics that the front wheels operated at greater circumferential slip than the rear wheels (slip on front wheels -- 20-50% greater than rear). This difference seems quite large, especially in view of the design practice of providing a front to rear braking distribution that is close to optimum for operation on the higher friction surfaces such as dry pavement (i.e., the conditions of this run).

To assess how much the measured difference in the effective push-out pressures influenced the results, the value for the rear brake was reduced and made equal to that for the front brakes; the computation was then repeated. This had the effect of increasing the rear brake output torque for all applied pressures. The computed circumferential slip for the front and rear brakes were then virtually equal, and the stopping distance was reduced approximately 6 percent. It should be noted that the push-out pressures could also have been made equal by increasing the value of the front brakes which would have resulted in an increase of the stopping distance while again producing virtually equal circumferential slip of the front and rear wheels.

2.5.5.3 "Rolling" Radius of the Tires

The validation maneuvers of this effort were initiated from a nominal initial velocity of 40 MPH as indicated by the vehicle speedometer. However, for validation of the computer simulation, a more precise determination of the speed is required. Because the individual wheel angular velocities were being measured quite accurately, it was planned to use this information and the measured deflected radius of the tire to compute the initial velocity as

$$U_0 = \Omega_0 R_d$$

The measured "deflected" tire radius (distance from wheel center to ground) was 12.56 inches with the vehicle loaded to the test configuration and with the tires inflated to the test pressure of 28 psi. For the straight ahead braking maneuver, the measured initial wheel velocity, Ω_0 , was 8.5 revolutions per second (mean value of the three repeat runs). Those measurements correspond to an initial vehicle speed of 38.1 MPH. However, a careful integration of measured vehicle accleration time history indicates an initial velocity of 41.6 MPH which is 9.2 percent greater than the above value; thus, there was an inconsistency in the measured results.

In an attempt to resolve this discrepancy, the calibration of the accelerometer and the reduction of the accelerometer data was checked and found to be correct. The wheel angular velocity data was also thoroughly checked and found to be correct. Using the vehicle velocity deduced from the measured acceleration and the measured wheel angular velocity, a "rolling" radius of 13.72 inches would be required for these measurements; yet, the "deflected" tire radius when remeasured was only 12.56 inches. This finding implied that the loaded pneumatic tire rolls forward a distance greater than 2π times its deflected radius which was confirmed by carefully measuring, for one of the tires on the vehicle, the distance traveled per revolution. These measurements, made for a very small forward velocity

of the vehicle, indicated an effective "rolling" radius of 12.90 inches. Although this radius is significantly greater than the measured deflected radius, it is less than required to explain the existing discrepancy. However, experimental evidence (Reference 13) indicates that the "rolling" radius also increases with speed. A discussion of this phenomenon is given below.

It is possible to construct a qualitative heuristic description of a physical process by which the tire can roll forward a distance greater than 2π times its deflected radius. This phenomenon is believed to be the result of internal elastic strains in the tire which allow the tread and/or carcass elements to be compressed (in the upstream circumferential direction) as they approach and enter the region of the tire/ground patch. As the wheel moves forward and these elements pass beneath the wheel, they recover from their elastic strains. If the tire were perfectly elastic and there was no slip of the tread elements relative to the ground, the recovery of the strained elements would have the effect of moving the wheel center forward an additional distance D per revolution, where

$$D = \int_0^{2\pi} \epsilon \, d\theta$$

$d\theta = ds/R_W$

ds = differential circumferential distance

R_W = undeformed tire radius

ϵ = effective circumferential strain of tread.

The effective circumferential strain of the tread is ultimately proportional to the normal stresses at the tire ground interface. Because these stresses are proportional to the tire vertical load, and its angular velocity, the additional distance a tire travels forward is proportional to its vertical load, its angular displacement, θ , and its angular velocity, $\Omega = \dot{\theta}$. This described phonomenon would be modified by other phenomena such as radial growth of the tire proportional to angular velocity due to the

centrifugal forces acting on the tire elements. These phenomenon discussed above would also provide a source of rolling resistance of a tire on a rigid surface.

The computer simulation only accounts for the variation of the "deflected" radius with vertical load and, for zero slip (i.e., traction or braking force equal zero), computes the wheel angular velocity as being proportional to the vehicle velocity and inversely proportional to the deflected radius. Therefore, to allow matching of the wheel angular velocity and the vehicle speed with the measured initial values, the deflected radius at time zero was made equal to 13.72 inches by using an artificial undeflected tire radius equal to 13.72 inches plus the static deflection due to vertical load. This approximation accounts for the total effect (due to load, angular displacement and velocity) at the initial speed and it neglects only the variations in the "rolling" radius which would accrue due to the variations of D resulting from the diminishing of the angular velocity throughout the event and the variations in the vertical load on the tire.

For the tires of these tests with an inflation pressure of 28 psi and operating at 40 MPH, the experimental results indicate a "rolling" radius 10 percent greater than the measured static deflected radius of the tires. Because it is the "rolling" radius that relates the vehicle speed to the wheel angular speed, use of the "rolling" radius, R_R (which is the larger of these two radii), in the simulation results in a smaller computer initial wheel angular velocity than if the value of the deflected radius is used. Also, the larger radius will result in a lower wheel angular deceleration, $d\Omega/dt$, for a given vehicle deceleration, a_x, time history, because they are related as follows (neglecting the relatively small effects of circumferential slip).

$$d\Omega/dt = a_x/R_R$$

These effects are observed in the computed wheel velocity time histories of a straight ahead stop presented in Figure 2.5-19. In this example, the deflected radius of the tire was used for run No. 1, and the "rolling" radius was used for run No. 2. It should be noted that although the "rolling" radius (i.e., distance tire moves forward per revolution divided by 2π) relates the vehicle speed to the wheel angular speed, the torque developed by the tire circumferential forces is proportional to the deflected tire radius.

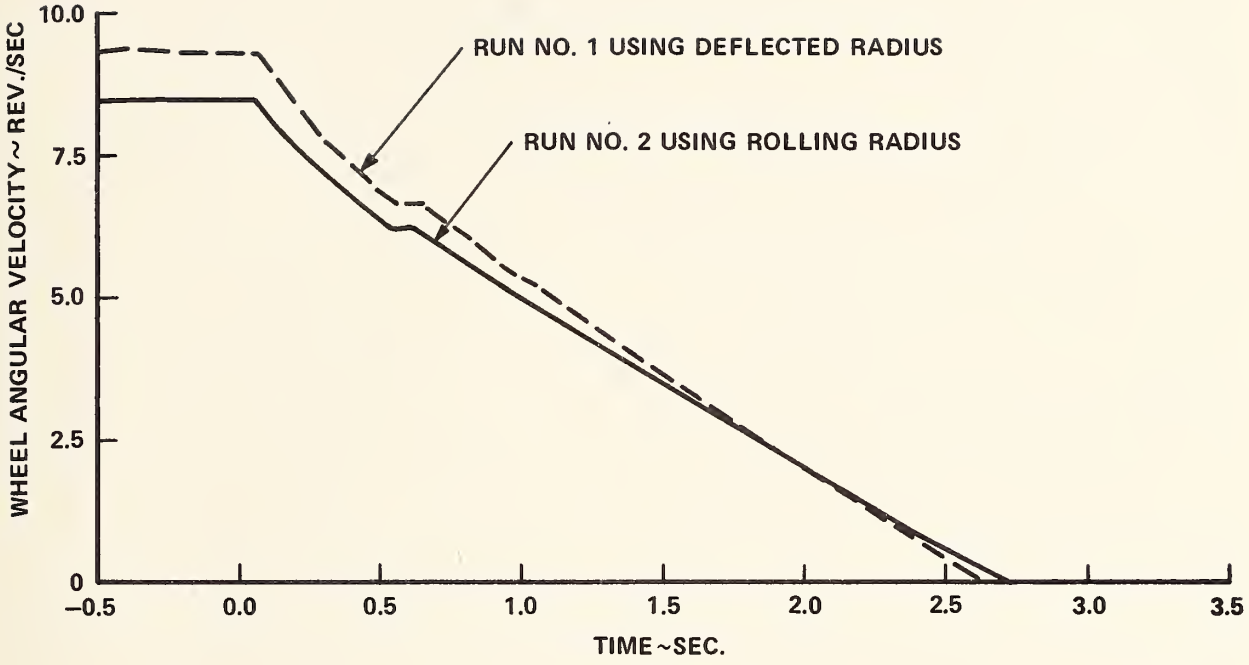

Figure 2.5-19 INFLUENCE OF A CHANGE IN THE ROLLING RADIUS

2.6 Braking In A Turn HVOSM-VD1

2.6.1 Test Vehicle and Instrumentation

The test vehicle and instrumentation used in this series of tests was the same as reported in Section 2.5.1.

2.6.2 Data Acquisition and Reduction

Data acquisition and reduction procedures used were the same as reported in Section 2.5.2.

2.6.3 Test Procedures

The test procedure for the combined cornering and braking was the same as that reported in Section 2.5.3 except for the addition of the application of a vehicle steer input. This was initiated manually by the driver as soon as the brake pedal was depressed. The steering input consisted of rapidly turning the steering wheel one-half turn and firmly holding it there until the vehicle stopped. This resulted in a steering input of seven degrees at the wheels. After a few practice runs, the driver was able to repeat the braking and steering inputs and their relative timing quite well.

2.6.4 Comparison of Predicted and Experimental Results

The responses measured in the repeated experiments of the combined cornering and braking maneuver are shown in Figure 2.6-1. It may be seen that the control inputs and their relative timing, and the vehicle responses were nearly identical for the three tests.

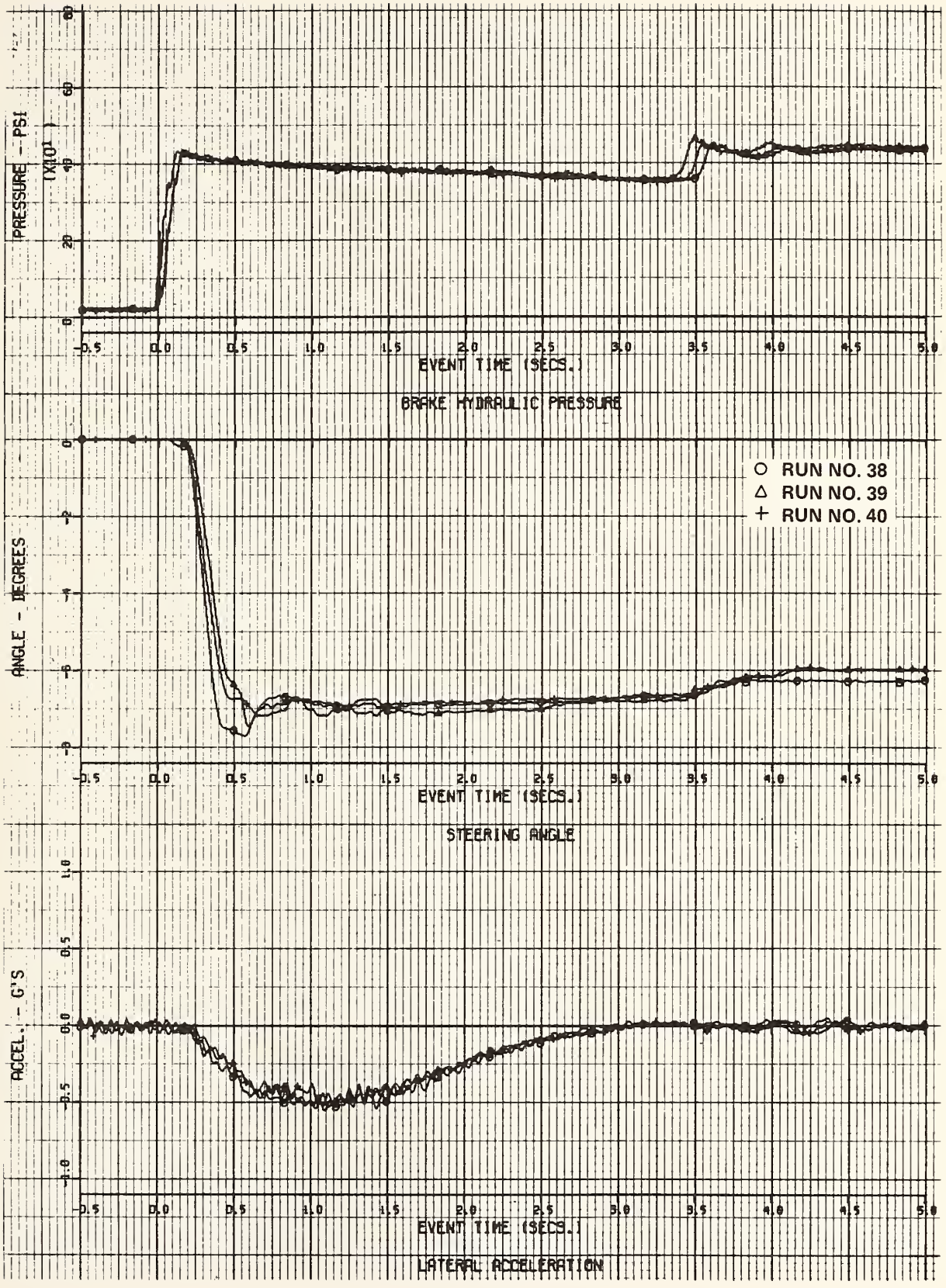

Figure 2.6-1(a) **EXPERIMENTAL TIME HISTORIES OF VEHICLE RESPONSES TO A COMBINATION CORNERING AND BRAKING MANEUVER**

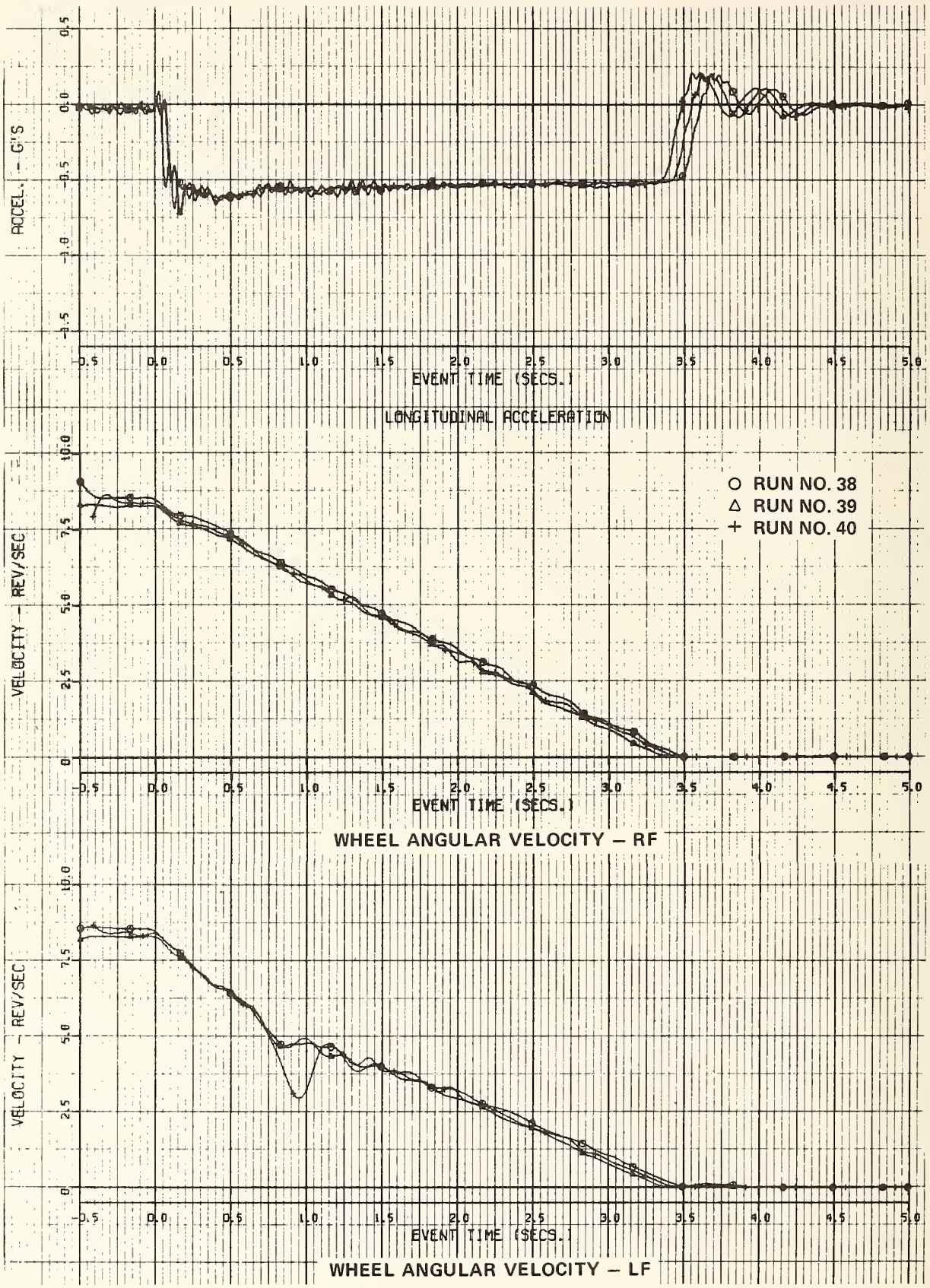
ACCEL. - G'S
0.5
0.0
-0.5
-1.0
-1.5
-0.5
0.0
0.5
1.0
1.5
2.0
2.5
3.0
3.5
4.0
4.5
5.0
EVENT TIME (SECS.)
LONGITUDINAL ACCELERATION
VELOCITY - REV/SEC
10.0
7.5
5.0
2.5
0
O RUN NO. 38
Δ RUN NO. 39
+ RUN NO. 40
EVENT TIME (SECS.)
WHEEL ANGULAR VELOCITY - RF
VELOCITY - REV/SEC
EVENT TIME (SECS.)
WHEEL ANGULAR VELOCITY - LF

Figure 2.6-1(b)

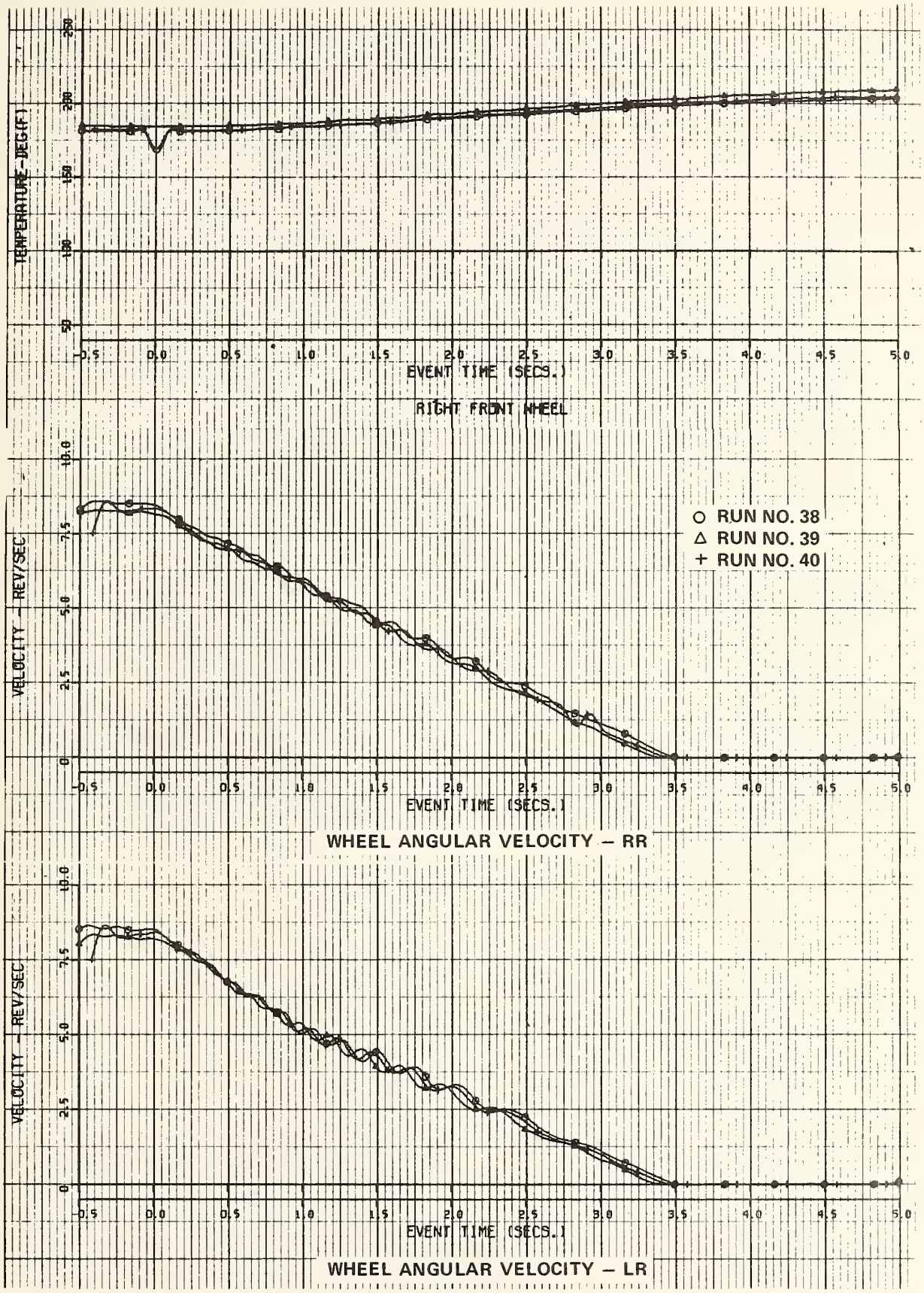
TEMPERATURE-DEG(F)
250
200
150
100
50
-0.5
0.0
0.5
1.0
1.5
2.0
2.5
3.0
3.5
4.0
4.5
5.0
EVENT TIME (SECS.)
RIGHT FRONT WHEEL
VELOCITY - REV/SEC
10.0
7.5
5.0
2.5
0
○ RUN NO. 38
△ RUN NO. 39
+ RUN NO. 40
EVENT TIME (SECS.)
WHEEL ANGULAR VELOCITY – RR
VELOCITY - REV/SEC
EVENT TIME (SECS.)
WHEEL ANGULAR VELOCITY – LR

Figure 2.6-1(c)

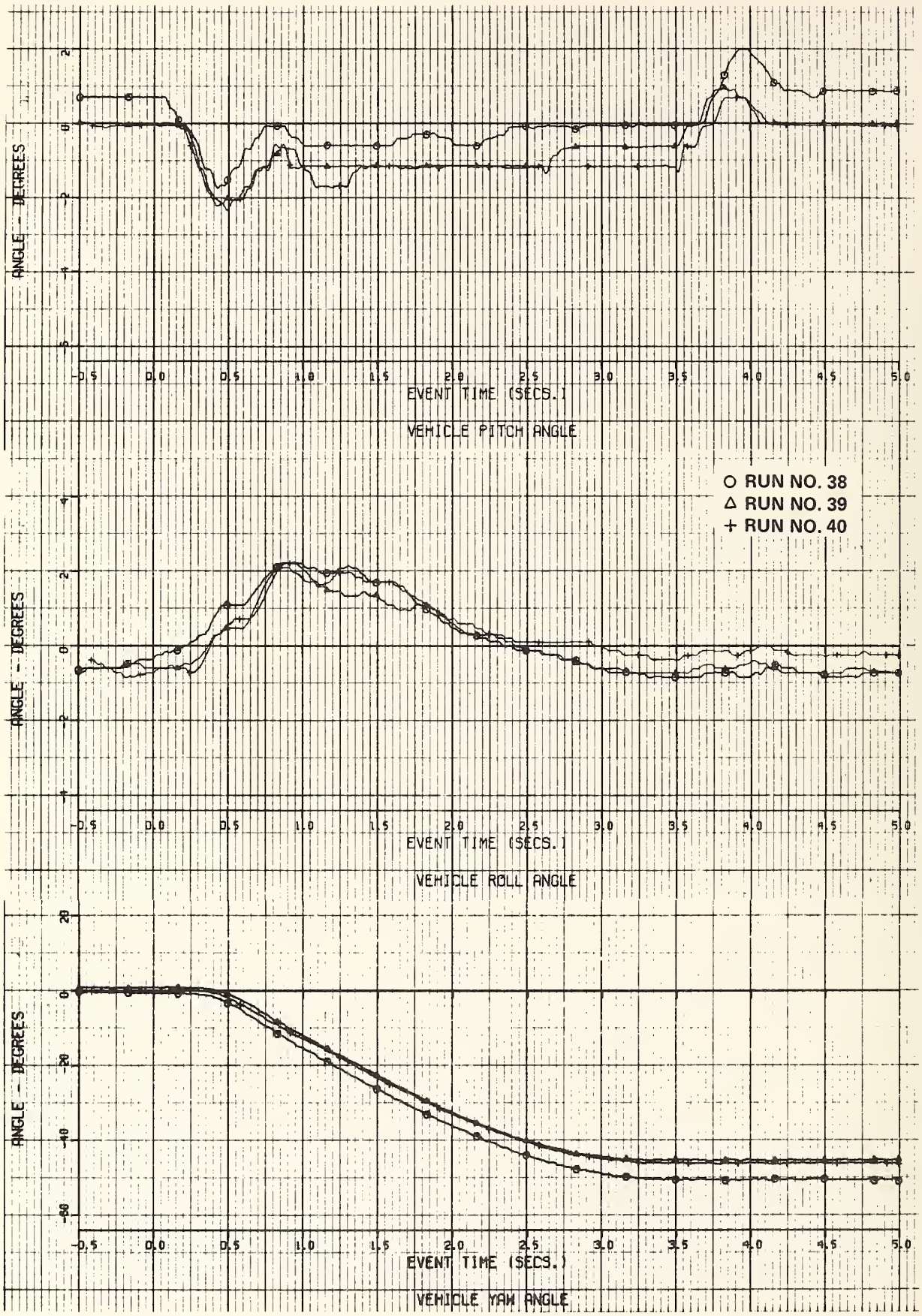
ANGLE - DEGREES
EVENT TIME (SECS.)
VEHICLE PITCH ANGLE
O RUN NO. 38
Δ RUN NO. 39
+ RUN NO. 40
ANGLE - DEGREES
EVENT TIME (SECS.)
VEHICLE ROLL ANGLE
ANGLE - DEGREES
EVENT TIME (SECS.)
VEHICLE YAW ANGLE

Figure 2.6-1(d)

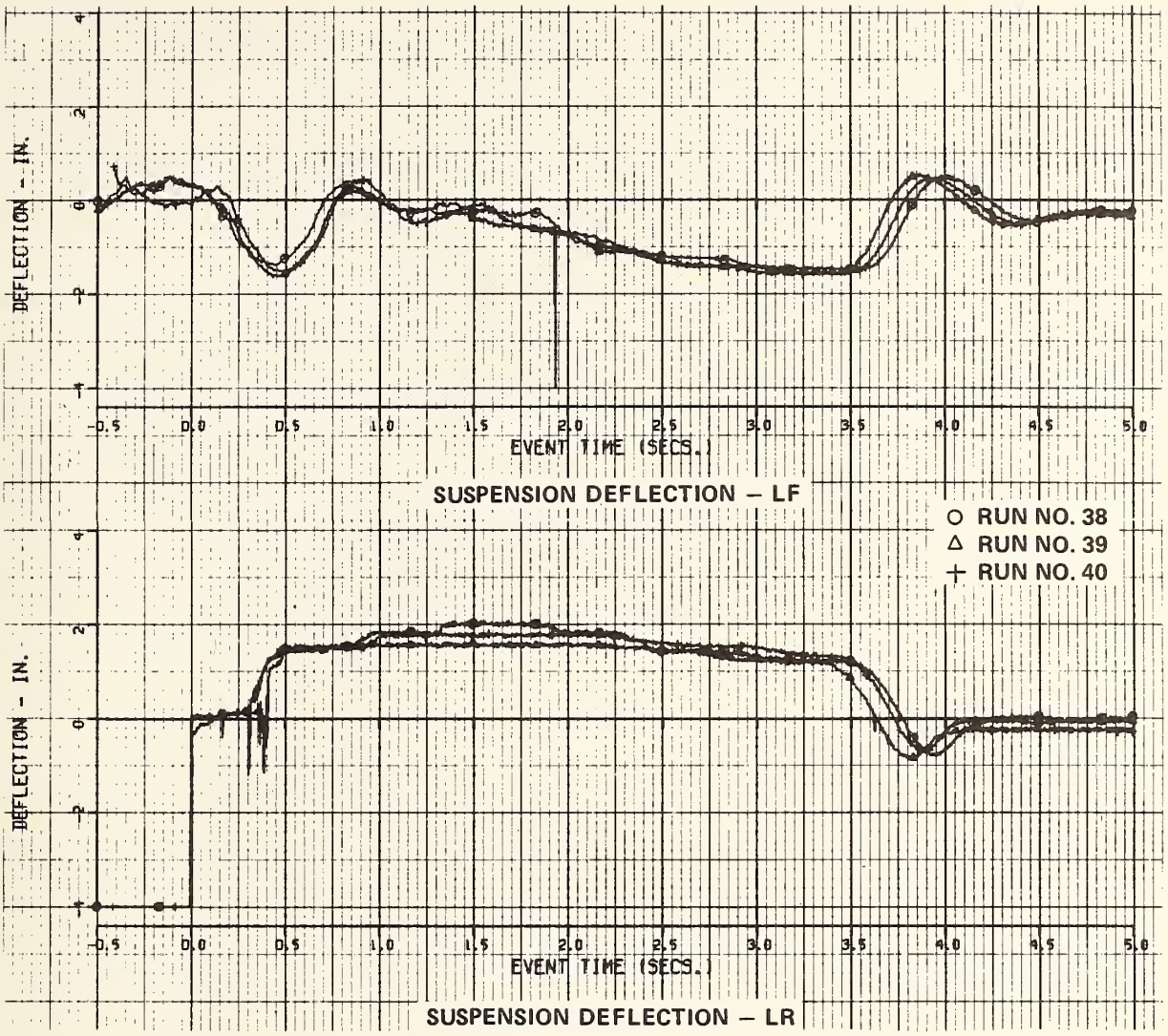
DEFLECTION - IN.
4
2
0
-2
-4
-0.5
0.0
0.5
1.0
1.5
2.0
2.5
3.0
3.5
4.0
4.5
5.0
EVENT TIME (SECS.)
SUSPENSION DEFLECTION – LF
O RUN NO. 38
Δ RUN NO. 39
+ RUN NO. 40
DEFLECTION - IN.
EVENT TIME (SECS.)
SUSPENSION DEFLECTION – LR

Figure 2.6-1(e)

In this series of tests, the vehicle was steered in a left turn. In one of the tests the steering input was slightly faster than for the other two runs, and it also had a small overshoot. As a result of this slight difference in the steering input, the yaw attitude is observed to be somewhat larger than that for the other runs throughout the duration of the event.

Table 2.6-1 presents the measurements obtained from the trajectory markings of the rear bumper squirt during the cornering stops. The definition of the measurements is illustrated in Figure 2.6-2.

Table 2.6-1
MEASUREMENTS OF TRAJECTORY FOR
COMBINED CORNERING AND BRAKING MANEUVER

RUN NO.	MEASUREMENTS INCHES			
	A*	B	C*	D
38	432	72	1193	279
39	449	58	1140	226
40	437	60	1162	234

*INCLUDING LAG DISTANCE = 65 INCHES

A,B,C,& D DEFINED IN FIGURE 3.10

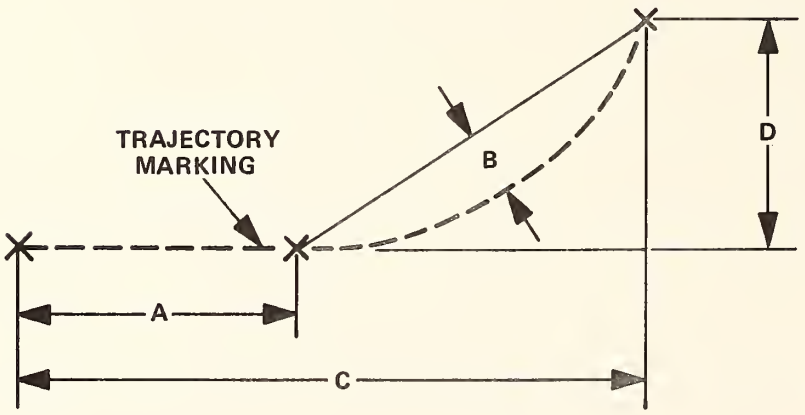

igure 2.6-2. MEASUREMENT DEFINITIONS FOR TRAJECTORIES OF CORNERING STOPS

The HVOSM inputs used in the braking in a turn simulations are shown in Figure 2.6-3 and the comparison of the measured and computed vehicle responses for the combined cornering and braking maneuver is presented in Figure 2.6-4. A comparison of the measured and computed final positions of the vehicle superimposed on a plot of the computed trajectory of the vehicle center of gravity is presented in Figure 2.6-5. As was the case for the straight ahead maneuver, the correlation between the measured and computed results is observed to be very good, especially with respect to the detailed characteristics of the wheel velocity time histories. In addition to predicting similar details of the initial variations of the wheel velocities as discussed for the straight ahead stops, the simulation has, for this cornering maneuver, faithfully predicted the characteristic differences that may be noted between the right and left wheels which arise due to the lateral weight transfer following the initial transient response.

The lateral weight transfer reduces the vertical load on the wheels on the inside of the turn (left side for this maneuver), while increasing the vertical load on the outside wheels. However, the same braking torque is applied to both the right and left wheels, thus they both must generate approximately the same (except for the relatively small difference in inertia torques) opposing torque due to the tire circumferential forces. To generate the same (except for the small difference arising from the difference in tire "deflected" radii) circumferential force as the outside tire while operating at a smaller vertical load, the inside tire must operate at a higher circumferential slip. Thus, the inside wheels operate at a lower angular velocity than the outside wheels. This effect is observed in both the measured and computed results.

```
BV53   BRAKING DYNAMICS VALIDATION - CORNERING STOPS - RUNS 38-40
                    VEHICLE DYNAMICS SIMULATION
  0.0      4.5      0.005              0.01     70.       1.3      60.0      0.0          1
 1.0                                                                                     2
 11.05    .608     .945     386.4    6000.0   40000.   40000.    -192.    453.6        3
 58.50    60.75    61.2     60.5       7.83     9.73     -2.0     14.68    4000.        4
 131.      0.5               1.3      58.0     0.10    266000.                          5
194.0     0.5               1.75     97.0     0.10    59244.0  46.52    0.059        6
 1300.    3.0      10.      8.4      3000.    1.71     .987      1.0     4200.        7
    0.0      0.0      0.0      0.0      0.0      0.0      0.0      0.0                  8
    0.0      0.0   -21.52    726.       0.0      0.0                                   9
 0.0      0.0      0.0      0.0      0.0      0.0      0.0      0.0                    10
  0.0      0.0      2.52     -97.     0.0      0.0                                    11
 -5.0     5.0      1.0                                                               12
-5.70  -3.90  -2.45  -1.30  -0.40   0.30   0.60   0.65   0.30  -0.40  -1.30
  0.0      4.5      0.1      0.0                                                      13
 0.0    0.0    0.0    0.0    0.0    0.0    0.0   -0.3   -3.0   -6.0   -6.9   -7.15  -7.0
-6.85  -6.8    -6.8   -6.9   -6.97  -6.95  -6.95  -6.95  -6.95  -6.95  -6.95  -6.95  -6.92
-6.91  -6.90   -6.90  -6.88  -6.86  -6.82  -6.80  -6.78  -6.77  -6.75  -6.72  -6.7   -6.7
-6.7   -6.6    -6.45  -6.32  -6.23  -6.2   -6.2
  0.0      6.0      0.25                                                             16
0.1079  0.1053  0.1030  0.1011  0.0994  0.0981  0.0971  0.0964  0.0959               21
0.0958  0.0960  0.0965  0.0973  0.0984  0.0998  0.1015  0.1035  0.1058
0.1085  0.1114  0.1147
 .092     .092     .092     .092     .092     .092     .092     .092     .092
 .092     .092     .092     .092     .092     .092     .092     .092     .092
 .092     .092     .092
 300.0    2.0      -2.9     300.0    2.0      4.3                                    23
 300.0    2.0      -4.3     300.0    2.0      4.5                                    24
  0.0     12.2     1.0                                                              25
  6.5     13.6     3.00                                          0.001              26
  29.     2.0    0.0      100000.                                                    27
0.0    .01    .02    .03    .04    .05    .06    .07    .08    .09    .10    .11    .12
.13    .14    .15    .16    .17    .18    .19    .20    .30    .40    .50    .60    .70
.80    .90   1.0
 0.0      0.17     0.30     0.48     0.65     0.75     0.83
 0.92     0.97     1.04     1.09     1.13     1.17     1.18
 1.19     1.23     1.25     1.23     1.20     1.19     1.17
1.08     1.04     1.01     1.0      1.0      1.0      1.0
 1.0
 0.0      0.17     0.30     0.48     0.65     0.75     0.83
 0.92     0.97     1.04     1.09     1.13     1.17     1.18
 1.19     1.23     1.25     1.23     1.20     1.19     1.17
 .08      1.04     1.01     1.0      1.0      1.0      1.0
```

```
FORMAT(13F6.3), PHIC(I),I=  1, 11
FORMAT(13F6.3), PSIF(I),I=  1, 13
FORMAT(13F6.3), PSIF(I),I= 14, 26
FORMAT(13F6.3), PSIF(I),I= 27, 39
FORMAT(13F6.3), PSIF(I),I= 40, 46
FORMAT(9F8.0,I8), APF(I),I=  1, 9
FORMAT(9F8.0),    APF(I),I= 10, 18
FORMAT(9F8.0),    APF(I),I= 19, 21
FORMAT(9F8.0),    APR(I),I=  1,  9
FORMAT(9F8.0),    APR(I),I= 10, 18
FORMAT(9F8.0),    APR(I),I= 19, 21
FORMAT(9F8.0,I8),NO.SLIP,NO.UGW,(UGW(I) 1,3 )
FORMAT(13F6.3), SLIP(J),J=  1, 13
FORMAT(13F6.3), SLIP(J),J= 14, 26
FORMAT(13F6.3), SLIP(J),J= 27, 29
FORMAT(7F10.5),     RHOS(J,  1),J=  1,  7
FORMAT(7F10.5),     RHOS(J,  1),J=  8, 14
FORMAT(7F10.5),     RHOS(J,  1),J= 15, 21
FORMAT(7F10.5),     RHOS(J,  1),J= 22, 28
FORMAT(7F10.5),     RHOS(J,  1),J= 29, 29
FORMAT(7F10.5),     RHOS(J,  2),J=  1,  7
FORMAT(7F10.5),     RHOS(J,  2),J=  8, 14
FORMAT(7F10.5),     RHOS(J,  2),J= 15, 21
FORMAT(7F10.5),     RHOS(J,  2),J= 22, 28
```

Figure 2.6-3 **COMPUTER PROGRAM INPUTS FOR CORNERING STOPS – CARD IMAGE FORMAT**

(1 of 7)

```
 1.0
 3.0     3.0     C.0      704.     1408.                                                    28    FORMAT(7F10.5),      RHOS(J,  2),J= 29, 29
200. 1200. 2200.                                                                                  FORMAT(9F8.0,I8),NO.FR',NO.SPEED,(SPEED 1,6 )
1.138     1.00        .930                                                                        FORMAT(13F6.3), FRCP(J),J=  1,  3
 .929      .792       .722                                                                        FORMAT(7F10.5),     RATIO(J,  1),J=  1,  3
  .719      .582       .513                                                                       FORMAT(7F10.5),     RATIO(J,  2),J=  1,  3
46.0     3.0     3.0      1.0      1.0     1000.    1000.                                   29    FORMAT(7F10.5),     RATIO(J,  3),J=  1,  3
 0.0     0.0     0.0      0.0      0.0      0.0     410.     425.     412.                  30    NTTS,IBTYP(1),IBTYP(2),AK1,AK2,PONE,PTWO
409.    405.    403.     402.     400.     398.     395.     390.     388.                        BRAKE PRES. TPC(I),  I=   1,  9
387.    386.    385.     383.     382.     381.     378.     375.     372.                                    TPC(I),  I=  10, 18
371.    370.    370.     369.     369.     368.     367.     365.     362.                                    TPC(I),  I=  19, 27
360.    357.    355.     355.     402.     437.     437.     437.     437.                                    TPC(I),  I=  28, 36
437.                                                                                                          TPC(I),  I=  37, 45
                                                                                                              TPC(I),  I=  46, 46
 0.0     0.0     0.0      0.0      0.0      0.0      0.0      0.0      0.0                  31    THROTTLE SET TTS(I),  I=   1,  9
 0.0     0.0     0.0      0.0      0.0      0.0      0.0      0.0      0.0                                    TTS(I),  I=  10, 18
 0.0     0.0     0.0      0.0      0.0      0.0      0.0      0.0      0.0                                    TTS(I),  I=  19, 27
 0.0     0.0     0.0      0.0      0.0      0.0      0.0      0.0      0.0                                    TTS(I),  I=  28, 36
 0.0     0.0     0.0      0.0      0.0      0.0      0.0      0.0      0.0                                    TTS(I),  I=  37, 45
 0.0                                                                                                          TTS(I),  I=  46, 46
 0.0     0.0     0.0      0.0      0.0      0.0      0.0      0.0      0.0                  32    TRANS. RATIO TTR(I),  I=   1,  9
 0.0     0.0     0.0      0.0      0.0      0.0      0.0      0.0      0.0                                    TTR(I),  I=  10, 18
 0.0     0.0     0.0      0.0      0.0      0.0      0.0      0.0      0.0                                    TTR(I),  I=  19, 27
 0.0     0.0     0.0      0.0      0.0      0.0      0.0      0.0      0.0                                    TTR(I),  I=  28, 36
 0.0     0.0     0.0      0.0      0.0      0.0      0.0      0.0      0.0                                    TTR(I),  I=  37, 45
 0.0                                                                                                          TTR(I),  I=  46, 46
   500     900    1300     1700     2100     2500     2900     3300     3700                33    ENGINE RPM,TRPME(I),  I=   1,  9
  4100    4500    4900                                                                                             TRPME(I),  I=  10, 12
   500     563     594      618      630      621      600      561      516                34    WIDEOPEN TH.TWOT(I),  I=   1,  9
   480     438     420                                                                                              TWOT(I),  I=  10, 12
     0    -120    -144     -165     -180     -192     -204     -216     -231                35    CLOSED THROT TCT(I),  I=   1,  9
  -249    -267    -288                                                                                              TCT(I),  I=  10, 12
 7.62    1.40    0.480    0.942               3.12     6.21     6.43     4.62               36    BRAKE PARAM.GN(I,1),  I=   1,  9
 1.0     9.25    0.384             10.0      10.E10   10.F10                                  .   BRAKE PARAM.GN(I,1),  I=  10, 16
 7.62    1.40    0.476    0.691               3.12     6.21     6.43     4.62               36    BRAKE PARAM.GN(I,2),  I=   1,  9
 1.0     9.25    C.381             10.0      10.E10   10.E10                                      BRAKE PARAM.GN(I,2),  I=  10, 16
170.    170.    170.     170.                                                               37    TAUO(I),I=1,4
.960    .974    .985     .996     1.00     1.03     1.01     1.00     .995                  38    LINING FADE  TLF(I),  I=   1,  9
.982    .972    .952     .930     .907     .859     .814     .770     .727                                   TLF(I),  I=  10, 18
.687    .645    .609     .586     .561     .536     .515     .500     .488                                   TLF(I),  I=  19, 27
.475    .465    .454     .444     .441     .438     .435     .432     .429                                   TLF(I),  I=  28, 36
.425    .422    .419     .416     .414     .410     .407     .404     .401                                   TLF(I),  I=  37, 45
.398    .395    .391     .388     .385     .382                                                            TLF(I),  I=  46, 51
170.    110.    192.  .9611E-4  .02853   60.336    0.10                                     39    TAUA,PZERO(1),PZERO(2),CONE,CTWO,CTHREE,ZETAB
                                                                                          9999
```

Figure 2.6-3 **COMPUTER PROGRAM INPUTS FOR CORNERING STOPS – CARD IMAGE FORMAT**

(2 of 7)

BV53 BRAKING DYNAMICS VALIDATION - CORNERING STOPS - RUNS 38-40
VEHICLE DYNAMICS SIMULATION
20JUL'71

INERTIAL DATA

MS	= 11.0500	LB.-SEC.**2/IN
MUF	= 0.6080	''
MUR	= 0.9450	''
IX	= 6200.0	LB.-SEC.**2-IN
IY	= 40000.0	''
IZ	= 40000.0	''
IXZ	=-192.000	''
IR	= 453.60	''
G	= 386.400	IN/SEC.**2

DIMENSIONS

A	= 58.5000	INCHES
B	= 60.7500	''
TF	= 61.2000	''
TR	= 60.5000	''
ZF	= 7.8300	''
ZR	= 9.7300	''
RHO	= -2.0000	''
RW	= 14.6800	''

SUSPENSION DATA

KF	= 131.000	LB./IN.
KR	= 194.000	LB./IN.
CF'	= 58.000	LBS.
CR'	= 97.000	LBS.
EPSILONF	= 0.100	IN./SEC.
EPSILONR	= 0.100	IN./SEC.
CF	= 1.300	LB-SEC/IN
CR	= 1.750	LB-SEC/IN

LAMBDAF	= 0.500	
LAMBDAR	= 0.500	
OMEGAF	= 0.0	INCHES
OMEGAR	= 0.0	INCHES
TS	= 46.520	INCHES
RR	= 59244.0	LB-IN/RAD
RF	=266000.0	LB-IN/RAD
KRS	= 0.059	ROLL STEER COEFF.

INITIAL CONDITIONS

PHIO	= 0.0	DEGREES	XCO'	= 0.0	INCHES	PO	= 0.0	DEG/SEC	UO	= 726.000	IN/SEC
THETAO	= 0.0	''	YCO'	= 0.0	''	QO	= 0.0	''	VO	= 0.0	''
PSIO	= 0.0	''	ZCO'	= -21.520	''	RO	= 0.0	''	WO	= 0.0	''
PHIRO	= 0.0	''	DELTA1	= 0.0	''	D(PHIR)/DT	= 0.0	''	D(DEL1)/DT	= 0.0	''
PSIFIO	= 0.0	''	DELTA2	= 0.0	''	D(PSIF)/DT	= 0.0	RAD/SC	D(DEL2)/DT	= 0.0	''
			DELTA3	= 0.0	''				D(DEL3)/DT	= 0.0	''

ACCELEROMETER POSITIONS

X1	= 0.0	INCHES	
Y1	= 0.0	''	
Z1	= 2.520	''	
X2	= -97.000	''	
Y2	= 0.0	''	
Z2	= 0.0	''	

DRIVER STEER CONTROL TABLE

T	PSIF	T	PSIF	T	PSIF	T	PSIF	T	PSIF	T	PSIF	T	PSIF	T	PSIF
0.0	0.0	0.60	0.0	1.20	-7.00	1.80	-6.95	2.40	-6.95	3.00	-6.86	3.60	-6.72	4.20	-6.32
0.10	0.0	0.70	-0.30	1.30	-6.85	1.90	-6.95	2.50	-6.92	3.10	-6.82	3.70	-6.70	4.30	-6.23
0.20	0.0	0.80	-3.00	1.40	-6.80	2.00	-6.95	2.60	-6.91	3.20	-6.80	3.80	-6.70	4.40	-6.20
0.30	0.0	0.90	-6.00	1.50	-6.80	2.10	-6.95	2.70	-6.90	3.30	-6.78	3.90	-6.70	4.50	-6.20
0.40	0.0	1.00	-6.90	1.60	-6.90	2.20	-6.95	2.80	-6.90	3.40	-6.77	4.00	-6.60		
0.50	0.0	1.10	-7.15	1.70	-6.97	2.30	-6.95	2.90	-6.88	3.50	-6.75	4.10	-6.45		

TIRE DATA

KT	1300.000	LB/IN
SIGMAT	= 3.000	INCHES
LAMBDAT	= 10.000	
A0	=4000.000	
A1	= 8.400	
A2	=3000.000	
A3	= 1.710	
A4	=4200.000	
AMU	= 0.987	
OMEGT	= 1.000	

TERRAIN TABLE ARGUMENTS

XB(BEGIN)	= 0.0	0.0	0.0	0.0	0.0	INCHES
XE(END)	= 0.0	0.0	0.0	0.0	0.0	''
X(INCR)	= 0.0	0.0	0.0	0.0	0.0	''
YB(BEGIN)	= 0.0	0.0	0.0	0.0	0.0	''
YE(END)	= 0.0	0.0	0.0	0.0	0.0	''
Y(INCR)	= 0.0	0.0	0.0	0.0	0.0	''
NO.X BOUNDS	= 0	0	0	0	0	
NO.Y BOUNDS	= 0	0	0	0	0	
AMUG	= 0.0	0.0	0.0	0.0	0.0	

NO.TERR.TAB.= 0

PROGRAM CONTROL DATA

START TIME	= 0.0	SEC
END TIME	= 4.500	''
INCR FOR INTEGRATION	= 0.0050	''
PRINT INTERVAL	= 0.010	''
THETA MAX (TO SWITCH)	= 70.000	DEG
UVWMIN(STOP)	= 1.300	
PQRMIN(STOP)	= 60.000	
INDCRB	= 0	
(=0.ND CURB,=1 CURB, =-1 STEER DEG. OF FREEDOM)		
MODE OF INTEGRATION	= 1	
(=0 VAR.ADAMS-MOULT., =1 RUNGE-KUTTA,=2 FIX.AM)		

Figure 2.6-3 **COMPUTER PROGRAM INPUTS FOR CORNERING STOPS – TABULAR FORMAT**

BV53 BRAKING DYNAMICS VALIDATION - CORNERING STOPS - RUNS 38-40
VEHICLE DYNAMICS SIMULATION
20JUL'71

FRONT WHEEL CAMBER
VS
SUSPENSION DEFLECTION

DELTAF INCHES	PHIC DEGREES
-5.000	-5.700
-4.000	-3.900
-3.000	-2.450
-2.000	-1.300
-1.000	-0.400
0.0	0.300
1.000	0.600
2.000	0.650
3.000	0.300
4.000	-0.400
5.000	-1.300

CURB IMPACT DATA

YC1'	=	0.0	INCHES
YC2'	=	0.0	''
ZC2'	=	0.0	''
DELTC	=	0.0	SEC(INTEG.INCR)
PHIC1	=	0.0	DEGREES
PHIC2	=	0.0	''
MUC	=	0.0	
IPSI	=	0.0	LB-SEC**2-IN
CPSI'	=	0.0	LB-IN
OMEGA PSI	=	0.0	RAD
KPSI	=	0.0	LB-IN/RAD
EPSILON PSI	=	0.0	RAD/SEC
TRAIL,FRONT(PT)	=	0.0	INCHES

SUSPENSION STOPS, EXTENSION AND COMPRESSION

	FRONT		REAR	
COMPRESSION				
KFC	= 300.000	LB/IN	KRC = 300.000	LB/IN
KFC'	= 2.000	LB/IN**3	KRC' = 2.000	LB/IN**3
OMEGFC	= -2.900	INCHES	OMEGRC = -4.300	INCHES
EXTENSION				
KFE	= 300.000	LB/IN	KRE = 300.000	LB/IN
KFE'	= 2.000	LB/IN**3	KRE' = 2.000	LB/IN**3
OMEGFE	= 4.300	INCHES	OMEGRF = 4.500	INCHES

BRAKING DYNAMICS

FRONT		
IDJF	=	0.0 LB-SEC**2 IN
IWJF,ROTA	=	12.200 ''
AXLE RAT	=	1.000
REAR		
IDJR	=	6.500 LB-SEC**2-IN
IWJR,ROTA	=	13.600 ''
AXLE RAT	=	3.000

WHEEL RADIUS-RADIAL SPRING FOR TABLE

RWHJR(BEGIN)	=	0.0	INCHES
RWHJE(END)	=	6.000	''
DRWHJ(INCRE.)	=	0.250	''

RW-HJ INCHES	FJP LBS	RW-HJ INCHES	FJP LBS	RW-HJ INCHES	FJP LBS	RW-HJ INCHES	FJP LBS
0.0	0.0	1.75	225.	3.50	0.115E 04	5.25	0.242E 04
0.250	91.0	2.00	211.	3.75	0.142E 04	5.50	0.231E 04
0.500	110.	2.25	253.	4.00	0.164E 04	5.75	0.262E 04
0.750	135.	2.50	234.	4.25	0.166E 04	6.00	0.249E 04
1.00	159.	2.75	283.	4.50	0.194E 04		
1.25	183.	3.00	256.	4.75	0.209E 04		
1.50	179.	3.25	0.105E 04	5.00	0.203E 04		

ANTI-PITCH TABLES FOR CIRCUMFERENTIAL TIRE FORCE

APF=	0.10790	0.10530	0.10300	0.10110	0.09940	0.09810	0.09710	0.09640	0.09590	0.09580	0.09600
	0.09650	0.09730	0.09840	0.09980	0.10150	0.10350	0.10580	0.10850	0.11140	0.11470	
APR=	0.09200	0.09200	0.09200	0.09200	0.09200	0.09200	0.09200	0.09200	0.09200	0.09200	0.09200
	0.09200	0.09200	0.09200	0.09200	0.09200	0.09200	0.09200	0.09200	0.09200	0.09200	

Figure 2.6-3 **COMPUTER PROGRAM INPUTS FOR CORNERING STOPS – TABULAR FORMAT**

(4 of 7)

BV53 BRAKING DYNAMICS VALIDATION - CORNERING STOPS - RUNS 38-40
VEHICLE DYNAMICS SIMULATION
20JUL '71

RHOS(SLIP,UGW),RATIO OF FRICTION COEFFICIENTS, CIRCUMFERENTIAL TO PEAK SIDE FORCE. UGW(I)=UG(I)*COS(PSIIP(I)) +VG(I)*SIN(PSIIP(I))
NO OF SLIP= 29, NO.OF UGW= 2 SLIP AND UGW GIVEN AS POSITIVE VALUES

SLIP	RHOS UGW(1)IN/SEC 0.0	UGW(2) 1.000E 05	UGW(3) 0.0	SLIP	RHOS UGW(1)IN/SEC 0.0	UGW(2) 1.000E 05	UGW(3) 0.0	SLIP	RHOS UGW(1)IN/SEC 0.0	UGW(2) 1.000E 05	UGW(3) 0.0
0.0	0.0	0.0	0.0	0.100	1.09000	1.09000	0.0	0.200	1.17000	1.17000	0.0
0.010	0.17000	0.17000	0.0	0.110	1.13000	1.13000	0.0	0.300	1.08000	1.08000	0.0
0.020	0.30000	0.30000	0.0	0.120	1.17000	1.17000	0.0	0.400	1.04000	1.04000	0.0
0.030	0.48000	0.48000	0.0	0.130	1.18000	1.18000	0.0	0.500	1.01000	1.01000	0.0
0.040	0.65000	0.65000	0.0	0.140	1.19000	1.19000	0.0	0.600	1.00000	1.00000	0.0
0.050	0.75000	0.75000	0.0	0.150	1.23000	1.23000	0.0	0.700	1.00000	1.00000	0.0
0.060	0.83000	0.83000	0.0	0.160	1.25000	1.25000	0.0	0.800	1.00000	1.00000	0.0
0.070	0.92000	0.92000	0.0	0.170	1.23000	1.23000	0.0	0.900	1.00000	1.00000	0.0
0.080	0.97000	0.97000	0.0	0.180	1.20000	1.20000	0.0	1.000	1.00000	1.00000	0.0
0.090	1.04000	1.04000	0.0	0.190	1.19000	1.19000	0.0				

RATIO(FR',SPEED), MODIFICATION FACTOR FOR TIRE-TERRAIN FRICTION COEFFICIENTS. SPEED= SQRT(UG(I)**2 + VG(I)**2). FR' =FRCP
NO.OF FRCP= 3, NO.OF SPEED= 3

FRCP,LB	SPEED,IN/SEC 0.0	SPEED,IN/SEC 704.0	SPEED,IN/SEC 1408.0	SPEED,IN/SEC	SPEED,IN/SEC	SPEED,IN/SEC
200.0	1.13800E 00	9.29000E-01	7.19000E-01			
1200.0	1.00000E 00	7.92000E-01	5.82000E-01			
2200.0	9.30000E-01	7.22000E-01	5.13000E-01			

Figure 2.6-3 **COMPUTER PROGRAM INPUTS FOR CORNERING STOPS – TABULAR FORMAT**

(5 of 7)

BV53 BRAKING DYNAMICS VALIDATION - CORNERING STOPS - RUNS 38-40
VEHICLE DYNAMICS SIMULATION
20JUL'71

BRAKING SYSTEMS WITH COMPUTED TORQUES

NTTS,(MAX 101),NO.OF PC,TS,TR ENTRIES =	46	TAUA	AMBIENT TEMPERATURE, DEG.F =	170.0
IBTYP(1) FRONT BRAKE TYPE =	3	PO(1)	FRONT,BRAKE PUSH OUT PRES.,PSIG=	110.00
IBTYP(2) REAR " " =	3	PO(2)	REAR, " " " " =	192.00
K1 SLOPE PR/PF (P1.LT.PF.LE.P2) =	1.0000	C1	COEFFICIENT FOR RESISTING FORCE=	9.61100E-05
K2 " " (PF.GT.P2) =	1.0000	C2	" " " =	2.85300E-02
P1 BRAKE PRES. FOR PR/PF CHANGE,PSIG=	1.00000E 03	C3	" " " =	6.03360E 01
P2 " " " " " =	1.00000E 03	ZETAB,THRESHOLD WHEEL SPEED TO LIMIT BRAKE TORQUE,RAD/SEC=		0.10

TABLES PC,TS,TR VARY WITH TIME
TT(J),J=1,NTTS, 0 TO 10 SECS. IN 0.10 SEC INCREMENTS

SEC TT	BRAKE MASTER CYL PRES.(PSIG) PC	THROTTLE SETTING TS	TRANSMISSION RATIO TR	SEC TT	BRAKE MASTER CYL PRES.(PSIG) PC	THROTTLE SETTING TS	TRANSMISSION RATIO TR	SEC TT	BRAKE MASTER CYL PRES.(PSIG) PC	THROTTLE SETTING TS	TRANSMISSION RATIO TR
0.0	0.	0.0	0.0	1.60	390.	0.0	0.0	3.20	368.	0.0	0.0
0.10	0.	0.0	0.0	1.70	388.	0.0	0.0	3.30	367.	0.0	0.0
0.20	0.	0.0	0.0	1.80	387.	0.0	0.0	3.40	365.	0.0	0.0
0.30	0.	0.0	0.0	1.90	386.	0.0	0.0	3.50	362.	0.0	0.0
0.40	0.	0.0	0.0	2.00	385.	0.0	0.0	3.60	360.	0.0	0.0
0.50	0.	0.0	0.0	2.10	383.	0.0	0.0	3.70	357.	0.0	0.0
0.60	410.	0.0	0.0	2.20	382.	0.0	0.0	3.80	355.	0.0	0.0
0.70	425.	0.0	0.0	2.30	381.	0.0	0.0	3.90	355.	0.0	0.0
0.80	412.	0.0	0.0	2.40	378.	0.0	0.0	4.00	402.	0.0	0.0
0.90	409.	0.0	0.0	2.50	375.	0.0	0.0	4.10	437.	0.0	0.0
1.00	405.	0.0	0.0	2.60	372.	0.0	0.0	4.20	437.	0.0	0.0
1.10	403.	0.0	0.0	2.70	371.	0.0	0.0	4.30	437.	0.0	0.0
1.20	402.	0.0	0.0	2.80	370.	0.0	0.0	4.40	437.	0.0	0.0
1.30	400.	0.0	0.0	2.90	370.	0.0	0.0	4.50	437.	0.0	0.0
1.40	398.	0.0	0.0	3.00	369.	0.0	0.0				
1.50	395.	0.0	0.0	3.10	369.	0.0	0.0				

Figure 2.6-3 **COMPUTER PROGRAM INPUTS FOR CORNERING STOPS — TABULAR FORMAT**

ENGINE RPM	ENGINE TORQUE WIDE OPEN THROTTLE LB-FT	ENGINE TORQUE CLOSED THROTTLE LB-FT
500.	500.	0.
900.	563.	-120.
1300.	594.	-144.
1700.	618.	-165.
2100.	630.	-180.
2500.	621.	-192.
2900.	600.	-204.
3300.	561.	-216.
3700.	516.	-231.
4100.	480.	-249.
4500.	438.	-267.
4900.	420.	-288.

	BRAKE PARAMETERS FRONT GN(I,1)	REAR GN(I,2)
1	7.62000E 00	7.62000E 00
2	1.40000E 00	1.40000E 00
3	4.80000E-01	4.76000E-01
4	9.42000E-01	6.91000E-01
5	0.0	0.0
6	3.12000E 00	3.12000E 00
7	6.21000E 00	6.21000E 00
8	6.43000E 00	6.43000E 00
9	4.62000E 00	4.62000E 00
10	1.00000E 00	1.00000E 00
11	9.25000E 00	9.25000E 00
12	3.84000E-01	3.81000E-01
13	0.0	0.0
14	1.00000E 01	1.00000E 01
15	9.99999E 10	9.99999E 10
16	9.99999E 10	9.99999E 10

INITIAL BRAKE TEMPERATURE, DEG.F
TAU0(1), RIGHT FRONT = 170.00
TAU0(2), LEFT " = 170.00
TAU0(3), RIGHT REAR = 170.00
TAU0(4), LEFT " = 170.00

TABLE LF VARIES WITH TEMPERATURE
TTAU(J),J=1,51, 0(DEG.F) TO 1000(DEG.F) IN 20 DEGREE INCREMENTS

BRAKE LINING FADE COEFFICIENTS

TTAU DEG.F	LF	TTAU DEG.F	LF	TTAU DEG.F	LF	TTAU DEG.F	LF
0.0	0.9600	260.0	0.9070	520.0	0.4880	780.0	0.4160
20.0	0.9740	280.0	0.8590	540.0	0.4750	800.0	0.4140
40.0	0.9850	300.0	0.8140	560.0	0.4650	820.0	0.4100
60.0	0.9960	320.0	0.7700	580.0	0.4540	840.0	0.4070
80.0	1.0000	340.0	0.7270	600.0	0.4440	860.0	0.4040
100.0	1.0300	360.0	0.6870	620.0	0.4410	880.0	0.4010
120.0	1.0100	380.0	0.6450	640.0	0.4380	900.0	0.3980
140.0	1.0000	400.0	0.6090	660.0	0.4350	920.0	0.3950
160.0	0.9950	420.0	0.5860	680.0	0.4320	940.0	0.3910
180.0	0.9820	440.0	0.5610	700.0	0.4290	960.0	0.3880
200.0	0.9720	460.0	0.5360	720.0	0.4250	980.0	0.3850
220.0	0.9520	480.0	0.5150	740.0	0.4220	1000.0	0.3820
240.0	0.9300	500.0	0.5000	760.0	0.4190		

Figure 2.6-3 **COMPUTER PROGRAM INPUTS FOR CORNERING STOPS — TABULAR FORMAT**

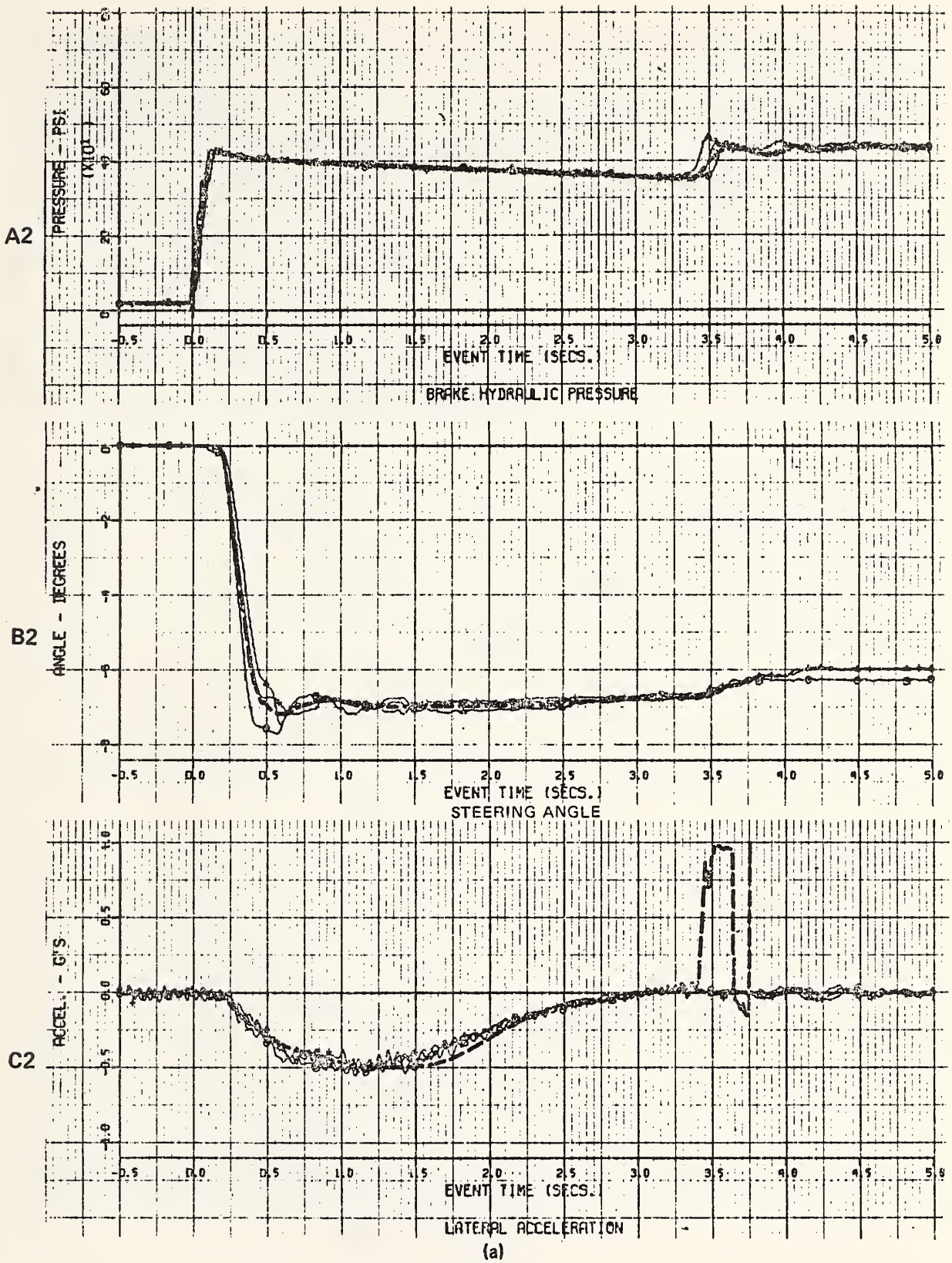

Figure 2.6-4 COMPARISON OF MEASURED AND COMPUTED VEHICLE RESPONSES – CORNERING AND BRAKING MANEUVER

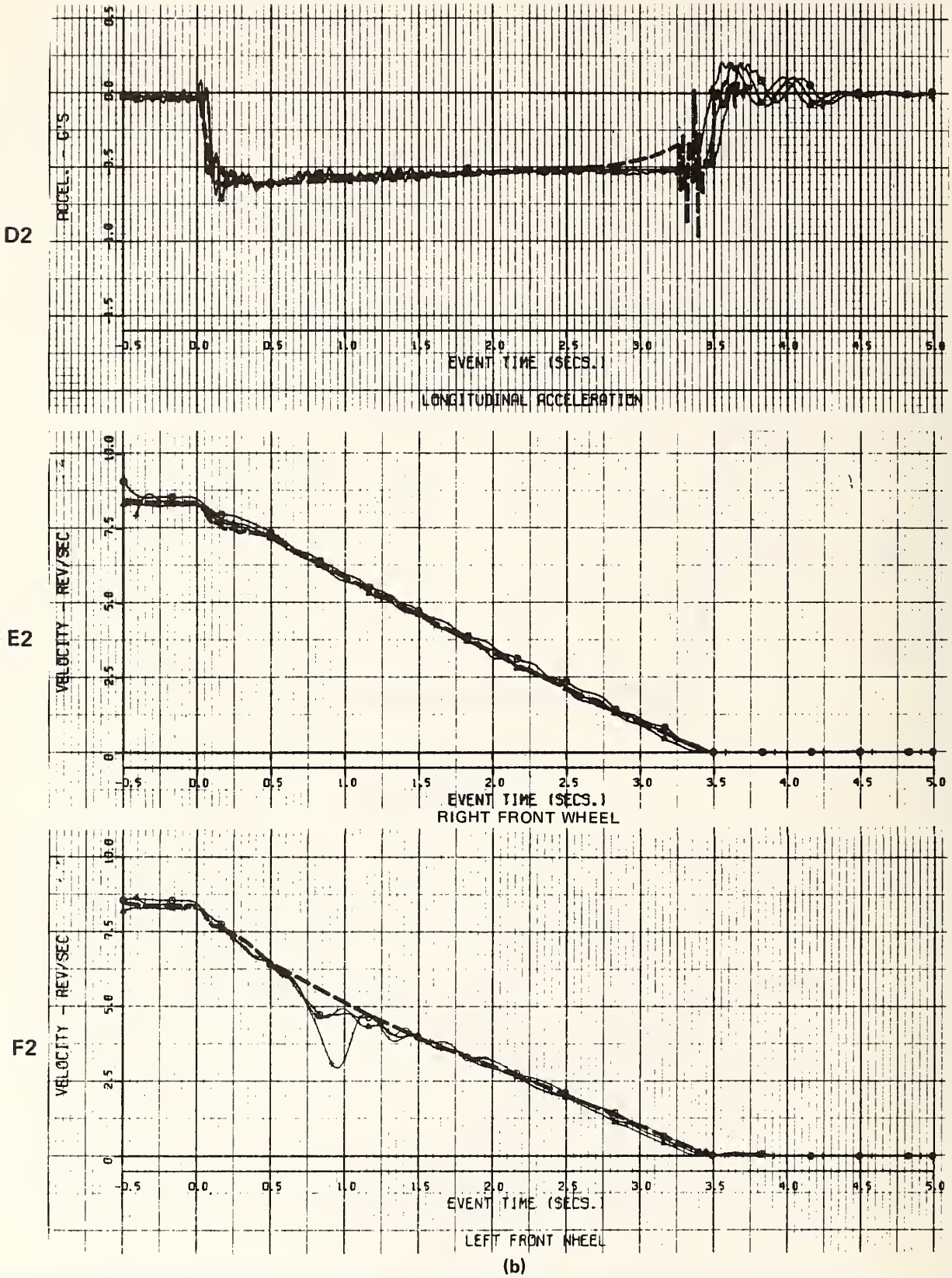

Figure 2.6-4 (Cont.) COMPARISON OF MEASURED AND COMPUTED VEHICLE RESPONSES – CORNERING AND BRAKING MANEUVER

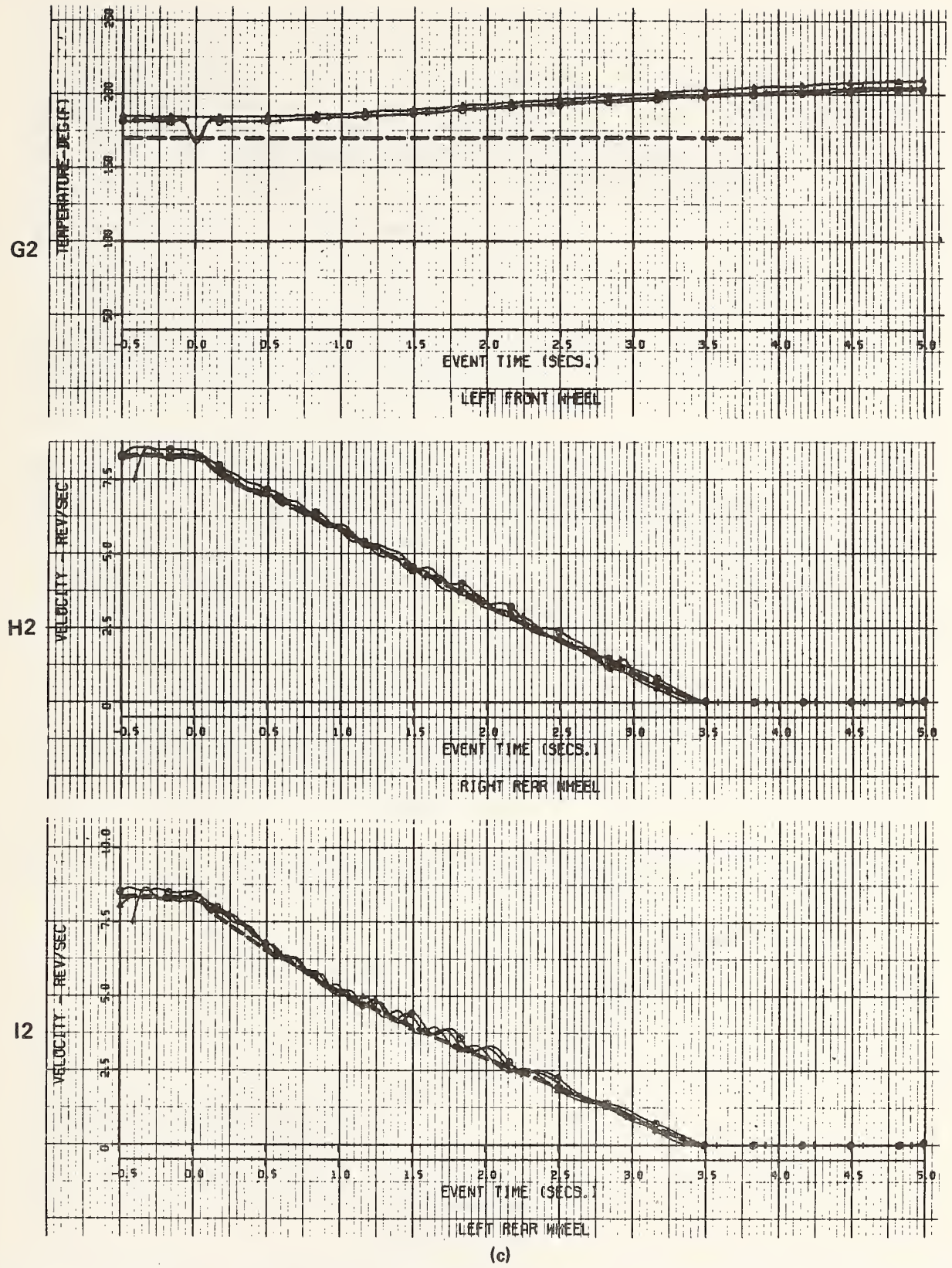

(c)

Figure 2.6-4 (Cont.) COMPARISON OF MEASURED AND COMPUTED VEHICLE RESPONSES – CORNERING AND BRAKING MANEUVER

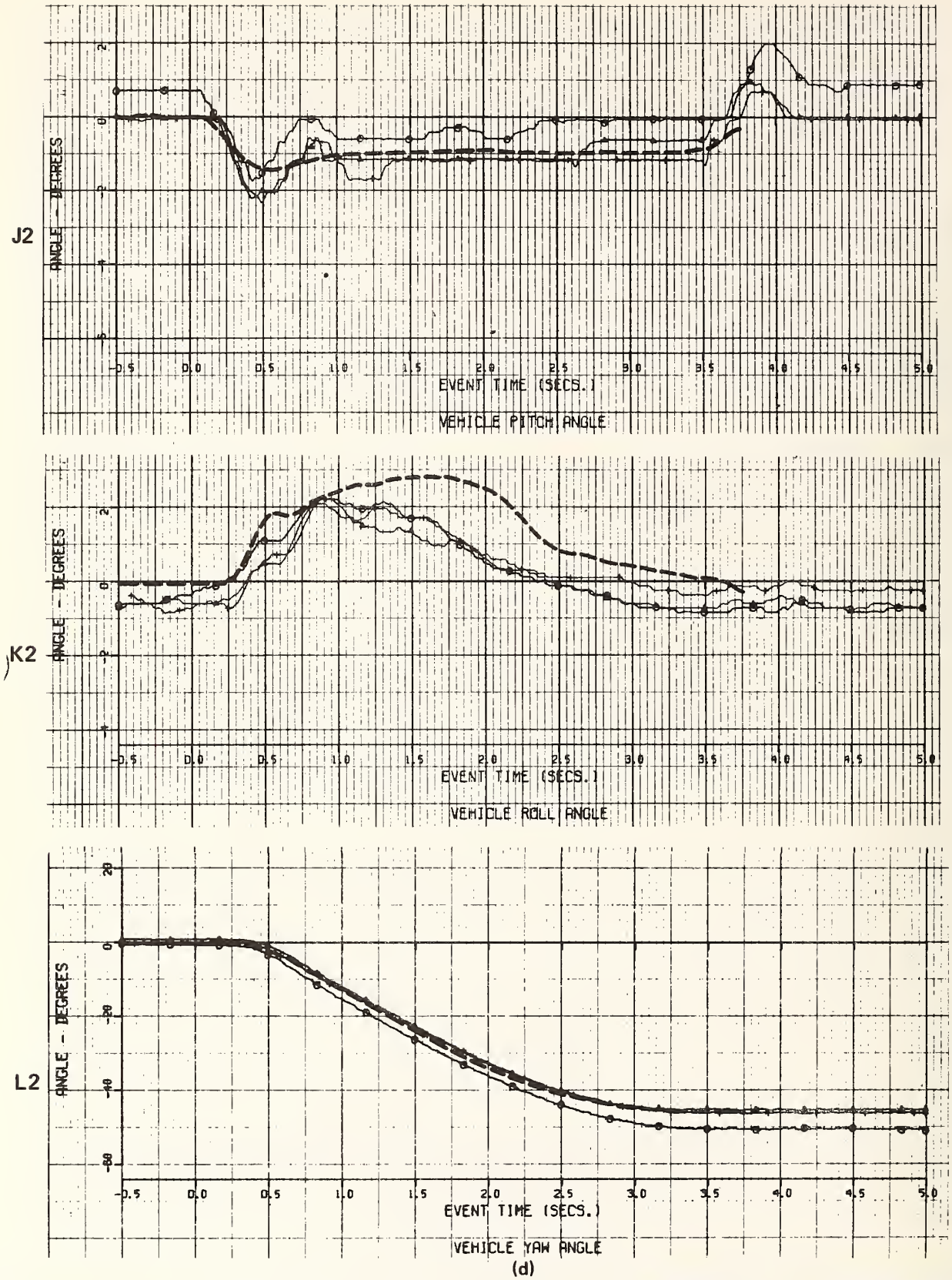

ure 2.6-4 (Cont.) COMPARISON OF MEASURED AND COMPUTED VEHICLE RESPONSES – CORNERING AND BRAKING MANEUVER

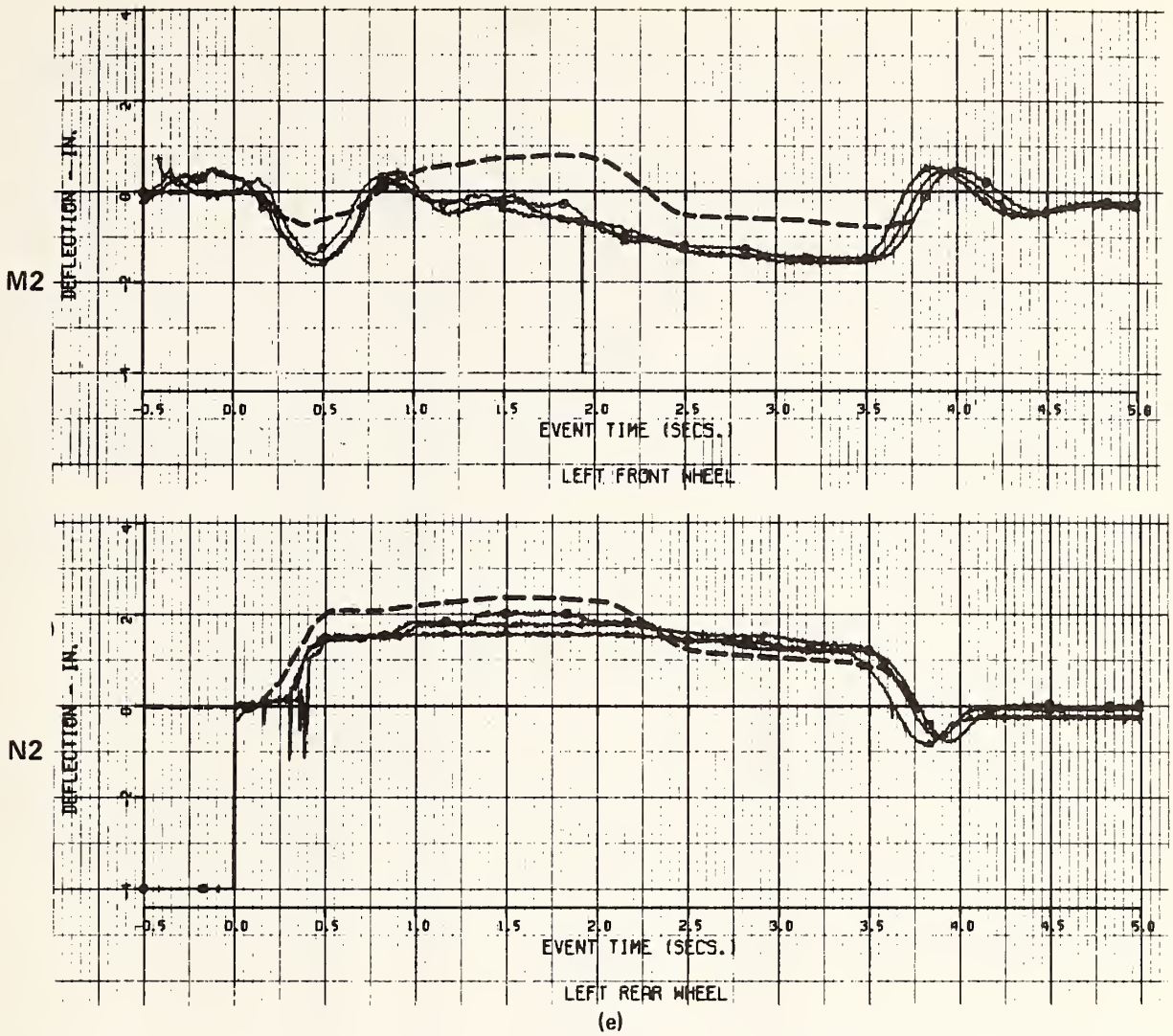

Figure 2.6-4 (Cont.) COMPARISON OF MEASURED AND COMPUTED VEHICLE RESPONSES – CORNERING AND BRAKING MANEUVER

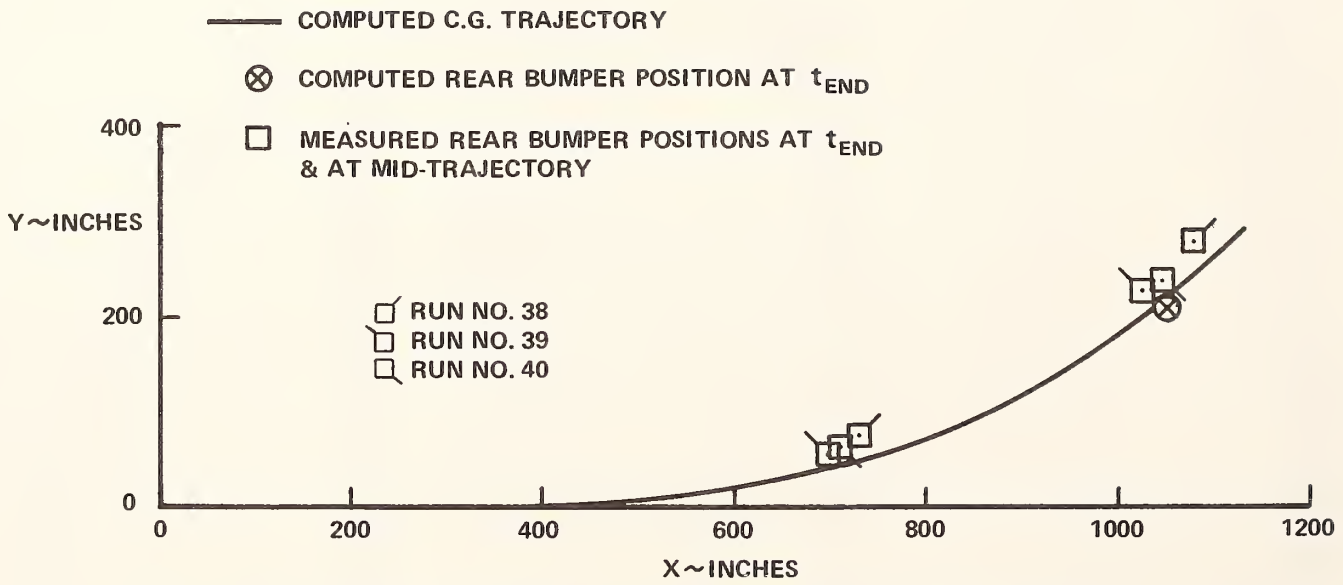

Figure 2.6-5 MEASURED AND COMPUTED STOPPING POSITIONS

Again, the correlation between measured and computed responses of the sprung mass relative to the unsprung masses is generally not as good as it is for the other vehicle responses. This is attributed to the assumed inputs for the suspension and shock absorber characteristics as explained in the above discussion of the straight ahead braking results. A consequence of the lateral weight transfer is observed for the time history of the measured left front wheel angular velocity at t = 0.7 sec when the wheel deceleration momentarily increased. This is the result of the rapid reduction in the vertical load on this wheel due to the sprung mass roll response as can be deduced from the roll attitude and front suspension deflection time histories. Because this detail of the sprung mass response was not so accurately predicted, the corresponding feature is not present in the predicted wheel angular velocity time history.

2.6.5 Vehicle Response Sensitivity

No vehicle response sensitivity analyses related explicitly to braking in a turn were conducted. However, the discussion of Section 2.5.5 applies equally to this comparison series.

3.0 HVOSM GENERAL COMPARISONS

In Section 2.0, rigorous validation tests of the HVOSM were reported in which detailed response measures from repeatable experiments were compared with HVOSM simulations of the same experiment. In this section, general comparisons between experimental and HVOSM responses are reported. Although these comparsions cannot be construed to constitute rigorous validation because either detailed response measurements were not made, the experiments were not demonstrated to be repeatable, or the vehicle characteristics were not sufficiently defined, they do demonstrate through either visual comparison or limited response measure comparison that the HVOSM does indeed predict the gross motions of a vehicle, at least qualitatively, in extreme maneuvers.

3.1 General Motors Bridge Parapet Comparison

In Reference 7, sequences of high speed photographs of a vehicle impacting a General Motors designed bridge parapet at 50 MPH and 12° are presented. Since no response data other than the photographs are available, and also since vehicle parameter and control inputs are not defined, a qualitative comparison between the actual event and the HVOSM was made.

Results of the comparison using the HVOSM-RD1 version are shown in Figure 3.1-1. In this comparison, the bridge parapet was simulated as a two-faced curb, and although sprung mass contact was not simulated, the pictorial sequence indicates a good correlation of general body motions.

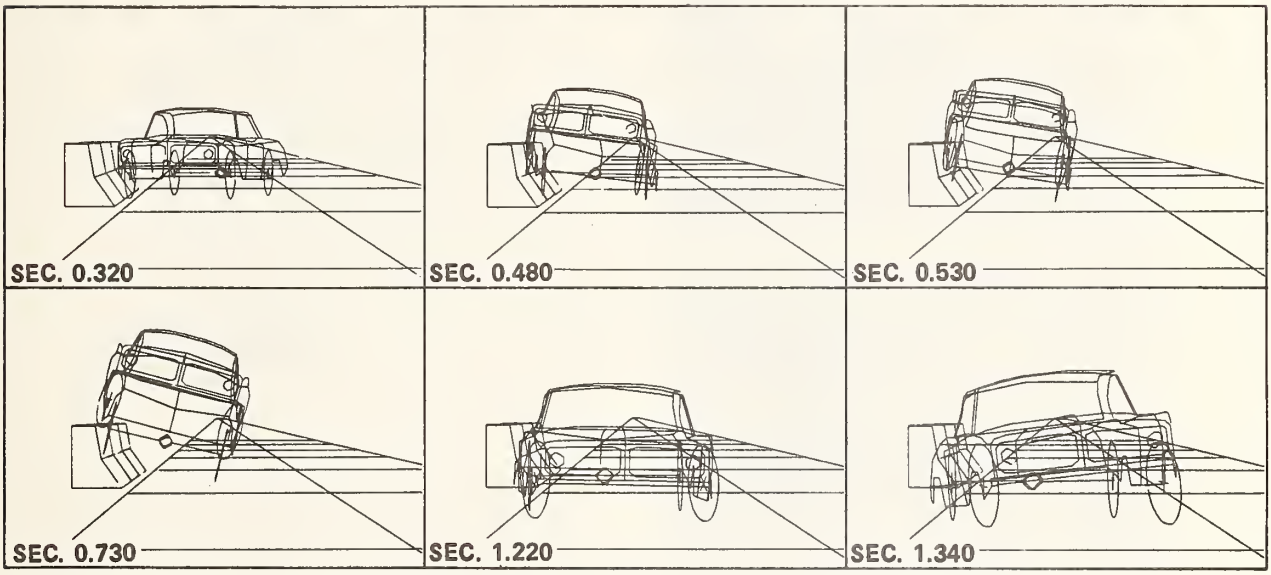

Figure 3.1-1 EXPERIMENTAL AND PREDICTED VEHICLE RESPONSES FOR A 50 MPH, 12° COLLISION WITH THE GENERAL MOTORS BRIDGE PARAPET

(REVISED 19 MARCH 1969)

3.2 Astro Spiral Jump

One application of the HVOSM has been the development of ramp geometry for an automobile thrill show stunt (Reference 14) in which the vehicle executes a 360° roll while airborne between take-off and landing ramps. Development of the complex ramp geometry, of course, assumed validity of the model, particularly with regard to suspension effects during takeoff and angular motion coupling while airborne. In subsequent full scale tests the assumption of validity was confirmed as indicated by the graphical comparison of Figure 3.2-1.

COMPUTER PREDICTION

EXPERIMENT

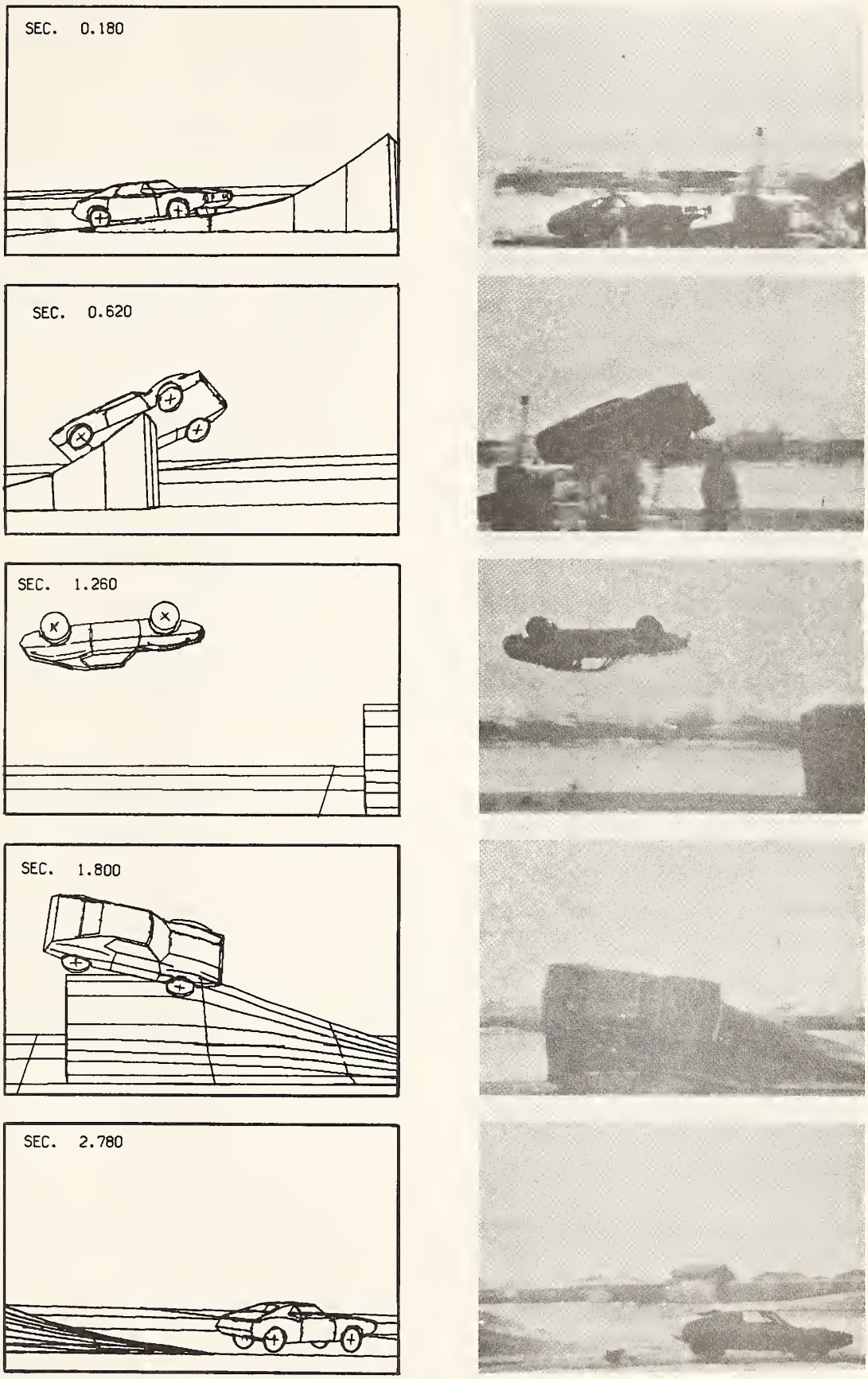

Figure 3.2-1 PREDICTED AND EXPERIMENTAL VEHICLE RESPONSES IN ASTRO SPIRAL JUMP

3.3 Embankment Comparisons

A total of six full-scale tests along with HVOSM comparisons were conducted by the Texas Transportation Institute (TTI) involving a vehicle leaving the roadway and traversing a roadside embankment. The test results and comparisons are reported, in detail, in Reference 8 and are summarized below.

Six tests were conducted, all in one day, for various encroachment conditions. Table 3.3-1 lists the details of each test. The primary reason for the tests was to provide a wide variety of conditions to simulate.

Each test was simulated by HVOSM. Input to the program consisted of embankment geometry, vehicle parameters, and test conditions. Vehicle parameters for the test car were obtained at TTI on another study (Reference 9) and are reported in Reference 8. Sears Supertread tires were used on the test car and their properties were available from the literature (Reference 6). A friction coefficient between the tire and the grassy slope was not available. However, skid tests were conducted at the Texas A & M Research Annex on grass and sod similar to that at the test site. The coefficient was found to be 0.5.

Three types of comparisons were made between test results and HVOSM output. These were plots of the right front tire track, plots of vertical acceleration versus time, and computer generated perspective drawings of the simulated vehicle at selected times adjacent to prints of frames from the high speed movie film. Figures 3.3-1 through 3.3-3 show the comparisons for Test No. 1. The grid lines shown on the tire track plots (see Figure 3.3-1) correspond to the chalked grid lines at the test site.

TABLE 3.3-1 TEST CONDITIONS

Test No.	Encroachment Angle (deg)	Encroachment Speed (MPH)	Comments
1	9.7	55.7	No problems.
2	13.8	45.1	Tie-rod failure locked right front tire over in full right steer position. Steer control lost and car went over back slope. No other vehicle damage occurred.
3	9.8	45.3	No problems.
4	20.4	47.0	Portable generator powering instrumentation trailer failed, causing loss of accelerometer data. Also, due to the large encroachment angle, sufficient time and space was not available to steer the car back after reaching the ditch bottom and the car went over the back slope. No vehicle damage occurred.
5	8.6	59.9	No problems.
6	13.3	63.6	Tie-rod failure locked right front tire over in right steer position. Steer control was partially lost and car went over back slopes. No other vehicle damage occurred.

The vertical acceleration was found to be the predominant component of the resultant acceleration, in both measured and simulated values. As a consequence, only the vertical acceleration component was plotted and compared. In the acceleration plots, as well as the other comparisons, time equal to 0.0 represents the time when the right front tire crossed the pavement's edge. A discussion of the comparisons for each test follows.

Test No. 1

In comparison with the others, this test was the most successful in terms of correlation between test data and HVOSM predictions. This could be expected since with each succeeding test the vehicle's suspension system was subject to progressive degradation. No mechanical failures occurred during Test No. 1, and as seen in Figures 3.3-1 through 3.3-3, the correlations of path, attitude and accelerations was excellent.

Test No. 2

By closely studying the movie film, it was determined that the front suspension system was subjected to relatively high vertical loads approximately 1.6 seconds after the car left the roadway. At that time the right front tire was approximately 27 feet laterally from the edge of the pavement (Y = 47 feet). This loading resulted in a tie-rod failure which locked the right front wheel over in a full right turn position (a steer angle of approximately 22 degrees). Prediction of such a failure is not within the capabilities of HVOSM. It was therefore decided that an attempt would be made to simulate the effect of the failure. This was done by programming in a locked over steer angle of 22.5 degrees at T = 1.6 seconds after the simulated vehicle left the roadway.

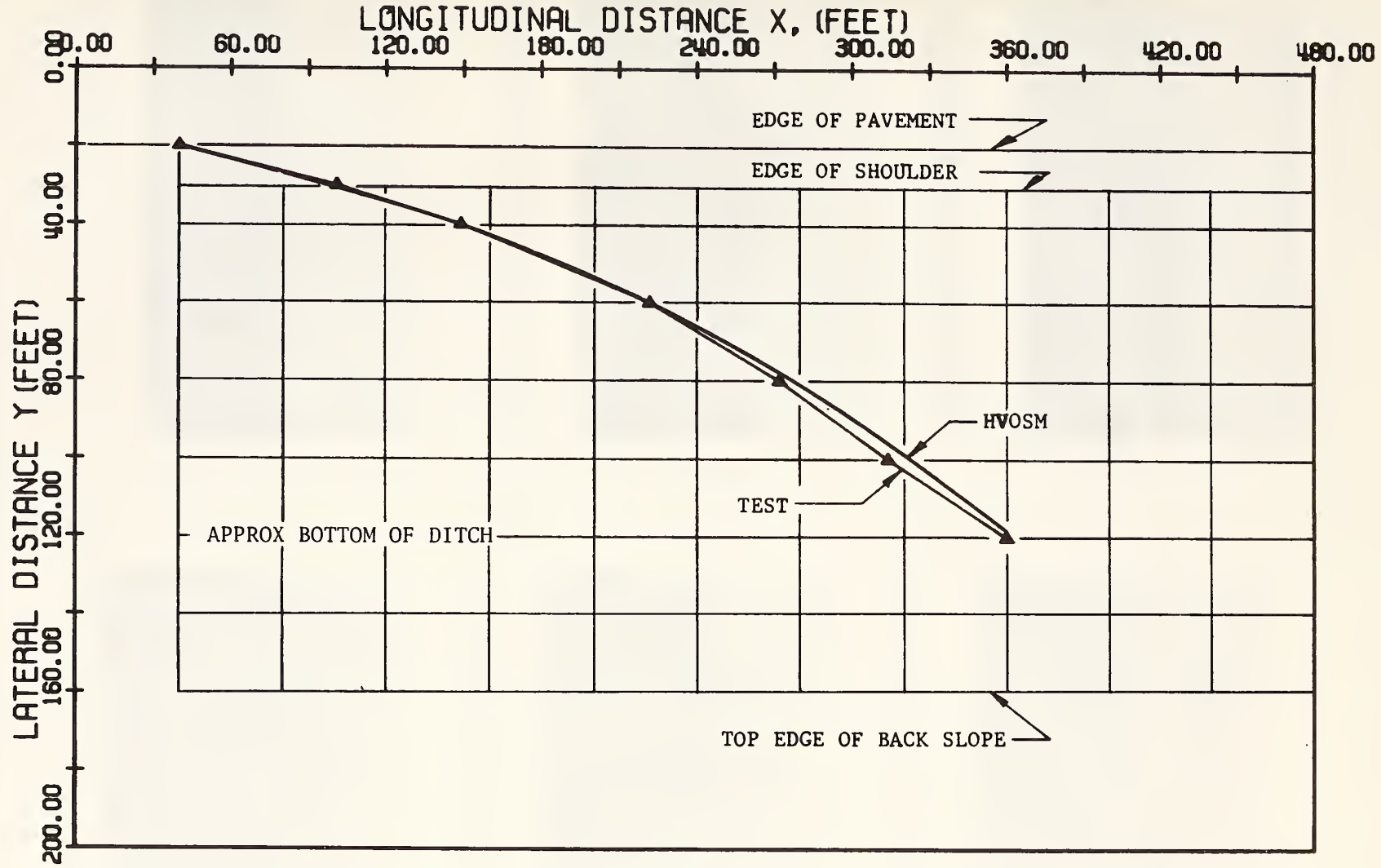

Figure 3.3-1 RIGHT FRONT TIRE TRACK, TEST NO. 1.

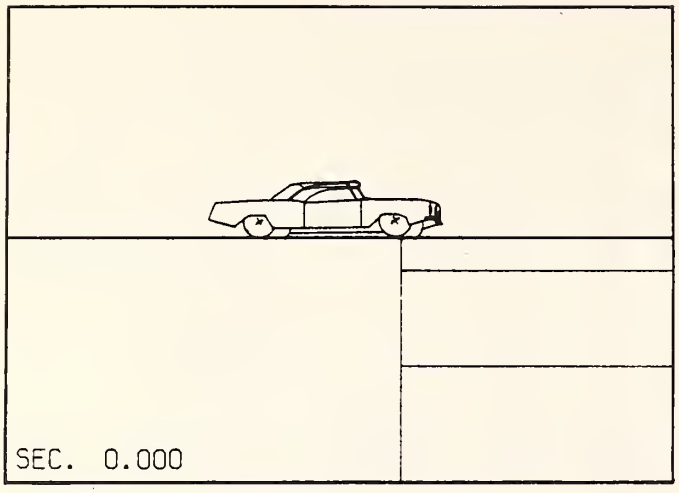

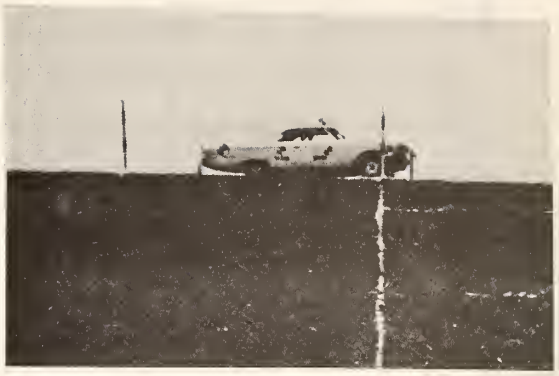

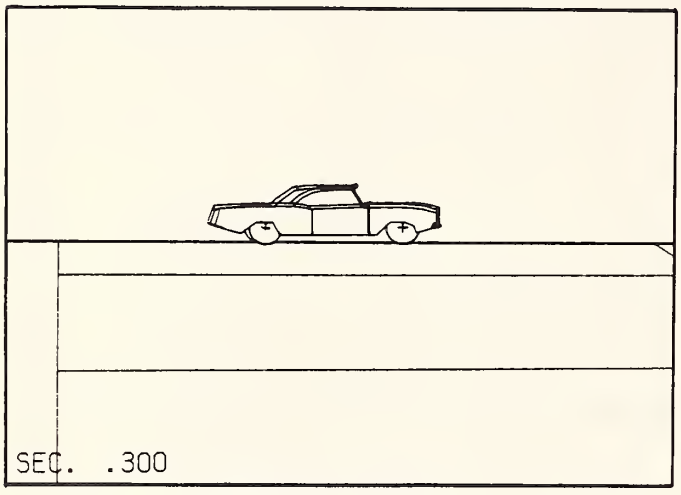

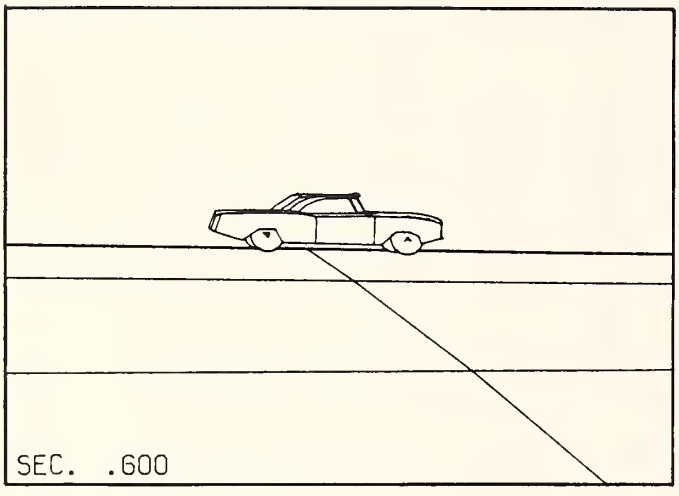

Figure 3.3-2 HVOSM VERSUS TEST RESULTS, TEST NO. 1, CAMERA NO. 1.

HVOSM

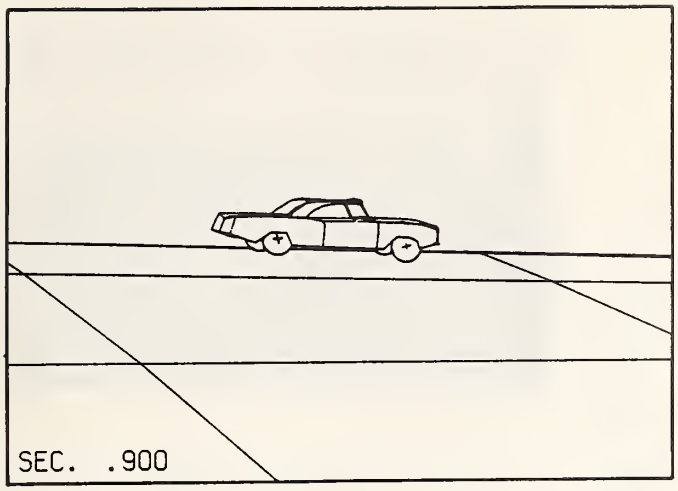

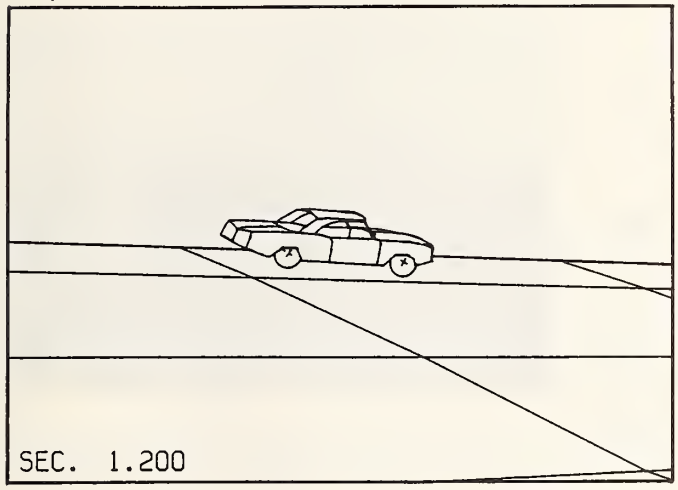

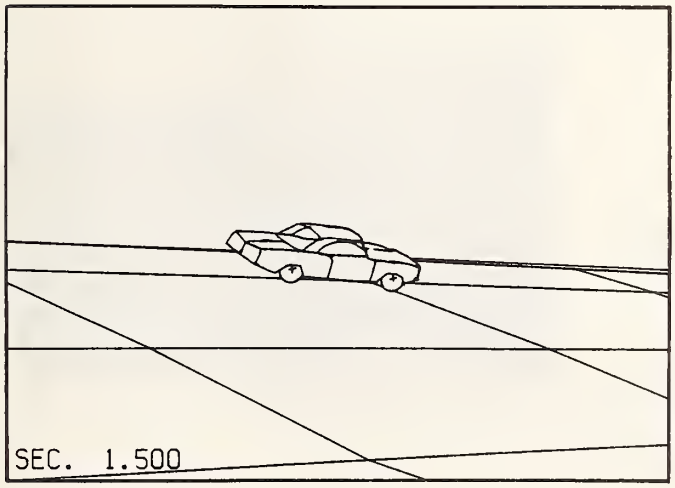

TEST

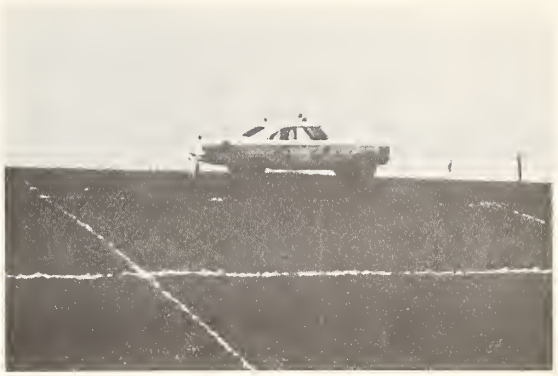

Figure 3.3-2 CONTINUED.

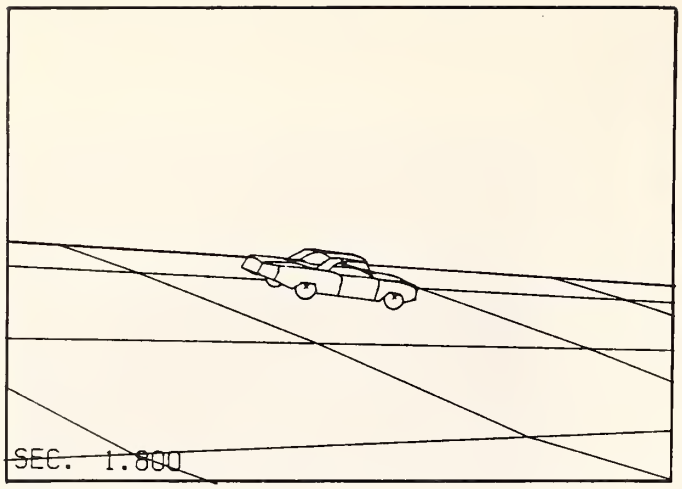

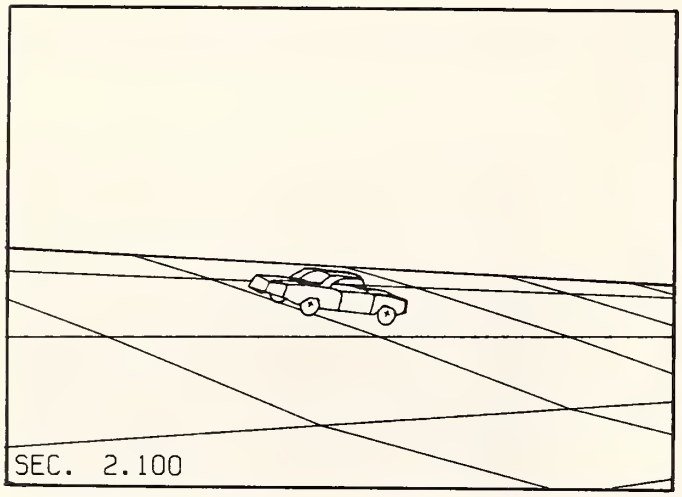

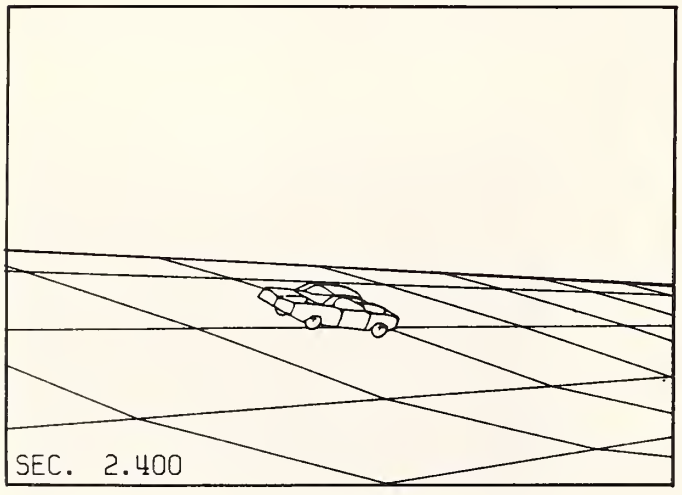

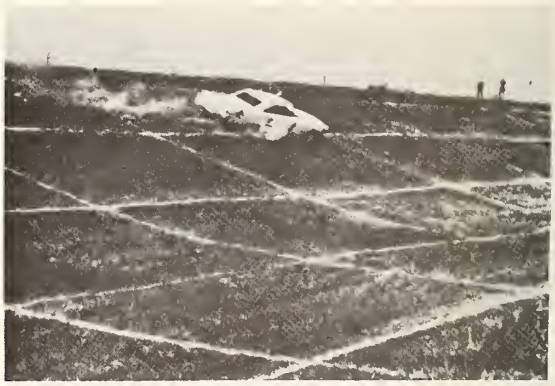

Figure 3.3-2 CONTINUED.

HVOSM

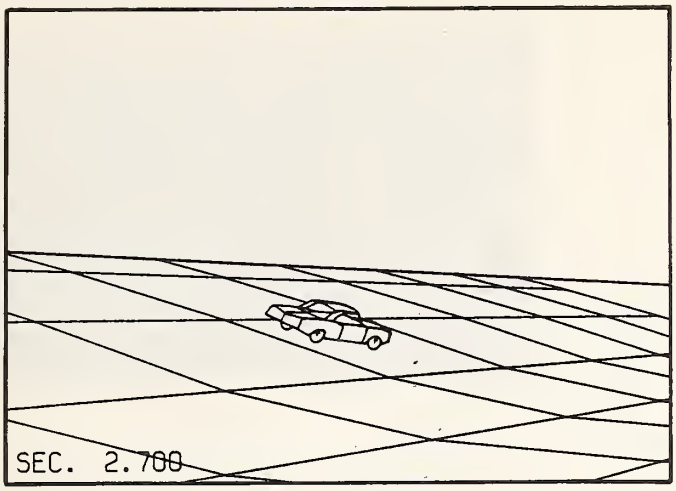

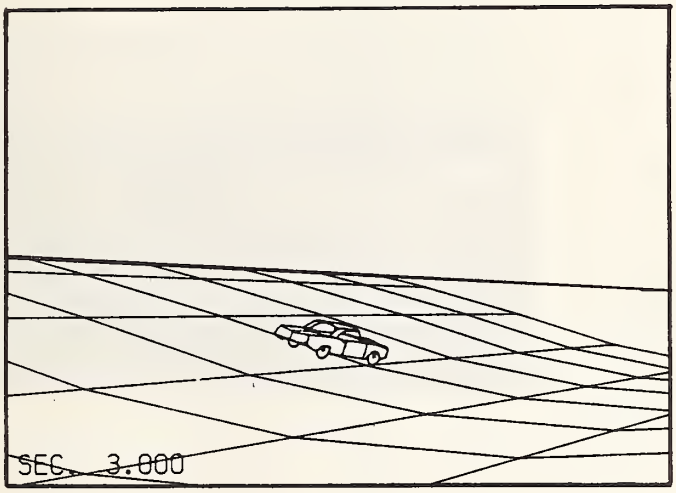

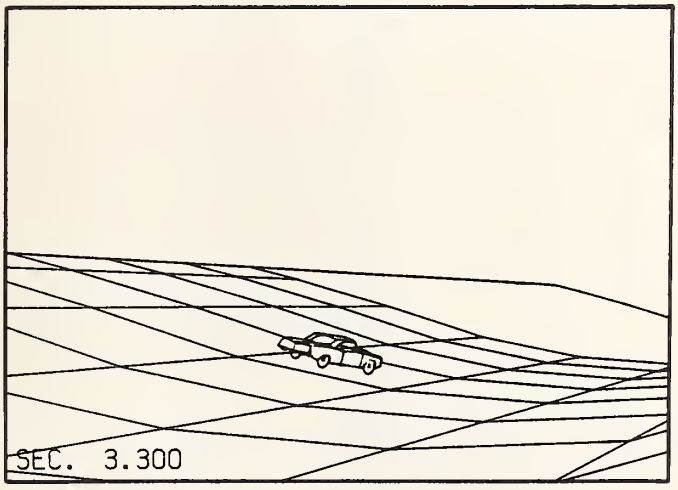

TEST

Figure 3.3-2 CONTINUED

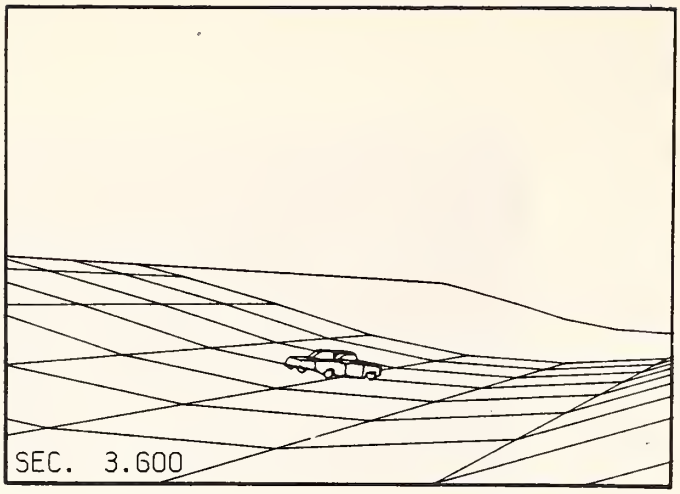

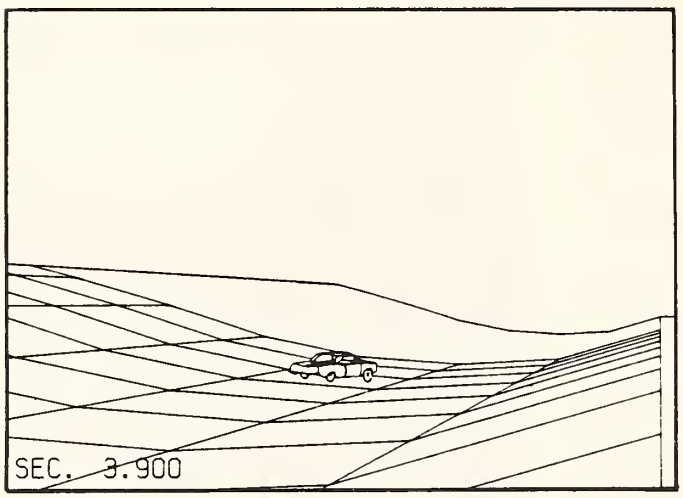

Figure 3.3-2 CONTINUED.

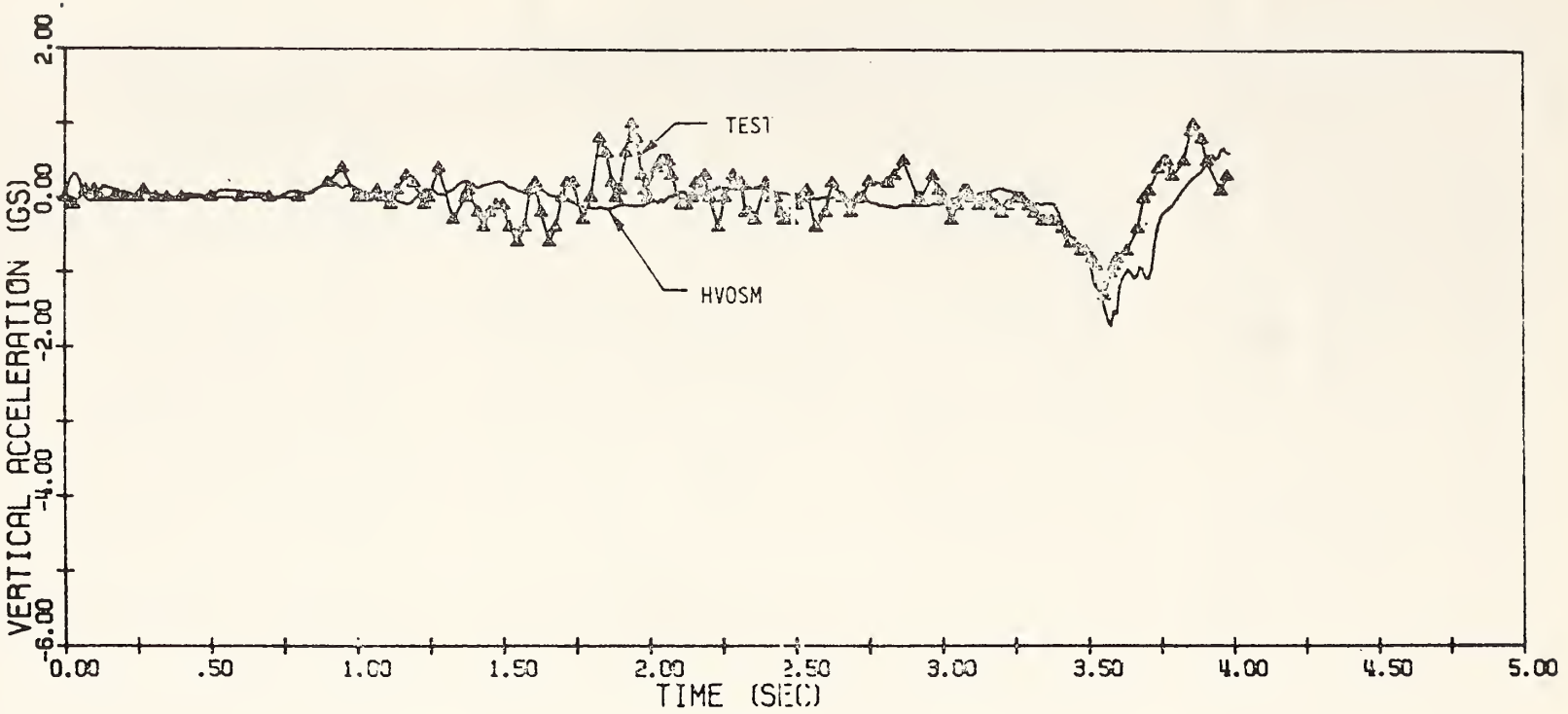

Figure 3.3-3 VERTICAL ACCELERATION VERSUS TIME, TEST NO. 1.

The plot of tire tracks (Figure 3.3-4) shows an increasing difference between test results and HVOSM predictions for Test No. 2. This disparity is attributed primarily to slight rutting that occurred in the test, an occurrence which could not be simulated by the version of HVOSM used by TTI at the time of this study. Although the grassy slope was hard and well compacted, the extreme steer angle that resulted when the wheel locked caused the tire to dig in slightly. As a consequence, larger than predicted side forces occurred, causing the test car to turn more sharply than the simulated car.

The mechanical failures and subsequent path differences undoubtedly contributed to the differences that occurred between the measured and predicted vertical accelerations in Test No. 2 (see Figure 3.3-5). A summary of the factors which probably caused differences between predicted and measured acceleration in Test No. 2 as well as the other tests, follows:

(1) Terrain Irregularities -- Limitations on the number of grid points that could be measured and that could be accepted by HVOSM precluded an exact simulation of the terrain. Local irregularities such as bumps and indentations could not be simulated. They undoubtedly caused unpredictable accelerations. In most cases, accelerations caused by irregularities would not be of major significance with regard to accident severity. The irregularities may, however, cause mechanical failures in the suspension system which could lead to a more hazardous condition later.

(2) Type and Location of Accelerometer Support -- The vibratory motion of both the accelerometer support and the vehicle's structural framework caused accelerations in the test car which, due to the limitations of the structural idealization, could not be computed by HVOSM. The degree to which structural vibration contributed to the measured values is unknown. It is probable, however, that the effect was small and would be characterized by relatively high frequencies of vibration.

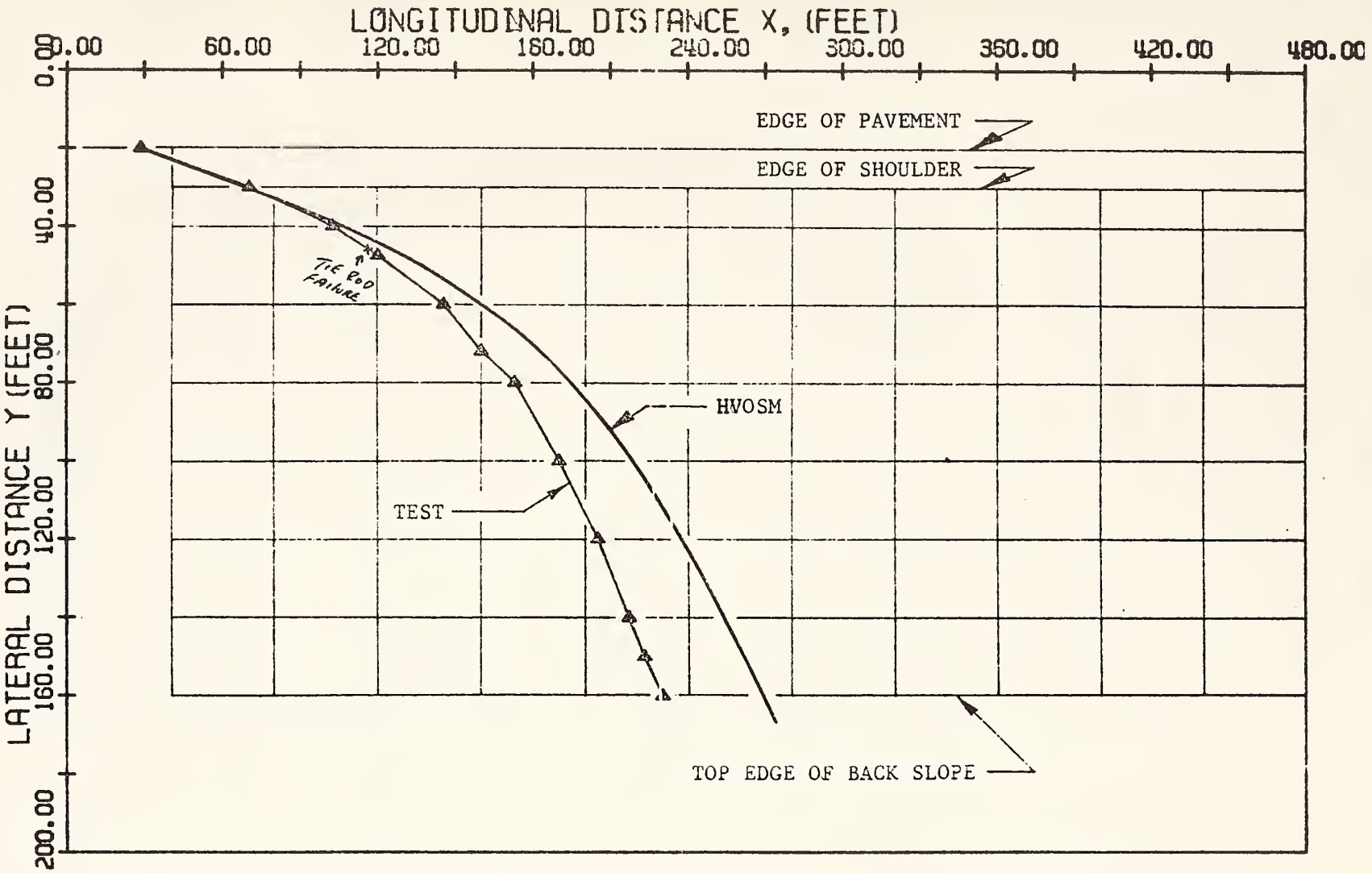

Figure 3.3-4 RIGHT FRONT TIRE TRACK, TEST NO. 2.

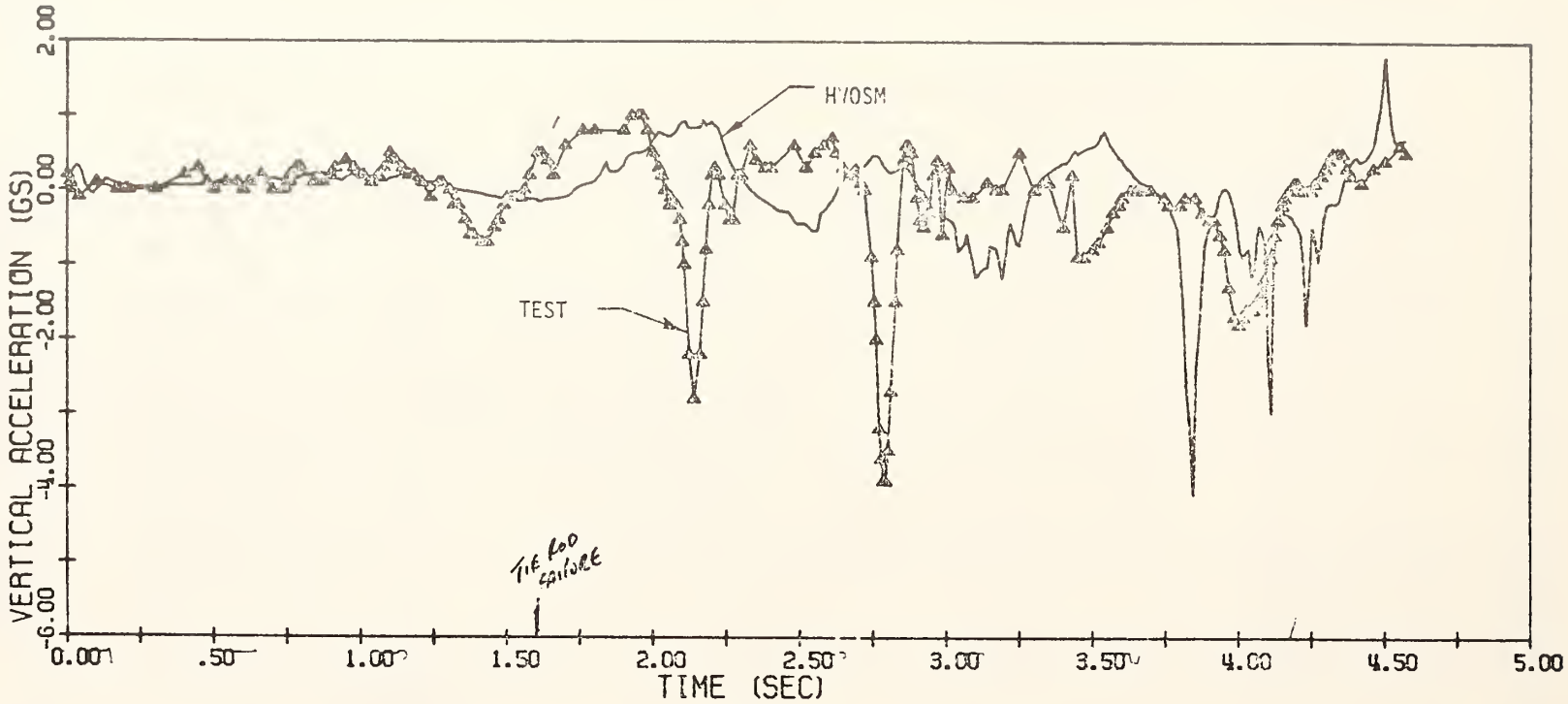

Figure 3.3-5 VERTICAL ACCELERATION VERSUS TIME, TEST NO. 2.

(3) Path Variations -- When the predicted and actual path did not closely compare, there was a twofold effect on the acceleration comparisons. First, the test car and the simulated car traversed different terrain which obviously caused some differences in accelerations. Secondly, the lateral position (in the Y direction) of the test car at any given time differed from the simulated vehicle. For example, in Test No. 2, the test car began traversing the back slope at approximately T = 4.0 seconds, while the simulated car entered it at approximately T = 4.6 seconds. Note that if the HVOSM curve in Figure 3.3-5 were shifted to the left the comparison would improve.

(4) Tire Rutting -- As discussed in a previous paragraph, some tire rutting occurred, especially for large steer angles. By studying the movie film it was observed that the front portion of the vehicle would undergo a bouncing or skipping type of motion during these large steer angles. The instability apparently caused some fluctuations in the measured accelerations that were not simulated by HVOSM.

Prior to conducting Test 3, the test car was returned to the Research Annex and new tie rod assemblies were installed. The steering system was then realigned.

Test No. 3

Comparisons of the tire track for this test (Figure 3.3-6) show good agreement up to the point where steer control was regained in the test car (at Y + 90 feet approximately). The simulated car remained in a no-steer control mode throughout the run.

A comparison of vertical accelerations for Test 3 (Figure 3.3-7) shows that the HVOSM trace approximated a mean of the test trace. Fluctuations in the test values are attributed to terrain irregularities and the effects of structural vibrations in the vehicle, as previously discussed.

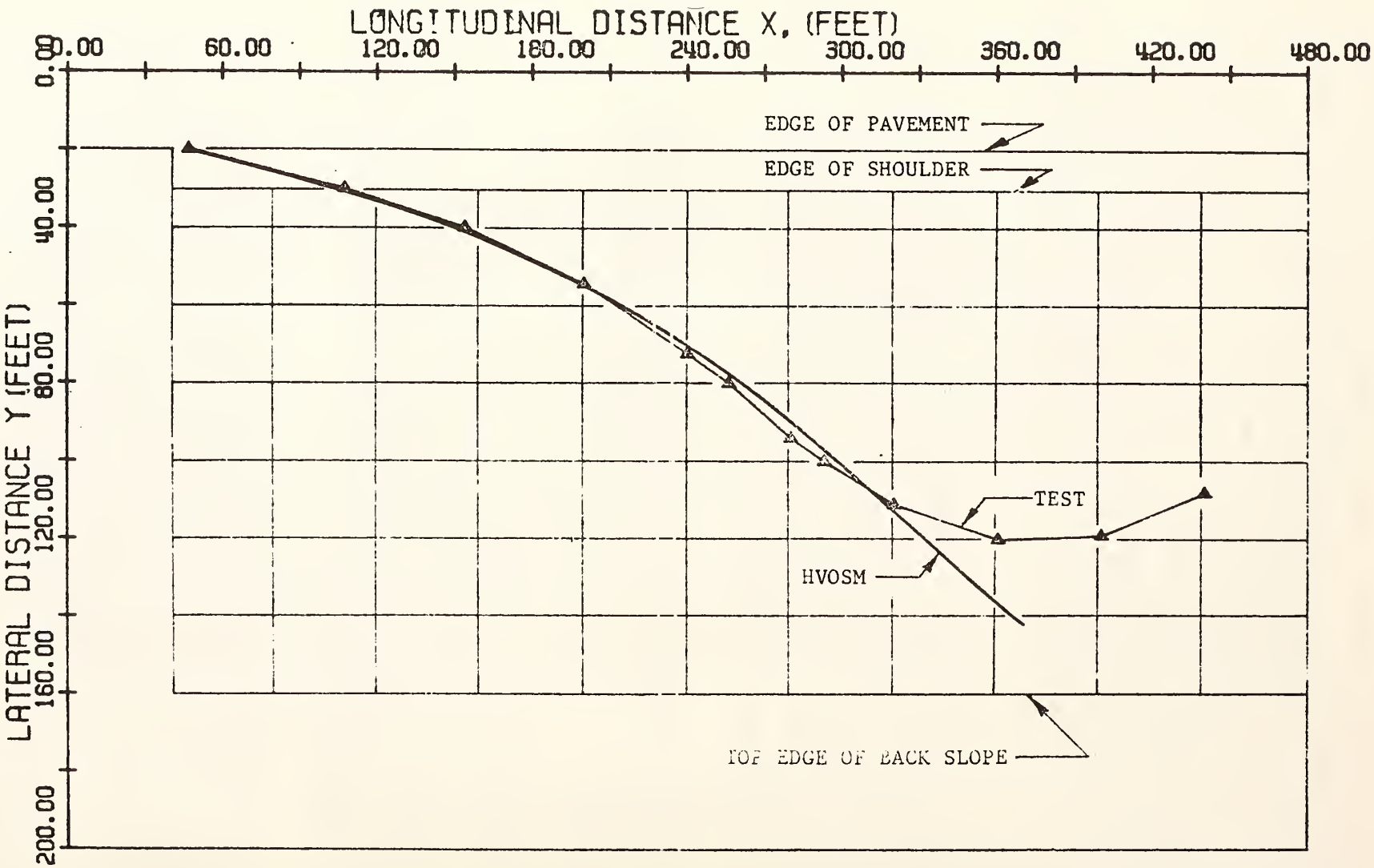

Figure 3.3-6 RIGHT FRONT TIRE TRACK, TEST NO. 3.

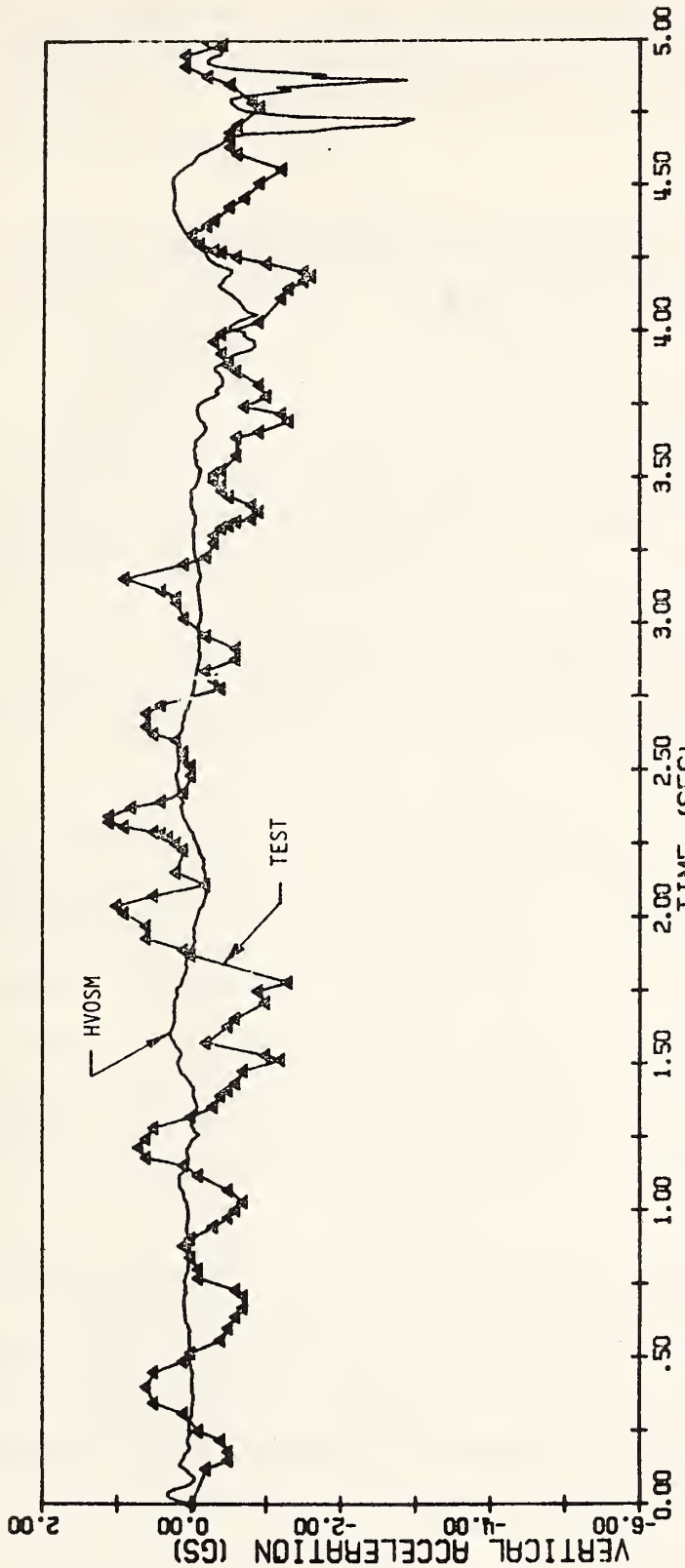

Figure 3.3-7 VERTICAL ACCELERATION VERSUS TIME, TEST NO. 3.

The relatively large accelerations of HVOSM between 4.5 seconds and 5.0 seconds were caused by the simulated vehicle entering the back slope.

Test No. 4

From the movie film it was observed that the front wheels of the test car went from a zero degree steer angle at T = 0.50 seconds to a full right turn at T = 1.0 seconds. They remained in a full right position until approximately T = 2.0 seconds, at which time they returned to a zero degree steer angle and remained at approximately zero for the remainder of the test. No suspension damage occurred during the test. The remote control operator reported that attempts to steer back to the left after the car reached the ditch bottom (at about T = 2.4 seconds) were unsuccessful. There was apparently some malfunction in the control system. Nevertheless, it is probable that the car could not have been redirected prior to going over the top of the back slope due to the large encroachment angle the car had upon entering the ditch bottom.

It is not certain what caused the front wheels in Tests 2 and 4 to turn sharply to the right after entering the side slope. However, it is interesting to note that the paths of Tests 2 and 4 were almost identical after the car reached a lateral distance of 20 feet off the edge of the pavement. In both tests the wheels turned sharply to the right at a lateral distance of approximately 27 feet off the edge of the pavement. An inspection of the side slope in that particular area showed no major irregularities, although there were local indentations and bumps which could have caused the problems.

In HVOSM the steer angle of the simulated car was programmed to be similar to that of the test car for Test 4. Upon leaving the roadway, the steer angle was zero up to T = 0.5 seconds. The steer angle was then increased linearly up to 22 degrees at T = 1.0 seconds. It was held at 22 degrees up to T = 2.0 seconds and was then decreased linearly back to zero at T = 2.5 seconds, where it remained for the duration of the simulation.

The tire track comparisons between test and simulation (Figure 3.3-8) showed reasonable agreement. The smaller turning radius of the test path is attributed to the added side forces created by the slight rutting that occurred during the test.

The generator supplying power to the instrumentation trailer failed during Test 4 and all accelerometer data were lost.

Test No. 5

No technical problems occurred during Test 5. The car left the road at a relatively shallow angle (8.6 degrees) and remained on the side slope during most of the test.

Good agreement between test and HVOSM tire tracks was obtained through most of Test 5. It can be seen in Figure 3.3-9 that steer control of the test car was regained and the car was steered back up the slope before it reached the ditch bottom. Note in Figure 3.3-9 the change in path curvature at an X distance of about 280 feet and a Y distance of about 66 feet. The ditch bottom begins at a Y distance of approximately 100 feet. The remote control operator related that he was "determined not to allow the car to hit the cotton patch again".

Although not planned, it is significant that steer back on the side slope was attempted. It had been speculated that if such a maneuver occurred, the car would likely roll over. Analysis of the film for this test showed that the car never appeared to be in danger of rolling over. It would be premature to conclude, however, that there are no conditions which would cause this car or any other car to roll over on a 3.5:1 side slope. As a matter of fact, tests at TTI on other studies have shown that when subjected to a particular sequence of severe steering and braking maneuvers, certain automobiles will roll over on a flat concrete pavement.

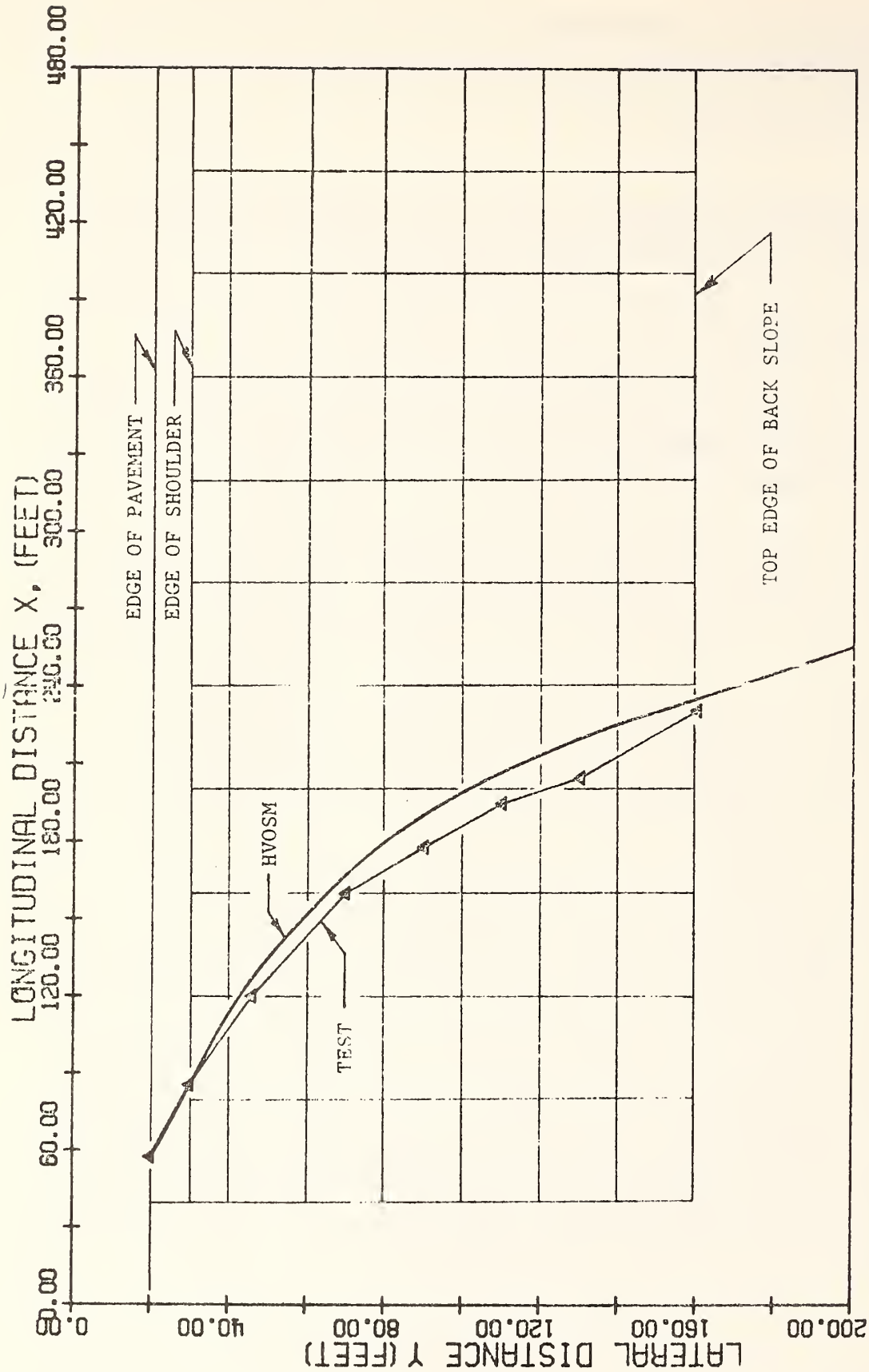

Figure 3.3-8 RIGHT FRONT TIRE TRACK, TEST NO. 4.

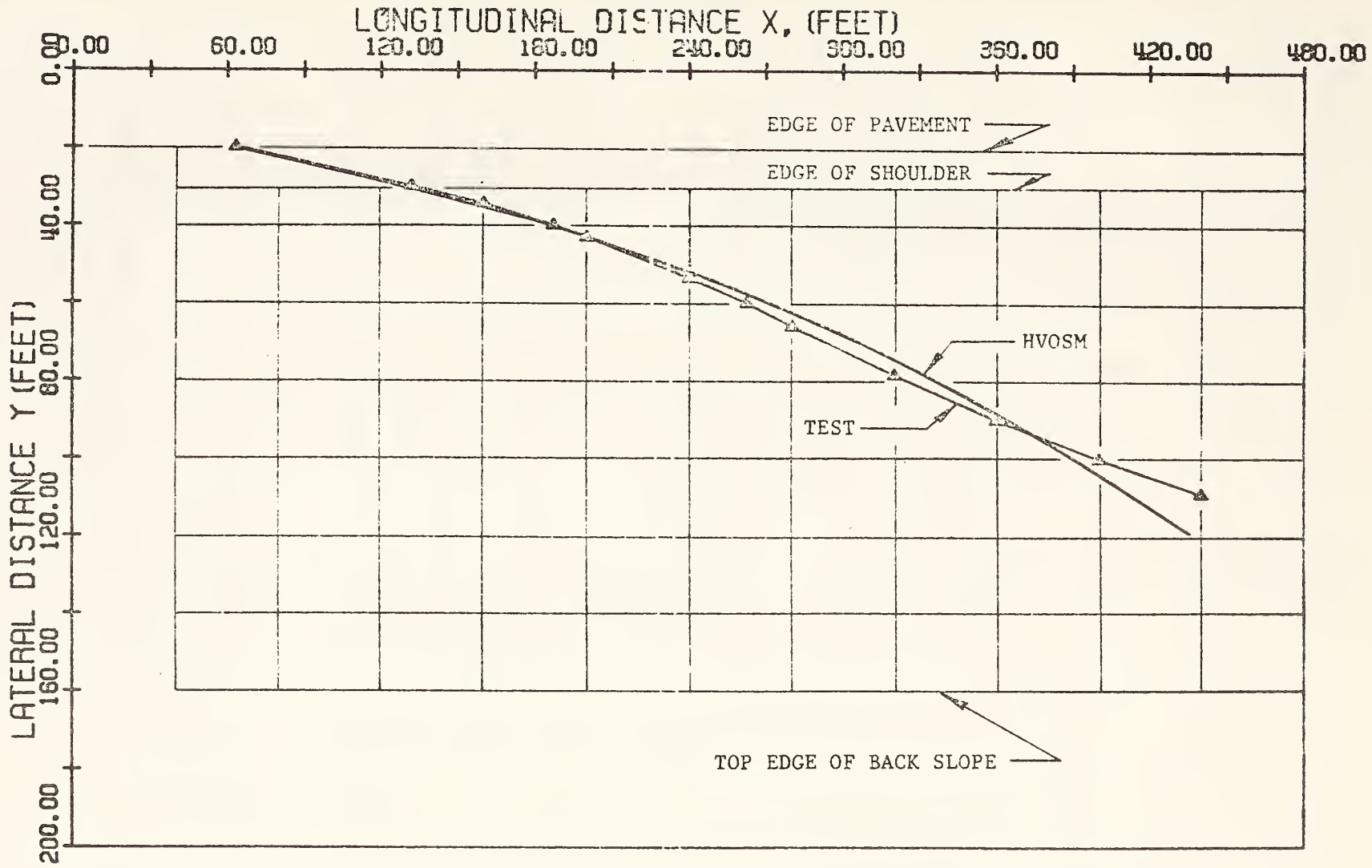

Figure 3.3-9 RIGHT FRONT TIRE TRACK, TEST NO. 5.

Reasonably good comparisons of accelerations were obtained in Test 5 (Figure 3.3-10), especially during the first half of the test. For the remainder of the test, the amplitude of the accelerations was comparable, but their variation with time differed. Differences in the latter phases of the test are attributed to path differences and differences in speed between tests and HVOSM.

Test No. 6

This test began with a moderate encroachment angle (13.3 degrees) and a relatively high encroachment speed (63.6 MPH). Large steer angles again occurred during this test. The front wheels turned sharply to the right at approximately T = 1.2 seconds (or Y = 50 feet, approximately). They remained in this position for about one second and then returned to approximately a zero steer angle. Examination of the suspension system after Test 6 showed that a tie-rod failure had again occurred, causing the right front tire to be locked in a partial right turn position (about 10 degrees). Repeated testing of the car had obviously caused degradation in the suspension system (loose ball joints, out of alignment, etc.).

It was decided to simulate Test 6 in HVOSM by assuming a free-wheeling condition (no steer control) throughout the test. In so doing the extent to which steer irregularities in the test affected the vehicle's path and attitude could be determined. As shown in Figure 3,3-11, the test and HVOSM paths agreed up to a Y = 70 feet, approximately. From that point the two paths began to diverge with the test vehicle turning more to the right. The attitude of the test and simulated vehicles remained relatively stable.

Differences in predicted and measured accelerations (Figure 3.3-12) are attributed to the factors presented in the discussion of Test No. 1. The test car enters the back slope at about T = 3.3 seconds while the HVOSM car enters it at T = 3.5 seconds. The large acceleration in the HVOSM car at

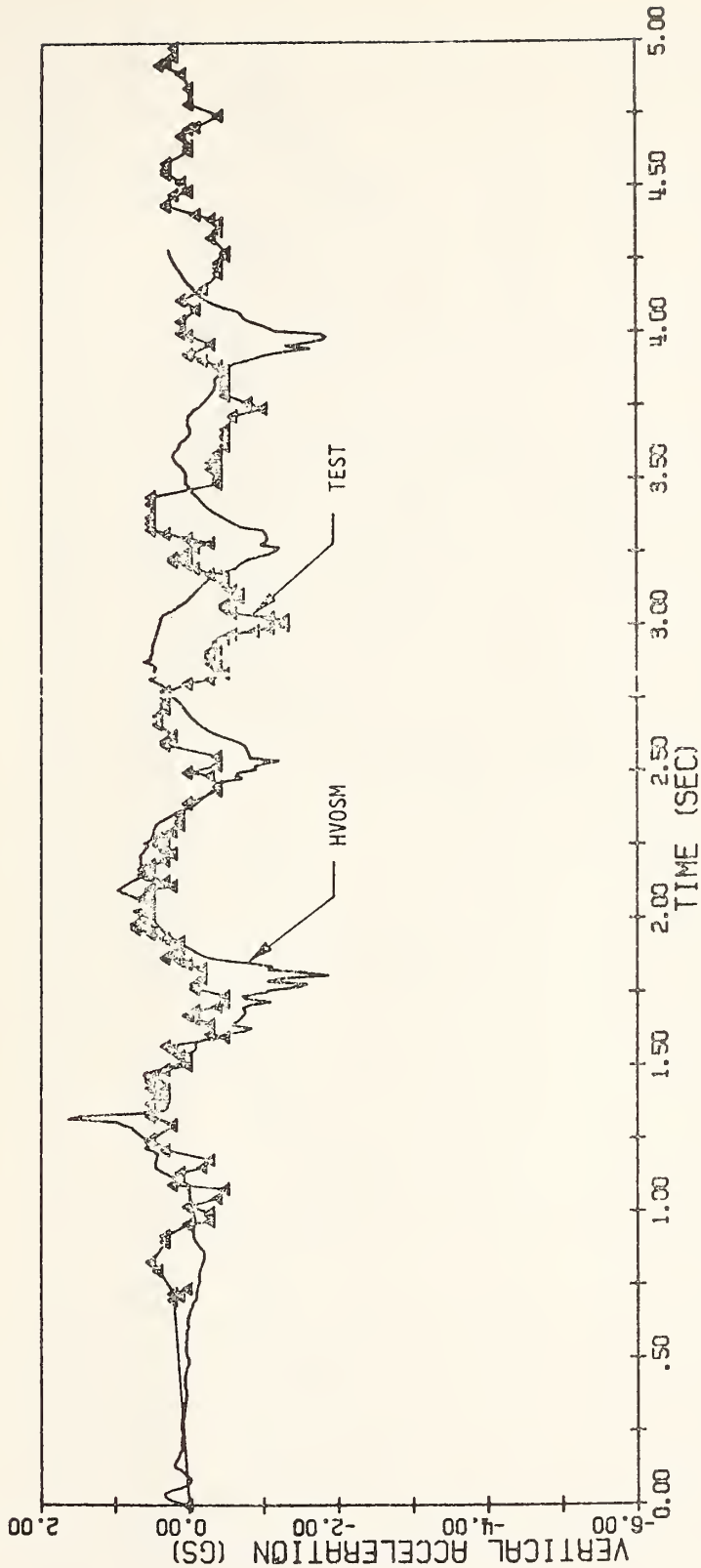

Figure 3.3-10 VERTICAL ACCELERATION VERSUS TIME, TEST NO. 5.

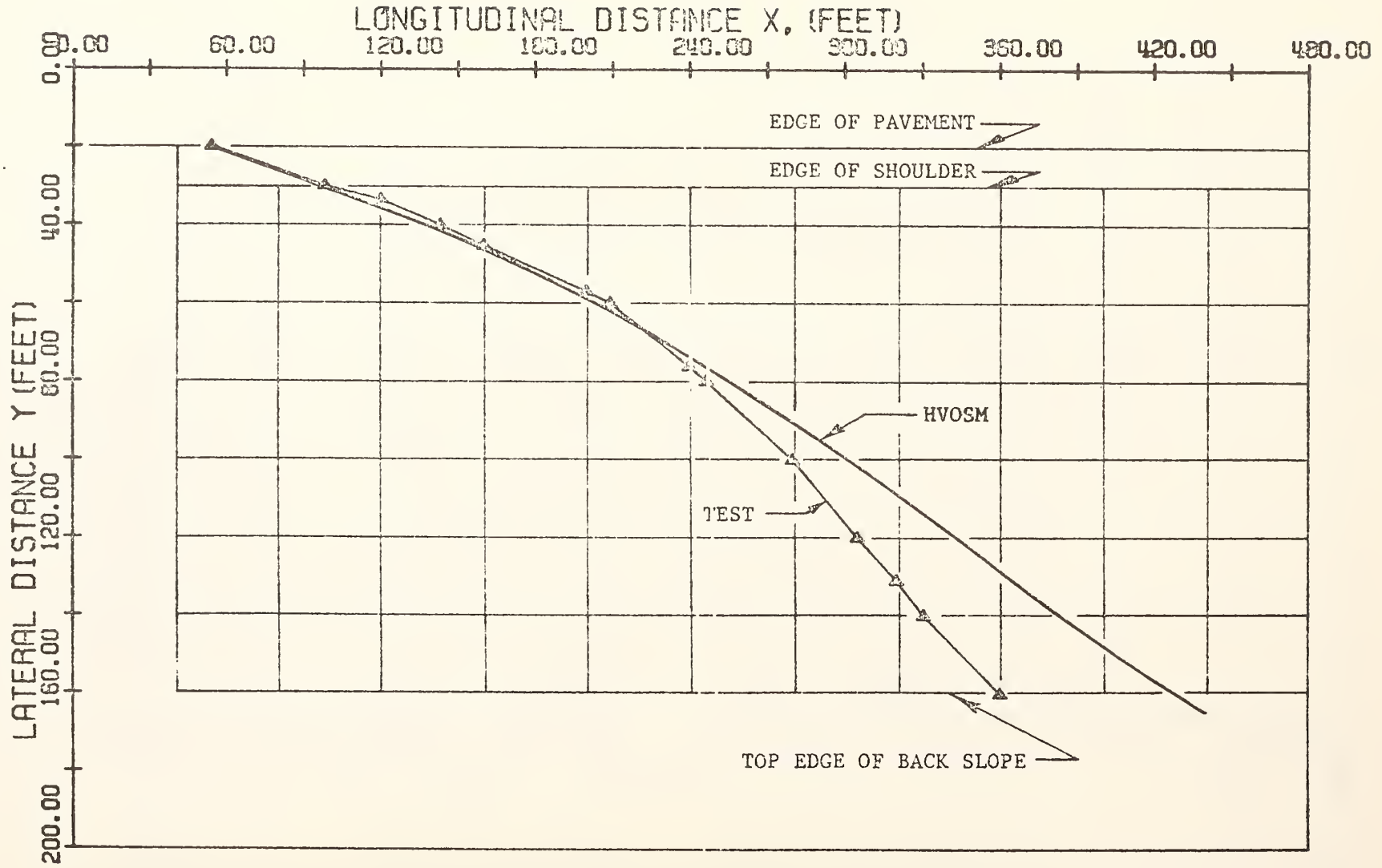

Figure 3.3-11 RIGHT FRONT TIRE TRACK, TEST NO. 6.

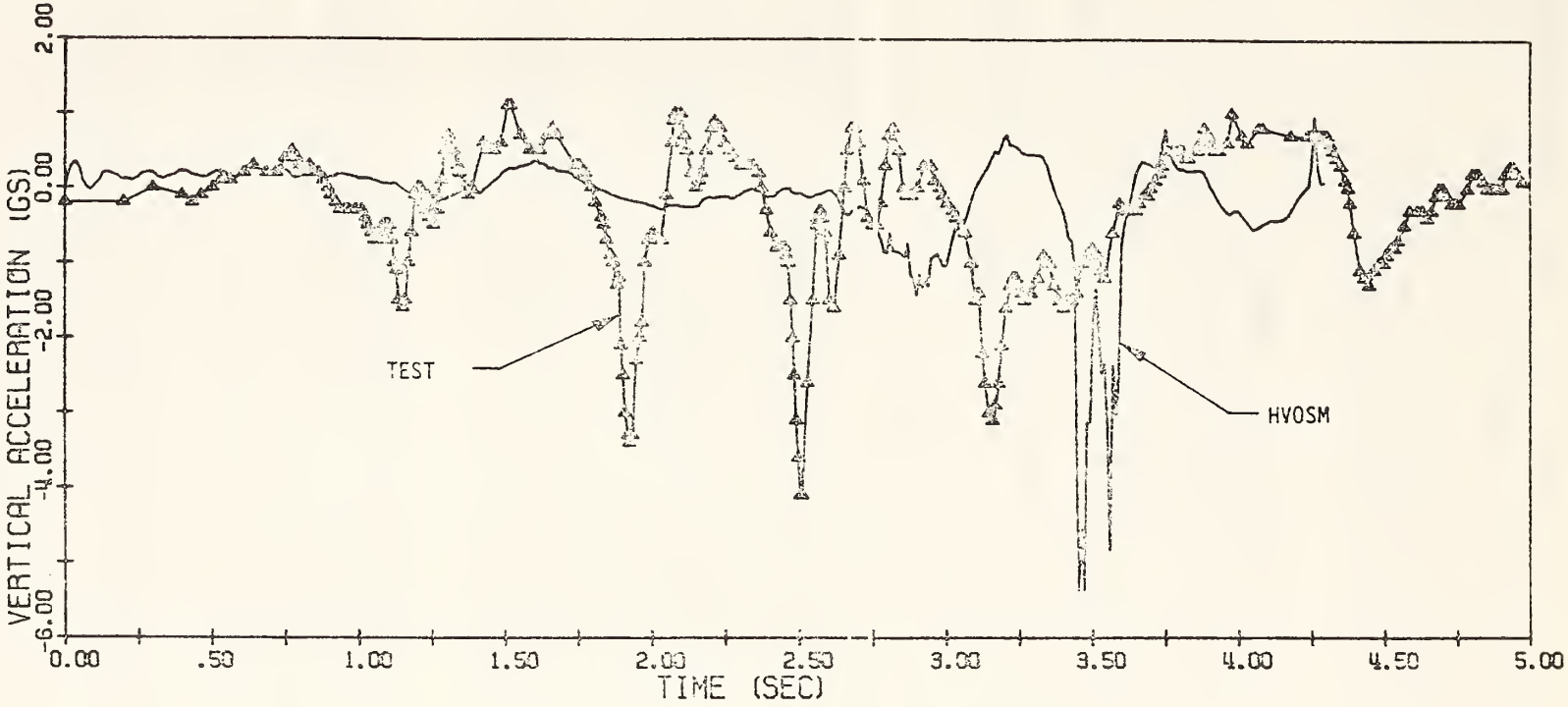

Figure 3.3-12 VERTICAL ACCELERATIONS VERSUS TIME, TEST NO. 6.

T = 3.5 seconds was caused by the back slope. The test accelerations were not larger during the back slope traversal because the test car brakes were applied just prior to entering the back slope. The remote control operator sensed that the car could not be redirected and was therefore attempting to stop it.

From an overall assessment of the comparisons, HVOSM was generally in reasonable agreement with the test results. The differences that did occur are attributed primarily to the mechanical failures in the test car's suspension system and their subsequent effects on the dynamic behavior of the car. It is known that the condition of the suspension system continued to deteriorate with each test. It is not known, however, just how much the suspension system deterioration contributed to causing each failure.

A wide variety of encroachment conditions were encountered in the study. Encroachment speeds ranged from 45.1 MPH to 63.6 MPH, and encroachment angles ranged from 8.6 degrees to 20.4 degrees. In addition, suspension failures (Tests 2 and 6) and the steer back on the side slope (Test 5) created special test conditions. This range of test conditions is believed to encompass many of the conditions that occur in run-off-the-road accidents. It is significant that for these conditions both test and simulation results showed that a car could traverse the embankment with no tendency to roll over.

Reasonably good correlations were obtained between test and predicted accelerations for Tests 1, 3 and 5, where no mechanical or electrical failures occurred.

4.0 REFERENCES

1. Kulp, D. L., "Determination of Selected Vehicle Properties on a 1963 Ford Galaxie-4-door Sedan for Cornell Aeronautical Laboratory, Inc.," Ford Motor Company, Test Order No. E-7012, 12 August 1968 (unpublished).

2. McHenry, R. R., Segal, D. J., DeLeys, N. J., "Determination of Physical Criteria for Roadside Energy Conversion Systems," CAL Report No. VJ-2251-V-1, June 1967.

3. No Author, "Drum Brake Design," Chrysler Institute of Engineering, Graduate School Lecture Notes, CH-6, January 24, 1952.

4. Newcomb, T. P. and Spurr, R. T., "Braking of Road Vehicles," Chapman and Hall, Ltd., 1967.

5. "Brake System Road Test Code - Passenger Car - SAE J843c," SAE Recommended Practice, SAE Handbook, 1971.

6. McHenry, R. R. and DeLeys, N. J., "Vehicle Dynamics in Single Vehicle Accidents - Validation and Extensions of a Computer Simulation," CAL Report No. VJ-2251-V-3, December 1968.

7. Lundstrom, Louis C., Skeels, Paul C., Englund, Blaine R., Rogers, Robert A., "A Bridge Parapet Designed for Safety," Highway Research Record Number 38, HRB Publication No. 1268, 1965.

8. Ross, H. E. and Post, E. R., "Comparisons of Full-Scale Embankment Tests with Computer Simulations - Volume One, Test Results and Comparisons," Texas Transportation Institute Report No. 140-7, December 1972.

9. Weaver, G. D., Marquis, E. L., and Luedecke, A. R., Jr., "Vehicle Dynamics on Roadway Slopes," Report No. 626A-1, Texas Transportation Institute, Texas A & M University, October 1971.

10. "Automobile Accidents Related to Railroad Grade Crossings - A Study of the Effects of Topography and a Computer-Graphics Display of Traffic Flow," Calspan Report No. VJ-2251-V-4, March 1969.

11. McHenry, R. R. and DeLeys, N. J., "Automobile Dynamics - A Computer Simulation of Three-Dimensional Motions for Use in Studies of Braking Systems and the Driving Task," Calspan Report No. VJ-2251-V-7, August 1970.

12. Anders, E. B., et al, "Digital Filters," NACA-136, December 1964 (Auburn Research Foundation, Inc., Auburn, Alabama).

13. Hadekel, R., "The Mechanical Characteristics of Pneumatic Tyres - A Digest of Present Knowledge," T.P.A. 3 Technical Information Bureau for Chief Scientist S & T Memo No. 10/52, November 1952.

14. McHenry, R. R., "The Astro Spiral Jump - An Auto Thrill Show Stunt Designed Via Simulation," presented at the Sixth Annual Simulation Symposium, Tampa, Florida, March 1973.

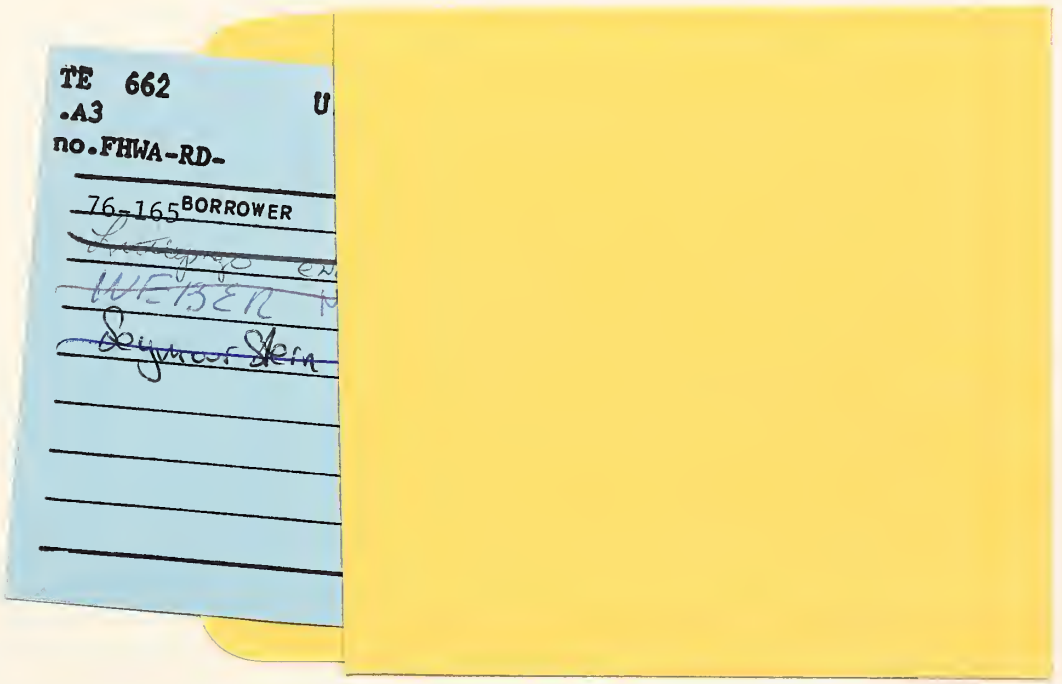
TE 662
.A3
no.FHWA-RD-
76-165
BORROWER